TRANSIENT STABILITY ANALYSIS OF INTEGRATED AC AND DC POWER SYSTEMS

A thesis
presented for the degree of
Doctor of Philosophy in Electrical Engineering

in the
University of Canterbury,
Christchurch, New Zealand

by

K.S. TURNER B.E.(HONS), M.E.

1980

CONTENTS

THE AUTHOR

The author was born in New Zealand, in 1950 and began undergraduate studies at the University of Canterbury in 1969 as a bursar with N.Z. Electricity. He completed a B.E. (Hons) degree in 1972 and an M.E. degree the following year. In early 1974 he joined the Dunedin staff of N.Z. Electricity and was responsible over the next 3 years for the installation and commissioning of Southward transmission on the N.Z. HVDC Link. During this time he was also involved in developing partial discharge testing for evaluating the aged condition of generators and in transient fault location on AC lines.

He returned to the University of Canterbury as N.Z. Electricity Power Fellow in 1977 to pursue investigations of HVDC transmission.

LIST OF PRINCIPAL SYMBOLS

For convenience the symbols used throughout this thesis are defined below. In some cases, symbols have alternative meanings but if there is any ambiguity of meaning this is clarified in the text or diagram.

Symbols

I	:	Current
V	:	Voltage
E_f	:	Synchronous Machine Field Voltage
Y	:	Admittance
R	:	Resistance
X	:	Reactance
X_c	:	Commutation Reactance
X'	:	Synchronous Machine Transient Reactance
X''	:	Synchronous Machine Subtransient Reactance
L	:	Inductance
C	:	Capacitance
S	:	Complex Power
P	:	Real Power
Q	:	Reactive Power
H	:	Inertia Constant of Rotating Machine
T'_{qo}, T'_{do}	:	Synchronous Machine Transient Open Circuit Time Constant
T''_{qo}, T''_{do}	:	Synchronous Machine Subtransient Open Circuit Time Constant
V_d	:	DC Voltage
I_d	:	DC Current
$V\angle\beta$	:	Thevenin Source Voltage
$E\angle\theta$	:	Converter Fundamental AC Terminal Voltage
$I\angle\psi$	:	Converter Fundamental AC Terminal Current
$Z_{th}\angle\mu$	:	Thevenin Delay Angle
α	:	Converter Delay Angle
u	:	Converter Commutation Angle
δ	:	$\alpha + u$ (converters)
δ	:	Generator Rotor Angle (for synchronous machines)
γ	:	Converter Extinction Angle
ϕ	:	Power Factor

π : 3.14159
t : Time
h : Integration Step Length
T : Period of Power System Frequency
ω : Angular Frequency
x^{sp} : Specified Value of x
$\dot{x}$: Derivative of x with respect to Time
$\angle x$: $\cos x + j \sin x$
j : Complex Operator
f(x) : Function of x
$\bar{x}$: Complex Variable x
x* : Complex Conjugate of x
[ ] : Matrix or Vector
$\surd$: Square Root
$\int$: Integration
Σ : Summation
a > b : a greater than b
a < b : a less than b
$\leftrightarrow$: Fourier Transform Pair
X : Convolution

Subscripts

α : TCS Capacitive Nodes
β : TCS Resistive Node with no Capacitive Connection
γ : TCS Inductive Nodes
δ : TCS Converter Inductive Nodes
l : TCS Inductive Branches
r : TCS Resistive Branches
k : TCS Converter Branches
r,m : Real and Imaginary Parts
r,i : Rectifier and Inverter Variables
d,q : Direct and Quadrature Axis Synchronous Machine Variables

Abbreviations

N.Z. : New Zealand
S.I. : South Island of N.Z.
N.I. : North Island of N.Z.
p.u. : Per Unit

HVDC	:	High Voltage Direct Current
TS	:	Transient Stability
TCS	:	Transient Converter Simulation
AVR	:	Automatic Voltage Regulator
DC	:	Direct Current
AC	:	Alternating Current
FFT	:	Fast Fourier Transform
msec	:	millisecond
cosh	:	hyperbolic cosine
cos	:	cosine
sin	:	sine
rms	:	Root Mean Square

ABSTRACT

This thesis describes the development of accurate models for representing power system converter loads in Transient Stability analysis.

An accurate load model is developed for rectifier loads, such as smelters and chlorine plants, in which all modes of rectifier operation are accounted for and the dynamics of the DC load represented.

The limitation of representing HVDC links with a Quasi-Steady State model are recognized and an alternative method is developed which uses interactive coordination between a transient converter simulation programme and a multi-machine transient stability programme. The algorithm provides an accurate AC system model for transient converter simulations and an accurate DC system model for transient stability analysis.

Case study results are presented which show the limitations of the Quasi-Steady State model and the algorithm is used to examine the possibility of using HVDC links for first swing stability improvement.

ACKNOWLEDGEMENTS

I would like to express my sincere thanks to my supervisor, Dr. C.P. Arnold, and my co-supervisor Professor J. Arrillaga for their guidance, encouragement and friendship throughout my research.

I also wish to acknowledge the generous cooperation and interest of my post-graduate colleagues, especially Bruce Harker and Doug Heffernan, in the many stimulating discussions we had as 'sparring' partners.

Special recognition is due to New Zealand Electricity for its wholehearted support of my work. I thank NZE for supporting me as a Power Fellow, for the draughting and technical expertise freely given by the Christchurch District Office and for the generous financial assistance provided to my supervisors for paper presentations overseas. In particular I thank Mr. C.V. Currie and Dr. P.S. Barnett for their cooperation.

I acknowledge a special debt to my wife Brenda for her unwavering encouragement, patience and faith.

"A good wife. who can
find?
She is far more precious
than jewels"

Proverbs 31.10.

CHAPTER 1

INTRODUCTION

During the past two decades, HVDC links have been established as competitive and attractive alternatives to AC transmission and this is evidenced by the number of HVDC schemes currently in operation or under construction. The prime motivation for their development has been large scale electric energy transport but, because of their easily controlled power transfer, HVDC links have demonstrated a significant stabilising influence in AC power systems (Pacific Intertie, Nelson River). There is now a growing trend for HVDC links to be used where system stability is the primary consideration. (Eel River, CU Project, Square Butte).

During the development stages of HVDC links, system planning was accomplished using small scale physical models. However such models lack flexibility in being able to change system parameters or represent large AC systems. With the advent of the modern digital computer, attempts were made to overcome the limitations of physical models using transient simulation in which the valves of each bridge are explicitly modelled. (Hingorani and Hay 1966, 1967). This method allows for the non-linearities introduced by the many discrete switchings taking place and was later refined to provide greater computational efficiency and flexibility. (Giesner 1971, Milias-Argitis et al 1976, Arrillaga et al 1977, 1978).

A comprehensive treatise on the steady state analysis of HVDC transmission was published by Kimbark, 1971 and, because of the number of HVDC links being planned, AC power system analysis programmes were extended to include HVDC link models. The models began to appear in load flow analysis about the same time. (Sato and Arrillaga 1969, Stott 1971, Reeve et al 1976, Arrillaga and Bodger 1977, 1978). The steady state models used for the loadflow problem were also implemented as Quasi-Steady States, (QSS), models in transient stability programmes, (Marshall et al 1974, Arrillaga et al 1977, Brameller et al 1979), and faults studies (Wong 1972, Lake 1978).

In the development of transient stability analysis the emphasis has been placed on deriving accurate models for the synchronous machines and their controllers. (Kimbark 1956). However with the availability of sophisticated computer programmes the complexity of system representation has increased and it is now recognized that inaccurate load models can lead to unrealistic system responses. (CAPS Working Group 1973). Moreover, although QSS models have been used for HVDC link representation in TS studies, the accuracy or applicability of such models have not been justified. It is during the disturbances used in TS analysis that the applicability of a QSS model is questionable. The QSS model cannot predict or determine the controllability of a converter and if normal valve firing sequences are disturbed by consequential valve malfunctions the QSS model cannot be used.

The objective of this work is to improve the modelling of large converter plant for TS analysis and to establish the accuracy and applicability (or otherwise) of the QSS model. This is done using Transient Converter Simulation, (TCS), for analysing the detailed behaviour of HVDC links.

An interactive procedure is developed here in which a multi-machine TS programme is used to provide the AC system representation required in TCS studies. The TS programme is used to derive a reduced AC network equivalent of the AC system that is time-variant and includes the transient and sub-transient effects of the dynamically responsive elements in the system. This time-variant equivalent is used for AC representation throughout a transient converter simulation of an HVDC link. The results obtained by the TCS are in turn processed to provide equivalents which represent the behaviour of the HVDC link and which are compatible with the TS study. The TCS results are therefore used to accurately represent the DC link during the disturbance period. As soon as the link behaviour returns to a quasi-steady state form the TCS can be terminated and the TS study continued using a QSS model. This interactive coordination of the two types of programme allows a detailed representation of the components of major

interest, (i.e. HVDC links), while providing an accurate and time-variant representation of the remaining parts of the system without increasing computation time.

In Chapter 2 the basic parts of a modern TS programme are reviewed. It includes both synchronous machine models and computational aspects and is based on a TS programme produced initially at the University of Manchester Institute of Science and Technology (Arnold 1976).

In Chapter 3 a model of a rectifier load is developed in which the dynamic effects of the DC load are represented. This introduces a need to improve the solution algorithm used for including the effect of the rectifier load in the AC network. For this purpose a unified algorithm is developed which uses the Newton-Raphson solution process for the rectifier without degrading the convergence properties of the AC system. With the dynamically responsive DC load included in the model, the response of the rectifier during disturbances can not be represented by the normal mode equations. The model is thus extended to account for the abnormal modes of rectifier operation.

To introduce the results of a transient converter simulation into the TS programme, so that the QSS model can be replaced during the disturbance period, it is necessary to derive TS compatible variables from the waveform orientated data provided by the TCS. Chapter 4 discusses the assumptions and errors associated with deriving fundamental frequency TS variables from distorted, noisy waveforms and also investigates approximations which reduce the computational effort required in processing the waveforms.

The QSS DC link model is discussed in Chapter 5 and the method of interactive coordination between the TS and TCS programmes is explained. Algorithms are derived so that the time-variant network equivalents for TCS may be derived with minimal change to the TS programme.

In Chapter 6 the results of three, worst case, fault studies are presented and the QSS and TCS models are compared in detail. The differences between the two models are

discussed to show the limits of applicability of the QSS model.

Chapter 7 uses the interactive capabilities of the TS and TCS programmes to demonstrate the feasibility of using a DC link for first swing stability improvement. A large number of preliminary studies are made using the QSS model only, to determine the effects of different machine models, systems and DC link parameters. Based on these studies three transient converter simulations are performed on different systems to determine the accuracy of the QSS model and the feasibility and effectiveness of the stability improvement control.

CHAPTER 2

ELEMENTS OF TRANSIENT STABILITY ANALYSIS

2.0 INTRODUCTION

The development of large interconnected AC power systems as we know them today, has been dependent on the fact that generators operating in parallel have a natural tendency to run in synchronism. Hence many machines can be connected to feed the same network. The degree of stability with which systems operate depends on a number of factors:

i) The size of individual generators.
ii) The position of the generators in a network.
iii) The strength of the transmission network.
iv) The distribution of load in the network.

Disturbances in a system, such as a fault, cause an interchange of inertial energy between the generators. The result is a change in speed of each individual machine and because this change is different for each, the machines swing relative to each other (and relative to a reference machine in the system) causing synchronising power to flow. If the swing of one machine relative to the next exceeds a certain limit, synchronism is lost, and the machines no longer continue to operate together, resulting in a collapse of the system.

The investigation of the ability of a system to remain in synchronism after a fault is known as Transient Stability Analysis. This problem has been the subject of thorough investigation since about 1920. Until the advent of the modern digital computer, calculations were made laboriously by hand using many simplifications to avoid complexity. Modern computer programmes for assessing transient stability are now capable of studying large systems with many machines to any degree of complexity required. With such a tool it is possible to determine whether any given power system will remain stable in any given operating condition when subjected to any given disturbance.

The purpose of this chapter is not to review the many approaches to TS analysis as they are at present. The intention is to present the fundamentals of TS analysis and to give an overview of a modern TS programme. This overview is based on a TS programme developed by Dr. C.P. Arnold and used extensively in conjunction with the modelling of converters throughout this work.

2.1 STEADY STATE STABILITY

During normal steady state operation of a power system, the system load is undergoing constant and relatively small fluctuations. These fluctuations cause small deviations from constant frequency which are corrected by a change in the power output of the generators, by governor action. The power transfer between the two machines of Fig. 2.1, for example, can be described by equation 2.1.

$$P_{12} = \frac{V_1 V_2}{X} \sin \delta \qquad (2.1)$$

where δ is the phasor angle between voltages V_1 and V_2, or the electrical angle between the rotors of the two machines. The variation of P_{12} with δ is illustrated in Fig. 2.1b. As load variations increase the power demand from a generator, the rotor angle increases to meet the demand. Figure 2.1b shows the maximum power which can be transmitted between the two machines is reached when $\delta = 90°$. This is the steady state stability limit for this system. If the load increases beyond this level, although δ increases, the power delivered decreases, and the machines lose synchronism.

The steady state stability limit can be increased by decreasing the transfer impedance. This is fixed for any given system and can only be decreased by the addition of more lines or transformers to strengthen the system. The limit can also be increased using an automatic voltage regulator (AVR) to increase V_1 or V_2. If the AVR is used to make excitation a function of power output then the steady state stability limit can exceed 90° As illustrated in Fig. 2.1b, although δ_1 exceeds 90°, power can still be

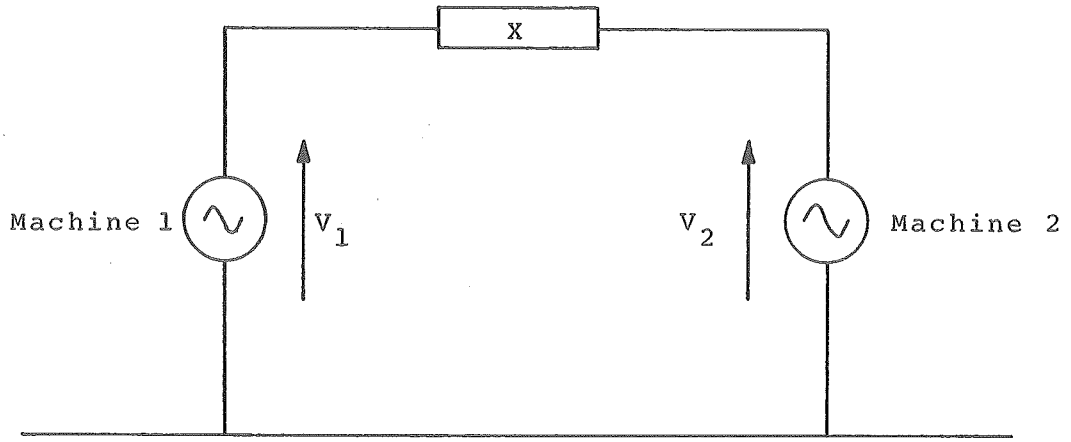

Fig. 2.1a Simple Two Machine System

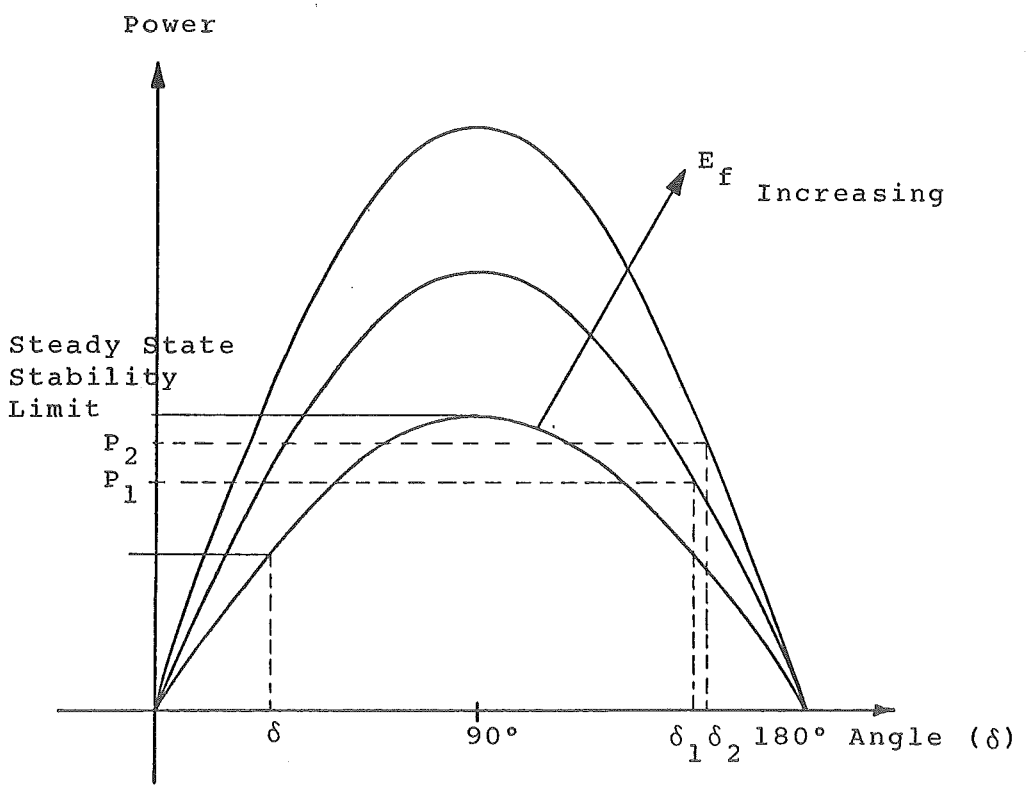

Fig. 2.1b Power Angle Curve for Two Machine System

increased, as δ increases to δ_2, by the increase in field voltage, E_f, modifying the P-δ curve. In normal system operation generators are generally operating well below their steady state stability limit with angles ranging up to 40°.

2.2 TRANSIENT STABILITY

Slow variations of load can be compensated by governor action. A sudden increase in load cannot be compensated for immediately, and during the interim period the extra energy taken by the load comes from the stored inertial energy of the system machines. The result is an oscillation in the rotor angles and, provided there is some damping in the system, the machines will settle to a new angle.

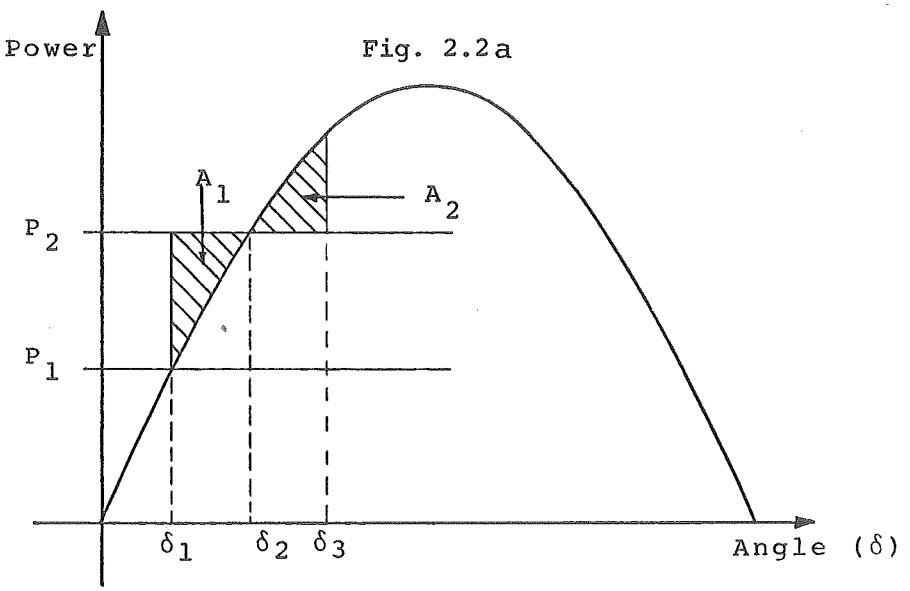

Fig. 2.2a

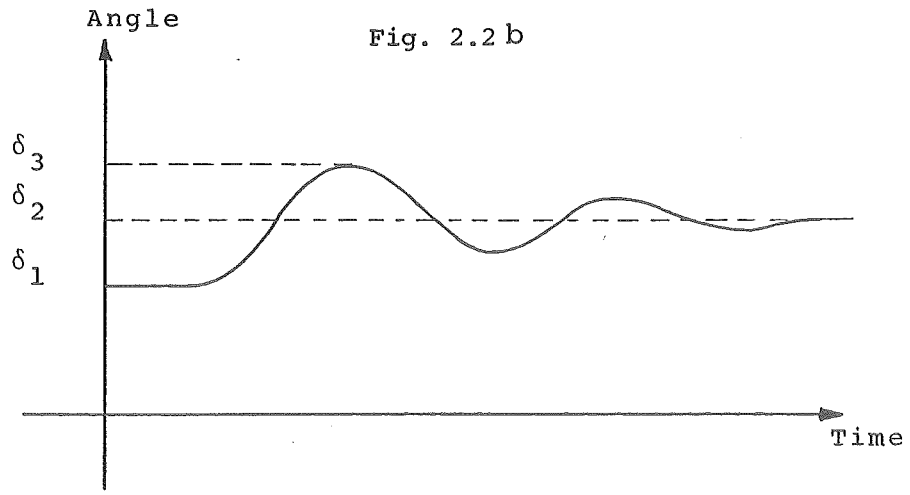

Fig. 2.2b

Fig. 2.2 Effect of Load Increase on δ.

Figure 2.2a illustrates the effect of a sudden electrical load increase, from P1 to P2 for a single generator feeding into an infinite bus. The deceleration of the machine (due to the electrical power output exceeding the mechanical power input) causes an angle increase to δ_2 but at this point it is still decelerating. The machine swings to angle δ_3 and, without damping, areas A1 and A2 would be equal. With damping the machine settles to a new operating point at δ_2. The response of the angle with time is illustrated in Fig. 2.2b.

The generator will remain transiently stable provided area A2 can always be equal to or larger than A1. This is known as the equal area criterion (Kimbark 1948). The transient stability limit is reached when A2 equals A1 but cannot increase further as is the case in Fig. 2.3. If the machine swings beyond δ_3 then stability will be lost.

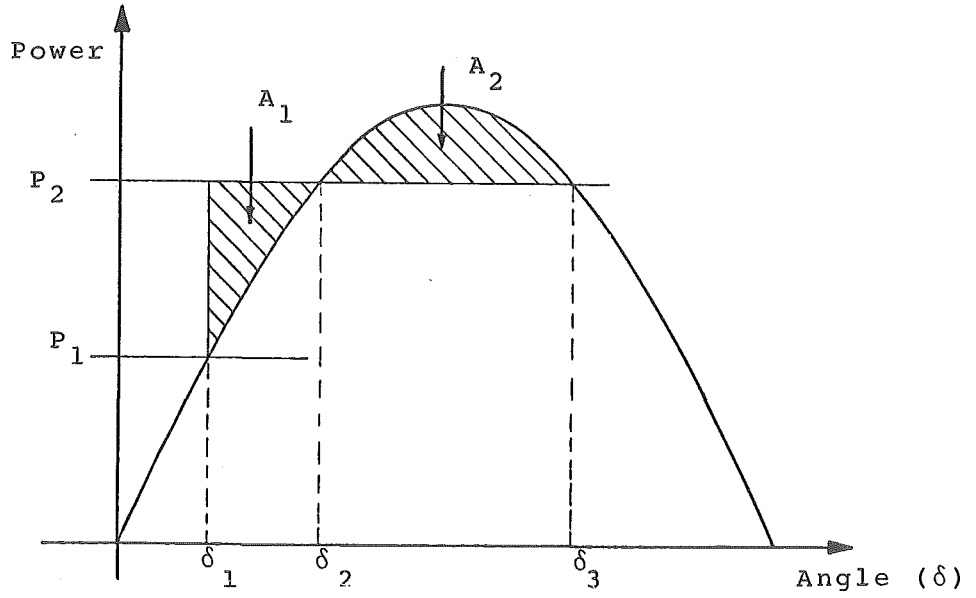

Fig. 2.3 Transient Stability Limit.

When a fault occurs in the system the power angle curve is instantaneously altered. Refering to Fig. 2.4, the output power drops from P1 to P2 and the machine accelerates (due to excess mechanical power).

At 3 the fault is cleared and a post fault P-δ curve is invoked. The electrical power jumps to P4 and the machine is now subjected to deceleration although its angle is still increasing. At 5 it reaches its peak swing angle and, provided damping is present, it settles to a new steady state angle of δ_6.

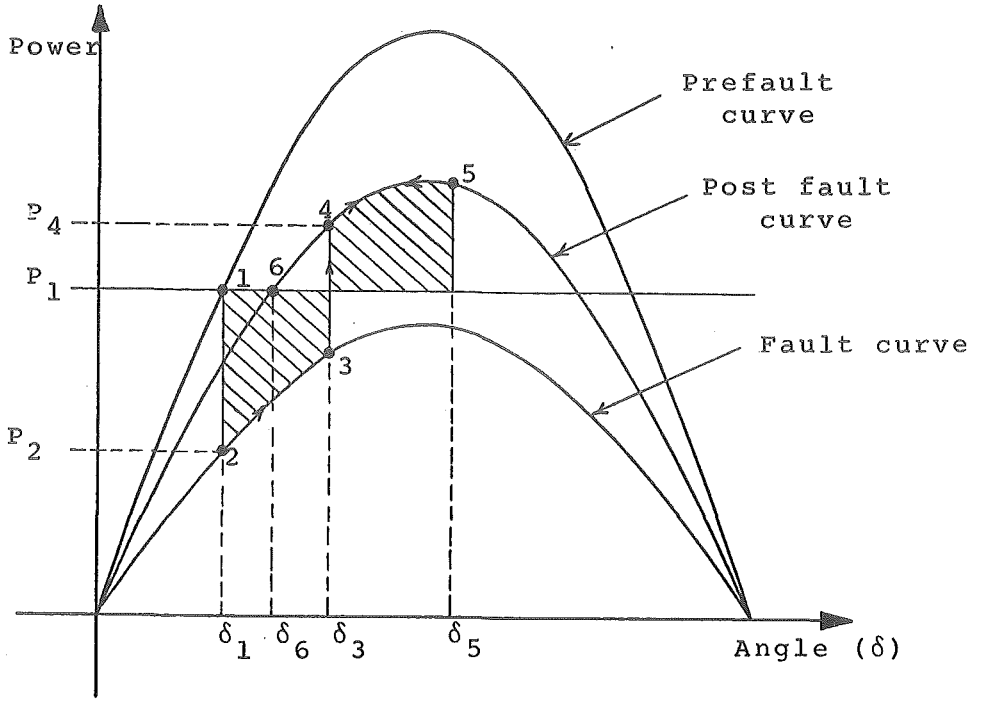

Fig. 2.4 Idealised Power Angle Curve for a Faulted System.

2.3 MULTI-MACHINE TRANSIENT STABILITY

The equal area criterion discussed in section 2.2 is useful to demonstrate TS principles and for solving TS problems involving only two machines. Its applicability is limited for any more than two machines.

One of the early approaches to solving the multi-machine stability problem involves a point by point method of solving the differential swing equations. Once the angular position is obtained at a given step the network is solved to determine a new electrical power for the solution of the swing equation at the next step. This method is extremely laborious, synchronous machine representation was in most cases limited to a voltage behind reactance and the method on its own could only be applied to small systems. As the size of the network increases the network part of the solution becomes increasingly more difficult.

This problem is overcome by the use of an AC network analyser. The network analyser is a scaled physical model of the system which, when given the relative machine angles (obtained by hand from the point by point solution of the swing equation), can provide the electrical power flows

around the network for the next point of the swing curve.

With the advent of the digital computer the alternating solution of the differential and network equations was implemented entirely on the computer, eliminating the need for any hand calculations. The complexity of the machine model could be increased and the system size was only limited by the amount and speed of the computing time available.

A number of different algorithms were developed to improve the efficiency of the computation, the most significant one being reported in 1972, (Dommel and Sato 1972) in which the differential and network equations were solved simultaneously. This new algorithm eliminated interface errors which occur when the differential and network equations are solved alternately,as with the earlier algorithms. This was done using an implicit rather than an explicit integration method allowing the differential equations to be algebraized, included in the network algebraic equations and solved simultaneously.

The trapezoidal rule is numerically stable, (Law 1972), and can be used with step lengths greater than the smallest time constant of the system,without instability or excessive errors. This allows detailed representation of machines, their AVR's and governors, induction motors and non-impedance loads without affecting the numerical performance of the programme. The models used for the various system elements are well known and their operational features will be presented without further justification.

2.4 MODELLING FOR TRANSIENT STABILITY STUDIES

The conditions throughout a network at a given step of a TS study are defined by:

i) A set of steady state algebraic equations of the network, loads and rotating machines, i.e.:

$$G(X,Y) = 0 \qquad (2.2)$$

ii) A system of differential equations which describe the dynamic behaviour of the machines and their controls, i.e.:

$$\dot{Y} = \mathbb{F}(X,Y,t) \qquad (2.3)$$

where X are the non integrable variables which depend on a set of algebraic constraints (examples of which are busbar voltages and electrical powers)

Y are integrable variables which depend on a set of time variant restraints (i.e. rotor angles or internal emf's)

and $\mathbb{G}$ and $\mathbb{F}$ are functions.

When there is a sudden disturbance to the system, variables X show a discrete change following the disturbance while variables Y are continuous as a discrete change in them is not possible by definition.

The solution of the TS problem using implicit integration involves the algebraization of equation 2.3 into the same form as equation 2.2 and subsequent solution of equation 2.2.

2.4.1 Network Representation

Lines, transformers and cables can be represented by a combination of series and parallel impedances, commonly in an equivalent π network as illustrated in Fig. 2.5.

For a line, Y_{ab} represents the transfer impedance and Y_{aa} the shunt susceptance. i.e.:

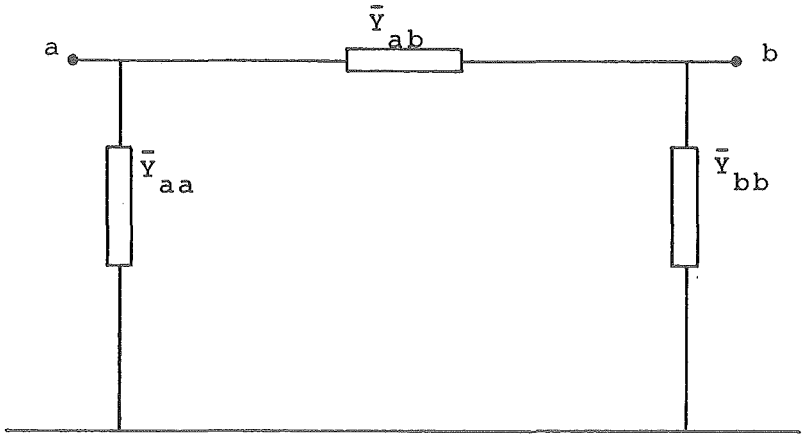

Fig. 2.5 π Equivalent Circuit for Network Elements.

$$\bar{Y}_{ab} = \frac{1}{R + jx} \tag{2.4}$$

$$\bar{Y}_{aa} = \bar{Y}_{bb} = -jB/_2 \tag{2.5}$$

The same applies for nominal tapped transformers and cables. For an off nominal tap transformer the elements are modified by the tap position. If the tap position, T, is given in % off nominal, then:

$$a = 1 + 0.01T \tag{2.6}$$

and
$$\bar{Y}_{ab_t} = a\bar{Y}_{ab} \tag{2.7}$$

$$\bar{Y}_{aa_t} = (a^2 - a)\bar{Y}_{ab} \tag{2.8}$$

$$\bar{Y}_{bb_t} = (1 - a)\bar{Y}_{ab} \tag{2.9}$$

In a nodal admittance formulation of the network, equation 2.2 is of the form:

$$[\bar{I}] = [\bar{Y}]\ [\bar{V}] \tag{2.10}$$

where $[\bar{I}]$ is a vector of injected currents, $[\bar{Y}]$ the network admittance matrix and $[\bar{V}]$ the vector of nodal voltages. Admittances $\bar{Y}_{ii}$ form diagonal elements of $[\bar{Y}]$ and $\bar{Y}_{ij}$, $i \neq j$ form off diagonal elements of $[\bar{Y}]$

2.4.2 Synchronous Machine Model

The most important model and one which affects TS results significantly is that of the synchronous machine. The model is made up of both algebraic and differential equations.

2.4.2.1 Algebraic equations - In a conventional d-q reference frame of representation the basic equations describing a synchronous machine are:

$$\begin{bmatrix} I_d \\ I_q \end{bmatrix} = \frac{1}{R_a^2 + X_d X_q} \begin{bmatrix} R_a & X_q \\ -X_d & R_a \end{bmatrix} \begin{bmatrix} E_d - V_d \\ E_q - V_q \end{bmatrix} \tag{2.11}$$

This is a steady state (synchronous) description but is equally valid for transient and subtransient behaviour by replacing synchronous reactances by transient or subtransient values and the voltage behind synchronous reactance by transient or subtransient respectively. i.e., for increasing degree of detail from left to right:

$$\begin{array}{ccccc} X_q & \rightarrow & X'_q & \rightarrow & X_q'' \\ E & \rightarrow & E' & \rightarrow & E'' \end{array} \qquad (2.12)$$

To interface the d-q model to the network frame of reference a transformation is required, i.e.:

$$(I_r + jI_m) = (I_d + jI_q)e^{-j(\frac{\pi}{2} - \delta)} \qquad (2.13)$$

In the network frame of reference the machine model can be summarised by:

$$\bar{I} = \bar{Y}_{fict}(\bar{E} - \bar{V}) + \bar{I}_{sal} \qquad (2.14)$$

where $$\bar{Y}_{fict} = (R_a - j(x_d + x_q)/2)/(R_a^2 + x_d x_q) \qquad (2.15)$$

$$\bar{I}_{sal} = \bar{Y}_{sal}(\bar{E} - \bar{V})^* e^{j2\delta} \qquad (2.16)$$

$$\bar{Y}_{sal} = j(x_d - x_q)/[2(R_a^2 + x_d x_q)] \qquad (2.17)$$

The Norton equivalent of equation (2.14) is illustrated in Fig. 2.6.

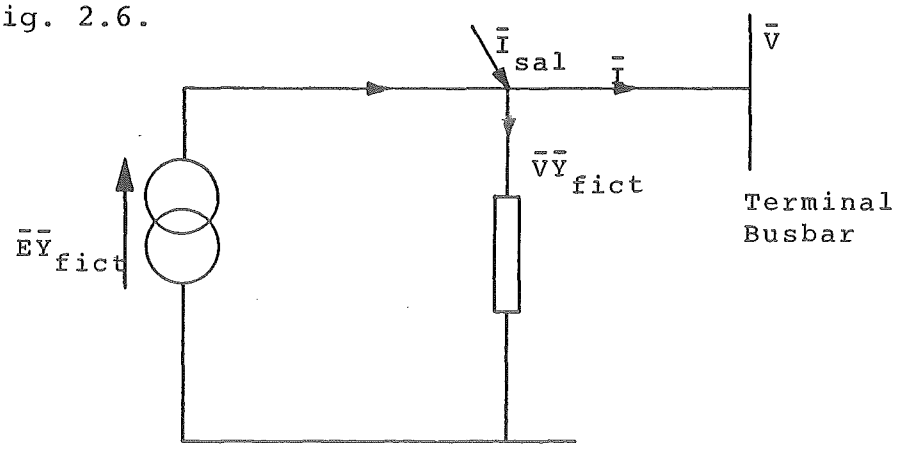

Fig. 2.6 Norton Equivalent of Synchronous Machine for Nodal Formulation.

In the nodal admittance formulation of equation 2.2 the admittance $\bar{Y}_{fict}$ can be included directly into the admittance matrix and the currents $\bar{I}_{sal}$ and $\bar{Y}_{fict}.\bar{E}$ become part of the vector of nodal injected currents. Since $\bar{I}_{sal}$ is a function of the unknown bus voltage, $\bar{V}$, solution of the generator equations is an iterative process.

2.4.2.2 Differential equations - The differential equations for the machine are related to two different effects:

i) The electro-mechanical response of the machine.

ii) The dynamic behaviour of electrical characteristics.

The electro-mechanical response is described by the well known swing equation, here given as two first order equations:

$$\dot{\omega} = \frac{\omega_o}{2H} (P_m - P_e - D_a\dot{\delta}) \qquad (2.18)$$

$$\dot{\delta} = \omega - \omega_o \qquad (2.19)$$

where P_m is the turbine shaft power, P_e is the electrical output power, D_a is a damping factor related to the change in positive sequence flux, ω_o is the nominal and ω the actual machine speed. The dynamic response of the flux linkages is governed by the transient and subtransient open circuit time constants. Their effect is introduced,in the transient state, by:

$$\dot{E}'_d = [(x_q - x'_q) I_q - E'_d] / T'_{qo} \qquad (2.20)$$

$$\dot{E}'_q = [E_f - (x_d - x'_d) I_d - E'_q] / T'_{do} \qquad (2.21)$$

and in the subtransient state by:

$$\dot{E}''_d = [E'_d + (x'_q - x''_q) I_q - E''_d]/T''_{qo} \qquad (2.22)$$

$$\dot{E}''_q = [E'_q - (x'_d - x''_d) I_d - E''_q]/T''_{do} \qquad (2.23)$$

Saturation, which affects only the mutual rotor-stator flux, modifies equations 2.14 and 2.20 to 2.23. Although saturation is a very nonlinear characteristic, linear approximations can be applied with acceptable accuracy, (Olive 1966), using saturation factors to preserve the linearity of the equations. As saturation cannot be easily presented briefly the details will be omitted.

2.4.3 Speed Governor

Without a governor model, the mechanical power, P_m, of equation 2.18 is assumed to remain constant. This assumption is reasonable when only first swing transient stability is being examined since governor action is relatively slow. For longer term studies governor action can have an appreciable affect on the shaft power and subsequent system response after the first swing. Governor response can also indicate trends in the longer term power-frequency balance problem.

The governor is normally modelled by a set of differential equations obtained from the transfer functions of a functional block diagram. The equations become part of equation 2.3. Standard governor models have been developed, (IEEE Committee Report Feb. 1973) and are widely used in many TS programmes. Separate documentation is unnecessary here. The present TS programme incorporates a range of models from a simple, to a fully detailed representation of both hydro and steam turbine governors.

2.4.4 Automatic Voltage Regulator

The purpose of the AVR is to control the terminal voltage, V, of the generator to a fixed value. This is done by monitoring the terminal voltage and varying the excitation voltage, Ef , of equation 2.21. This provides a secondary change to the rotor-stator flux linkages apart from their natural response given by equations 2.20 to 2.23.

Standard AVR models are available, (IEEE Committee Report Jan. 1973), and these models are incorporated, with varying degrees of complexity depending on data available,in the present programme.

2.4.5 Loads

Most commerical and domestic loads can be represented as constant impedances. With this representation a nominal impedance is calculated, based on the initial power and voltage obtained from a loadflow. This impedance can be included directly into the admittance matrix of equation 2.10.

Non impedance type load models can be used for specific applications where the impedance load characteristic is not representative. In such cases, constant current and constant power characteristics, as illustrated in Fig. 2.7, can be used.

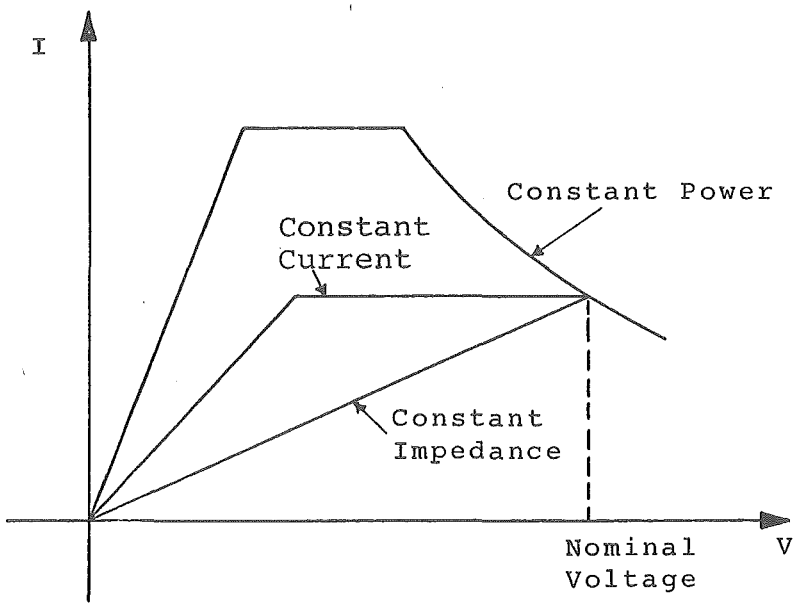

Fig. 2.7 Non Impedance Load Characteristic.

This type of load is included in the TS programme by calculating the nominal admittance of the load and modifying the characteristics by calculating an injected current which represents the deviation of the chosen characteristic from an impedance. The injected current is added to the nodal current vector, $[\bar{I}]$, of equation 2.10. Special precautions have to be taken to ensure that abnormally large injected currents, which may upset the numerical stability of the programme, are not required to produce the chosen characteristic. The low voltage part, of the non-impedance characteristics illustrated in Fig. 2.7, is modified to avoid this

Special industrial induction motor loads can also be represented with a detailed induction motor model developed recently, (Arnold et al 1979).

The functional relationships between the network, synchronous machine, governor, AVR and loads, in TS modelling, are illustrated in Fig. 2.8.

2.5 COMPUTATIONAL CONSIDERATIONS

The major part of the computational effort used in TS studies is required in the solution of equation 2.10. The size of matrix $[\bar{Y}]$ goes up as the square of the number of buses in the system. One of the attributes of $[\bar{Y}]$ is that it is very sparse, i.e., for a 100 bus system only about 4% of the 10,000 elements in $[\bar{Y}]$ are non zero. However solution of equation 2.10, by computing the inverse of $[\bar{Y}]$ explicitly, i.e.

$$[\bar{V}] = [\bar{Y}]^{-1} [\bar{I}] \qquad (2.24)$$

results in a full matrix $[\bar{Y}]^{-1}$ requiring much greater storage and processing. Because of the iterative nature of the TS problem and the number of steps for a complete run, computation methods requiring $[\bar{Y}]^{-1}$ explicitly, become prohibitive for large systems, even on modern very fast computers.

A highly efficient algorithm has been developed, (Zollenkopf 1970), for the direct solution of sparse networks without the formation of $[\bar{Y}]^{-1}$ explicitly. This method, bifactorisation, is very fast as it preserves the sparsity of the original matrix and only processes non zero elements. The method is based on the technique of Gaussian Elimination in which $\bar{Y}$ is reduced to a matrix, $\bar{U}$, in upper triangular form, i.e.

$$[\bar{I}]'' = [\bar{U}] [\bar{V}] \qquad (2.25)$$

It is thus possible to solve for $[\bar{V}]$ by backward substitution. Using this approach, $[\bar{Y}]$ can be represented by its upper and lower triangular matrices and a unit diagonal matrix $[\bar{D}]$ such that:

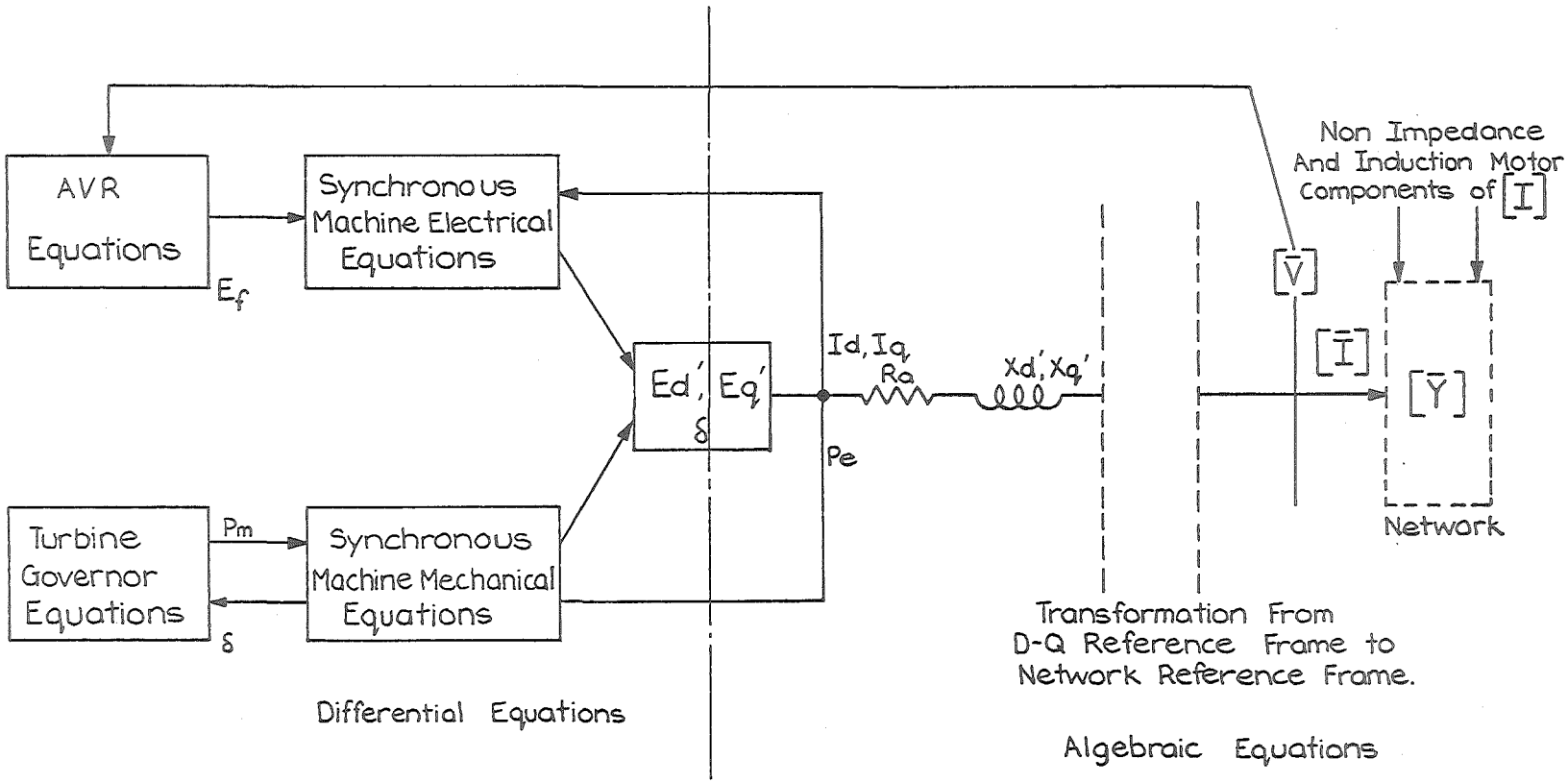

Fig. 2.8 Functional Relationships of a T.S. Model (in the Transient State)

$$[\bar{Y}] = [\bar{L}][\bar{D}][\bar{U}] \qquad (2.26)$$

$$\text{and} \quad [\bar{I}] = [\bar{L}][\bar{D}][\bar{U}][\bar{V}] \qquad (2.27)$$

In this form $[\bar{L}] = [\bar{U}]^T$ and hence only one half of the admittance matrix need be stored.
The modified vector, $[\bar{I}]''$, can be obtained by forward substitution on $[\bar{L}]$ and many solutions for $[\bar{V}]$ can be obtained without re-triangularisation provided $[\bar{Y}]$ remains unchanged. Re-triangularisation is therefore only necessary when the system is subjected to a topological change.

If $[\bar{Y}]$ is sparse then $[\bar{L}]$ and $[\bar{U}]$ are also likely to be sparse and ordered elimination uses highly efficient sparsity programming to store and process only the non zero elements. During the elimination, pivots are selected to obtain maximum preservation of the sparsity of the arrays. The elimination is initially simulated, to determine the pivot ordering in advance and to organise the subsequent elimination processing so that it can be executed very rapidly without storage being wasted.

The algorithm, outlined above, has been implemented in the present TS programme. Its performance has proved to be highly successful making the programme one of the fastest available at the present time.

2.6 SUMMARY

The basic features of a modern TS programme have been presented. Considerable effort has been spent on the development of TS analysis in the past as evidenced by its prominence in the literature. A lot of effort has been spent on improving modelling techniques to make the programmes a more effective tool for power system analysis. Most of the material presented here can be found in the literature but as a basic reference the author would refer the reader to Kimbark 1948, 1956.

CHAPTER 3

MODELLING RECTIFIER LOADS

3.0 INTRODUCTION

Transient stability is generally regarded as a problem of keeping dynamic power system elements in synchronism. Because of this, the traditional emphasis in developing models for TS analysis, has been placed on generator representation and efficient computational techniques for digital computer implementation. It is only relatively recently that importance has been attached to load modelling and the contribution which loads make to system damping. (Concordia 1975). Emphasis has been placed on induction motor response (Brereton et al 1957, Iliceto and Capasso 1974, Hakim and Berg 1976) and investigations of composite load dynamics. (CAPS Working Group 1973.) Little consideration has been given to large rectifier loads.

Rectifier loads with high power ratings and sophisticated power electronic control have become common in power systems.

Figure 3.1 illustrates the primary transmission system of the South Island, (SI), of New Zealand which includes a large aluminium smelter and DC link. DC links require separate treatment and are considered later in this work. The rectifier load at the smelter represents some 13% of the total SI installed capacity. Since this load is constant it can represent up to 50% of the SI load during periods of light load. The size of this load is sufficiently large to affect the dynamic response of the system and an accurate representation of it is therefore important.

In this chapter an accurate representation for rectifier loads is developed. The model includes the dynamic effects on the DC side of the rectifier and is extended to include abnormal modes of operation during large disturbances. The model is therefore accurate for the wide range of conditions that may prevail during TS analysis. A second (unified) algorithm is developed to improve the convergence of the TS

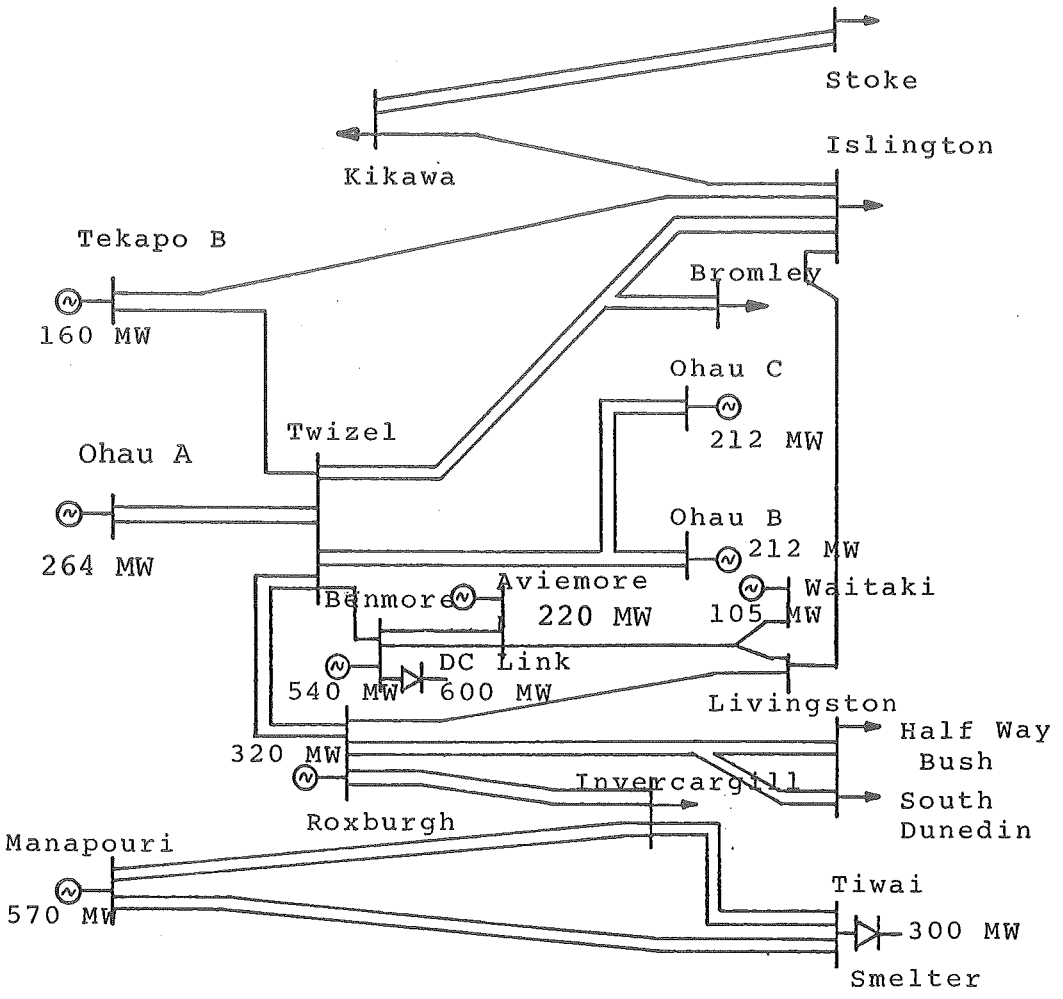

Fig. 3.1 New Zealand South Island Primary System

programme which showed considerable deterioration in convergence when the dynamic DC load is modelled using the more conventional sequential algorithm.

3.0.1 Model Application

Rectifier loads utilise a number of control methods, i.e., diode or thyristor elements in full or half wave rectification. Although the particular load considered in this work is an aluminium smelter the model is applicable to any large rectified load (such as chlorine plants) by specifying the correct input parameters.

In the case of the NZ smelter, coarse voltage control is achieved using a tap changer and fine control is obtained using series saturable reactors. The saturable reactor

control affects diode conduction in an identical manner to a normal thyristor bridge (Fuji Electric 1972) but the equivalent of the delay angle has a much more limited range. This action is illustrated in Fig. 3.2.

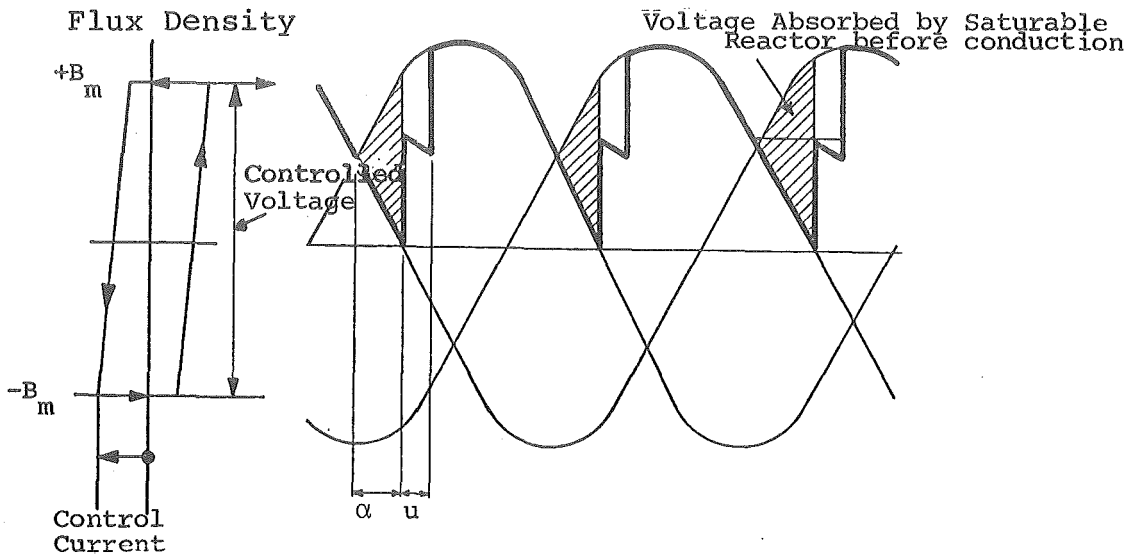

Fig. 3.2 Saturable Reactor Control of Diode Conduction.

The thyristor controlled biasing voltage maintains the series saturable reactor at a high impedance until the forward voltage is high enough to cause saturation of the reactor. During this period commutation cannot take place and the reactor absorbs the forward voltage equivalent to the shaded area in Fig. 3.2. As soon as saturation is reached the reactor impedance drops and normal commutation takes place.

The range of control, exerted by the saturable reactors at the Tiwai smelter is equivalent to a delay angle range from 3 to 20 degrees.

3.1 BASIC RECTIFIER MODEL

Large rectifier loads generally consist of parallel and/or series connected 3 phase full wave bridges. For smelter applications converters are paralleled on the DC side to achieve the high currents required for smelters. For simplicity of modelling it is possible to reduce these connections to a single equivalent bridge but consideration has to be given to the evaluation of commutation reactance.

3.1.1 Commutation Reactance of Parallel Bridges

Figure 3.3 is a single line connection diagram of one potline at the Tiwai smelter.

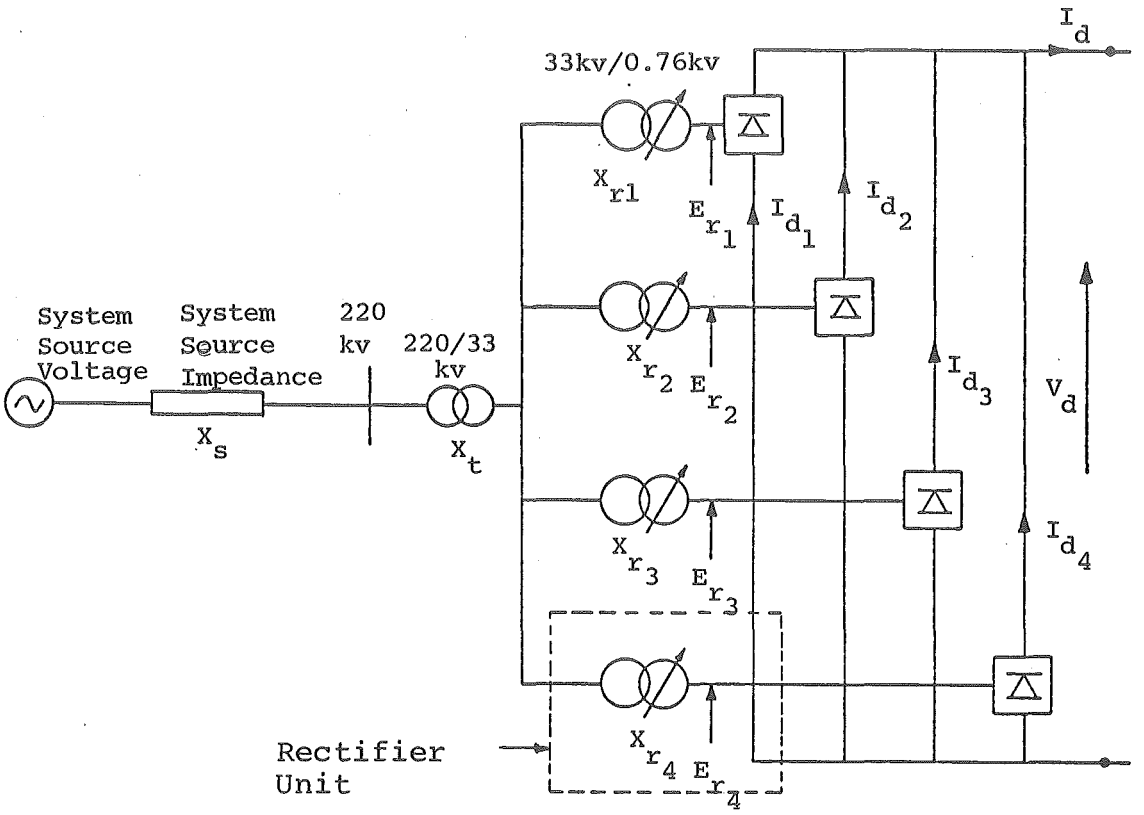

Fig. 3.3 Single Line Connection Diagram for one Potline at Tiwai Smelter.

The source voltage for one of the bridges is defined as the voltage appearing on the DC line during the period when no commutation is taking place, i.e. the purely sinusoidal voltage nearest the rectifier. (Uhlmann 1975). For the case illustrated in Fig. 3.3, this would be the system source voltage. If filters are connected on the 220kv or 33kv bus's then the voltage at the filter bus would become the source voltage since, ideally, it would be purely sinusoidal. The commutation reactance is defined as the reactance between the source voltage and the converter.

When considering a single bridge (bridge 1) of Fig. 3.3, the commutation reactance, X_{c1}, is:

$$X_{c1} = X_s + X_t + X_{r1} \qquad (3.1)$$

However with multiple bridges which are phase shifted in relation to each other, the high pulse number of the system means that the voltage at the 33kv bus is essentially sinusoidal and can therefore be considered as the source voltage of the system. In this case the commutation reactance of a single bridge becomes:

$$X_{c1} = X_{r1} \tag{3.2}$$

Although the network reactance does not contribute to the commutation reactance, it still affects the source voltage in the normal AC manner by theregulating effect of an AC current through an impedance.

Since the 4 bridges are under the same controller it is assumed that:

$$E_{r1} = E_{r2} = E_{r3} = E_{r4} = E_r \tag{3.3}$$

$$I_{d1} = I_{d2} = I_{d3} = I_{d4} \tag{3.4}$$

$$\text{and} \quad 4I_{d1} = I_d \tag{3.5}$$

In this case the parallel combination of Fig. 3.3 can be modelled as a single equivalent bridge, Fig. 3.4, in which:

$$X_c = \frac{X_{r1}}{4} \tag{3.6}$$

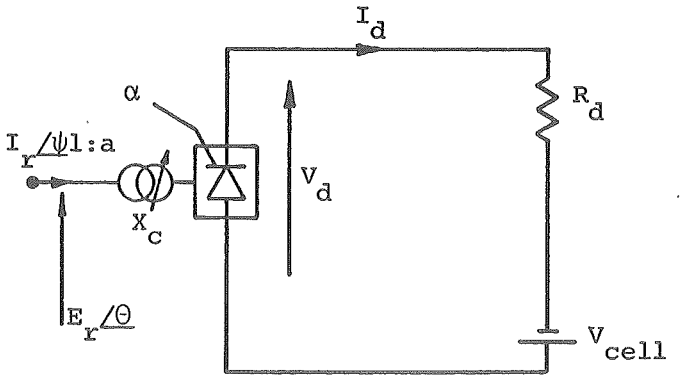

Fig. 3.4 Smelter Rectifier Load Equivalent.

The chief component in any commutation reactance is the converter transformer reactance (i.e. X_r). However when there is more than one bridge, connected with the same phase angle, the system component of commutation reactance can become significant.

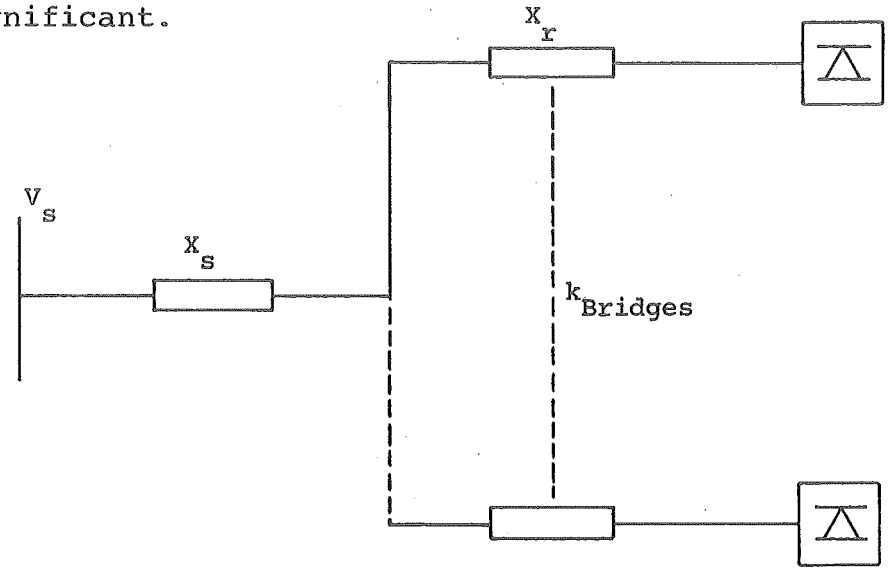

Fig. 3.5 Commutation Reactance for k Bridges Connected with the Same Phase Angle.

Referring to Fig. 3.5, for k bridges all with the same connection phase angles, the system reactance will be commutating k times the current of a single bridge and in this case with commutation reactance of one bridge is:

$$X_{cl} = kX_s + X_r \qquad (3.7)$$

This assumes each bridge is operating with the same direct current.

3.1.2 Basic Assumptions

Further assumptions are made in formulating a basic rectifier model. These are:

i) The rectifier source voltages are balanced, three phase waveforms with negligible distortion.

ii) The losses in the converter transformer are negligible.

iii) The thyristor (or diode) elements of the converter behave as ideal switches and are lossless.

iv) The DC current and voltage are smooth.

v) Control action affecting delay angles is considered to be instantaneous.

vi) No tap changer action takes place during or immediately after a sudden disturbance.

These assumptions are well documented and accepted elsewhere (Kimbark 1971) and will not be justified separately in this work.

3.1.3 Basic Converter Equations

A number of basic equations can be derived from first principles (Kimbark 1971, Adamson et al 1960), to interrelate the variables in Fig. 3.4. The constants in the following equations are given with the source voltage, E_r, as a phase to phase quantity referred to the secondary side of the converter transformer by the tap, a. In terms of the DC voltage:

$$V_d = \frac{3}{\sqrt{2}\pi} aE_r(\cos\alpha + \cos\delta) \qquad (3.8)$$

In terms of DC current:

$$I_d = \frac{aE_r}{\sqrt{2}X_c} (\cos\alpha - \cos\delta) \qquad (3.9)$$

Using equation 3.9, the commutation angle can be eliminated from equation 3.8 to give a more convenient form for DC voltage: i.e.

$$V_d = \frac{3\sqrt{2}}{\pi} aE_r \cos\alpha - \frac{3X_c}{\pi} I_d \qquad (3.10)$$

Using Fourier analysis the fundamental component of AC current at the terminals of the converter transformer can be related to the DC current by:

$$I_r = \frac{\sqrt{6}}{\pi} \left[\frac{1 \angle -2\alpha - \angle -2\delta - j2u}{4(\cos\alpha - \cos\delta)}\right] I_d \qquad (3.11)$$

The expression in parentheses is commonly equated to a constant, k_1. Referring to the system side of the transformer:

$$I_r = ak_1 \frac{\sqrt{6}}{\pi} I_d \tag{3.12}$$

For normal operating conditions of a converter, k_1 can be approximated to unity with less than a 1% error. With a commutation angle of 60° the error is 4.3%.

An approximation for the power factor at the converter transformer can be obtained by equating real AC and DC powers across the converter: i.e.

$$V_d I_d = \sqrt{3}\, E_r I_r \cos\phi \tag{3.13}$$

$$\text{where } \phi = \theta - \psi$$

Substituting for I_r with equation 3.12 and V_d with equation 3.8 gives

$$\cos\phi = \frac{1}{2k_1} (\cos\alpha + \cos\delta) \tag{3.14}$$

Using Kirchoffs laws around the DC current loop provides:

$$V_d = I_d R_d + V_{cell} \tag{3.15}$$

The above set of equations are fundamental to quasi-steady state models of converters.

3.1.4 Per Unit System

In order to use AC per unit quantities in the DC equations and to keep the DC variables in the same order of magnitude as the AC ones, a per unit system was introduced for the DC variables. The system uses the same base MVA on both the AC and DC sides of the converter and is illustrated in Fig. 3.6.

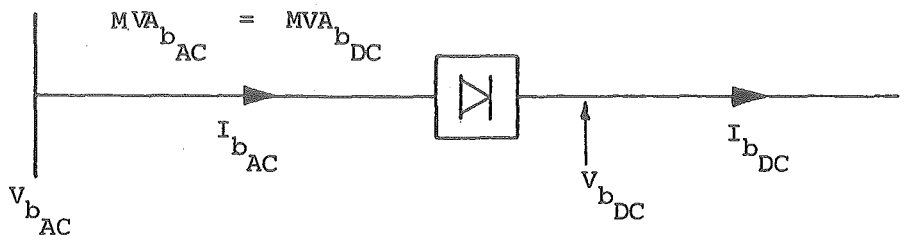

Fig. 3.6 Per Unit Definitions.

The AC terminal voltage referred to the DC base becomes:

$$E_{r(pu)_{DC}} = E_{r(pu)_{AC}} \frac{V_{b\ AC}}{V_{b\ DC}} \tag{3.16}$$

The commutation reactance, given on an AC base, also has to be modified before it can be used in the DC equation, viz:

$$X_{c(pu)_{DC}} = X_{c(pu)_{AC}} \left(\frac{V_{b\ AC}}{V_{b\ DC}}\right)^2 \tag{3.17}$$

Hence equation 3.10, in terms of per unit quantities becomes:

$$V_{d(pu)_{DC}} = \frac{3\sqrt{2}}{\pi} aE_{r(pu)_{DC}} \cos\alpha - \frac{3}{\pi} X_{c(pu)_{DC}} I_{d(pu)_{DC}} \tag{3.18}$$

3.1.5 Sequential Algorithm Formulation

As discussed in Chapter 2, the TS programme used for this work sequentially solves the network and generators. A vector of injected currents $[\bar{I}]$, which account for the generator's behaviour, is used to obtain a new estimate of the vector of nodal voltages $[\bar{V}]$ by solving

$$[\bar{V}]_{i+1} = [\bar{Y}]^{-1} [\bar{I}_{inj}]_i \qquad (3.19)$$

at the ith iteration.

The rectifier model is included in a similar way. From an initial loadflow a nominal bus shunt admittance $\bar{Y}_o$ can be calculated for the rectifier from:

$$G_o = P_o / |\bar{E}_r|^2 \qquad (3.20)$$

$$B_o = - Q_o / |\bar{E}_r|^2 \qquad (3.21)$$

where E_r is the nominal AC bus voltage obtained from the initial loadflow solution and:

$$\begin{aligned} \bar{S}_o &= P_o + j\, Q_o \\ \bar{Y}_o &= G_o + j\, B_o \end{aligned} \qquad (3.22)$$

$\bar{Y}_o$ is included directly into the network admittance matrix $[\bar{Y}]$. The rectifier is solved at each iteration of the TS run and any departure from the impedance characteristic is accounted for by calculating an injected current using:

$$\bar{I}_{r_{inj}} = (\bar{Y}_o - \bar{Y})\, \bar{E}_{r_i} \qquad (3.23)$$

where $$\bar{Y} = \frac{\bar{S}^*}{|\bar{E}_{r_i}|^2} \qquad (3.24)$$

and $\bar{E}_r$ is the terminal voltage at the rectifier obtained from the previous iteration. $\bar{I}_r$ can then be included in the current vector of equation 3.19 which, after solution, produces a new value for $\bar{E}_r$ and therefore a new rectifier state. The process is iterated to convergence as the dynamic equipment and rectifier settle to a solution. The algorithm is illustrated in the flow chart of Fig. 3.7.

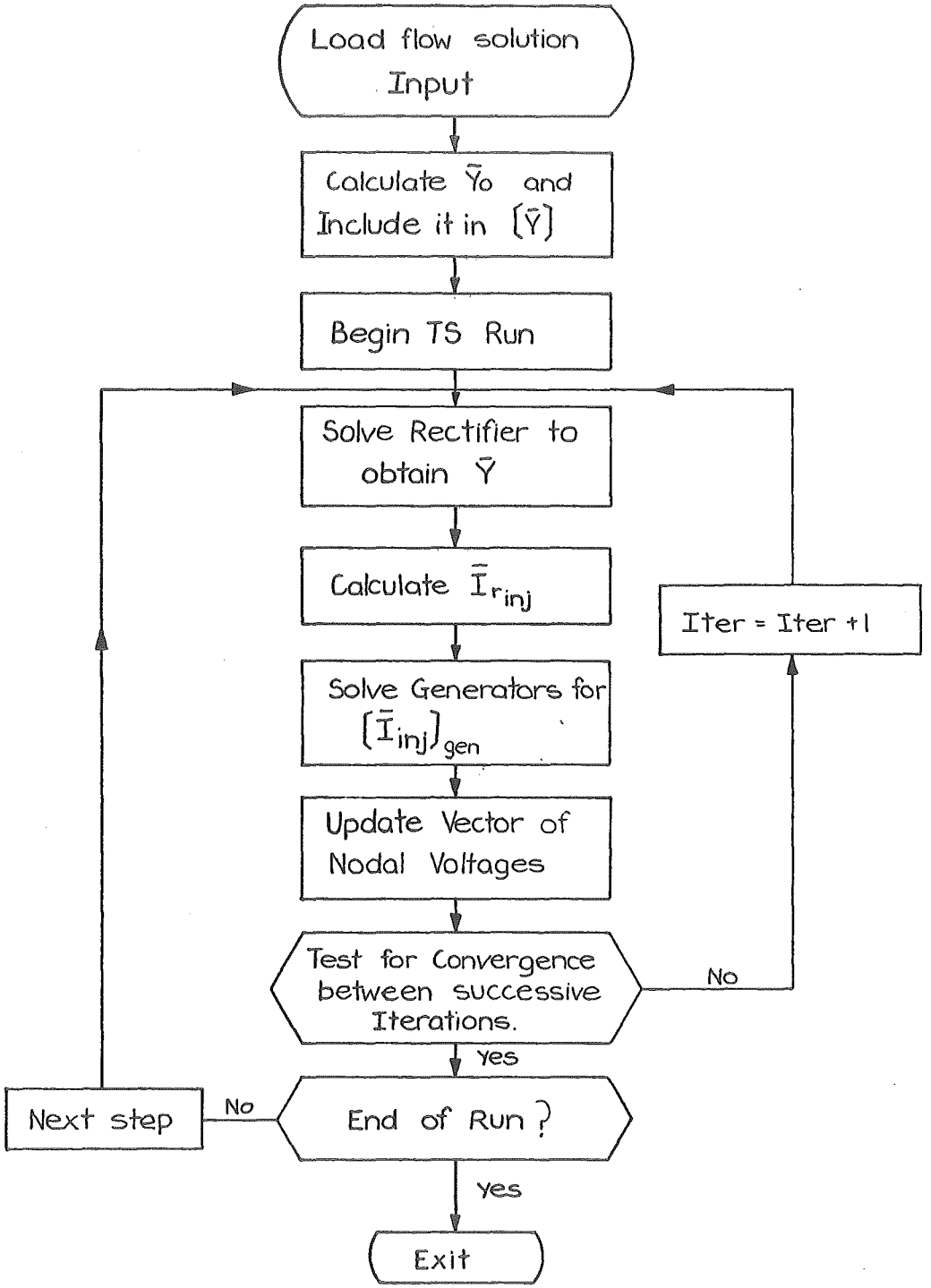

Fig. 3.7 Rectifier Load Sequential Algorithm Flow Diagram.

3.1.5.1 Rectifier solution - With a given AC terminal voltage and specified control regime, a simple rectifier can be solved directly without iteration. Constant current control is normally used for smelting applications and, provided the delay angle is within its specified control range, the DC current can be calculated from Fig. 3.8 by:

$$I_d = I_{d_{set}} - V_d/A \tag{3.25}$$

where A is the constant current controller gain.

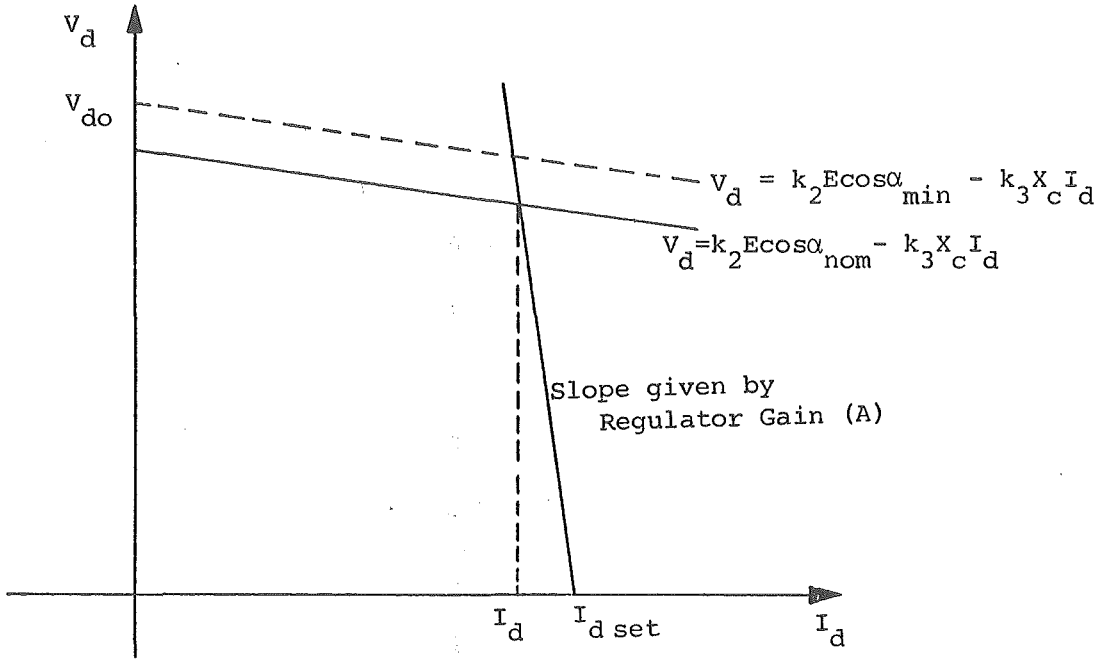

Fig. 3.8 Simple Rectifier Control Characteristic.

Substituting for V_d with equation 3.15, I_d can be solved for directly using:

$$I_d = (AI_{d\,set} - V_{cell})/(A + R_d) \tag{3.26}$$

With this given current the delay angle can be obtained using equation 3.10. If the delay angle is within the limits of its permissible operating range, the AC power factor can be obtained and the power flow evaluated, i.e.:

$$S = V_d I_d + j\,(V_d I_d \tan\phi) \tag{3.27}$$

If α lies outside the range of the controller limits the control changes to constant α mode. Using equations 3.10 and 3.15 I_d can be calculated by:

$$I_d = (\frac{3\sqrt{2}}{\pi} aE_r \cos\alpha_{limit} - V_{cell})/(R_d + 3X_c/\pi) \quad (3.28)$$

where $\alpha_{limit} = \alpha_{min}$ or α_{max}

Protection limits and disturbance severity determine the rectifier operating characteristic during a disturbance. Shutdown occurs if I_d reaches a specified minimum, (or zero), and the existence of cell counter voltage will cause shutdown before the AC terminal voltage reaches zero.

3.2 DYNAMIC DC LOAD REPRESENTATION

The basic rectifier model outlined in section 3.1 assumes that both α and I_d can change instantaneously as determined by the behaviour of the AC terminal voltage. This may be valid for some rectifier loads but data for the NZ smelter (Fuji Electric 1972) indicates that:

i) The controller time constant is of the same order as the integration step length of the TS programme (10 msec).

ii) The DC load time constant is much larger and is 113 msec.

Because of the very small controller time constant it is not necessary to model control dynamics. For a severe disturbance the rectifier is subject to a large drop in voltage which forces the control angle to its minimum quickly (via the proportional control loop). During the fault period, α will remain on its minimum value if the rectifier continues to operate and will also remain there during the post fault period as the voltage recovers. Because of the rapidly changing behaviour of the network during a TS study the fine delay angle control will be unable to exert any significant control over the DC load current and hence the controller response does not require detailed representation.

However the time constant of the DC load is of the same order as the fault period itself and will modify the performance of the rectifier considerably. In order to realistically examine the effects which rectifiers have on transient stability the time constant must be taken into account.

3.2.1 Implicit Integration for Dynamic DC Loads

As soon as α reaches its limit the dynamic response of the DC current is described by:

$$V_d = I_d R_d + V_{cell} + L \dot{I}_d \tag{3.29}$$

where L is the equivalent inductance of the DC load. Substituting for V_d using equation 3.10, 3.29 can be written in the form:

$$\dot{I}_d = f(t) + C \tag{3.30}$$

i.e. $$\dot{I}_d(t) = AE_r(t)\cos\alpha(t) - B\, I_d(t) + C \tag{3.31}$$

where $$A = \frac{1}{\tau R_d} \frac{3\sqrt{2}}{\pi} a \tag{3.32}$$

$$B = \frac{1}{\tau}\left(\frac{3X_c}{\pi R_d} + 1\right) \tag{3.33}$$

$$C = V_{cell}/\tau R_d \tag{3.34}$$

and τ = DC Load Time Constant.

By using the trapezoidal integration method, for any time function $x(t)$,

$$x(t + h) = x(t) + \frac{h}{2}(\dot{x}(t) + \dot{x}(t + h)) \tag{3.35}$$

where h is the integration step.

Applying equation 3.35 to 3.31 produces an algebraic form of equation 3.29 which can be implemented directly with the TS programme, i.e.:

$$I_d(t+h) = K_a E_r(t+h)\ \cos\alpha(t+h) + K_b \qquad (3.36)$$

$$\text{where}\quad K_a = h/(2 + Bh) \qquad (3.37)$$

$$K_b = (1 - 2BK_a) I_d(t) + AK_a E_r(t)\ \cos\alpha(t) + 2K_a C \qquad (3.38)$$

The constants K_a and K_b can be evaluated at the beginning of each step, using the results of the previous step. The current values of E_r and $\cos\alpha$ provide a new estimate for I_d at time $t+h$. Since α is normally on its limit and therefore constant, it is not required explicitly in equation 3.36 and can be absorbed in the constant K_a.

3.2.2 Limitations of the Sequential Algorithm

The basic rectifier model of section 3.1.5 does not depart greatly from an impedance characteristic and hence the injected current required to compensate for its characteristic is not large. Figure 3.9 demonstrates the difference between the two characteristics.

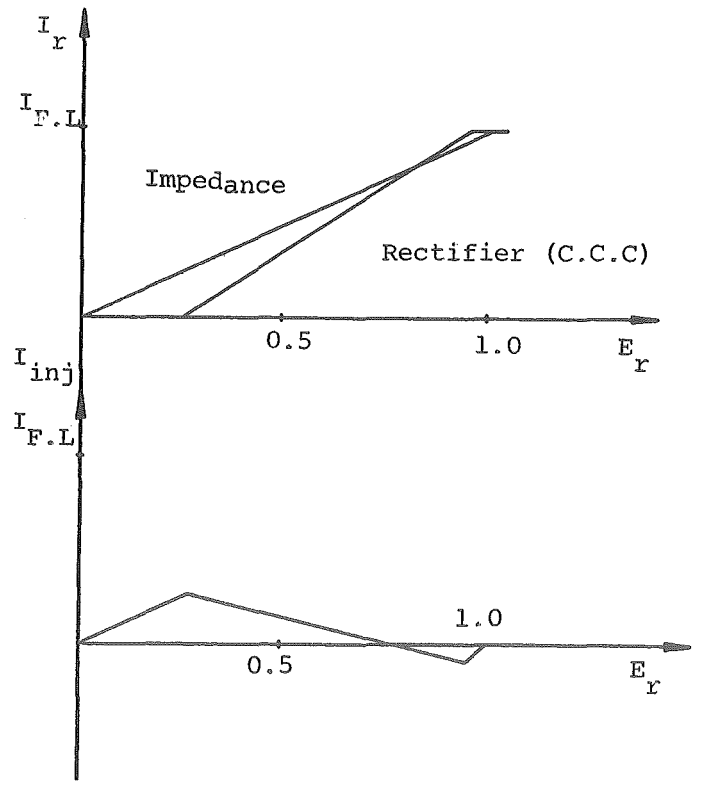

Fig. 3.9 Difference between Impedance and Simple Rectifier Characteristic (for $V_{cell} \neq 0$).

The rectifier characteristic is well behaved with the injected current tending to zero as the voltage approaches zero, as distinct from non impedance type loads, (constant current or constant power), in which the current does not drop naturally to zero at low voltage. No convergence problems were experienced with the basic rectifier model but non impedance type loads have created convergence difficulties when implemented in the sequential algorithm. (Stott 1979).

When the basic model is modified to account for the dynamic behaviour of the DC load, the injected current departs widely from that of an impedance characteristic during stages of the transient stability run. Immediately after a fault application the voltage drops to a low value but the injected current magnitude remains essentially the same due to the slow rate of change of DC load current. Similarly on fault clearance, the voltage recovers sharply but the injected current remains low.

With this characteristic the sequential solution method exhibited similar convergence problems to those experienced with non impedance loads. When the fault was applied at some distance from the rectifier terminals there was no deterioration in convergence of the AC system since the injected currents required to account for the DC load behaviour are moderate. As the fault was moved towards the rectifier and the AC voltage at the rectifier terminals during the fault decreased, the number of iterations to convergence progressively increased.

The problem appears to be due to the phase of a large injected current vector being affected by the phase variations of a small voltage vector, with successive iterations. The phase variations of the large current vector upsets the smooth convergence of the sequential algorithm.

3.2.3 Model Limitations

A second factor was observed as the fault was brought progressively closer to the rectifier. The slow response of the DC current after fault application required that normal load currents had to be commutated by a lowered AC voltage.

This led to a rapid rise in commutation angle immediately after fault application and commutation angles exceeding 60° were observed. This mode of operation is outside the valid range of the normal mode equations and to model dynamic effects it is necessary to extend the model to represent abnormal modes of operation. In addition, an improved algorithm is required to eliminate the convergence problems of the sequential algorithm.

3.3 ABNORMAL MODES OF OPERATION

3.3.1 Mode Classification

The full range of rectifier operation can be classified into four modes. (Giesner and Arrillaga 1970).

Mode 1 - Normal operation. Only two valves in the bridge are involved in simultaneous commutation at any one time. This mode extends up to a commutation angle (u) of 60°.

Mode 2 - Enforced delay. Although a commutation angle greater than 60° is desired, the forward voltage across the incoming thyristor is negative until either the previous commutation is complete or until the firing angle exceeds 30°. In this mode u remains at 60° and α can range up to 30°.

Mode 3 - Abnormal operation. In this mode periods of 3 phase short circuit and DC short circuit exist when two commutations overlap. During the period there is a controlled safe short circuit which is cleared when one of the commutations is complete. During the short circuit period 4 valves are conducting.

Mode 4 - Continuous three phase and DC short circuit caused by two commutations taking place continuously. In this mode the commutation angle is 120° and the AC and DC current paths are independent.

Table 3.1 summarises the conditions for the different modes of operation.

TABLE 3.1 RECTIFIER MODES OF OPERATION

Mode	Firing Angle α	Overlap Angle u
1	$0° \leqslant \alpha \leqslant 90°$	$0° \leqslant u \leqslant 60°$
2	$0° \leqslant \alpha \leqslant 30°$	$60°$
3	$30° \leqslant \alpha \leqslant 90°$	$60° \leqslant u < 120°$
4	$30° \leqslant \alpha \leqslant 90°$	$120°$

3.3.2 Equations for Abnormal Operation

Equations 3.8 and 3.9 do not apply for a converter operating in mode 3. These two equations are modified for abnormal operation and become: (Kimbark 1971).

$$V_d = \frac{3\sqrt{3}}{\sqrt{2}\pi} aE_r(\cos\alpha' + \cos\delta') \tag{3.39}$$

$$I_d = \frac{aE_r}{\sqrt{6}X_c}(\cos\alpha' - \cos\delta') \tag{3.40}$$

where $\alpha' = \alpha - 30°$ (3.41)

$\delta' = \delta + 30°$ (3.42)

An equivalent form of equation 3.10 can also be derived, i.e.:

$$V_d = \frac{3\sqrt{6}}{\pi} a\, E_r \cos\alpha' - \frac{9X_c}{\pi} I_d \tag{3.43}$$

In mode 2 both normal and abnormal equations are valid. In mode 4, $V_d = 0$ and I_d depends on the natural response of the DC network under short circuit.

Equation 3.11 is only valid for modes 1 and 2 and its use cannot be extended into mode 3. As an initial investigation the waveforms of mode 3, for a range of α and u, were subjected to Fourier analysis (computationally) to determine how good the approximation of equation 3.12 was. The results are illustrated in Fig. 3.10 and, for $\alpha = 30°$,

show errors up to 10% with a commutation angle of 120°.

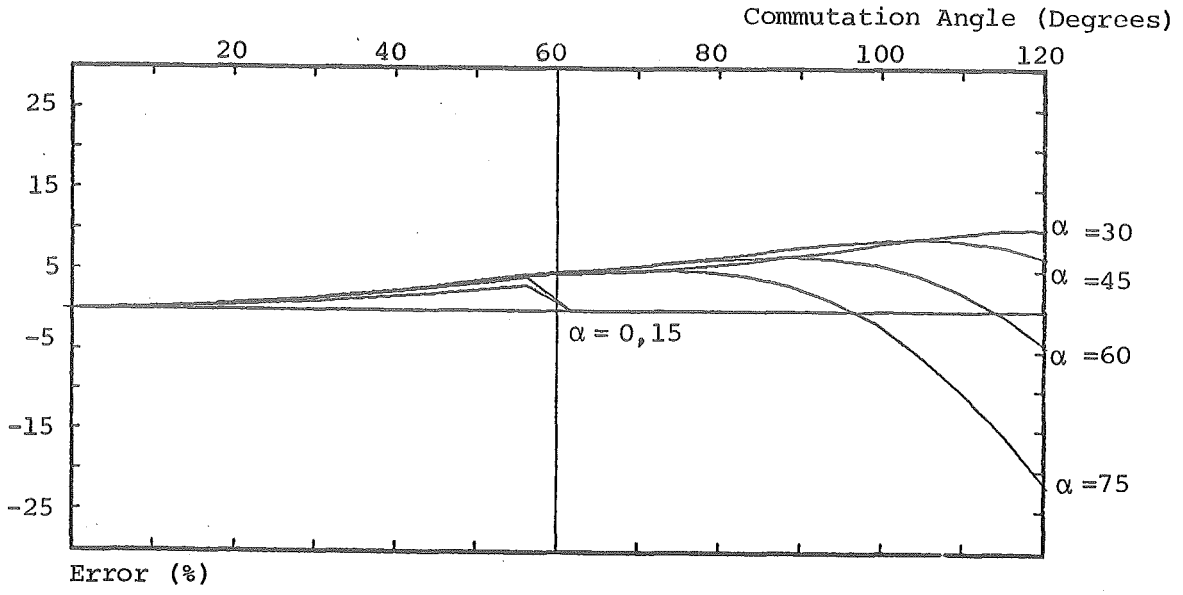

Fig. 3.10 Error in Approximation $I_r = \frac{\sqrt{6}}{\pi} I_d$.

A new expression, equivalent to equation 3.11, was derived using an analytical approach, (appendix A1), and the expression for K_1 in mode 3 is:

$$K_1 = \sqrt{3}\,\frac{(\angle -2\alpha' - \angle -2\delta' - j2u)}{4(\cos\alpha' - \cos\delta')} \qquad (3.44)$$

This expression gave identical results to those in figure 3.10.

Equations 3.40, 3.43 and 3.44 form the basis for extending the simple rectifier model into abnormal modes of operation.

3.4 UNIFIED ALGORITHM

To avoid the convergence difficulties of the sequential solution, an alternative algorithm was developed for the rectifier load. It combines the rectifier and network solutions into a unified process. It does not affect the sequential solution of the other components of the power system with the network.

3.4.1 Algorithm Proposal

The basis of this approach is to reduce the AC network, excluding the rectifier, to an equivalent Thevenin source

voltage and impedance as viewed from the rectifier terminals. This equivalent of the AC system, along with the rectifier, can be described by a set of non-linear simultaneous equations which can be solved by the standard Newton-Raphson algorithm described in appendix A2. The solution of the reduced system yields the fundamental AC current at the rectifier terminals which can then be superimposed on the rest of the AC network.

The network equivalent impedance is obtained by injecting 1 PU current into the network at the rectifier terminals while all other nodal injected currents are zero. With an injected current vector of this form, a solution of equation 3.19 gives the driving point and transfer impedances in the resulting voltage vector, i.e.:

$$[\bar{Z}] = [\bar{V}'] = [\bar{Y}]^{-1} [\bar{I}_{inj}] \qquad (3.45)$$

where

$$[\bar{I}_{inj}] = \begin{bmatrix} 0 \\ \vdots \\ 0 \\ \bar{I}'_r \\ 0 \\ \vdots \\ 0 \end{bmatrix} \quad \text{and} \quad \bar{I}'_r = 1 + jo \qquad (3.46)$$

The equivalent circuit illustrated in Fig. 3.11 is now solved to find the rectifier current $(\bar{I}_r)$ by using the Newton-Raphson technique.

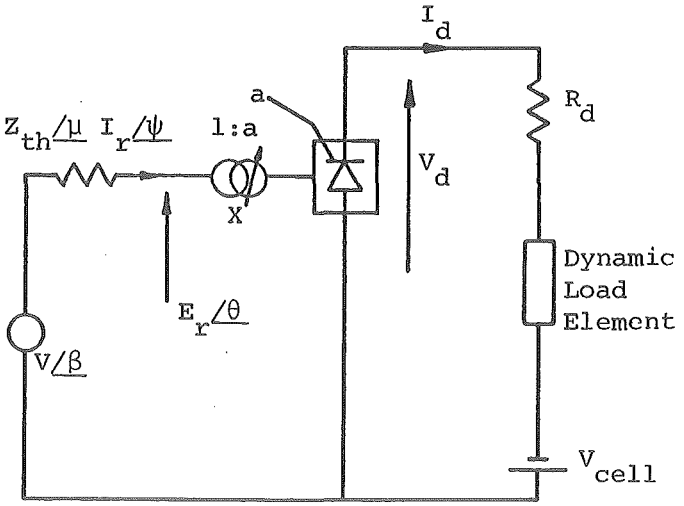

Fig. 3.11 Equivalent System for Newton-Raphson Solution.

The effect of the rectifier on the rest of the system can be determined by superposition, i.e.:

$$[\bar{V}] = [\bar{V}^o] + [\bar{Z}]\ \bar{I}_r \tag{3.47}$$

where

$$[\bar{V}^o] = [\bar{Y}]^{-1}\ [\bar{I}^o_{inj}] \tag{3.48}$$

and $[\bar{I}^o_{inj}]$ are the injected currents due to all other generation and loads in the system.

If the network remains constant, vector $[\bar{Z}]$ is also constant and only needs re-evaluation on occurrence of a discontinuity such as line switching, fault application or removal, or motor switching.

With this approach the unified algorithm can be implemented without any disturbance to the sequential method adopted for generator solution. The advantages of both methods are combined to provide good convergence for the rectifier element which departs considerably from an impedance characteristic. Although the programming required for the rectifier is more complex, it represents only a small part of the total TS programme.

3.4.2 Formulation of Equations for Normal Operation

The equivalent system of Fig. 3.11 contains 7 variables:

$$E_r,\ I_r,\ \theta,\ \psi,\ \alpha,\ V_d,\ I_d \tag{3.49}$$

With these variables 4 independent equations can be written using Kirchoffs law and the equations of section 3.1.3. These are:

$$V\underline{/\beta} - E_r\underline{/\theta} - (Z_{th}\underline{/\mu}\ ,\ I_r\underline{/\psi}\ ) = 0 \tag{3.50}$$

$$V_d - \frac{3\sqrt{2}}{\pi}\ a\ E_r \cos\alpha + \frac{3}{\pi}\ X_c\ I_d = 0 \tag{3.51}$$

$$V_d\ I_d - \sqrt{3}\ a\ E_r\ I_r \cos(\theta - \psi) = 0 \tag{3.52}$$

Equation 3.50 represents 2 equations since it is complex. Substituting for V_d and I_r using equations 3.12 and 3.15 reduces the number of variables to 5. i.e.:

$$E_r,\ \theta,\ \psi,\ \alpha,\ I_d \tag{3.53}$$

A fifth equation, representing the control specification, can be written. With constant current control, (i.e. when α is within its limits), the control specification is given as:

$$I_d - I_d^{sp} = 0 \tag{3.54}$$

Equations 3.50 through 3.52 and 3.54 represent $[F(\bar{x})] = 0$ of the Newton-Raphson process and $[\bar{x}]^T$ is given by 3.53.

When α reaches a specified lower limit (α min), the control specification given by equation 3.54 changes to:

$$\alpha - \alpha_{min} = 0 \tag{3.55}$$

and equation 3.51 is replaced by the algebraic form of the differential equation for I_d as derived in equation 3.36. i.e.:

$$I_d - k_a E_r \cos\alpha - k_b = 0 \tag{3.56}$$

Since these equations are for normal operation, the value of K_1 in equation 3.12 is close to unity. The commutation angle, u, is not explicitly included in the formulation, to keep the dimension of the Jacobian to a minimum. K_1 is evaluated at the end of each iteration, after claculation of u, and this value is used for the next iteration. Since the variation of K_1 is small in the normal mode, its evaluation in this manner does not affect the convergence of the Newton-Raphson algorithm.

3.4.3 Formulation of Equations for Abnormal Operation

In mode 3 the errors involved in equation 3.12 are more significant. For this reason the number of variables used in the problem formulation is increased to include the commutation angle explicitly. A linearised form of equation 3.44 is obtained for $\alpha = 30°$, from Fig. 3.10, to simplify the expression. In the range of $120 > u > 60$ the value of K_1 can be obtained from:

$$f_1(u) = 1.01 - 0.0573u \qquad (3.57)$$

where u is in radians.

In addition the equation for commutation is included and $[F(\bar{x})] = 0$ becomes:

$$V\angle\beta - E_r\angle\theta - Z\angle\mu \left(\frac{\sqrt{6}}{\pi} f_1(u)\ I_d\right)\angle\psi = 0 \qquad (3.58)$$

$$\frac{\sqrt{2}}{\pi} a E_r \cos(\theta - \psi)\ f_1(u) - \frac{\sqrt{6}}{\pi} a E_r \cos\alpha' + \frac{3X_c}{\pi} I_d = 0 \qquad (3.59)$$

$$I_d - k'_a a E_r \cos\alpha' - k'_b = 0 \qquad (3.60)$$

$$\cos(\alpha + u + 30) - \cos\alpha' + \sqrt{6}\, X_c I_d / a E_r = 0 \qquad (3.61)$$

$$\alpha - \alpha_{min} = 0 \qquad (3.62)$$

In mode 4 the AC and DC systems are both short circuited at the converter and operate independently. In this case the system equivalent of Fig. 3.11 is reduced to that of Fig. 3.12.

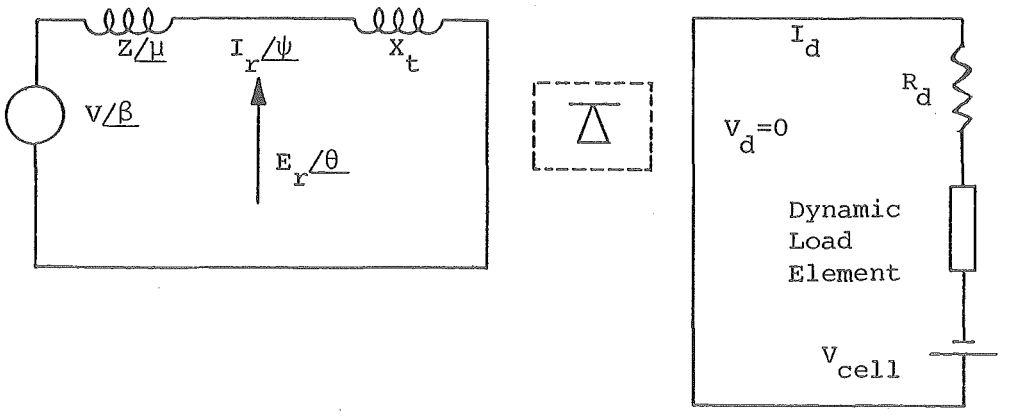

Fig. 3.12 Rectifier Load Equivalent in Mode 4 Operation.

3.4.3 Formulation of Equations for Abnormal Operation

In mode 3 the errors involved in equation 3.12 are more significant. For this reason the number of variables used in the problem formulation is increased to include the commutation angle explicitly. A linearised form of equation 3.44 is obtained for $\alpha = 30°$, from Fig. 3.10, to simplify the expression. In the range of $120 > u > 60$ the value of K_1 can be obtained from:

$$f_1(u) = 1.01 - 0.0573u \qquad (3.57)$$

where u is in radians.

In addition the equation for commutation is included and $[F(\bar{x})] = 0$ becomes:

$$V\angle\beta - E_r\angle\theta - Z\angle\mu \left(\frac{\sqrt{6}}{\pi} f_1(u)\ I_d\right)\angle\psi = 0 \qquad (3.58)$$

$$\frac{\sqrt{2}}{\pi} a E_r \cos(\theta - \psi)\ f_1(u) - \frac{\sqrt{6}}{\pi} a E_r \cos\alpha' + \frac{3X_c}{\pi} I_d = 0 \qquad (3.59)$$

$$I_d - k'_a a E_r \cos\alpha' - k'_b = 0 \qquad (3.60)$$

$$\cos(\alpha + u + 30) - \cos\alpha' + \sqrt{6}\, X_c I_d / a E_r = 0 \qquad (3.61)$$

$$\alpha - \alpha_{min} = 0 \qquad (3.62)$$

In mode 4 the AC and DC systems are both short circuited at the converter and operate independently. In this case the system equivalent of Fig. 3.11 is reduced to that of Fig. 3.12.

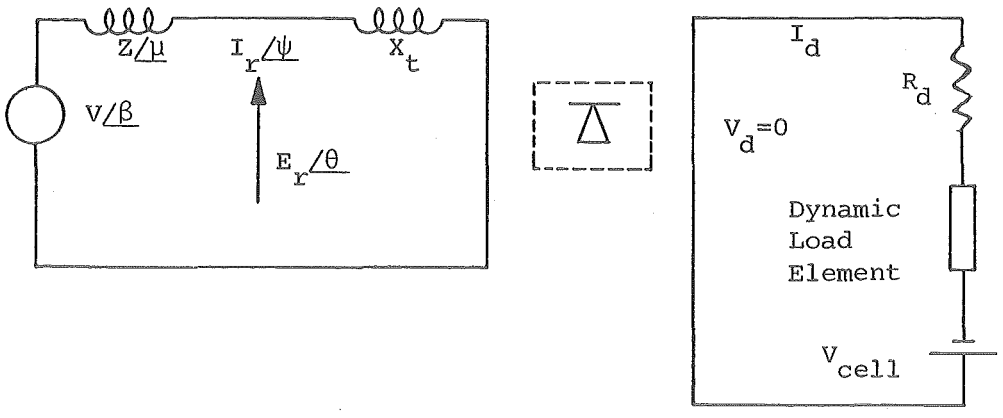

Fig. 3.12 Rectifier Load Equivalent in Mode 4 Operation.

The network equivalent can be solved directly and the DC current is obtained from the algebraic form of the differential equation (i.e. equation 3.60).

3.4.4 Programme Implementation

The unified algorithm is more complex to implement than the sequential algorithm. A flow diagram of the algorithm is illustrated in Fig. 3.13.

Particular attention has to be paid to obtaining good starting values for the Newton-Raphson algorithm and to ensuring that the correct mode is chosen.

3.4.4.1 Calculation of initial conditions - The success and rapid convergence of the Newton-Raphson algorithm partly depends on obtaining good starting values for the variables of the problem. Since the initial Jacobian represents an initial estimate of the slopes of the tangent hyperplanes which approximate the functions being solved (Stott 1974), an error in initial estimates may mean that these slopes are incorrect. The algorithm may therefore begin to seek a solution in the wrong direction and this may lead to divergence or convergence to an incorrect answer. A common case observed in converter modelling is to converge to a solution for which the converter is a source of reactive power instead of a sink.

Loadflow results are used at the start of a TS run and during the normal running of the study, the values from the previous step are used as initial conditions for the next step. With step lengths ranging from 10 to 25 msec, the Newton-Raphson algorithm obtained convergence in 2 or 3 iterations.

Discontinutities during the study require a special calculation of the initial conditions as the network change can be large. A new network equivalent impedance and voltage is obtained immediately after a discontinuity and, since I_d does not change instantaneously, an estimate of E_r can be made using equation 3.12 and:

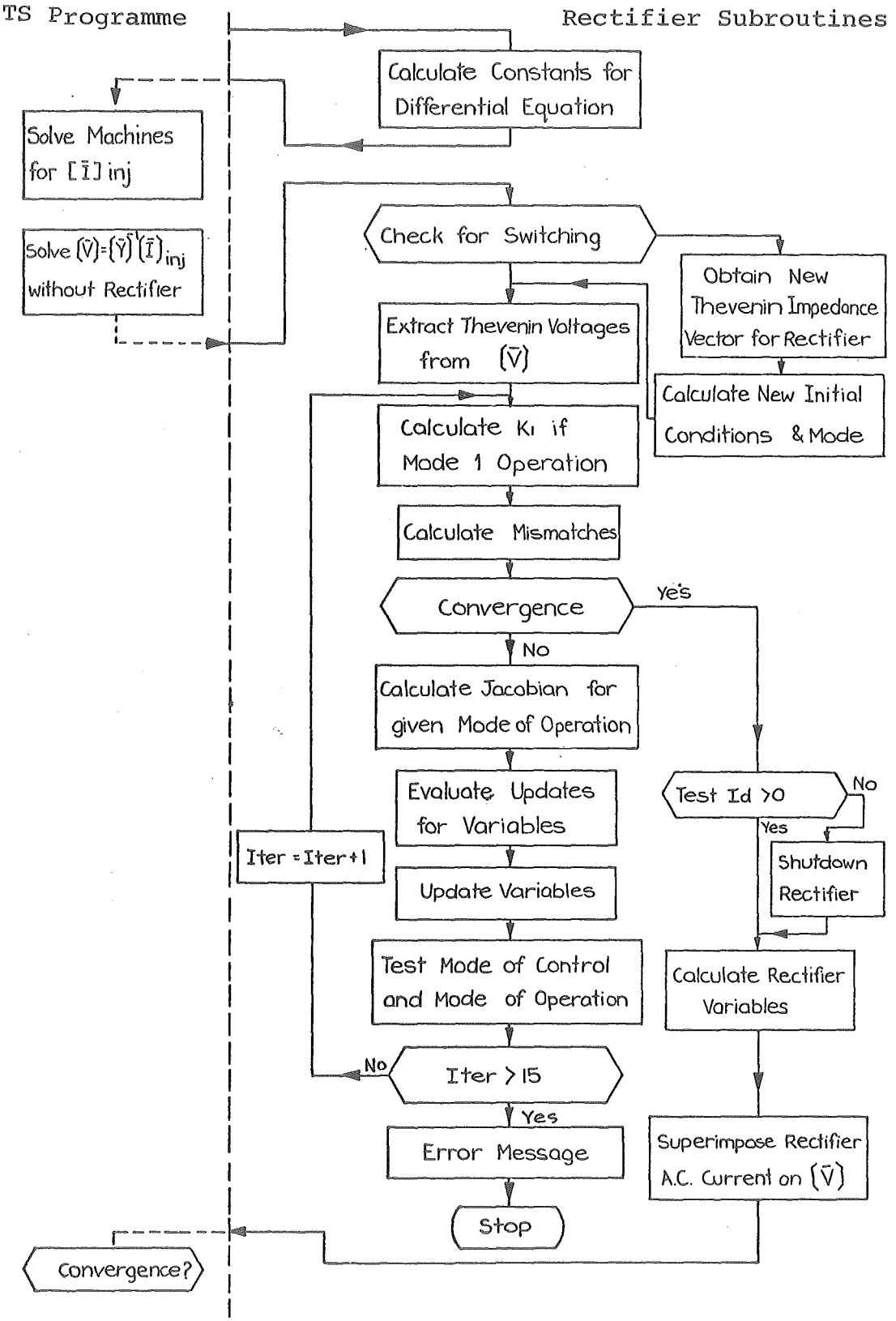

Fig. 3.13 Unified Algorithm Flow Diagram.

$$E_r = V - I_r Z_{th} \qquad (3.63)$$

Power factor is obtained using the converter equations of section 3.1.3, Θ is set to β and ψ is calculated using:

$$\phi = \Theta - \psi \qquad (3.64)$$

The initial conditions so obtained give convergence in 2 to 5 iterations for the first overall iteration of the whole system and only 1 or 2 iterations on successive system iterations. Reconvergence of the AC system is unaltered by the rectifier.

3.4.4.2 Choice of operating mode - Choice of operating mode after a discontinuity is just as important as good initial conditions. The incorrect choice can lead to an attempt to solve the wrong set of equations for the prevailing conditions. This may lead to failure of the algorithm and study termination. Mode choice is made using a factor K_m (Giesner and Arrillaga 1970) where:

$$K_m = \frac{\sqrt{2} X_c I_d}{a E_r} \qquad (3.65)$$

The range of K_m for each mode is as follows:

Mode 1 $\quad K_m < \cos(60° - \alpha)$

Mode 2 $\quad \cos 60° - \alpha < K_m < 0.8660$

Mode 3 $\quad 0.8660 < K_m < 1.1547$

Mode 4 $\quad 1.1547 < K_m$

Immediately after a discontinuity, the choice of mode is influenced by the estimate made for E_r. If the value of K_m indicates mode 4, iterations are made in mode 3, to check that the commutation angle will in fact reach 120°. This test is repeated at the beginning of each time step so that reversion to mode 3 can be determined correctly.

In modes 1, 2 and 3 K_m is evaluated at the end of each iteration of the Newton-Raphson process to determine when a mode change will take place. Because of the continuity of the normal and abnormal equations across their respective mode boundaries, no sudden steps are observed in the variables and mode changing during a solution does not upset convergence of the algorithm. In mode 2, the normal equations are used and mode 2 is implemented by a change in the control specification.

3.4.4.3 Control specification - A particular advantage of the Newton-Raphson formulation is the flexibility it affords to the setting of control specifications. The normal specifications are either constant current or constant delay angle. During the transition through mode 2, the commutation angle is fixed at 60° and the enforced delay is calculated. This can be easily accomplished by replacing equation 3.55 by:

$$\cos^{-1}\left[\cos\alpha - \frac{\sqrt{2}X_c I_d}{a E_r}\right] - \alpha - u^{sp} = 0 \qquad (3.66)$$

where $u^{sp} = 60°$.

Equation 3.56, (or 3.60), also becomes a control specification when reconverging after a discontinuity. This equation reduces to:

$$I_d - k_b = 0 \qquad (3.67)$$

for zero step length, holding I_d at its previous value.

3.5 COMPARISON OF SEQUENTIAL AND UNIFIED ALGORITHMS

The network illustrated in Fig. 3.1 was used as a test system to examine the convergence properties of the sequential and unified algorithms. The disturbance applied to the network was a three phase line fault located at various points of the system. Line switching and fault clearance occurred 140 msec later, this being the primary

fault clearing time for the system. For longer studies auto-reclosure of lines took place 360 msec after line opening. In all studies the rectifier steady state load was constant at 288 MW and 105 MVAR and generators were modelled to include transient and subtransient effects and automatic voltage regulators and governors were included. All other loads were of the impedance type.

The most difficult computational problem occurred when reconverging after a discontinuity. Once reconvergence had been achieved, and the first integration step following this had been successfuly solved, the solution was numerically well behaved.

Table 3.2 presents a comparison of the convergence properties of the two algorithms.

In cases 1, 2 and 4 the number of iterations required to reconverge after three different discontinuities during each study was used as the basis for comparison. Cases 1, 3 and 4 were more severe faults than case 2 when observed from the rectifier terminals.

In case 1, the unified algorithm showed a slight advantage when reconverging following a discontinuity. However the number of iterations required during the integration procedure was almost identical. The slight increase in the time step iterations using the unified method was due to a tighter tolerance being set for the convergence of the rectifier variables of the Newton-Raphson process in all studies.

TABLE 3.2 COMPARISON OF SEQUENTIAL AND UNIFIED ALGORITHMS

Case	Fault Position	Rectifier Model	Algorithm	Iterations to Reconverge			Total Iterations for 1 Second Study
				Fault On	Fault Off	Auto Reclose	
1	Manapouri	Basic	Sequential	5	5	4	324
			Unified	2	4	3	332
2	Roxburgh	Dynamic	Sequential	27	6	6	346
			Unified	3	5	3	364
3	Manpouri fault X=0.0060	Dynamic	Sequential	Failed	-	-	-
			Unified	3	3	3	302
4	Manapouri fault X=0.0065	Dynamic	Sequential	8	Failed at first Time Step after Fault Application		
			Unified	3	3	3	298

Considering case 2, it can be seen that the rate of reconvergence after a discontinuity, using the sequential method, was slow. This was so, even though the rectifier model operated in mode 1 throughout the study with a maximum commutation angle of 35°. However once reconvergence was achieved the number of time step iterations compared favourably with the unified method.

The unified algorithm was clearly superior in case 3 as divergence occurred when the sequential method was used. Case 4 demonstrated that convergence problems also occur, using the sequential method, during the time step iterations, but these difficult cases do not cause problems to the unified method. The unified method consistently gave reconvergence after a discontinuity within 5 iterations and the number of time step iterations was also small provided the step length was suitable for the system as a whole. A fixed step length of 0.01 sec was used for all the cases in Table 3.2.

3.6 RESULTS

Three rectifier models were used to examine the differences in maximum swing angle when each is used for TS analysis. The standard approach to constant loads is to model them as an impedance and this method has been used in NZ in the past. The model developed in this work is used to assess the validity of the impedance model and the effect of modelling the dynamic DC load is also examined in comparison to the basic rectifier model.

3.6.1 System Studied

The two systems of Fig. 3.14 were used for TS analysis.

These are subsystems from Fig. 3.1 with high and low short circuit ratios at the smelter terminals. The Roxburgh

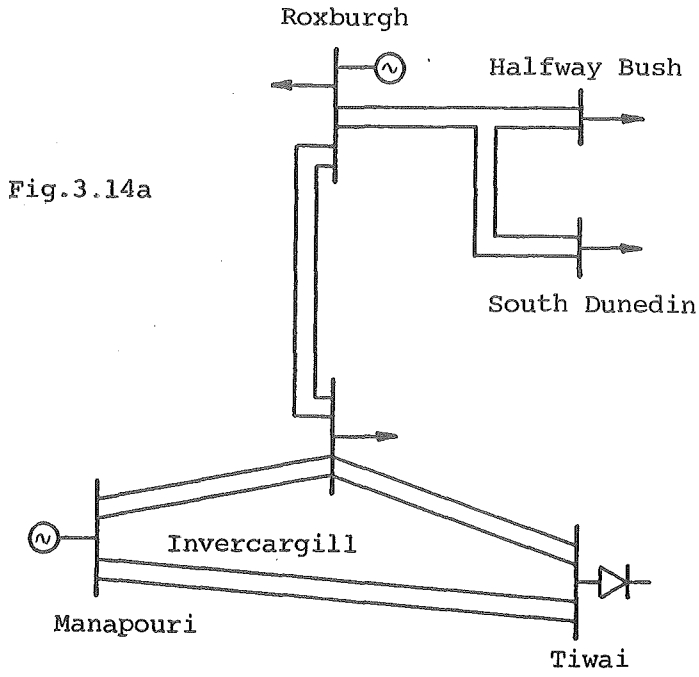

Fig.3.14a

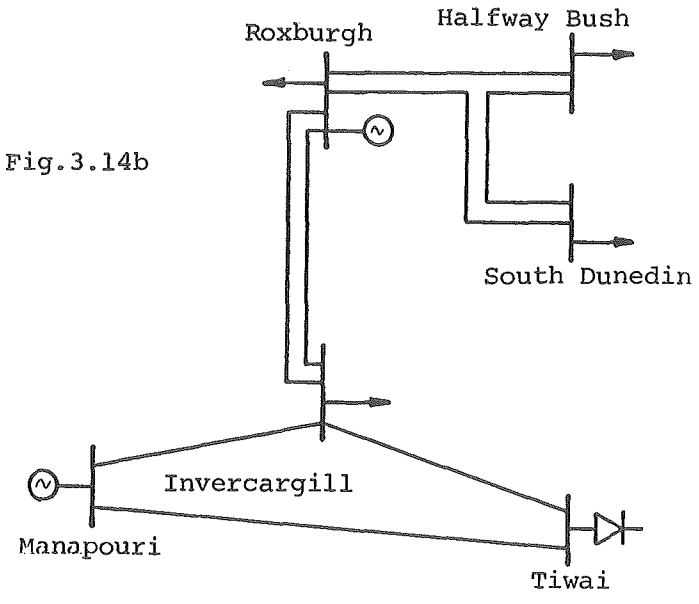

Fig.3.14b

Fig. 3.14 Sub-Systems Used for Results in Table 3.2.

generator was used as the swing machine with the majority of system generation coming from the Manapouri generator. This ensures that the swing of the Manapouri machine is sufficient to observe the differences between the various models and the case studied.

The disturbance applied to the network was a three phase line fault. For certain studies a small fault reactance was included to support the system voltage during the fault. This permitted specific rectifier behaviour to be observed.

The studies were continued only long enough to record first swing stability and the results are presented in Table 3.3.

3.6.2 Discussion of Results

With the stronger system, Fig. 3.14a, the difference between the rectifier models is small. The rectifier is seen to have much more influence when the system is weaker, (Fig. 3.14b). This is clearly shown by the results of corresponding cases, like A2 and B2 where the differences between the impedance and dynamic models are 2% and 14.8% respectively.

A comparison between cases B1 and B2 illustrates the importance of accurate rectifier representation. As the fault sets closer, the rectifier is forced into increasingly nonlinear operating modes.

Fig. 3.15 illustrates the differences in power and voltage behaviour for case B3, under the three alternative rectifier models.

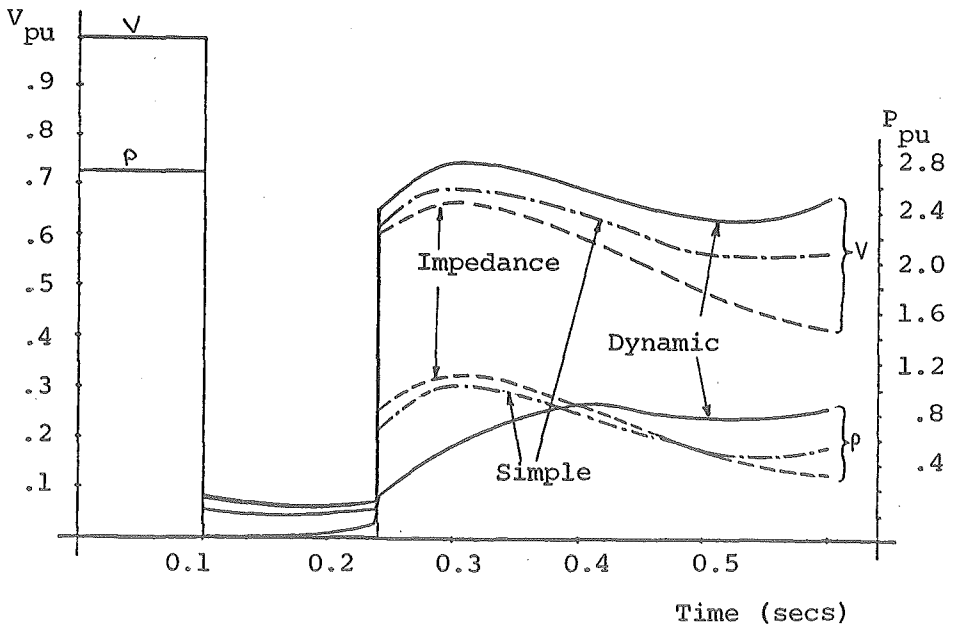

Fig. 3.15 Voltage and Power at Rectifier Bus for Case B3.

TABLE 3.3 EFFECTS OF RECIFIER MODELS ON TRANSIENT STABILITY

Network	Case	Manapouri Generation (MW)	Impedance Load (MW)	Fault Position	First Swing Maximum - Manapouri			Difference between Impedance and Dynamic Model
					Impedance Model	Basic Model	Dynamic Model	
A	1	450	260	Manapouri	40.6°	38.9° (1)	40.3° (4)	0.7%
	2	450	260	Invercargill	25.1°	25.0° (1)	24.6° (3)	2.0%
	3	570	340	Manapouri	75.2°	73.1° (1)	73.2° (4)	2.7%
	4	570	340	Invercargill	53.4°	53.0° (1)	57.4° (3)	3.7%
B	1	450	260	Manapouri	66.0°	60.1° (2)	62.6° (4)	5.1%
	2	450	260	Invercargill	37.2°	36.4° (1)	31.7° (4)	14.8
	3	570	340	Invercargill	92.0°	82.0° (1)	72.0° (3)	21.7%
	4	570	340	Invercargill (5)	Unstable	98.0° (1)	84.0° (3)	-

(1) Rectifier Shutdown during fault
(2) No Rectifier Shutdown during fault
(3) Short Circuit at Rectifier Terminals after Fault Application
(4) No Short Circuit at Rectifier Terminals after Fault Application
(5) Fault Period Increased by One Cycle

With the dynamic rectifier model the power demand during and immediately after the fault is seen to be substantially reduced and voltage recovery throughout the system is improved. Although the governor action was adequately represented, the mechanical power input for the three cases is almost constant during the period up to the first swing. Swing curves for case 3B are illustrated in Fig. 3.16.

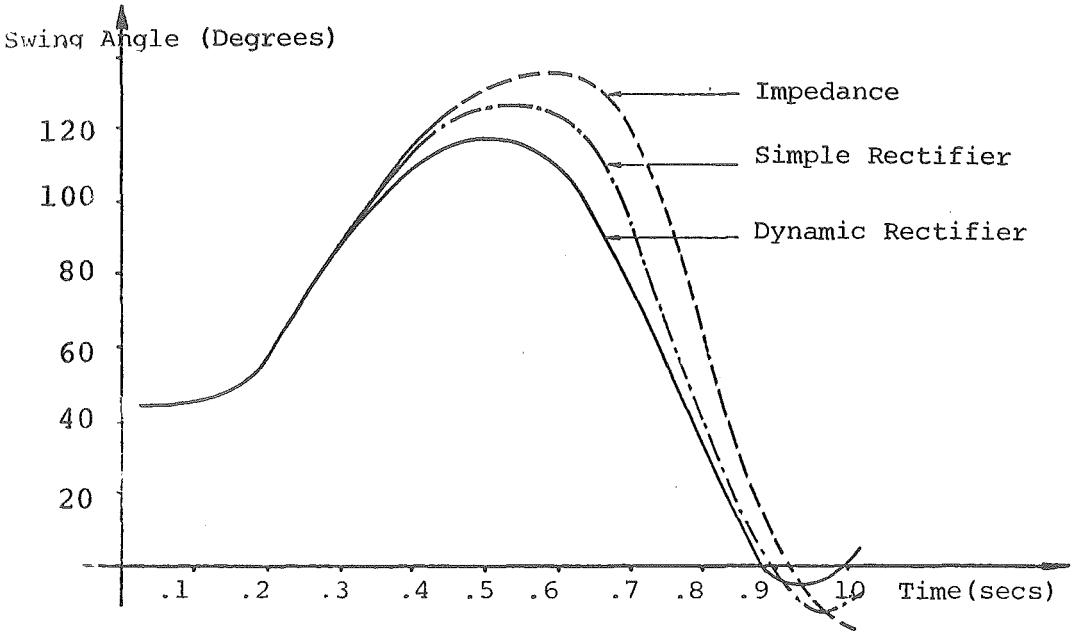

Fig. 3.16 Swing Curves for Case B3 of Table 3.3.

In case B4, fault clearance was delayed by one cycle and the impedance representation led to instability, while under the basic and dynamic rectifier models, marginal stability was observed.

The topology of the system, proximity of the fault to the rectifier and the rectifier protection limits are also factors in determining the extent of the rectifier effect on transient stability. If the fault is distant from the rectifier in a system with high short circuit capacity, then the impedance type representation gives somewhat conservative results. For systems with low short circuit capacities however, the results with the impedance type representation are too conservative to be practical and full rectifier representation is essential.

3.6.3 Rectifier Performance

Rectifier behaviour during the fault is influenced by the proximity of the fault, the system short circuit capacity and the DC load time constant. For close faults in weak systems with dynamic DC loads, the rectifier is forced into mode 4 operation. As the DC current decays, the operation changes to modes 3, 2 and then 1. Figure 3.17 shows the rectifier operation in all 4 modes for case B3.

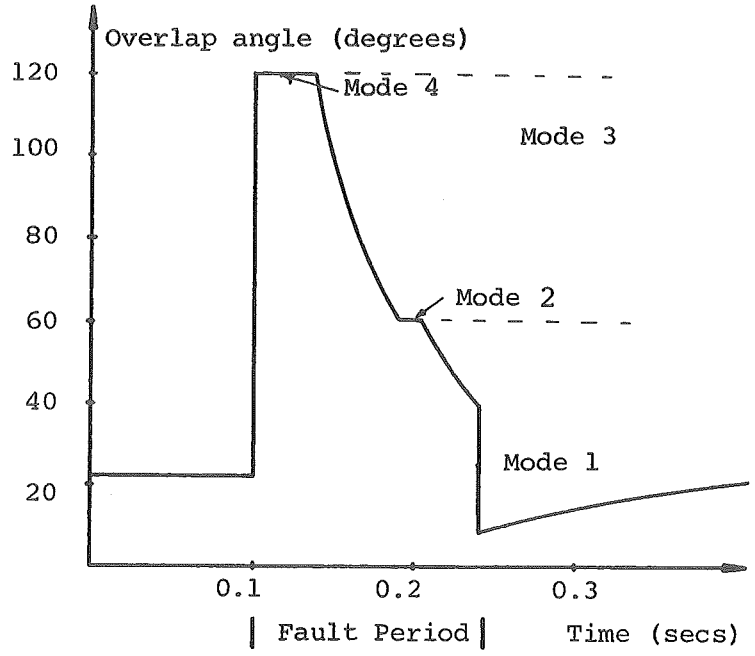

Fig. 3.17 Rectifier Overlap Angle vs. Time for Case B3.

For very short DC load time constants, the period in which the rectifier will be in abnormal modes will be small and an impedance or simple rectifier model will provide sufficiently accurate representation.

During the fault the rectifier will be operating at a very low power factor due to the abnormally large commutation angle. The rate of change of power factor is determined by the DC load time constant. As soon as the fault clears, the sudden increase in AC terminal voltage results in a very small commutation angle and the power factor is close to unity. As an example of the rectifier behaviour, Table 3.4 shows the ratio of MW/MVAR during the various stages of the study in case B3.

TABLE 3.4 RATIO OF MW/MVAR OF RECTIFIER for CASE B3.

Run Time	MW/MVAR	P.F.
Pre Fault	3.0	0.95
During Fault	0.0 - 1.5	0.0 - 0.83
Early Post Fault	6.5 - 4.5	0.98 - 0.97
At Swing Maximum	3.9	0 .97

The reduction in MVAR demand during the post fault period helps to give rise to a greater recovery of system voltages.

3.7 CONCLUSIONS

The results obtained from the three different methods of modelling a rectifier load show clearly the need for detailed modelling of the rectifier. This is particularly important for disturbances which occur in a weak system and are relatively close to the rectifier. In the case studied, the response of the rectifier, when detailed modelling is used, is such that a second short circuit exists in the network at the rectifier terminals. For a heavily loaded and concentrated system this extra disturbance may have considerably greater effect than has been shown here. The dynamic behaviour of the DC load modified the simple model performance and required an extension into abnormal modes of operation. This extension has been justified by the variation in the results for the models.

Two algorithms for including non impedance loads have been evaluated. The sequential algorithm, though simple to implement, failed when the load characteristic departed significantly from an impedance characteristic.

The unified algorithm demonstrated its convergence superiority throughout all the studies performed. Although the specific load model used with the algorithm was a rectifier, the two methods used are equally applicable to other non impedance types of load.

CHAPTER 4

DERIVATION OF TRANSIENT STABILITY COMPATIBLE EQUIVALENTS FROM TRANSIENT CONVERTER SIMULATION WAVEFORMS

4.0 INTRODUCTION

As discussed in section 3.0, accurate load models are an essential part in the realistic assessment of transient stability. Special attention has been paid to the modelling of high voltage direct current (HVDC) links, (Marshall et al 1974, Elamin 1975, BRAMELLER 1979). To date, because of its very fast controls, HVDC modelling has assumed a quasi-steady state, (QSS), form; i.e. using equations which describe the link behaviour in the steady state. However the highly non-linear behaviour of HVDC systems can only be predicted with reasonable confidence using a QSS model under clearly defined steady state operating conditions. During disturbances there is no guarantee that normal converter operation will remain within the region of applicability of the steady state equations, or that the converters will retain controllability. Therefore in systems containing relatively large HVDC transmission schemes and with disturbances at or close by the converter terminals only a fully detailed elemental transient analysis can provide accurate simulation of the converter behaviour.

The purpose of this chapter is to investigate the characteristic differences between Transient Converter Simulation, (TCS), and Transient Stability, (TS), modelling so that the limitations of using a QSS DC link model in a TS study can be overcome. The fundamental differences between TCS and TS studies are discussed. The form of the TCS results and how they may be processed to make them compatible for use in a TS study is investigated. Approximations are also examined to make the reduction process simple and computationally inexpensive.

A brief account of the principles used in TCS is included to show clearly the fundamental differences of the two study forms. More extensive discussions of TCS may be found in Heffernan 1980 or Al-kashali 1976.

4.1 TRANSIENT CONVERTER SIMULATION CONCEPTS

When investigating a 3 phase network in which many discrete switchings take place, for example HVDC converters, a single phase lumped parameter model is not sufficiently accurate during transient conditions. Distortions in individual phases and unbalance between phases can cause large deviations in the voltage crossovers between phases. These distortions influence the discrete switching times of the converter and may result in conditions which prevent normal switchings from taking place.

The transient converter simulation referred to in this work is a general technique in which system elements are explicitly represented, on a 3 phase basis, by inductive, capacitive and resistive elements. Connections between the elements are made based on the topology of the system being modelled. The behaviour of the network is defined by branch currents and nodal voltages and is determined by two fundamental factors:

i) Algebraic constraints in which the basic electric network laws relate currents and voltages at nodes and branches.

ii) Topological constraints which represent the way in which the elements are connected, to form the system under study.

Nodal, cut set, mesh or any other equivalent alternative method may be used to obtain a solution of the network.

In the case where converters are included in a system, each switching action requires a rearrangement of the network topology. Computational efficiency can be improved by employing diakoptics to separate out the elements which undergo frequent switching so that the whole network is not involved in the topological changes. Further improvements can be made by identifying various types of nodes and grouping these nodes with the aid of incidence matrices.

4.1.1 Formulation of Equations

Four basic equations represent the network laws governing the elements of a system.

i) Kirchoffs current law.

$$I_l + I_r + I_c = 0 \qquad (4.1)$$

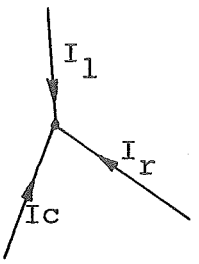

Fig. 4.1

ii) Inductive branch equation.

$$V_a + E_l - L_l\dot{I}_l - R_lI_l - V_b = 0 \qquad (4.2)$$

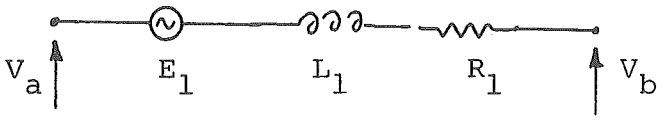

Fig. 4.2

iii) Resistive branch equation.

$$V_a + E_r - R_rI_r - V_b = 0 \qquad (4.3)$$

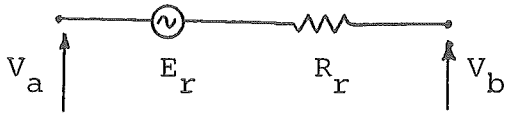

Fig. 4.3

iv) Capacitive branch equation.

$$\dot{V}_\alpha = C_\alpha^{-1} I_\alpha \qquad (4.4)$$

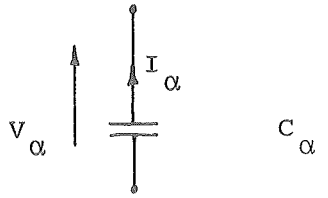

Fig. 4.4

It is convenient to segregate the system nodes according to the type of branches interconnected by them. This segregation defines α nodes (which have at least one capacitive connection), β nodes (which have at least one resistive connection but no capacitance), γ nodes (with only inductive components) and δ nodes (converter nodes, involving only inductive components, i.e. converter transformer and smoothing reactor). Thus the topological changes caused by valve switchings can be implemented by altering only the matrices involving converter (k) branches and δ nodes.

Using a state variable formulation, state variables can be defined as:

$$\psi_l = I_l L_l \tag{4.5}$$

$$\psi_k = I_k L_k \tag{4.6}$$

$$Q_\alpha = C_\alpha V_\alpha \tag{4.7}$$

When equations 4.1 to 4.4 are adapted to this state variable formulation with the above nodal representation, the following equations define the network:

$$\dot{\psi}_l = E_l - R_l I_l - K^t_{l\alpha} V_\alpha + K^t_{l\beta} V_\beta + K^t_{l\gamma} V_\gamma \tag{4.8}$$

$$\dot{\psi}_k = -R_k I_k + K^t_{k\alpha} V_\alpha + K^t_{k\beta} V_\beta + K^t_{k\delta} V_\delta \tag{4.9}$$

$$\dot{Q}_\alpha = -K_{\alpha l} I_l - K_{\alpha k} I_k - K_{\alpha r} I_r \tag{4.10}$$

where $K_{\beta l}$, etc. represent branch-node incidence matrices and suffixes l and r refer to inductive and resistive branches.

4.1.2 Solution and Results

The set of simultaneous differential equations of 4.8 to 4.10 are solved using a suitable single step numerical integration algorithm. The single step method is necessary

because of the many discontinuities resulting from converter topology changes. (Duke 1979, Al-kashali 1976). A very short step length is required for the integration algorithm for the following reasons:

i) The elemental representation of the system introduces very small time constants and, for numerical stability, an integration step length of a similar order is required.

ii) A high degree of resolution is required about switching points to determine accurate switching times.

iii) Converter topological changes introduce frequent disturbances to the network causing rapid rates of change of variables.

Integration step lengths of about 1° of fundamental frequency are normally used. (Heffernan 1980).

The output of a TCS is a sequence of samples of the system nodal voltages and branch currents, for each individual phase,spaced approximately 1° apart. Two examples of plotted sample sequences obtained by TCS are shown in Fig. 4.5 and they illustrate the detailed response characteristics which can be modelled.

Nonlinear characteristics of converter switching and fault disturbances introduce a high degree of distortion to the phase voltages and currents. Because of the short step length, frequencies up to 9 khz can be represented in the voltage and current waveforms but for power system purposes the range of interest extends only to about 1.5 khz.

Although a high degree of resolution of system behaviour is obtained from such a short step length, it introduces a major limitation. TCS is extremely expensive in terms of computation time. The simulated time of TS studies can often extend up to 10 seconds, (500 cycles), and the computational requirements are a function of the system size. TCS time for the same computational expense is limited to only a few cycles. For a typical 12 pulse DC link model representing the NZ DC transmission scheme and

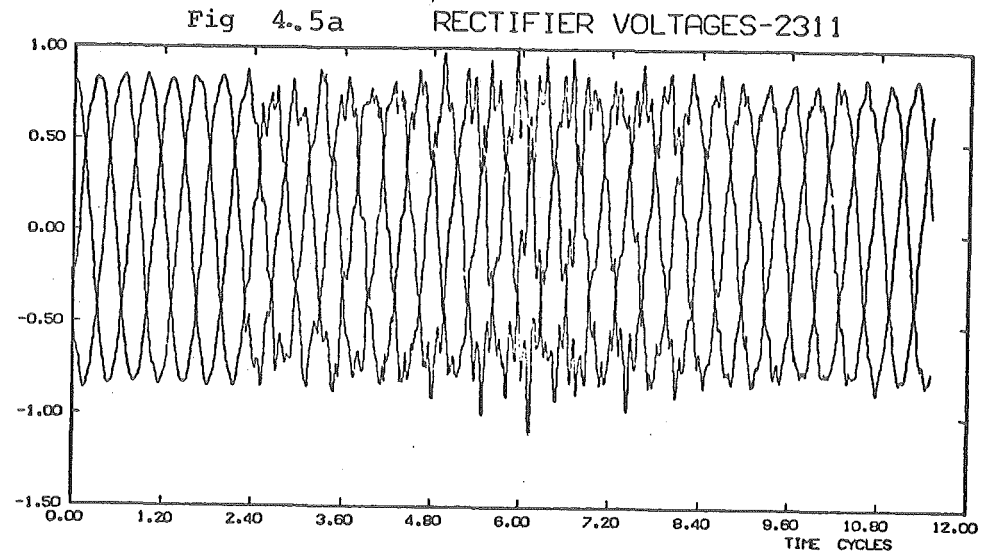

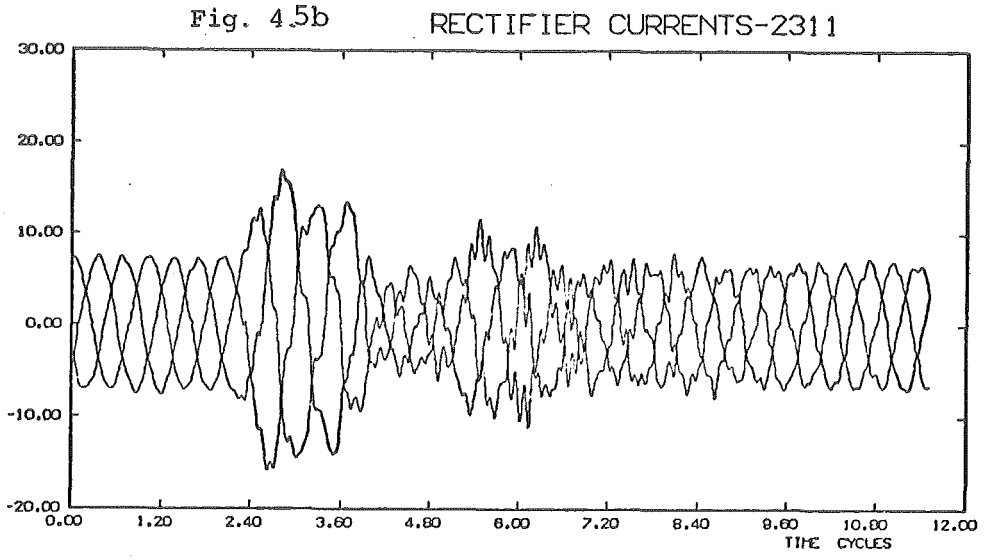

Fig. 4.5 Rectifier TCS Waveforms for an Inverter Terminal Fault.

disturbed by a fault in the AC system, a study period of 10 cycles (0.2 seconds) took 3000 seconds processing on a Burroughs B6718 computer. A TS study of the same case extending for 0.5 seconds simulation time took 27 seconds on the same computer. The ratio of the computing time is in the order of 300:1 and it is clear that TCS cannot be used for the full TS period when DC links are represented.

4.2 CONVERTER MODELLING FOR TRANSIENT STABILITY

As outlined in Chapter 2, the TS study uses a lumped parameter model of the system and uses integration step lengths in the order of 0.01 to 0.05 seconds. This is several hundred times greater than the step length of the TCS. Because of the limitation of the QSS link model during transient disturbances a TCS is necessary for accurate modelling of the link performance but its results cannot be incorporated directly in a TS study.

Some compromise is therefore required between the accurate, but computationally prohibitive, transient converter simulation and the computationally efficient, but less detailed, transient stability study. A compromise which exploits the advantages of both these methods is achieved by simultaneously performing transient stability and transient converter simulations with periodic coordination of the results. In this way the detailed converter model is provided with a time-variant Thevenin equivalent for correct AC system representation (Heffernan, Arrillaga et al 1980). Similarly, from the transient converter simulation, accurate power frequency information can be derived to represent the DC system behaviour at the converter terminals. The computational requirements are minimised by restricting the use of the transient converter simulation to the most disturbed part of the study; as the DC link regains normal controllability and attains predictable behaviour, this detailed simulation is replaced by a quasi-steady state model.

4.2.1 Transient Stability Requirements

Transient Stability is normally a fundamental frequency, single-phase, rms study and is therefore based on the assumptions of balanced and sinusoidal waveforms. In the presence of HVDC links, such assumptions are extended to the voltage and current waveforms at the converter terminals. On the other hand, transient converter simulation is waveform orientated and exhibits the distortions and non-linearities associated with converter operation.

It is therefore necessary to derive fundamental

frequency quantities from TCS voltage and current waveforms before information can be transferred from the TCS to the TS study.

4.2.2 Choice of Variables

Two variables are needed to transfer the converter information from the TCS to the TS study. A number of alternatives are available, i.e. real power, reactive power, voltage magnitude and current magnitude. Various definitions have been offered for reactive power in the presence of distorted waveforms (Shepherd et al 1972, Sharon 1973, Micu 1973) but a meaningful value of reactive power can only be obtained from sinusoidal components of voltage and current of the fundamental frequency. This fundamental frequency reactive power can only by derived from spectral analysis of the voltage and current waveforms and since both these variables can be used on their own, reactive power becomes redundant. The above problems do not exist in the definition of real power and further justification for its use as a variable is given in section 4.4.

The choice of the second variable is between voltage and current magnitude. Since the converter acts as a current harmonic source, the current waveform, particularly during and immediately after a disturbance, exhibits greater distortion and modulation effects than the voltage waveform. This has been tested in many TCS studies, and is illustrated in Fig. 4.5 and Figs. 4.6 and 4.7. The spectral analysis of the voltage waveform is, therefore, less prone to error and the voltage magnitude is a better choice of variable.

The specification of voltage and real power is required at each integration step of the TS study when the Quasi-Steady State DC link model is replaced by the results of a TCS involving the DC link.

To obtain fundamental components of voltage and power, Fourier processing of the TCS waveforms is required and this must be performed over at least one fundamental cycle of the waveforms. A component of voltage and power can be obtained

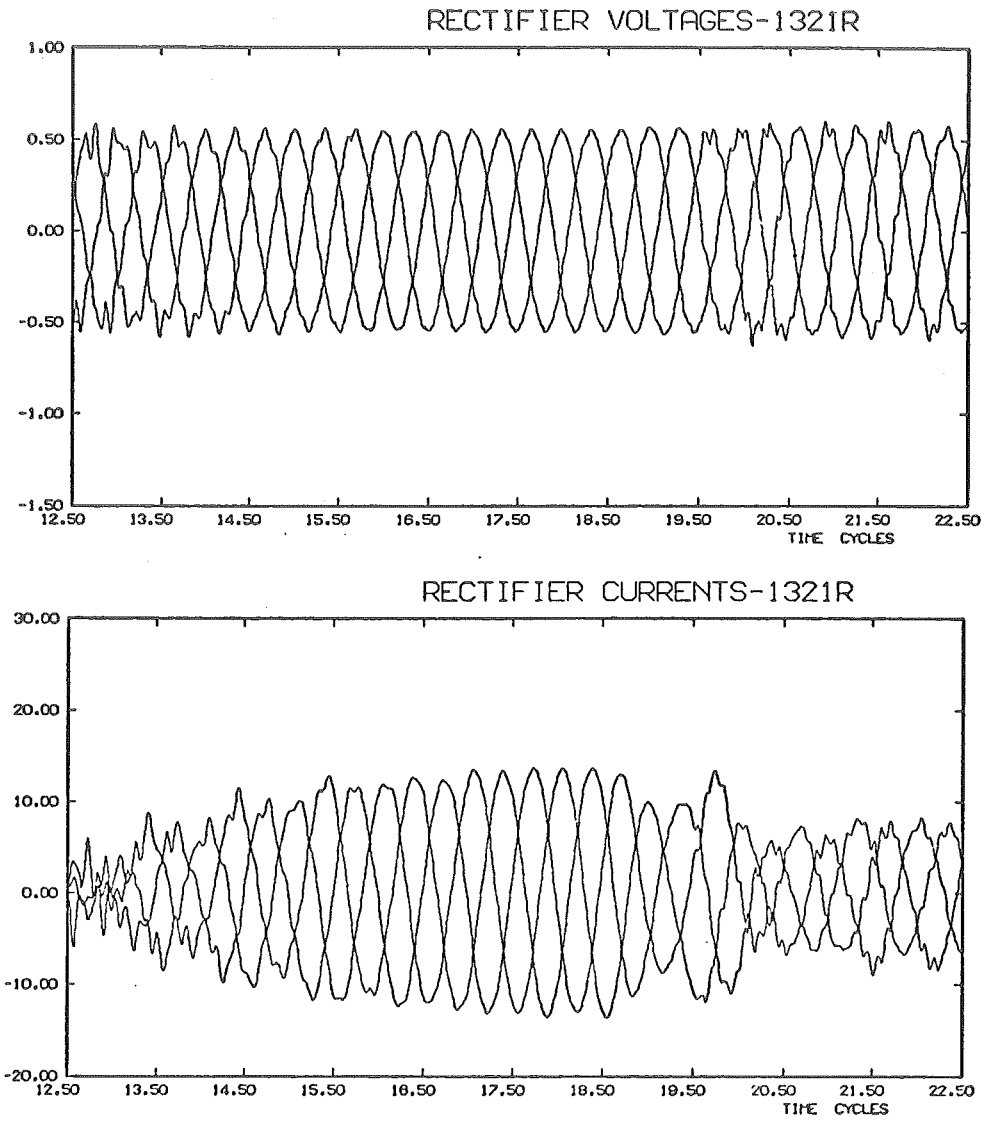

Fig. 4.6 Comparison Between TCS Waveforms at the Rectifier Terminal During Current Setting Changes.

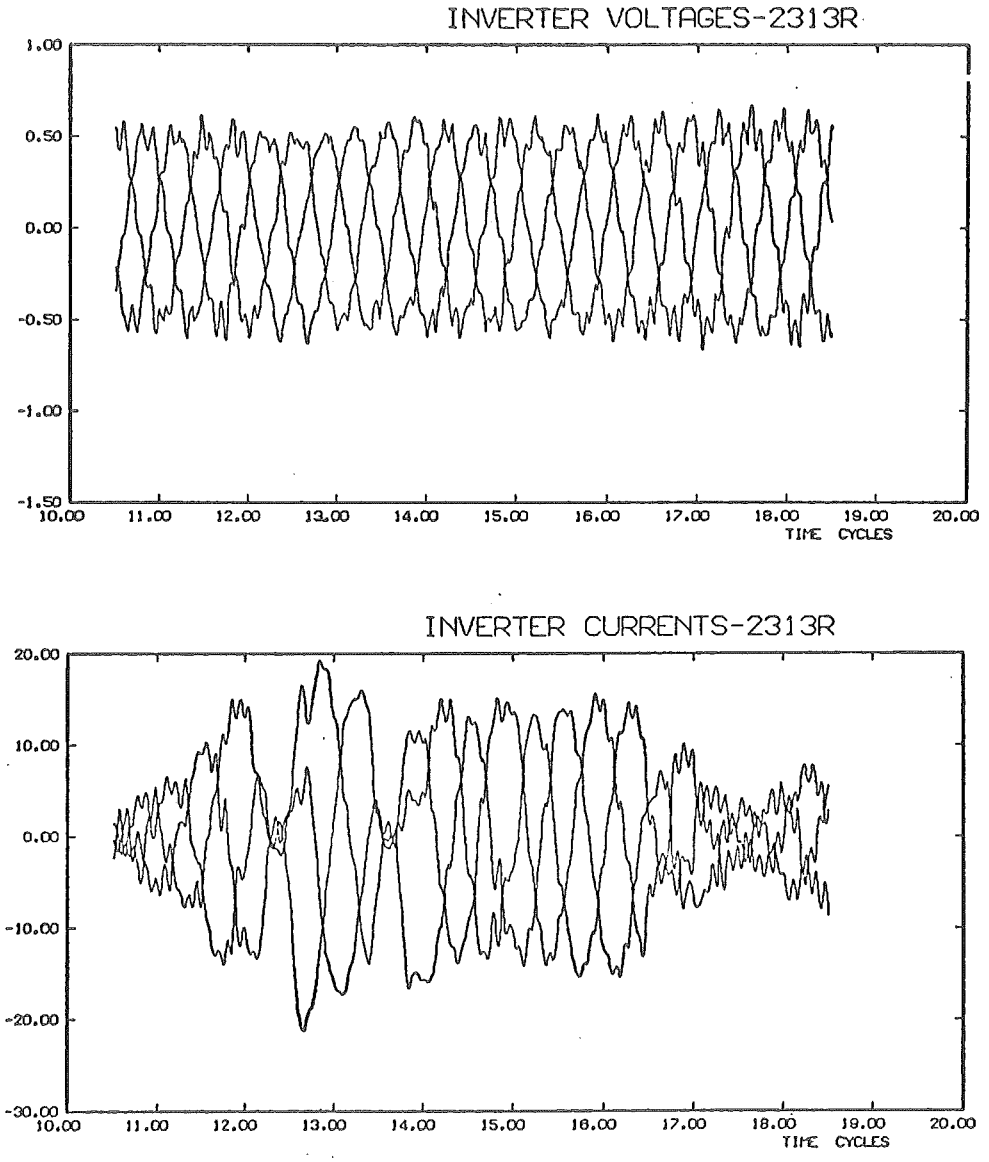

Fig. 4.7 Comparison Between TCS Waveforms at the Invertor Terminal During Commutational Failures.

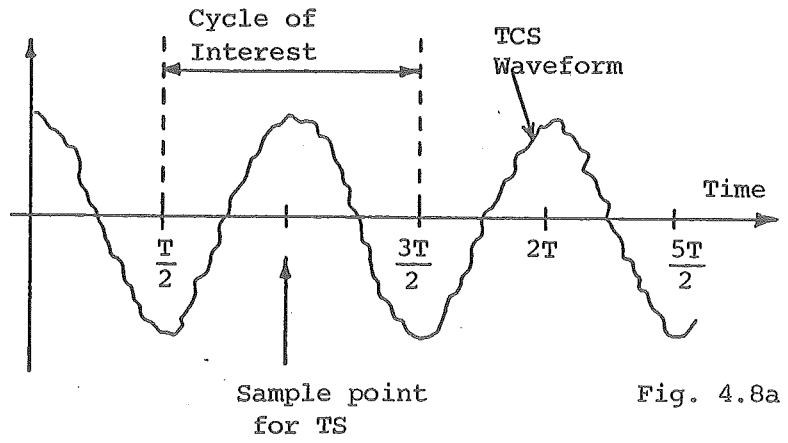

Fig. 4.8a

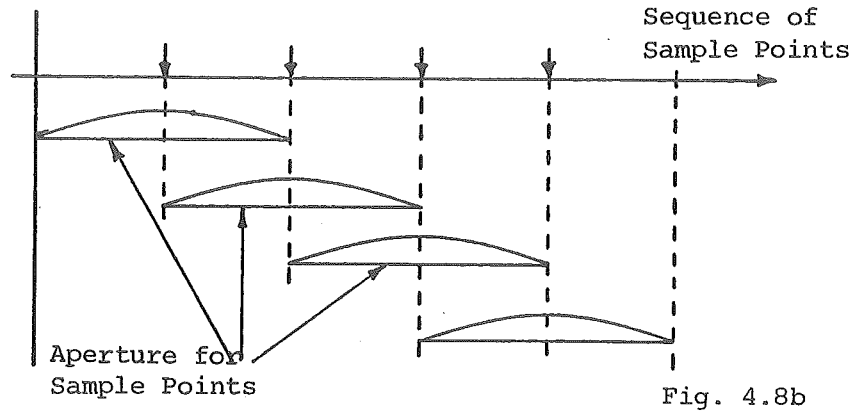

Fig. 4.8b

Fig. 4.8 Interaction Between TS Sample Points and a TCS Waveform.

at any sample point using a complete cycle (period T) spanning T/2 both sides of the sample point as illustrated in Fig. 4.8a. The sampling points must be synchronised with the TS study integration steps and, in order to ensure that sufficient samples are used (Lathi 1968), the TS programme step length should not exceed half of one fundamental cycle. In the studies performed using this programme the step length and sample rate was fixed at half a cycle of the fundamental frequency as illustrated in Fig. 4.8b.

4.3 ANALYSIS OF TRANSIENT CONVERTER SIMULATION WAVEFORMS

The following definitions are used to clarify the terminology relating power system periodic and non-periodic waveforms:

i) Periodic waveform: A waveform, periodic in the observation window T where 1/T is the fundamental power system frequency, (e.g. 50 Hz).

ii) Non-periodic waveform: A waveform not periodic in the observation window T .

The voltage waveforms at the terminals of a DC link during typical disturbances, such as those illustrated in Figs. 4.9 and 4.10 cannot be interpreted in terms of simple periodic waveforms for the following reasons:

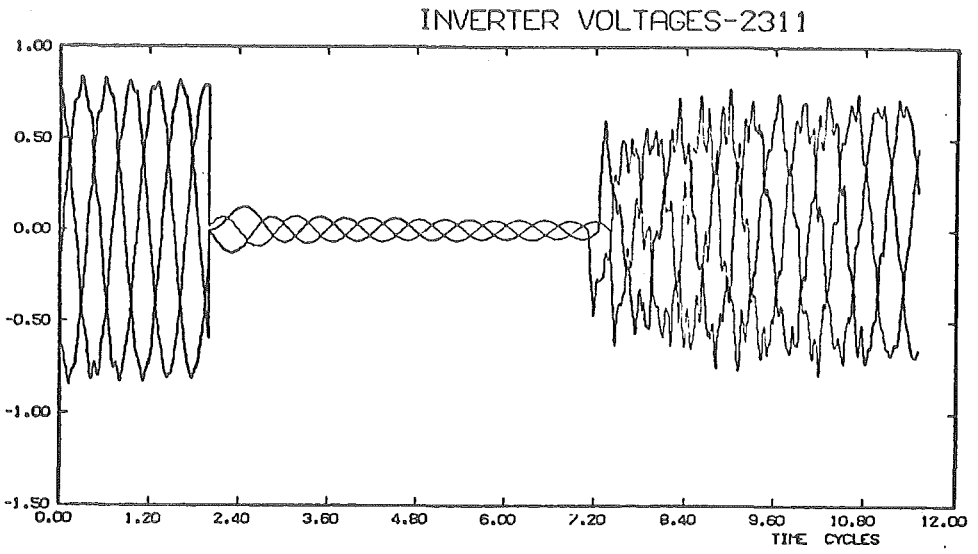

Fig. 4.9 TCS Waveform for a 3-Phase Fault at the Inverter Terminal.

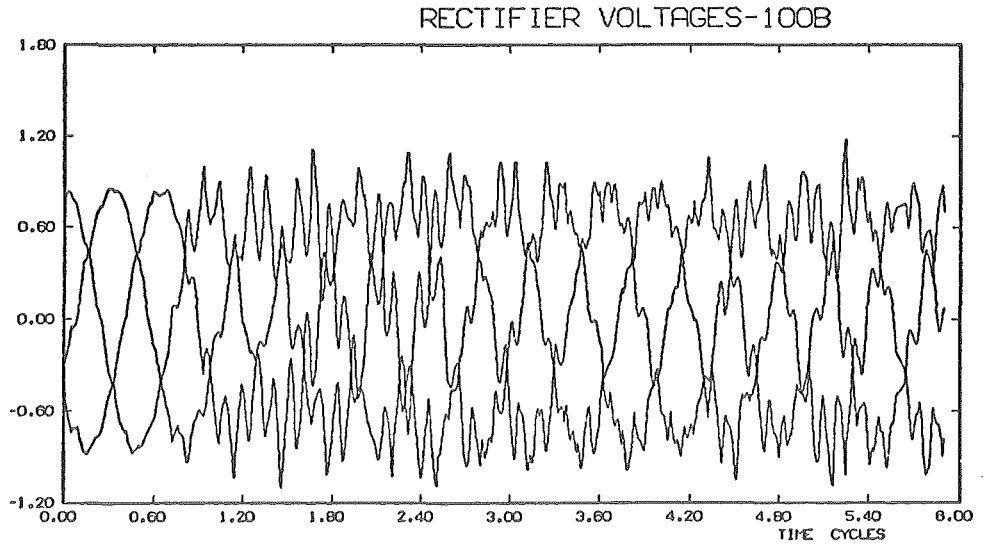

Fig. 4.10 Rectifier TCS Waveforms for a Single Phase Fault in the Inverter AC System.

i) Converter control action introduces deviations in the equidistant firing regime and valve firings do not necessarily occur periodically.

ii) The nonlinear behaviour of the converter excites disturbances which are not periodic in T.

iii) The network equivalent source is given in a constant frequency frame of reference but the TS study deviates from constant frequency after a disturbance, effectively altering the fundamental period.

These effects can be classified in terms of modulation, frequency mismatch and non periodic noise. Their presence means that simple fundamental component of voltage (or current) cannot be obtained merely by using a standard discrete Fast Fourier Transform (FFT), (Cochran et al 1967), on the samples which make up the TCS waveforms of Figs. 4.9 and 4.10. The presence of non periodic frequencies contribute to the spectral component evaluated at fundamental frequency. It is therefore necessary to consider the magnitude of these contributions to assess their individual effect on the identification and meaning of a fundamental component and thus ensure that the correct values of voltage and power are available for the TS study.

4.3.1 Effect of Modulation

Figure 4.9 illustrates the effect of a fault applied for a duration of 5 cycles and close to the invertor AC busbar of a DC link. There is a step change in voltage at the time of fault application and removal. In the TS study of this fault the integration step is adjusted to obtain a solution immediately before and after a discontinuity. However, performing an FFT to obtain a fundamental component from the cycle spanning either side of the discontinuity involves a half period of pre-discontinuity and a half period of post-discontinuity. The Fourier analysis of the waveform of this cycle in effect produces an averaging of the two parts of the cycle. The existence of a fundamental component is meaningless in this case and the result is incompatible with the requirements of the TS study.

The problem is overcome by extrapolating the results of the FFT on the immediate pre-discontinuity and post-discontinuity cycles to provide TCS data point at each respective solution in the TS study. This is discussed in section 5.2.2.

Apart from the discontinuities, the amplitudes of the voltages in Fig. 4.9, in the post fault period, are modulated by the slower dynamic response of the AC system. This response is derived from a TS study for which the fastest oscillations are in the order of 1-5 Hz. The Fourier analysis of each fundamental cycle, at intervals of half a cycle, reflects the much lower modulating frequency in the amplitude of the fundamental component from each cycle, and no special treatment is required for these modulating effects.

4.3.2 Effect of Frequency Mismatch

One of the basic assumptions in TS modelling is that frequency deviations are so small that parameter values remain constant. However, the Fourier analysis of the TCS waveforms, for a nominal frequency fundamental component (i. e. 50 or 60 Hz) can result in a small mismatch between the frequency of the variables at the converter terminals and the actual system frequency in the TS study.

The TCS is only used as a substitute for the Quasi-Steady State AC-DC model during, and for a short period after the fault. In this relatively short period (10-15 cycles) the deviation from nominal frequency is small. Typical results taken from the New Zealand system, for a fault relatively close to a converter and a synchronous machine, show a deviation of approximately 0.25 ms (1.25%) in the period of the system frequency. If the frequency mismatch is not taken into account when processing the TCS results the error introduced into a 1 p.u. fundamental of voltage or current is 0.65% (Appendix A4). Since real power is obtained from both voltage and current, it may be in error by up to 1.3%. However TS data is not normally provided to an accuracy better than 5% and therefore the errors associated with frequency mismatch are not significant.

4.3.3 Fourier Transforms of Periodic Waveforms with Noise

An outline of the fundamental equations of Fourier analysis and convolution, used in this section, is given in Appendix A3.

Figures 4.11a and 4.11b illustrate single cycles of

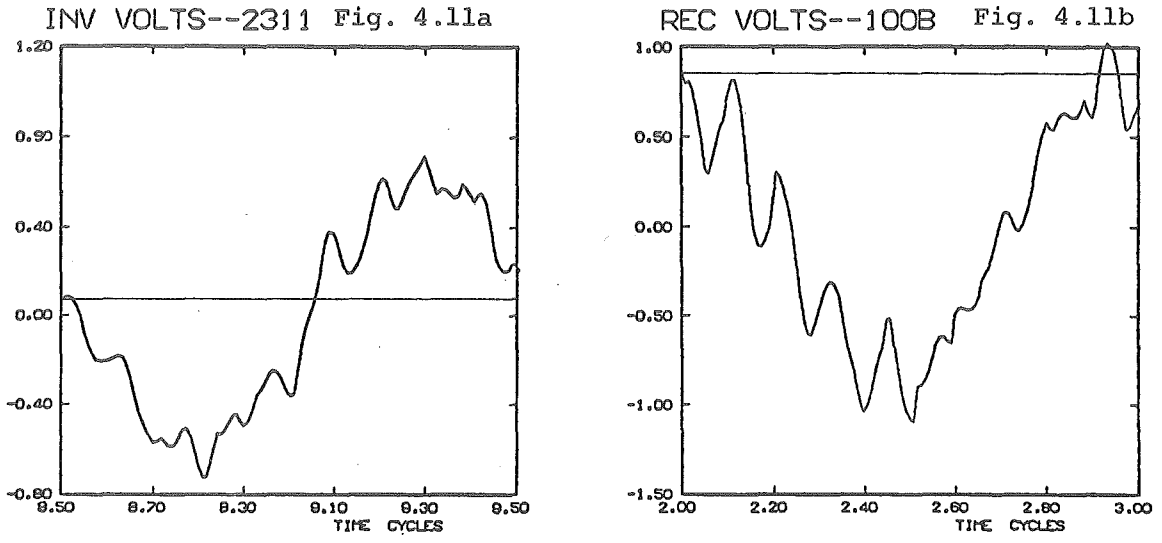

Fig. 4.11 Single Cycles of One Phase Obtained from TCS Waveforms of Figures 4.9 and 4.10.

one phase of the inverter and rectifier voltage waveforms taken from distorted periods of the results presented in Figs. 4.9 and 4.10. The discontinuities at the boundaries of these individual cycles show that considerable levels of non periodic frequencies exist in the waveforms due to the non-linearities associated with control action, filter response and converter behaviour. If these waveforms are assumed to be periodic and are subjected to Fourier transformation to obtain the spectral components of the signals (in particular the fundamental component), a phenomenon known as spectral leakage (Harris 1978) occurs. Spectral leakage results in the non periodic noise contributing to each of the periodic spectral components present, introducing uncertainty in their identification by the Fourier transformation.

The phenomenon of spectral leakage is best explained with the use of the convolution theorem (Lathi 1968).

In order to make the Fourier Transform of a periodic signal $f_T(t)$ finite, it is necessary to multiply the periodic signal, in the time domain, by a unit gate function, $g(t)$, where:

$$g(t) = 1 \text{ for } |t| < \frac{T}{2} \qquad (4.11)$$

$$g(t) = 0 \text{ for } |t| > \frac{T}{2} \qquad (4.12)$$

Figure 4.12a shows the gate function and its spectrum, $G(\omega)$. In the frequency domain this multiplication is equivalent to the convolution of $F(\omega)$ with $G(\omega)$, i.e.

$$f_T(t) \longleftrightarrow F(\omega) \qquad (4.13)$$

$$f_T(t) \cdot g(t) \longleftrightarrow F_g(\omega) \qquad (4.14)$$

where $F_g(\omega) = F(\omega) \otimes G(\omega)$ (4.15)

and $\longleftrightarrow$ denotes a Fourier Transform pair.

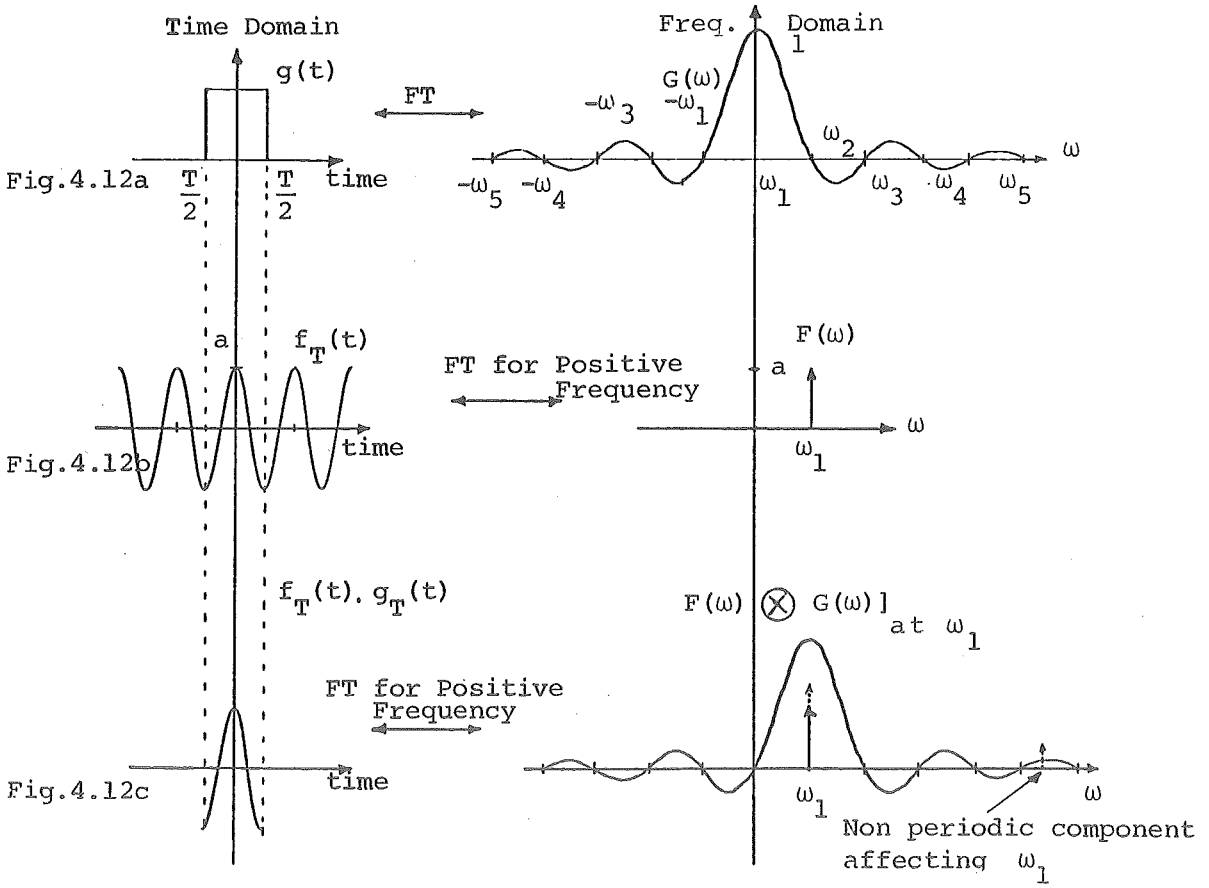

Fig. 4.12 Convolution and the Effect of Spectral Leakage on the Component at ω.

When $f_T(t)$ contains only the fundamental frequency, ω_1, as shown in Fig. 4.12b, the convolution of $F(\omega)$ and $G(\omega)$ at ω_1 is illustrated in Fig. 4.12c. The value of the convolution at ω_1 is the sum of the spectral components multiplied by their respective gate coefficients. When $f_T(t)$ is purely periodic in the aperture T then all the spectral components are integer multiples of ω_1 and lie at the zero crossings of $G(\omega)$ and hence the only spectral component which contributes is the one being evaluated, i.e. the component of ω_1 in the case of Fig. 4.12c.

However in the presence of an interfering spectral component which is not periodic in the aperture T, the product of it and $G(\omega)$ will no longer be zero. As shown by the dotted component at 5.3 ω_1 in Fig. 4.12c, this leads to an error in the identification of ω_1. The further from ω_1 the interfering spectral component is, the smaller is the coefficient of $G(\omega)$ and the less interference it has on the evaluation of the component at ω_1.

Because of the effect of spectral leakage, it is not possible to obtain the fundamental components of waveforms, such as those of Figs. 4.11a and 4.11b, with any degree of certainty by simple application of an FFT. However if the effect of spectral leakage can be minimised by filtering, it is possible to determine the magnitude of the effect by a direct comparison with spectral analysis of a waveform obtained by simple application of the FFT.

4.3.3.1 Spectral leakage reduction - The gate function is a particular case of a group of functions known as window functions. By proper choice of window function the effects of spectral leakage can be reduced. (Harris 1978). The method by which this is achieved is best observed in the frequency domain.

Figure 4.13 shows some of the more common discrete windows with their Fourier transforms.

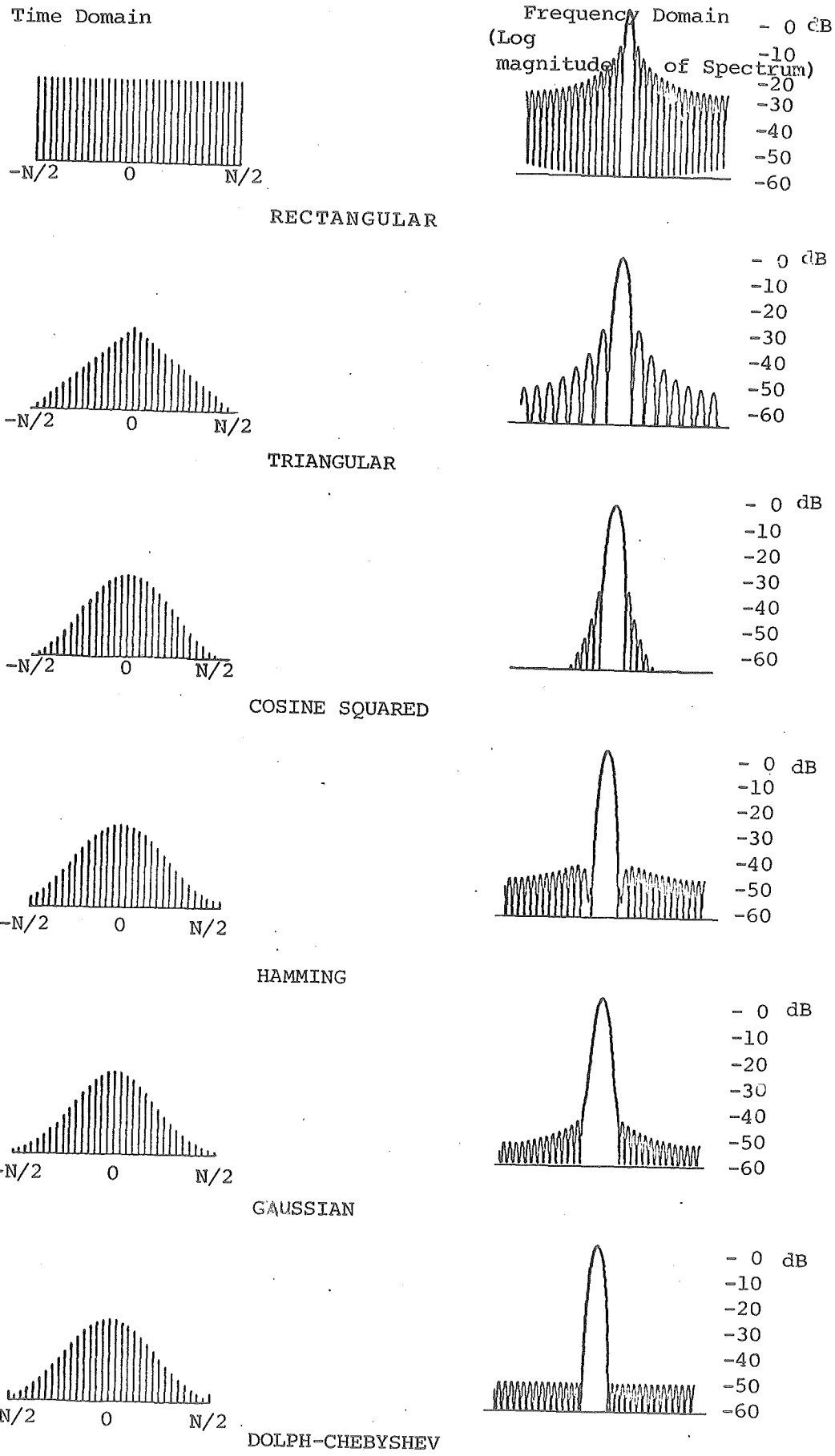

Fig. 4.13 Fourier Transform Pairs of Common Windows.

In the case of the gate function the sidelobe level is large and the rate of decay of the sidelobes is slow. This means that when evaluating the fundamental component of a signal, interfering spectral components near to it will be weighted heavily, contributing greater interference to the fundamental than for the other windows illustrated in Fig. 4.13. Hence, if the sidelobe level can be reduced quickly to a very low level, the contribution from interference outside the mainlobe will be reduced to a minimum. Observing this process in the time domain, the multiplicative weighting of the window brings the discontinuities at the boundaries of one cycle smoothly towards zero.

4.3.3.2 Choice of window - The objective in choosing a window to minimise spectral leakage is to obtain a mainlobe which is as narrow as possible (i.e. so that it only includes the spectral component of interest), with minimal sidelobe levels to reduce the contribution from interfering spectral components. These two specifications are interrelated for realisable windows and a compromise is required between mainlobe width and sidelobe level. The Dolph-Chebyshev window provides the narrowest possible mainlobe width for a given specified sidelobe level. (Harris 1978). It was chosen for this filtering application and its discrete form is realised in the frequency domain by:

$$w(k) = \frac{(-1)^k \cos\left(N\cos^{-1}\left[\beta \cos\left(\frac{\pi k}{N}\right)\right]\right)}{\cosh\left[N\cosh^{-1}(\beta)\right]} \qquad (4.16)$$

for $0 < k < N-1$ and k an integer.

$$\beta = \cosh\left[\frac{1}{N}\cosh(10^{\alpha})\right] \qquad (4.17)$$

and where the inverse hyperbolic cosine is defined by:

$$\cosh^{-1} x = \frac{\pi}{2} - \tan^{-1}\left(x/\sqrt{1 - x^2}\right) \text{ for } |x| < 1.0 \qquad (4.18)$$

$$= \mathrm{Ln}\left[x + \sqrt{x^2 - 1.0}\right] \text{ for } |x| > 1.0 \qquad (4.19)$$

and N = number of samples.

The time domain samples are obtained by performing a discrete inverse FFT on w(k). The sidelobe levels of the window remain below a specified constant maximum which can be controlled by the parameter α of equation 4.17. With $\alpha = 4.0$ the sidelobes are 80 db, (0.01%), down on the mainlobe magnitude.

When using windows for filtering, very low sidelobe levels are required to minimize the cummulative contributions of spectral components outside the mainlobe, including periodic contributions. This is because window spectral components, other than those of the gate function, are not necessarily zero at the periodic frequencies. The Dolph-Chebyshev window is well suited for this application as the constant sidelobes can be reduced to any desired level by the choice of a suitable value for the paremeter α.

4.3.3.3 Mainlobe width limitation - The comparison between the gate function and the Dolph-Chebyshev windows of Fig. 4.13 illustrates that the use of very low sidelobe levels results in a sacrifice in terms of the width of the mainlobe. In the case of the Dolph-Chebyshev window the mainlobe is much wider than that of the gate function. When positioned for the evaluation of w_1 by convolution in the frequency domain, (i.e. as for the gate function of Fig. 4.12c), the DC component and the 2nd and 3rd harmonics are included within the mainlobe. Because of the nature of the TCS waveforms, significant levels of DC and 2nd and 3rd harmonics may be present and this, coupled with the weighting of the mainlobe window coefficients, can cause considerable interference to the fundamental component evaluated. This represents a serious disadvantage in the use of windows and, for the purposes of evaluating a fundamental component from TCS waveforms, it restricts the identification of spectral leakage effects to higher order frequencies and noise outside the mainlobe.

4.3.3.4 Algorithm to overcome mainlobe width limitation - By applying the principle of convolution to the discrete TCS data and using the trigonometric form of

the Fourier Transform (Appendix A3) the complex fundamental Fourier component of $[w(k).f(k)]_{k=1}^{N}$ is:

$$X_1 = w_o C_1 + w_1 C_2 + w_2 C_3 + w_{-2} C_{-1}$$

$$+ w_{-3} C_{-2} + w_{-4} C_{-3} + w_{-1} C_o$$

$$+ \sum_{n=3}^{N/2} w_n C_{n+1} + \sum_{n=4}^{N/2-1} w_{-n+1} C_{-n} \qquad (4.20)$$

where w - discrete window coefficients in the frequency domain

$C_n = C_{-n}$ - complex periodic Fourier components (subscript refers to harmonic order).

By pre-processing the discrete TCS waveform samples taken from the cycle of interest, the DC content of the samples can be removed thereby eliminating C_o of equation 4.20. The samples are then spaced equally (refer Appendix A5), and the window is applied in the time domain by multiplicative weighting. In addition, since the last two terms of equation 4.20 includes all the higher order harmonics and noise but weighted with window coefficients in the order of 0.01%, they can also be neglected. Equation 4.20 can therefore be reduced to:

$$X_1 = C_1(w_o + w_{-2}) + C_2(w_1 + w_{-3}) + C_3(w_2 + w_{-4}) \qquad (4.21)$$

In equation 4.21, X_1 is obtained from an FFT of the TCS time domain samples multiplied by their respective time domain window coefficients. The window coefficients in the frequency domain are known by equation 4.16 and the only unknowns are the three harmonics. By using three windows, each with a different α parameter, and applying them to the same cycle of TCS data, three simultaneous equations of the same form as equation 4.21 can be obtained. This algorithm requires three applications of the FFT for each cycle of data and solution of the simultaneous equations permits the

evaluation of a filtered spectral component, C_1.

4.3.3.5 Algorithm tests - The algorithm was tested on 32 sample discrete sinusoidal data of the form:

$$f_T(t) = c_1 \cos(\omega_1 t + \phi_1) + \sum_{n=2}^{7} c_n \cos(\omega_1 t + \phi_n) \qquad (4.22)$$

where $c_1 = 1.0$

$c_n = 0.2$ for $n = 2$ to 7.

On this purely sinusoidal data the window filtering introduced an error of 0.16% into the identification of c_1 due to the contribution from higher harmonics. When a non periodic component, magnitude 0.2, was introduced into $f_T(t)$ at $5.65\omega_1$ the error in identifying ω_1 by direct application of the FFT to the data was 2%, but by using window filtering this was reduced to 0.36%.

The series represented by equation 4.22 constitutes a severe test as it uses a high amplitude for every harmonic. Even so, the algorithm performance is well within the accuracy range of power system calculations.

In this test windows with α values of 3.2, 3.5 and 3.8 were used. Further work could be directed towards investigating the effect of using different α parameters on the accuracy with which spectral components can be identified. However the algorithm performance, for the purposes of filtering TCS waveforms for power system applications, appears to be satisfactory.

4.3.3.6 Significance of spectral leakage in TCS waveforms - The algorithm described in the previous section was used to compare the filtered and unfiltered amplitudes of TCS voltages and currents at both DC link terminals for a number of case studies. The comparison was made using many cycles taken from periods of maximum distortion during each case study, typical examples being illustrated in Fig. 4.11.

The difference between direct and filtered fundamental amplitudes was found to be small. From the results of over 100 different cycles of TCS waveform, differences of up to 0.7% were relatively common for very distorted waveforms. The maximum difference observed was 1% and this was for the cycle illustrated in Fig. 4.11b.

These differences are not far outside the limits of accuracy of the filtering method itself and it can therefore be concluded that spectral leakage does not contribute significant errors when identifying the fundamental components of TCS waveforms.

It is therefore possible to obtain fundamental powers and voltages from TCS waveforms by simple application of an FFT, in the presence of modulation, frequency mismatch and non periodic noise. This can be done with the same degree of accuracy that other input data is obtained for transient stability studies.

4.4 ALTERNATIVE TO SPECTRAL ANALYSIS

As section 4.3 has shown, a simple fundamental component of a TCS waveform is not readily obtainable and is also subject to interpretation and error. Approximations can be used to avoid the need to perform spectral analysis of the TCS waveform. The evaluation of average or rms quantities from the converter waveforms includes the contributions of all harmonic components and this violates the sinusoidal assumption made in TS studies. However, the rms approximation can be compared with the fundamental component to determine whether it represents a sufficiently accurate alternative to spectral analysis.

Both the rms and fundamental quantities illustrated in the figures of this section have been obtained by processing TCS data over one cycle. In order to compare these quantities through a study, an rms and fundamental quantity was obtained 36 times per cycle, (i.e. every 10°), and the two quantities plotted together. Referring to Fig. 4.8b this means that the aperture for each plotted point overlaps the apertures of the

points either side by 350° A Fourier series was used to obtain only the fundamental of the TCS data because of the computing requirements of the FFT algorithm for such a large number of analyses over the period of a case study (typically 7000 Fourier transforms). This reduces the computational effort of the spectral analysis to 20% of the full FFT requirement. Because of the small errors detected due to spectral leakage, window filtering was not used.

4.4.1 RMS Approximation for Voltage

The rms value of a voltage, V(t), is defined over a period T as

$$V_{rms} = \sqrt{\frac{1}{T} \int_{o}^{T} v(t)^2 \, dt} \qquad (4.23)$$

For discrete data this becomes:

$$V_{rms} = \sqrt{\frac{1}{N} \sum_{n=1}^{N} (V_n)^2} \qquad (4.24)$$

where N = the number of samples.

RMS values for discrete data are easily and quickly evaluated in relation to spectral analysis.

Figures 4.14a and 4.14b show a comparison of fundamental voltage (positive sequence) and rms voltage for the TCS waveforms of Figs. 4.9 and 4.10. Figure 4.14b represents a severely distorted case with a 5% difference observed during the period immediately after disturbance initiation. This coincides with the period of maximum distortion in Fig. 4.10 at which time harmonic content is high. The effect of using one cycle for obtaining the fundamental or rms voltage is clearly shown in Fig. 4.14a during the cycle spanning fault application and removal, (i.e. at 2 and 7 cycles). While Fig. 4.9 shows a sudden discontinuity at these times, Fig. 4.14a demonstrates the averaging effect of processing, emphasising the need for extrapolation to obtain compatible TS samples at discontinuities.

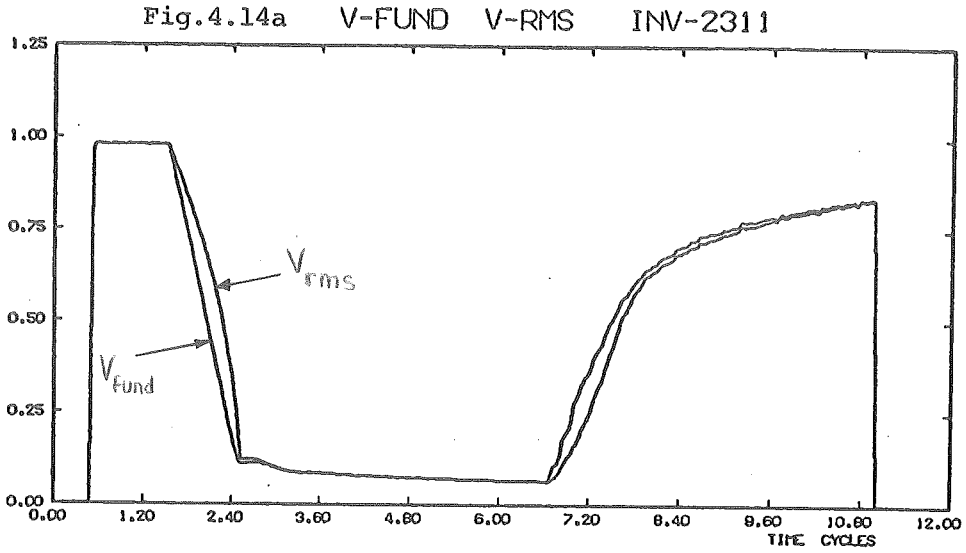

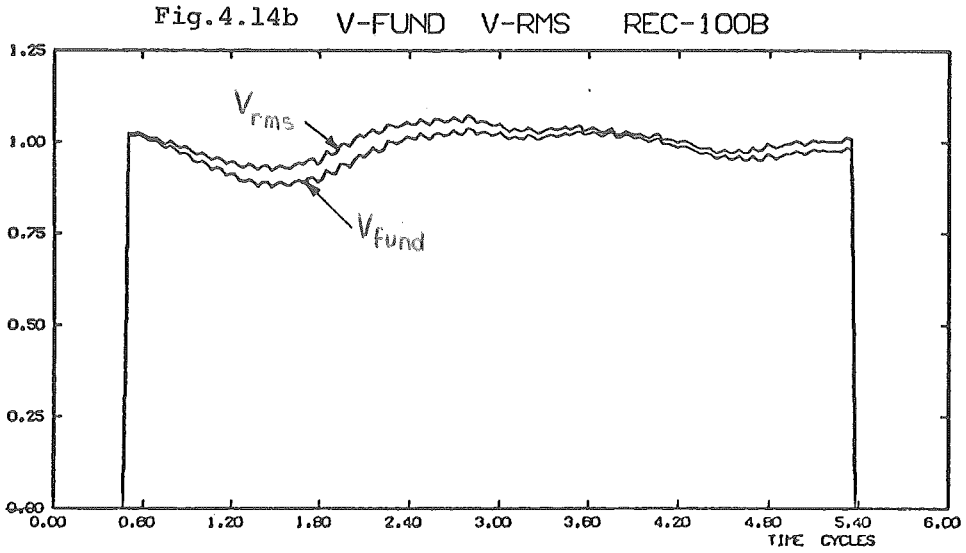

Fig. 4.14 Comparison of RMS and Fundamental Voltages for the TCS Waveforms of Figures 4.9 and 4.10.

4.4.2 RMS Approximation for Power

Apparent power is defined as:

$$s(t) = v(t) \cdot i(t) \tag{4.25}$$

The real component of $s(t)$ is the average value of $s(t)$ taken over a period, T. i.e.

$$P_{rms} = \frac{1}{T} \int_{0}^{T} v(t) \cdot i(t)\, dt \tag{4.26}$$

This is readily evaluated from discrete signals using:

$$P_{rms} = \frac{1}{N} \sum_{n=1}^{N} V_n \, i_n \qquad (4.27)$$

The real power evaluated in this way is the sum of fundamental and harmonic real powers. The results from many TCS's have shown that, in general, the harmonic real power is small and that the rms approximation for real fundamental power is a good one. Figures 4.15a and 4.15b show the two representative curves. In the case of Fig. 4.15a, although the maximum error is 4%, the cummulative error over the simulation period is small. The maximum error occurs for a short period when highly distorted signals exist.

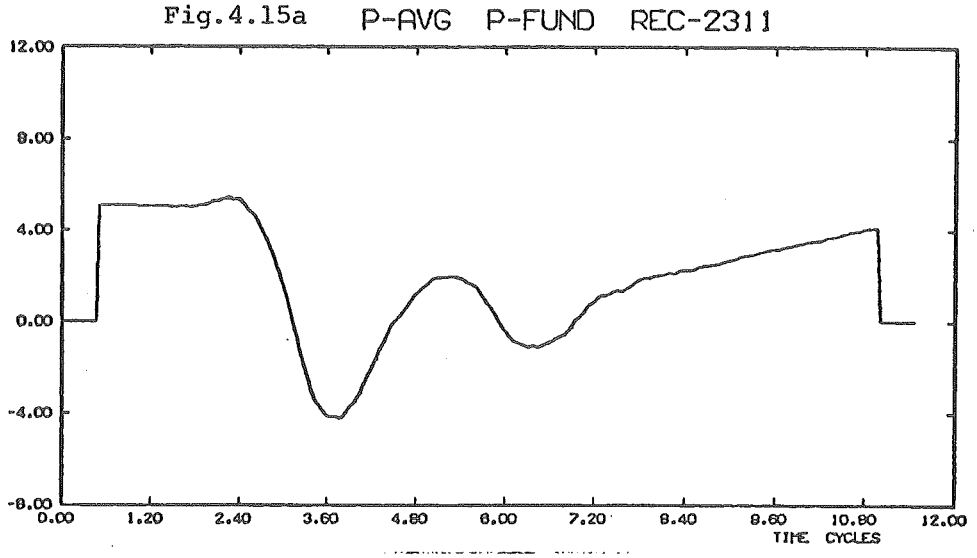

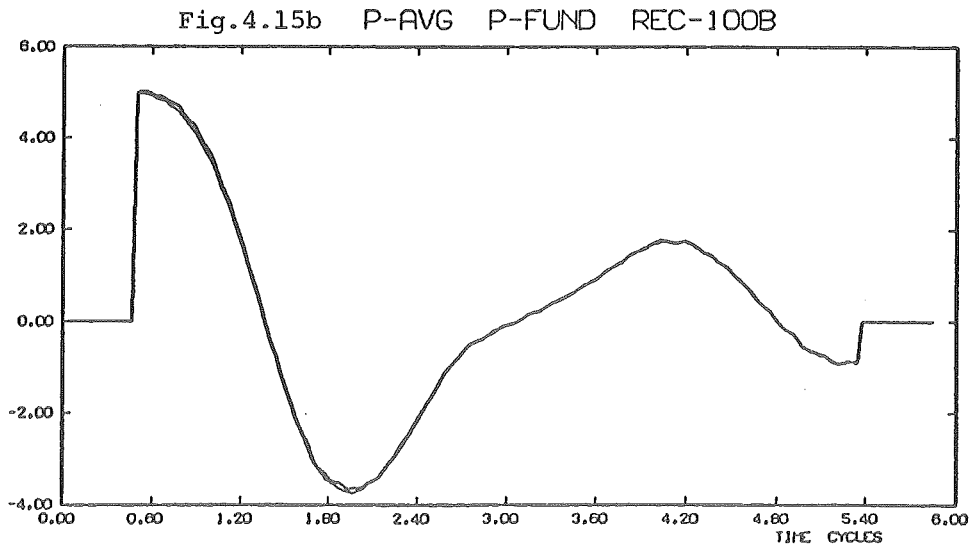

Fig. 4.15 Comparison of RMS and Fundamental Powers for the Cases Presented in Figures 4.9 and 4.10.

The harmonic power flow can only result from in-phase components of harmonic currents and voltages. Considering the relatively low resistive component of the converter transformer and the large X/R ratio of the AC system, the in-phase component of the harmonic currents and voltages are very small. Therefore the use of rms power is a good approximation and spectral analysis is not needed to derive the power variable.

It is for this reason that in section 4.2.2 it was chosen as one of the variables to transfer the converter information from the TCS to the TS study.

4.5 CONCLUSION

The feasibility of deriving transient stability compatible variables from transient converter simulation waveforms has been examined and demonstrated.

An efficient technique has been developed for processing the aperiodic and distorted waveforms obtained from a TCS so that the information may be used directly in a TS study. From the choice of waveforms available it has been shown that power and voltage magnitude are suitable variables for transferring such information.

The information is transferred at each step of the TS study and the problem posed by system discontinuities has been considered and overcome. The use of spectral analysis and window filtering has shown that sufficient accuracy and considerable computing saving can be achieved by judicious approximations. It has been shown that the use of rms power in place of fundamental power introduces only very small errors. However in the case of the converter voltage, the use of rms voltage can lead to significant errors.

It is therefore necessary to retain the spectral analysis to determine a fundamental voltage magnitude from the transient converter simulation waveforms but the rms approximation for power avoids the need for spectral analysis of current.

The techniques developed have application wherever distorted and aperiodic waveform information requires analysis. One such application is harmonic analysis of waveforms obtained by fast digital sampling of power system data.

CHAPTER 5

MODELLING DC LINKS WITH TRANSIENT CONVERTER SIMULATION INPUT

5.0 INTRODUCTION

The interactive use of both a QSS DC link model and a transient converter simulation of the AC-DC system provides an efficient and accurate DC link representation for TS studies. This proposal combines the advantages of both models. The transient converter simulation accurately models the DC link during and after a disturbance and once the link response has settled a QSS model is used to represent the link for the rest of the study period.

The combination of both models avoids the limitations of either model used independently. The QSS model assumes controllable DC link operation and this assumption has not been proved to be valid, especially during or immediately after a disturbance. The inclusion of a dynamically responsive DC line and controls (Brameller et al 1979) does not avoid this assumption. By using a full transient simulation for all elements, limited stability studies can be performed but this approach is computationally very expensive even for quite short studies. (Vovos and Galanos 1979). It would be impractical to use this approach for 2 or 3 second studies of large multimachine systems.

This chapter outlines the formulation and application of the QSS DC link model in the TS programme. The formulation is based on the unified method of Chapter 3. This chapter also covers the details of including TCS results into the TS programme and discusses the interaction of the two programmes.

5.1 QSS MODEL FORMULATION

The formulation uses the same basic DC equations presented in section 3.1. The assumptions discussed in that section also apply and the number of equations is increased

to cover a two terminal DC link. By formulating the equations with separate DC currents for each converter, this model can be extended to the multiterminal case.

5.1.1 Choice of Algorithm

The DC link model can be formulated using either the sequential or unified algorithms discussed in Chapter 3.

The sequential approach is relatively simple to implement and has been successfully used by Heffernan 1977. However, Heffernan's work deals with relatively small deviations from nominal operation and has not been used for major fault disturbances. It has been shown, in Chapter 3, that for severe disturbances where a large injected current is required at low voltage, the sequential algorithm degrades the convergence properties of the TS programme.

The unified algorithm is an iterative procedure which is more complex to implement and computationally more expensive than the sequential one. However it has already demonstrated its superior ability to maintain the good convergence properties of the TS programme even under difficult system conditions such as severe faults. Similar findings have been reported in loadflow investigations using a similar algorithm. (Harker 1980).

A DC link may not produce the same conditions as the dynamically responsive rectifier load model of Chapter 3 and the sequential algorithm could be used. However the unified algorithm was chosen for the following reasons:

i) It has been demonstrated that it does not affect the convergence properties of the TS programme under severe disturbances. Abornal DC link behaviour can be investigated if required.

ii) The use of TCS results for a period during the TS study favours the use of a robust algorithm which does not affect the TS programme convergence. TCS results may deviate considerably from the QSS model and, during faults, would provide conditions similar to those of the dynamically

responsive rectifier load model.

iii) It would be impractical to provide different algorithms for the QSS and TCS models.

iv) Computational efficiency is not of prime importance at this stage because of the investigative nature of this work. In addition the DC link model forms only a small proportion of the computational requirements of the full TS study.

v) The unified algorithm offers a flexible means for implementing DC link control (and link reversal) by substituting the necessary control equations into the Newton-Raphson formulation as discussed in section 3.4.

The disadvantages of complexity are not considered important in terms of the advantages outlined above.

5.1.2 Per Unit System

A per unit system is used for DC link variables to avoid numerical instabilities and provide comparable convergence tolerances to those used in the AC system. For simplicity a common MVA and voltage base is used across each converter. If the voltage base chosen is obtained from the nominal value of the converter source voltage referred to the secondary of the converter transformer, the DC voltage can be readily obtained without introducing the turns ratio of the converter transformer. In addition the impedance base of the AC and DC systems is the same and hence

$$X_{pu\,(\text{DC base})} = X_{pu\,(\text{AC base})} \qquad (5.1)$$

and the AC commutation reactance can be included directly into the DC equations without modification. This system is simpler than that used in section 3.1.4 by avoiding the need to multiply by the ratio of the voltage bases. In using this system the DC current referred to the AC side is modified by a factor of $\sqrt{3}$. i.e.:

$$MVA_{b_{DC}} = MVA_{b_{AC}} \qquad (5.2)$$

$$V_{b_{DC}} I_{b_{DC}} = \sqrt{3} V_{b_{AC}} I_{b_{AC}} \quad (5.3)$$

and since $$V_{b_{DC}} = V_{b_{AC}} \quad (5.4)$$

$$I_{b_{DC}} = \sqrt{3}\, I_{b_{AC}} \quad (5.5)$$

This is reflected in the equation relating fundamental AC current to DC current, i.e.:

$$I_{pu_{AC}} = \frac{3\sqrt{2}}{\pi} a\, I_d \text{ (pu)} \quad (5.6)$$

For a DC link, it is unlikely that the AC base voltage will be the same at both rectifier and inverter systems. This means that while the DC current is continuous through the DC link the per unit value of DC current is different at each end. To avoid unnecessary complications the variable I_d in the equation across the DC line, is used in kilo amps. Since most links operate with a nominal current in the order of 1 - 2 KA, the value of I_d is of a similar order as the other per unit variables.

5.1.3 Quasi-Steady State Equations

The unified algorithm is implemented by reducing the AC system, at each terminal of the DC link, to its Thevenin equivalent. The resulting subsystem, as shown in Fig. 5.1, is solved by the Newton-Raphson algorithm described in appendix A2. For simplicity, the filters at the link terminal are not included in Fig. 5.1 and are treated separately.

The system of Fig. 5.1 has a total of 15 possible variables:

$$I_d,\ (E_i,\ \theta_j,\ I_j,\ \psi_j,\ \alpha_j,\ Vd_j,\ a_j)\ j = 1,2$$

where j refers to a converter.
However the dimension of the problem can be reduced to 9 to minimise the dimension of the Jacobian matrix while still retaining sufficient flexibility for TS purposes.

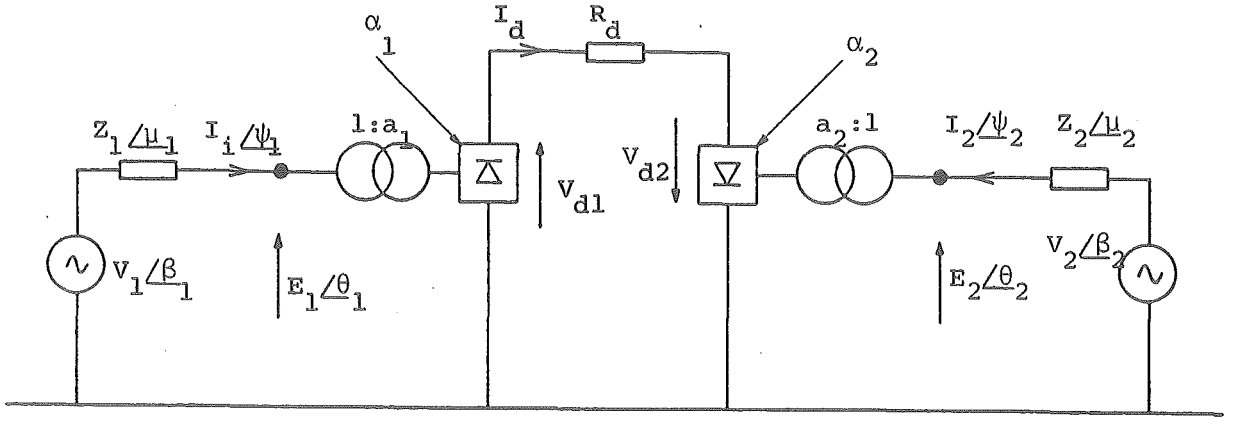

Fig. 5.1 AC and DC System for Unified Algorithm.

i) It is not necessary to include the converter transformer tap as a variable since it is assumed that no tap changing takes place during a TS study.

ii) AC and DC currents are related by equation 5.6 and hence I_j can be substituted for in terms of I_d.

iii) The DC voltage is not required explicitly as it can be expressed in terms of E_j, α_j and I_d. i.e.:

$$V_{d_j} = \frac{3\sqrt{2}}{\pi} a_j E_j \cos\alpha_j - \frac{3}{\pi} X_{c_j} I_d \qquad (5.7)$$

The set of independent equations for the link are derived from:

i) Equating voltages at the Thevenin source:

$$V_j\angle\beta_j - (Z_j\angle\mu_j I_j\angle\psi_j) - E_j \angle\theta_j = 0 \qquad (5.8)$$

ii) Equating powers across the converter:

$$V_{d_j} I_d - \sqrt{3}\ E_j\ I_j \cos(\theta_j - \psi_j) = 0 \qquad (5.9)$$

Using equations 5.6 and 5.7, this can be rewritten as:

$$a_j E_j \cos\alpha_j - \frac{1}{\sqrt{2}} X_{c_j} I_d - a_j E_j \cos(\theta_j - \psi_j) = 0 \qquad (5.10)$$

iii) Applying ohms law across the DC line:

$$V_{d1} + V_{d2} - I_d R_d = 0 \qquad (5.11)$$

or, eliminating V_{d1} and V_{d2}

$$\frac{3\sqrt{2}}{\pi}(a_1E_1\cos\alpha_1 + a_2E_2\cos\alpha_2) - \frac{3}{\pi}(X_{c1} + X_{c2} + R_d)\,I_d = 0 \qquad (5.12)$$

In this formulation the delay angle α is retained explicitly for both rectifier and inverter. This increases the versatility of the model for considering power flow reversal during a study period.

For power flow from terminal 1 to terminal 2 (i.e. terminal 1 is a rectifier and terminal 2 an inverter)

$\alpha_1 < 90$ and V_{d1} is positive

$\alpha_2 > 90$ and V_{d2} is negative.

Hence these equations are general for power flow in either direction. The QSS model for a two terminal DC link thus consists of 7 equations obtained from 5.8, 5.10 and 5.12, in terms of the following 9 variables:

$$I_d,\ (E_j,\ \Theta_j,\ \psi_j,\ \alpha_j)\ j = 1,2 \qquad (5.13)$$

Two control equations are required to fully specify the system. For normal operation under constant current control, these would be:

$$I_d - I_d^{sp} = 0 \qquad (5.14)$$

$$\gamma_2 - \gamma_2^{sp} = 0 \qquad (5.15)$$

5.1.3.1 Control equation - Since γ is not an essential variable in the formulation of the problem, the dimension of the Jacobian can be decreased if it is included implicitly. Control equation 5.14 can be written in terms of the problem variables of 5.13 and an alternative form can be derived for equation 5.15.

Referring to Fig. 5.2, areas A1 and A2 are equal since the voltage during commutation is the average of the two commutating phases.

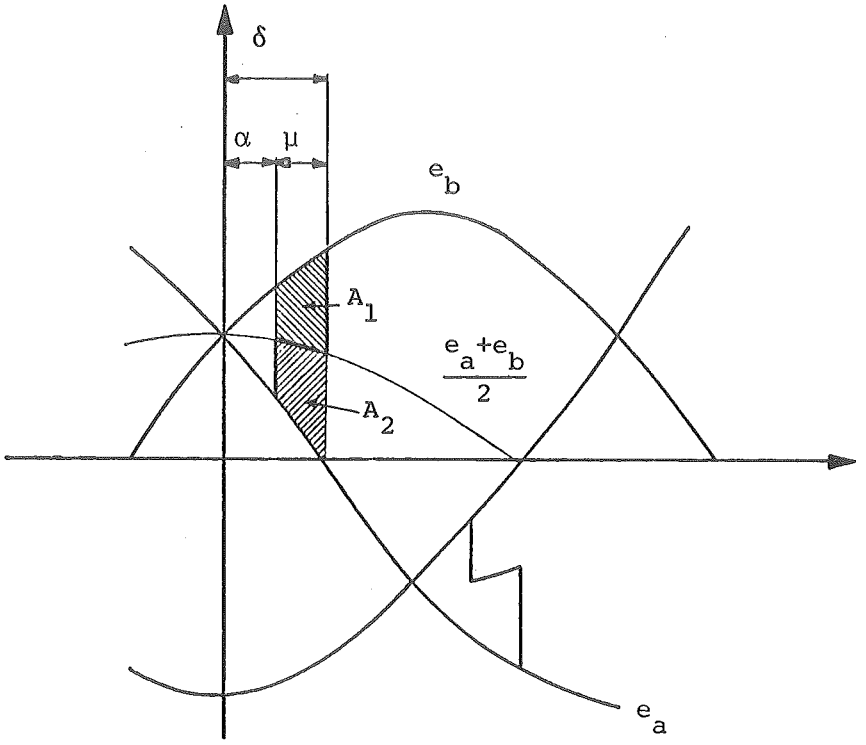

Fig. 5.2 Commutation From Phase a to Phase b.

Equation 5.7 can be written in terms of either α or δ, i.e.:

$$V_d = V_{do} \cos\alpha - {}^3/_\pi \, X_c \, I_d \qquad (5.16)$$

or

$$V_d = V_{do} \cos\delta + {}^3/_\pi \, X_c \, I_d \qquad (5.17)$$

This result can also be derived using

$$V_d = V_{do}(\cos\alpha + \cos\delta)/2 \qquad (5.18)$$

(Kimbark 1971).
Eliminating V_d from equations 5.16 and 5.17 by subtraction and substituting

$$\delta = \pi - \gamma \qquad (5.19)$$

the result is an alternative form of control equation 5.15, i.e.:

$$\cos\gamma^{sp} + \cos\alpha_2 - \frac{\sqrt{2}\, X_{c2} I_d}{a_2 E_2} = 0 \qquad (5.20)$$

5.1.3.2 Series bridges - Under the assumptions of balanced 3 phase AC voltages, converters operating in series can be reduced to a single equivalent bridge. To maintain flexibility in the model should a reduction in the number of operating bridges be required, the formulation accounts for series bridges.

For bridges in series, equation 5.7 is scaled by the number of bridges, NBG, i.e.:

$$V_{d_{Link}} = NBG \cdot V_{d_{Bridge}} \qquad (5.21)$$

5.1.3.3 Including filters in the DC link model -

Filters can be represented either as a shunt element in the TS programme or directly included in the DC link model. They are essential if the assumption of undistorted, balanced voltages at the converter terminals is to be valid. They are therefore included in the DC link formulation.

The addition of filters modifies Fig. 5.1 and equation 5.8. Equation 5.9 is not affected since the filters are considered lossless and do not consume real power. Fig. 5.3 shows filters included at a link terminal.

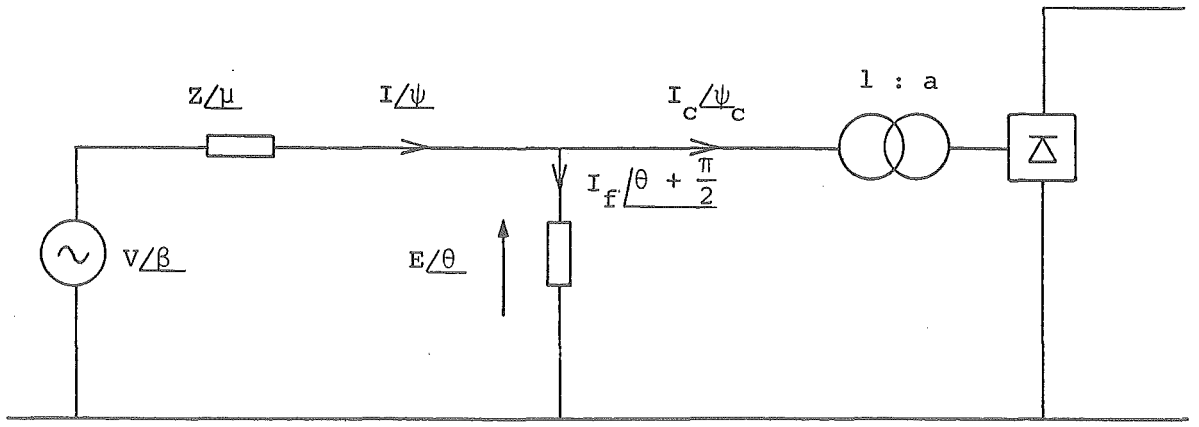

Fig. 5.3 Link Terminal With Filters.

Using Kirchoffs laws at the filter node

$$I \angle \psi = I_c \angle \psi_c + I_f \angle \theta + \pi/2 \qquad (5.22)$$

where $I_f = E. B_f$ and B_f is the filter admittance.

I_c is related to I_d by equation 5.6 so 5.8 becomes:

$$V_j \angle \beta_j - Z_j \angle \mu_j \left[K I_d \angle \psi_{c_j} + E_j B_j^f \angle \theta_j + \pi/2 \right]$$

$$- E_j \angle \theta_j = 0 \qquad (5.23)$$

and $K = \frac{3\sqrt{2}}{\pi} a$

5.1.4 DC Link Control

The Newton-Raphson algorithm allows a flexible implementation of different control modes of the DC link. The basic control characteristics of a link are shown in Fig. 5.4.

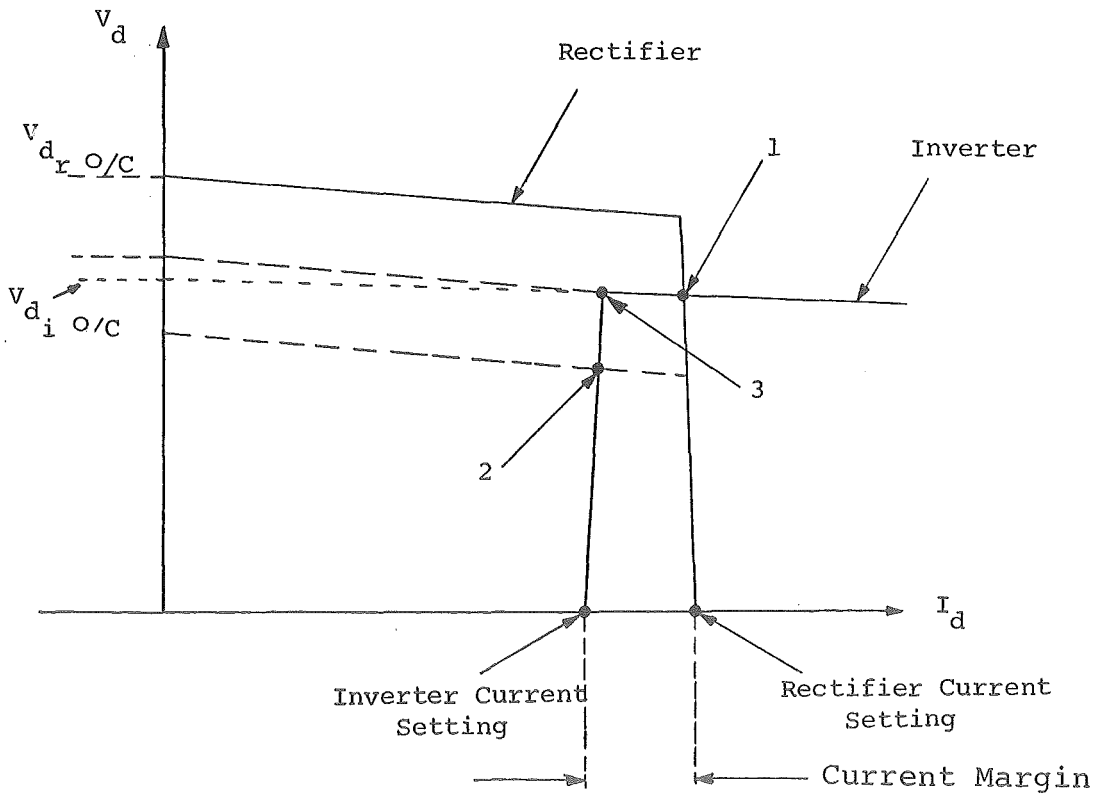

Fig. 5.4 Basic DC Link Control Characteristics.

Three modes of operation are possible:

Mode 1 - operating point 1. This is the normal mode of operation and $V_{dr_{o/c}} > V_{di_{o/c}}$. In this mode the inverter operates on minimum extinction angle (to minimise reactive power consumption) and the rectifier on constant current. The DC link remains in this mode for any drop in AC voltage at the inverter terminal. The control equations 5.14 and 5.15 apply.

Mode 2 - a drop in AC rectifier voltage reduces α_r to its minimum and the inverter takes over control of current. The link operates at point 2 and the control equations become:

$$I_d - (I_d^{sp} - I_{d_{margin}}) = 0 \qquad (5.24)$$

$$\alpha_1 - \alpha_{1_{min}} = 0 \qquad (5.25)$$

Mode 3 - A third mode can be invoked in the transition from points 2 to 1 in Fig. 5.4. In this case both rectifier delay angle and inverter extinction angle are on their minimum and the DC current is determined (within the limits of this mode) by the prevailing AC voltages at the link terminals. This mode usually occurs as the rectifier AC voltage recovers after a disturbance. The control equations become:

$$\alpha_1 - \alpha_{1_{min}} = 0 \qquad (5.26)$$

$$\gamma_2 - \gamma_{2_{min}} = 0 \qquad (5.27)$$

The control equations are written for power flow from converter 1 to converter 2. For power flow in the opposite direction the subscripts of the control equations must be exchanged.

5.1.4.1 Modification of control characteristics - The control characteristic of Fig. 5.4 is drawn for a particular case in which the rectifier commutation reactance, X_{cr}, is greater than the inverter commutation reactance,

X_{ci}. For this case there is only one operating point during the transition from 3 to 1 or vice versa. However if X_{cr} is less than X_{ci} this would not be the case and multiple operating points would exist, as illustrated in Fig. 5.5a (exaggerated).

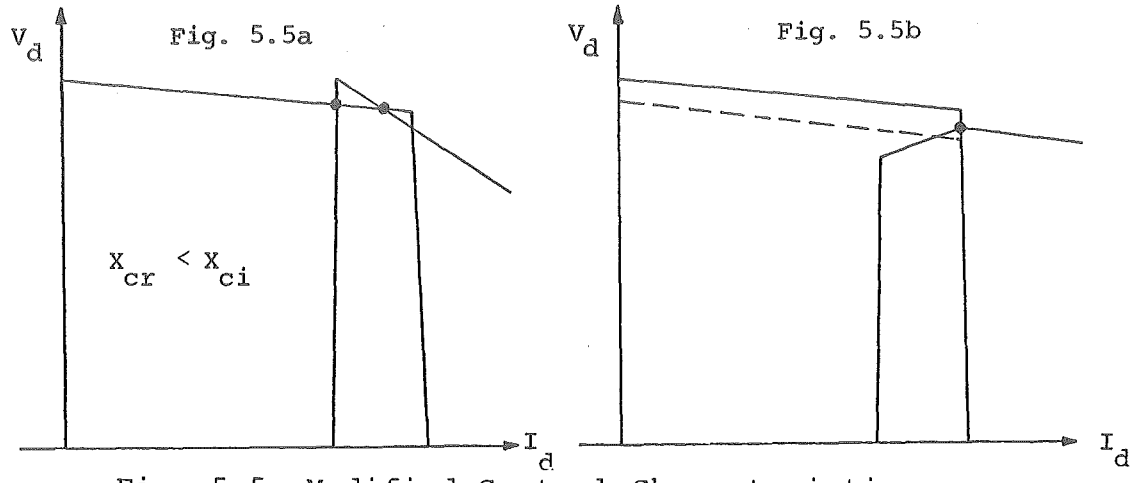

Fig. 5.5 Modified Control Characteristic.

This effect in a digital model can cause an incorrect solution or failure of the algorithm. This difficulty can be overcome (Ainsworth 1977) by modifying the characteristic to that of Fig. 5.5b. It was found to be unnecessary for the NZ DC link case since $X_{cr} > X_{ci}$ and the modified characteristic was not implemented in this model.

5.1.4.2 Implementation of control mode changes - Mode changes are detected when the DC current or a firing angle reaches specified limits. Mode changes after a sudden disturbance are detected and applied at the calculation of new initial conditions. During the iterative process the most common form of mode change takes place during recovery after an AC disturbance in the rectifier AC system. Because of the iterative nature of the unified algorithm a mode change may be detected at any iteration during a solution at any given time. Since the convergence pattern of the Newton-Raphson algorithm is oscillatory, a mode change may be detected early in the iterative loop when the final solution may be only very close to the mode change boundary.

The procedure adopted in this work is to perform one iteration in mode 3 as soon as a mode change is indicated.

i.e.: In transferring from mode 2 to mode 1 a forced iteration is performed in mode 3. Because of the continuity of the equations across the mode change boundaries the forced solution in the middle mode indicates whether an alternative mode choice needs to be made or whether the solution can proceed in the present mode. In some cases, during rapidly changing AC system conditions (i.e. loss of synchronism of a generator), the intermediate mode is not necessary and the forced solution in this mode causes abnormally large updates of some variables. Early in the model testing, this resulted in divergence of the Newton-Raphson algorithm because of the poor starting values for successive iterations. This problem was corrected by restricting variables to feasible values, i.e.:

$$\left.\begin{array}{l} 0 < \alpha_r < \pi/2 \\ \frac{\pi}{2} < \alpha_i < \pi \\ 0 < E_{r,i} \\ 0 < (\theta - \psi)_r \\ (\theta - \psi)_i < \pi \end{array}\right) \qquad (5.28)$$

Extensive testing of this mode changing procedure in many subsequent studies confirmed the success of this approach.

5.1.5 Calculation of Initial Conditions

During a TS study, sudden disturbances, network changes and rapid variations in network variables can be experienced. As discussed in section 3.4.4.1, it is essential that, at every step during the study period, the DC link solution begins with good estimates for the DC variables. In contrast, when the Newton-Raphson algorithm is used in a loadflow study (Harker 1980) it is only necessary to make one estimate for initial conditions.

In the TS case new initial conditions are calculated by a separate estimating process as described below. This

is used at the beginning of a study and immediately after a discontinuity, (i.e. fault application or switching operation). In the initial stages of the model development, a check was made on the rates of change of Thevenin source voltages ($V\angle\beta$ of Fig. 5.1). This was done by comparing the source voltage between successive steps, in case large changes were observed and new initial conditions had to be calculated during the run. However it was found that, apart from the discontinuities of the study, the solution from the previous step provided sufficiently accurate starting values for the next step.

The calculation of initial conditions is based on the new Thevenin voltages obtained for the converters at the beginning of each step. These are obtained from the first estimate of the network state at each step and are generally close to their final value at that step. Referring to Fig. 5.1 and variables given in 5.13 the initial estimates are made by the following procedure:

i) Estimate for E obtained by $E_j = V_j$

ii) Estimate for θ obtained by $\theta_j = \beta_j$

iii) Estimate for ψ_j obtained using an assumed link terminal power factor of 0.9

iv) Using equations 5.16 (or 5.17) in which α (or γ) is set to its minimum and with the DC current on its setting, the maximum DC voltage possible at both terminals can be obtained.

v) By evaluating the LHS of equation 5.11, with the DC voltage calculated from (iv) above, and testing for sign, the control mode of the link can be determined.

vi) With the control mode chosen, the value of α at the terminal controlling current, can be evaluated and the two control variables can be set to their specified values.

This procedure has been successfully used for a large number of TS studies with excellent reliability.

5.1.6 Algorithm Performance

The Newton-Raphson algorithm converges rapidly when given good starting values and this feature was noticeable for this application. The iterative and computational performance quoted here has been generalised from a large number of TS studies.

i) Convergence after a discontinuity usually takes only 3-4 iterations and sometimes, (5% of cases), took 5 iterations.

ii) During the rest of the TS run, convergence at the first AC iteration of a new step took 2 and sometimes 3 iterations. In most cases the total number of iterations per step was 3-4.

The computation time required for a two terminal DC link model is independent of the size of the AC system. In a real time study period of 1 second duration, the CPU time used by the DC link routine was approximately 12 seconds on a Burroughs B6700 computer. This is equivalent to the solution time for a 4 busbar, 5 line, 3 machine system. Hence for a study in a large system the DC link computation time becomes insignificant.

The times quoted here are times for a development programme written in FORTRAN IV and no attempt has been made to achieve optimum programme efficiency.

5.1.7 Programme Options

A number of options have been included in the QSS model to provide facilities for subsequent studies.

i) Application and removal of a DC line fault at specified times during the study.

ii) Under voltage shutdown of the link. This occurs when the AC voltage has dropped to 30% of its nominal operating level. Although filters are included in the link formulation, special provision is made, during the link shut-down, for them to remain connected to the AC system.

iii) Ramped increasing of DC current setting when the link restarts from a shutdown.

iv) Fixed percentage changes in nominal current setting at specified times.

v) Changes to nominal current setting determined by the slip of a specified machine.

vi) DC link power flow reversals at specified times with or without the ramped setting response.

vii) Provision to replace the QSS model, for a part of the study, with results derived from a transient converter simulation. To demonstrate the programming organisation of the QSS model a flow diagram is given in Fig. 5.6. In this flow diagram arrows from the side indicate entry to the DC link subroutine from the TS programme.

5.2 INCLUSION OF TRANSIENT CONVERTER SIMULATION RESULTS

When a detailed transient converter simulation has been performed on a system, the TS compatible equivalents derived from the results, (as per chapter 4), can be used to replace the QSS model during the most disturbed part of the study. When the response of the DC link has settled the TCS is terminated. The TS study then reverts back to using the QSS DC link model for the remainder of the study.

5.2.1 Solution At the Link Node Using TCS Input

The information from the TCS is embodied in real power (P_{dyn}), and voltage, (E_{dyn}), variables obtained from processing of the TCS waveforms. These become the specifications at the link terminal node when the QSS model is removed. Using the unified algorithm, the system equivalent of Fig. 5.7 is solved, given the P_{dyn} and E_{dyn} specifications.

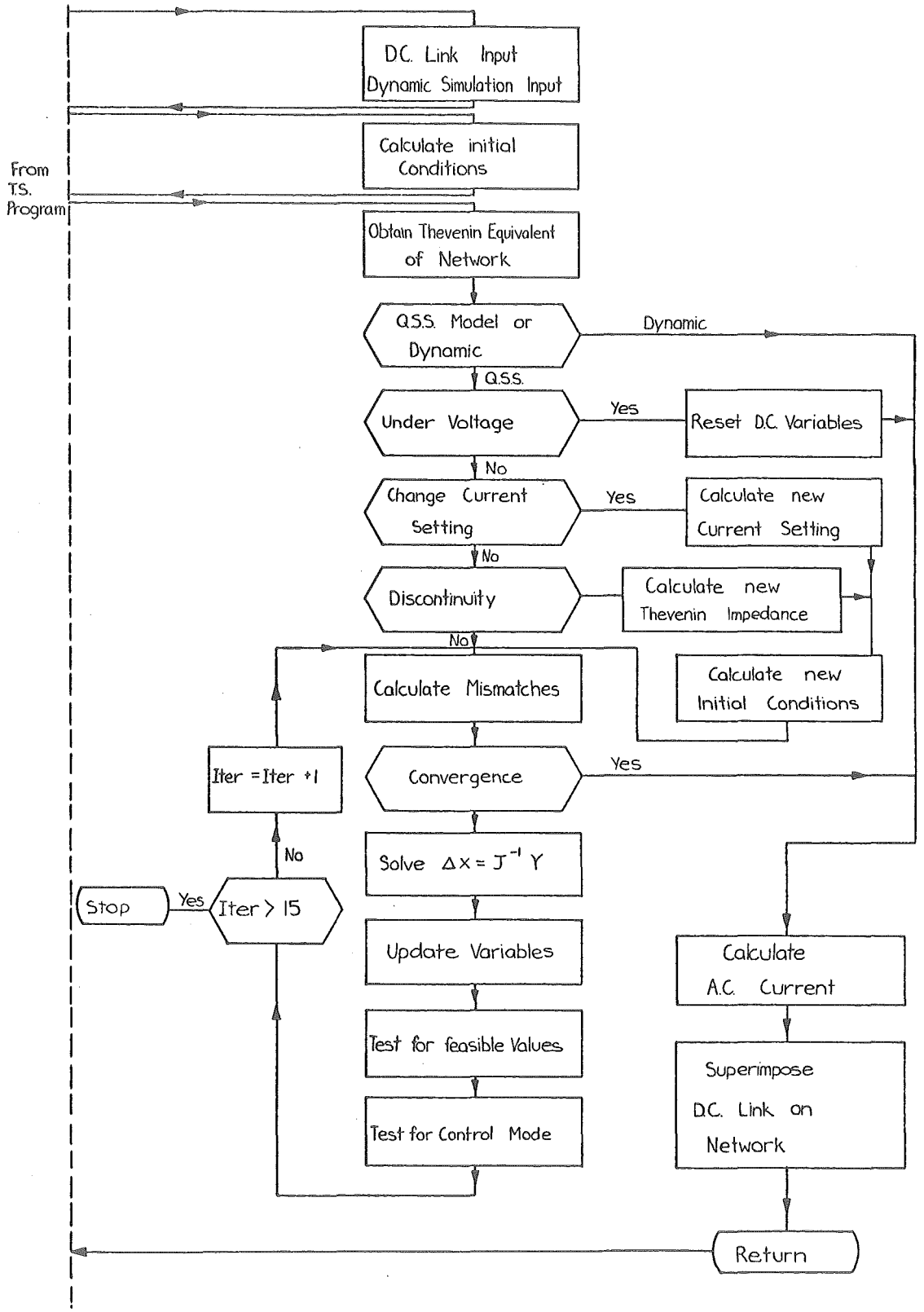

Fig. 5.6 QSS DC Link Model - Programme Flow.

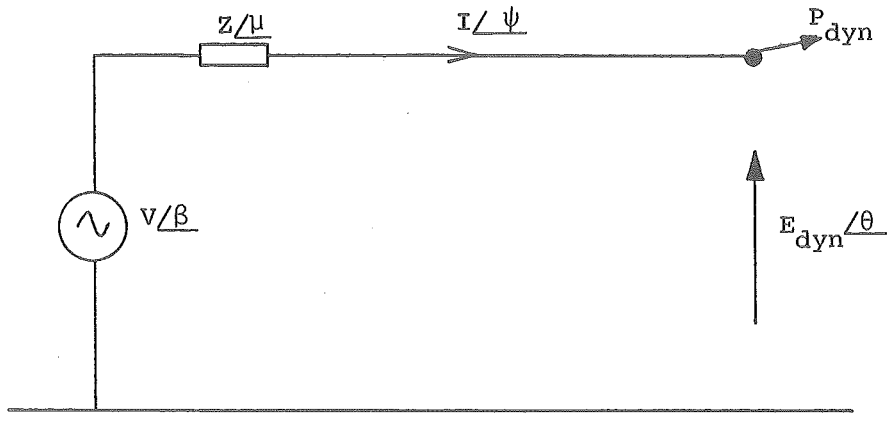

Fig. 5.7 Equivalent System for Including TCS Data.

This system can be solved directly for the AC currents which can then be superimposed on the AC network in the same way as the AC current from the QSS model.

$$\text{Using} \quad \bar{S} = \bar{E} \cdot \bar{I}^* \tag{5.29}$$

$$\text{where} \quad \bar{E} = E_{dyn} \angle \theta \tag{5.30}$$

$$\text{and} \quad \bar{I} = (V \angle \beta - E_{dyn} \angle \theta)/Z \angle \mu \tag{5.31}$$

$$\text{we obtain} \quad \bar{S} = (E_{dyn} \cdot V \angle \theta + \mu - \beta)/Z - (E_{dyn}^2 \angle \mu)/Z \tag{5.32}$$

Taking real parts of equation 5.32 and rearranging, θ can be solved for directly.

$$\text{i.e.} \quad \theta = \beta - \mu + \cos^{-1}\left[(P_{dyn} Z)/(E_{dyn} \cdot V) + (E_{dyn} \cdot \cos\mu)/V\right] \tag{5.33}$$

The AC current can now be obtained using equation 5.31. This solution requires little computational effort when compared to the QSS link model.

5.2.2 Alignment of TCS Input with TS

The TCS results are reduced to a sequence of data points, spaced 0.01 seconds (half a cycle) apart and

represent the fundamental component over the cycle spaced about that point. The integration step of the TS study is fixed at 0.01 seconds to coincide with the data points from the TCS. In the TS study, at a disturbance initiation, a new solution is obtained for the system immediately after the disturbance application. However, because the TCS results are essentially waveform orientated, a correct data point cannot be obtained at the new solution after disturbance application.

It is therefore necessary to extrapolate the processed TCS data points to provide, as closely as possible, a representation of the link performance immediately before or after a disturbance application. This effect is demonstrated in Fig. 5.8 in which the discrete integration steps of the TS study are related to the data points obtained from TCS.

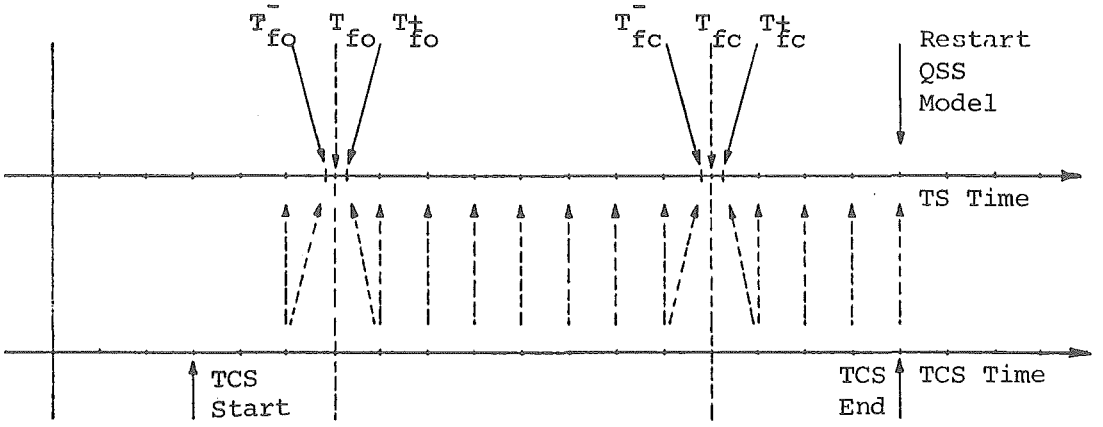

Fig. 5.8 Data Alignment Between TCS and TS Programmes.

Fault clearance requires special consideration as the mechanism differs for the two models. In the TS model the inherent assumption is made that at the time of fault clearance, T_{fc}, all three phases clear simultaneously and a new solution is obtained immediately (i.e. at T_{fc}^+). For the TCS, although the decision is made to clear the fault at T_{fc}, only one phase will open within 60° of T_{fc} (i.e. at the first current zero), the remaining phases opening in the following 120°. This would appear to distort the alignment of the two models for the TS solution at T_{fc}^+.

However the disturbance caused by the first phase clearance has the greatest influence on d.c. link control, and in spite of the TCS clearing delay, the post fault TCS data, obtained by processing one full cycle after T_{fc}, can be used to superimpose the immediate effect of the fault clearance on the TS solution at T_{fc}^{+}.

At the first and last points of the TCS data sequence, the QSS model is solved as well, to provide a check on the accuracy of matching between the two programmes and the two link models. Initially the final point of the TCS data was used for calculation of the QSS model initial conditions but this was found to be unnecessary and the method outlined in section 5.1.5 was retained.

5.2.3 Interactive Coordination Between Programmes

In the early stages of this work the system equivalent used for TCS was obtained from an AC-DC faults programme. (Lake 1978). Obtaining a TCS whose results corresponded to a TS study, required a considerable degree of coordination between 4 programmes. Figure 5.9 is a flow diagram showing the interaction between the loadflow, faults, TCS and TS programmes. It was necessary to ensure the system data used by each programme was identical before results from a TCS, via the left hand path of Fig. 5.9, were compatible with the TS study. However the initial studies performed using a fixed system equivalent (i.e. Via the left hand path of Fig. 5.9), showed a considerable mismatch between the TS and TCS programmes. In the case of the TS study the system equivalent of Fig. 5.7, used for introducing TCS results, is time variant while the faults programme fixed equivalent is only valid at one instant in time.

The mismatch was eliminated by using the TS programme to generate a time variant system equivalent for the TCS via the right hand path of Fig. 5.9.

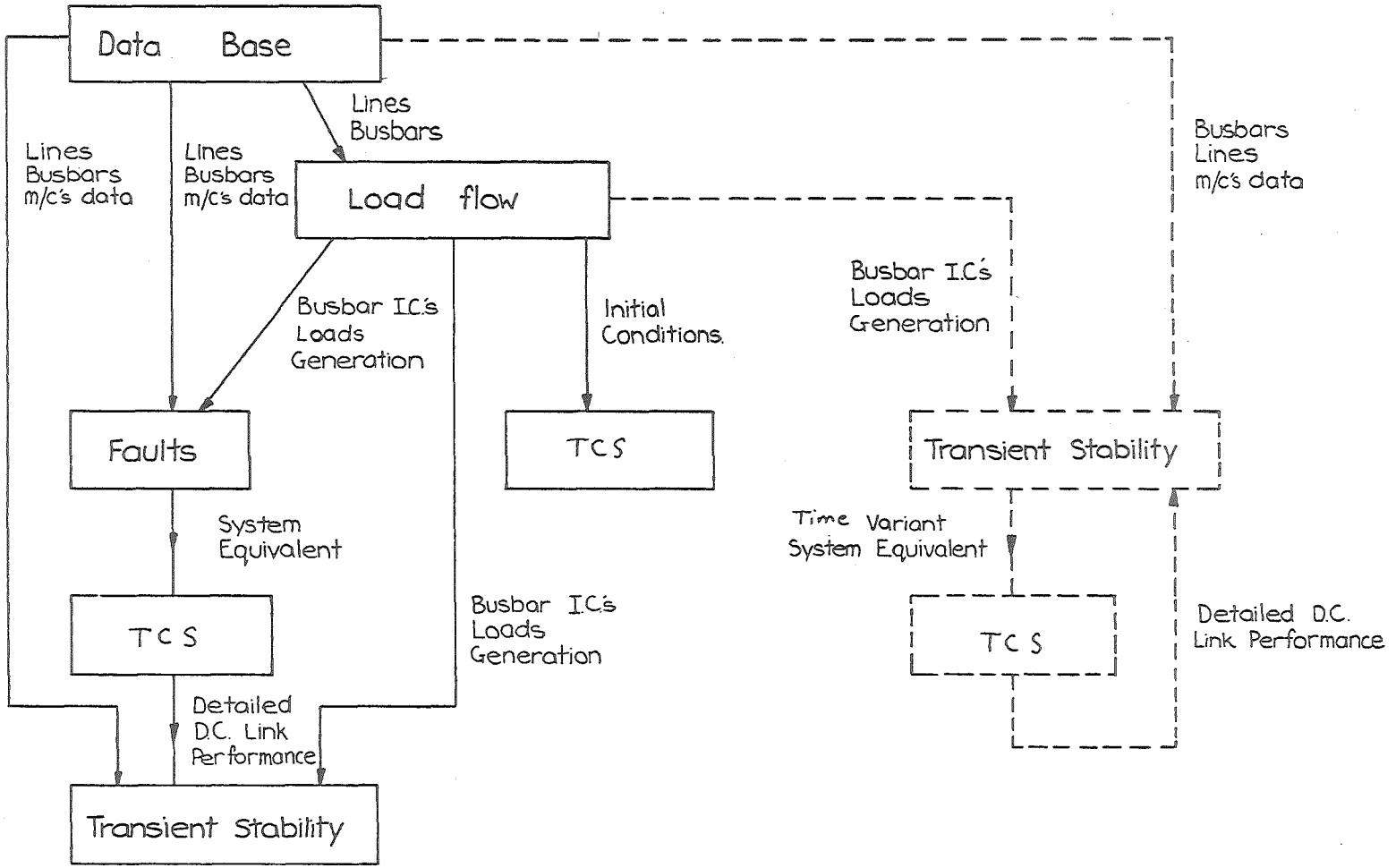

Fig. 5.9 Coordination Between Programmes.

At every integration step of the transient stability programme (every ½ cycle), the AC network is reduced to a Thevenin equivalent at each DC link terminal. Such equivalents at each time step constitute a reduced representation of the AC system as seen from the converter terminals and they include all associated generator effects. In order to provide explicit representation of a faulted bus within the AC system, a third Thevenin equivalent can also be obtained, at each integration step of the transient stability study, by looking back into the AC network from that point. Therefore the transient stability study produces a time variant sequence of network equivalents, the variation of which will be a function of the disturbance investigated.

Initial time-variant network equivalents are obtained for a QSS solution of the DC link model in the transient stability study and these are transferred to the first transient simulation of the convertor network.

An iterative process can be used, as detailed in Fig. 5.10, to improve the interaction between the two programmes. Two such iterations were performed for the severe inverter fault case discussed in the next chapter but inspection of the Thevenin equivalent sequences obtained showed differences of less than 1%.

It is possible to observe the trends as a transient convertor simulation progresses, since the simulation may be halted at any particular stage. By storing all state variable information at the last time step, the analysis may be restarted using this information for the exact initial conditions of the succeeding stage. The transient converter simulation will thus consist of n consecutive stages, and if necessary, between any two of these stages it is possible to interactively modify the performance of the QSS DC link model according to the transient converter simulation results. This provides very closely matched time-variant AC network equivalents for succeeding transient converter simulation stages.

Although several short duration transient stability runs may be required with this approach, these are

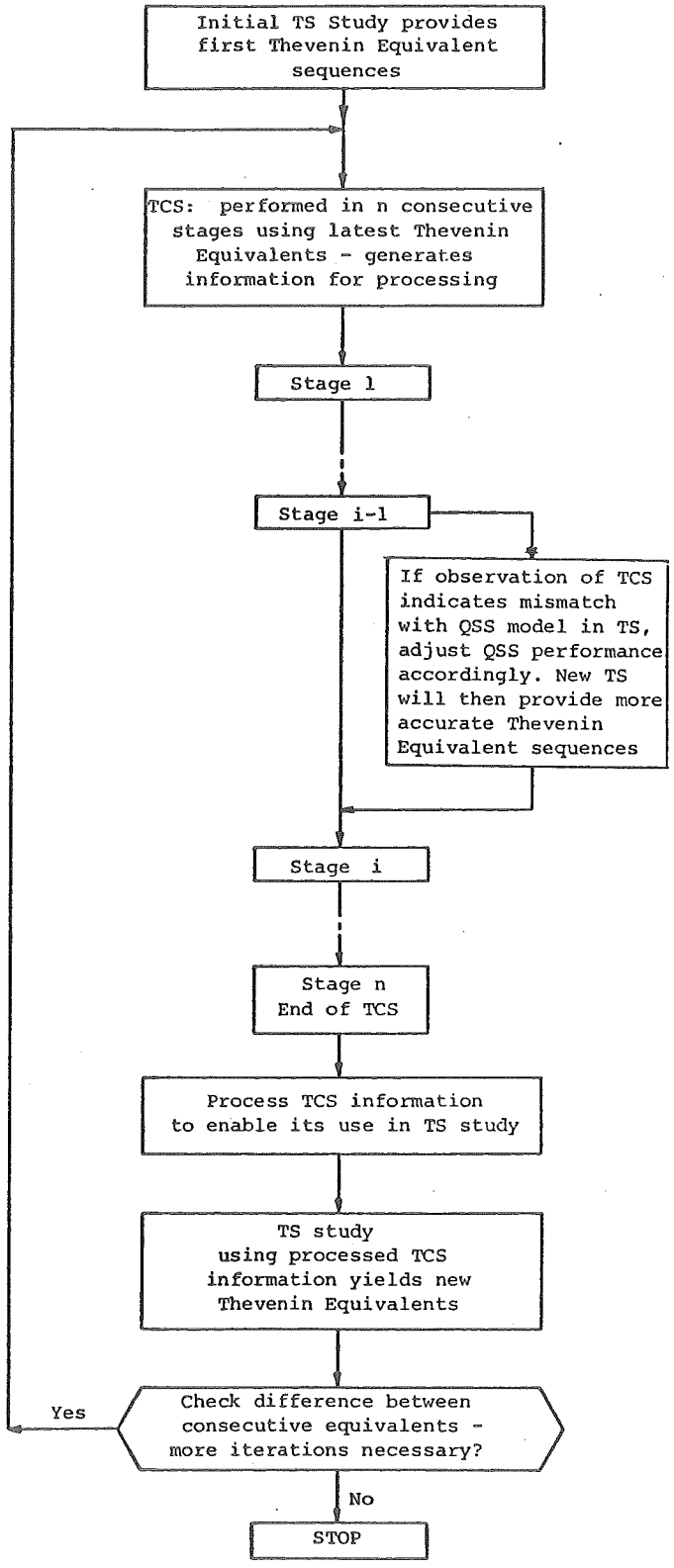

Fig. 5.10 Flow Diagram of Interaction Between Transient Convertor Simulation (TCS) and Transient Stability (TS) Programmes.

relatively inexpensive and they minimise the computing time of the transient converter simulation by eliminating the need for the iterative process.

5.2.4 System Equivalents for TCS

The fixed system equivalent obtained from the faults programme retains explicitly the faulted bus of the AC system. This is important to the TCS programme as it allows studies to include effects of the DC link nonlinearities in the fault current. (Arrillaga et al 1980).

5.2.4.1 Obtaining time variant equivalents - The provision of a time variant system from the TS programme is simplified for the DC fault case. For this case it is not necessary to provide explicit fault bus representation since the fault is contained within the DC system being simulated. The equivalent provided for the TCS programme in this case is exactly the same as that obtained for the QSS DC link model.

The provision of a time variant equivalent for an AC fault case is complicated by the technique used for applying a fault in the TS programme. The fault admittance is included directly in the admittance matrix of the network when the fault is to be present. (Arnold 1976). In this situation the fault bus is included implicitly in;

$$\bar{V} = [\bar{Y}]^{-1} [\bar{I}] \qquad (5.34)$$

This difficulty was solved by eliminating direct fault inclusion in the admittance matrix and instead solving for the fault current using the Thevenin equivalent at the faulted node. The fault current can then be superimposed onto the network in the same way as the injected current obtained at the DC link nodes.

It is necessary to solve both the fault and the DC link simultaneously because of the mutual coupling between them; i.e.

$$V_{m_f} = V_m + Z_{mm}I_m + Z_{mn}I_n - Z_{mp}I_f \qquad (5.35)$$

and similarly for the other link and fault nodes, where I_m and I_n are injected currents due to the link at terminals m and n and I_f is the fault current at fault node p.

The simultaneous solution can be achieved by reformulating the DC link model completely so that the fault equations 5.35 are directly included in the Newton-Raphson algorithm. However this special formulation is only required to provide the time variant equivalent for TCS and only during the fault period. The need to reformulate the DC link model for this specific, and little used case, does not justify the extra computational and programming effort for a facility not required in normal TS studies.

5.2.4.2 Algorithm for simultaneous fault and link solution - A simple algorithm was devised which retained the existing DC link model but involved it in a simultaneous solution of the fault when it was applied.

The solution of the fault is obtained by the simple network of Fig. 5.11 where V_p and Z_{pp} are the Thevenin voltage and impedance at the fault bus. The fault current

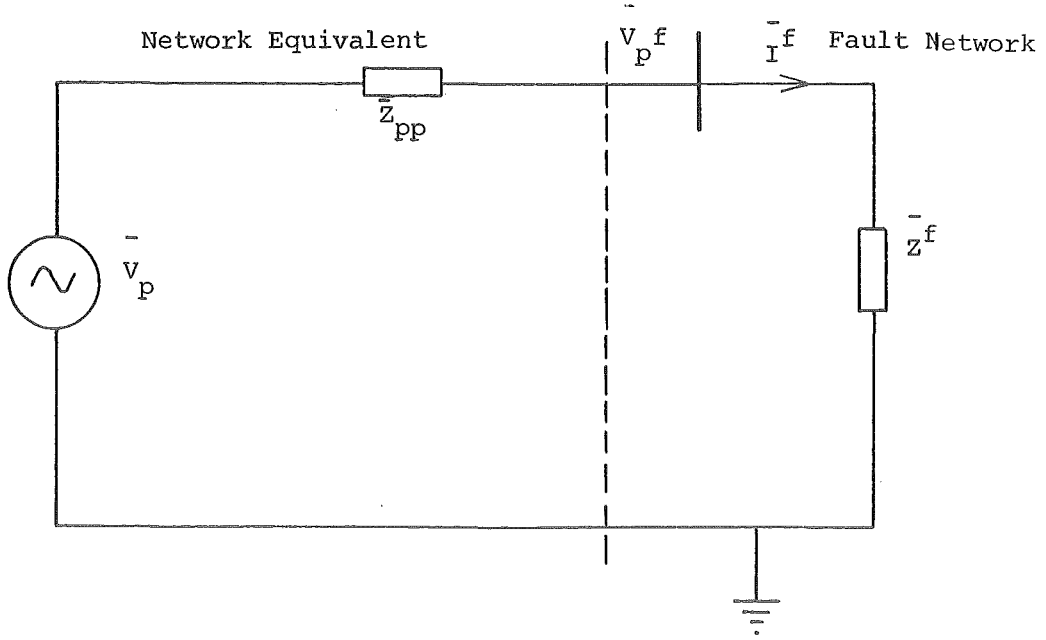

Fig. 5.11 Fault Bus Representation.

is obtained from:

$$\bar{I}_f = \bar{V}_p / (\bar{Z}_{pp} + \bar{Z}_f) \qquad (5.36)$$

For this to be a correct solution the Thevenin theorem states (Skilling 1965) that all other voltage and current sources must be present, i.e., the network equivalent at the fault bus must be obtained with the DC link injected currents included. The converse also applies in obtaining the correct solution for the DC link. The solutions of both link and fault were combined in the algorithm of Fig. 5.12.

The algorithm relies on a good estimate of the DC injected currents at the first iteration of each step if the speed of convergence of the TS programme is not to be impeded. The link solution obtained at the previous step proved to be quite successful except for the first iteration after fault application. In this case, since the fault has a dominant effect on the network, it is solved alone at the first iteration. A new DC link solution can then be obtained for entry into the algorithm at A of Fig. 5.12. This starting process is illustrated in Fig. 5.13.

5.2.4.3 Algorithm tests - The algorithm was tested against the normal fault representation to ensure accuracy and observe any degradation in convergence. Accuracy was not affected but, at some steps during the run, convergence required an extra iteration of the TS programme. For the case examined, the normal fault representation required a total of 57 iterations during a 5 cycle fault period while the superimposed fault case required 61.

The network equivalent for TCS is obtained from the last iteration at each time step. Since the fault and DC link are automatically solved simultaneously, the equivalent required for the TCS programme does not have either the link or fault included.

It is not possible to compare the equivalents from the faults and TS programmes directly. The faults programme

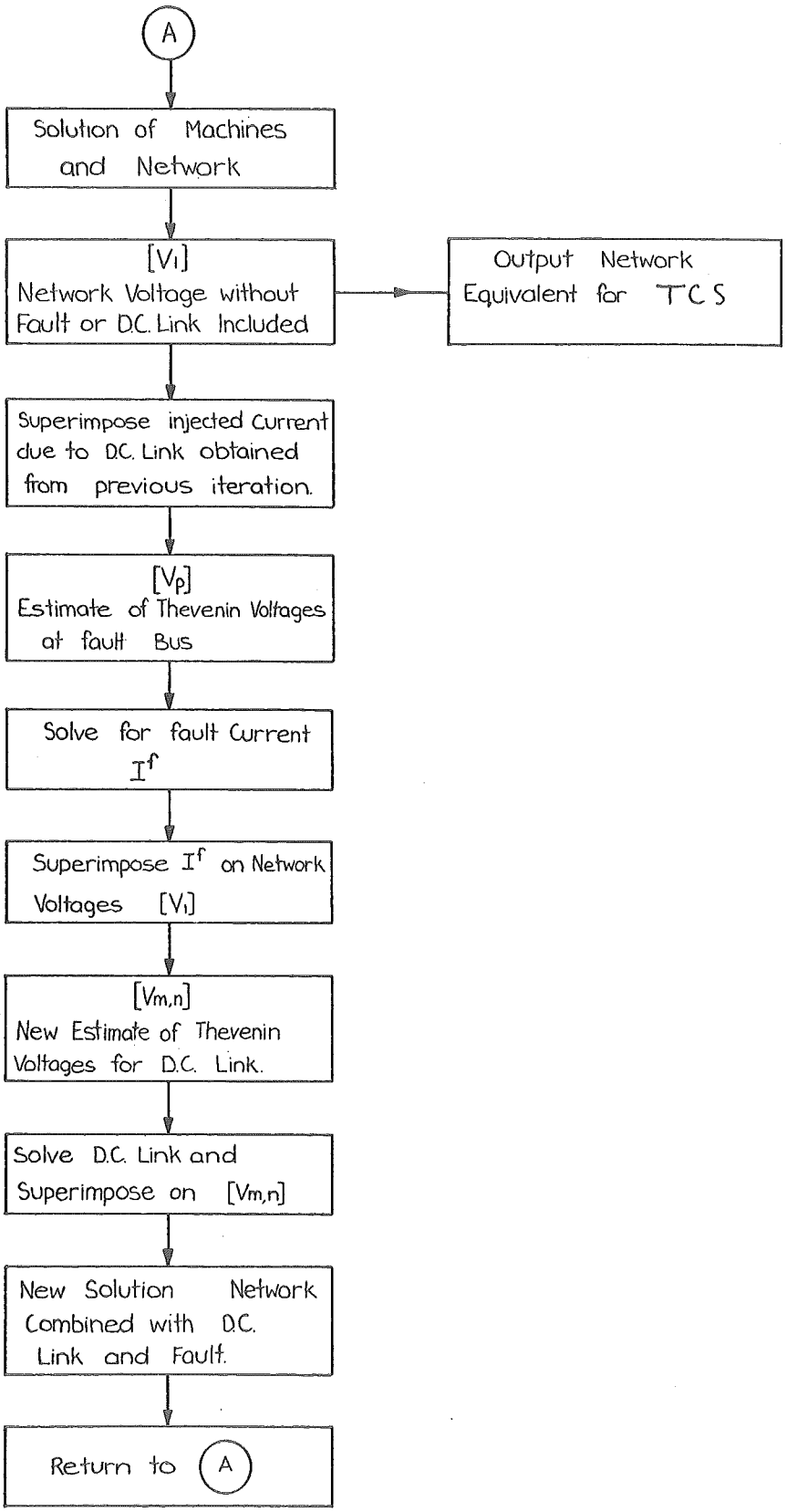

Fig. 5.12 Simultaneous Solution of Fault and DC Link.

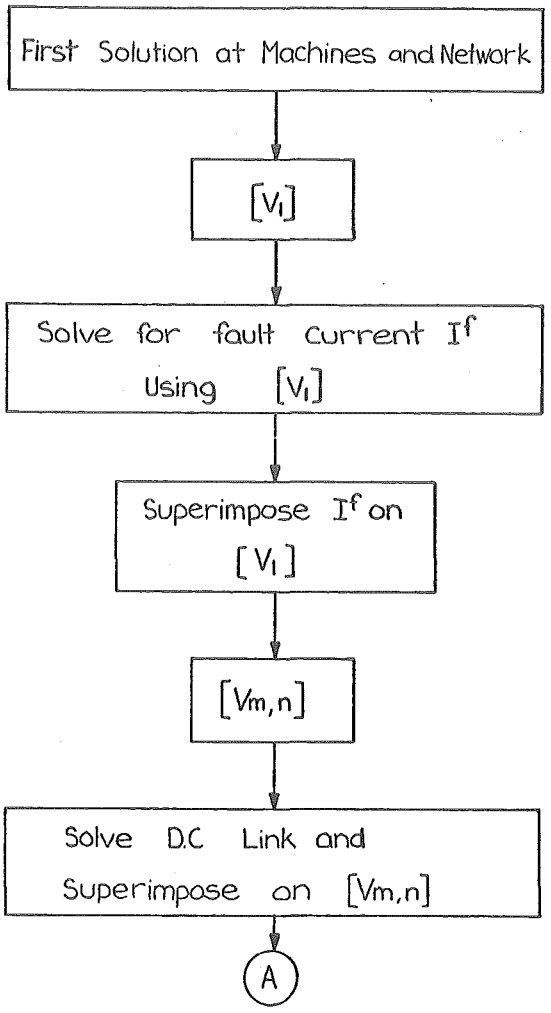

Fig. 5.13 Starting Process After Discontinuity.

uses the generator transient reactance, X'_d , in its admittance matrix so as to obtain a fault current which is valid approximately 3 cycles after fault application. The TS programme includes the subtransient reactance, X''_d , where this is available, in the admittance matrix and the Thevenin voltage reflects the dynamic response of the network. To ensure that correspondence existed between the faults and TS equivalents a short simulation was performed with no disturbances applied, to confirm that the results were identical. No discernible difference was observed between the two runs.

5.3 CONCLUSION

The choice of the unified algorithm for the QSS model, although more complex to programme, has proved to be very reliable and has not affected the convergence properties of the AC part of the TS programme. The model is adaptable to

a wide range of special performance features related to DC links, many of which have been included for subsequent studies. The computational effort for the QSS model is small when compared with that required for large AC systems and this could be further improved by optimised programming.

The use of the unified approach to include TCS results has proved to be simple and reliable. As a result of a number of studies, no convergence problems have been experienced even with conditions which lead to failure of the sequential method. The interactive model developed provides a useful tool in assessing convertor controllability during disturbances and provides an alternative to the use of physical simulators. A technique has been outlined for evaluating time variant equivalents, to provide interactive coordination between the TCS and TS programmes, without modification to the existing QSS model. The approach does not increase the number of variables in the QSS model and is only required once, before a transient converter simulation is to be performed.

CHAPTER 6

STUDIES WITH COMBINED TCS AND QSS DC LINK MODELS

6.0 INTRODUCTION

The purpose of this chapter is to combine the QSS model presented in Chapter 5 with the processed transient converter simulation (TCS) results, obtained by the methods discussed in Chapter 4, to examine the effect of DC link models in transient stability studies. The differences between the TCS and QSS results are discussed with the reasons why these differences occur. The effects that these differences have on TS analysis are presented. In addition, the accuracy of the approximations, discussed in section 4.4, is monitored to ensure that they can be applied for these TCS results.

6.0.1 System Studied

The NZ primary generation and 220 kv transmission network was used for the studies discussed. The SI network is illustrated in Fig. 3.1 and the NI system in Fig. 6.1.

Data for this network and the DC link connecting the NI and SI systems is readily available and is included in Appendix A6. The normal direction of power flow for the DC link is from the SI to the NI although the link was modified in 1976 to become bidirectional. The studies that are presented in this chapter are for DC power flow in its normal direction. The AC network at the Benmore (rectifier) terminal is relatively strong and the generators and filters at Benmore are used for reactive power compensation. The AC network at the Haywards (inverter) terminal is supported by synchronous condensers and filters. The Haywards terminal is close to a large load centre and this load has some influence on the inverter AC terminal conditions.

The NZ DC link consists of a 500 kv bipolar transmission line of 535 km from Bemore to Cook Strait, 40 km of

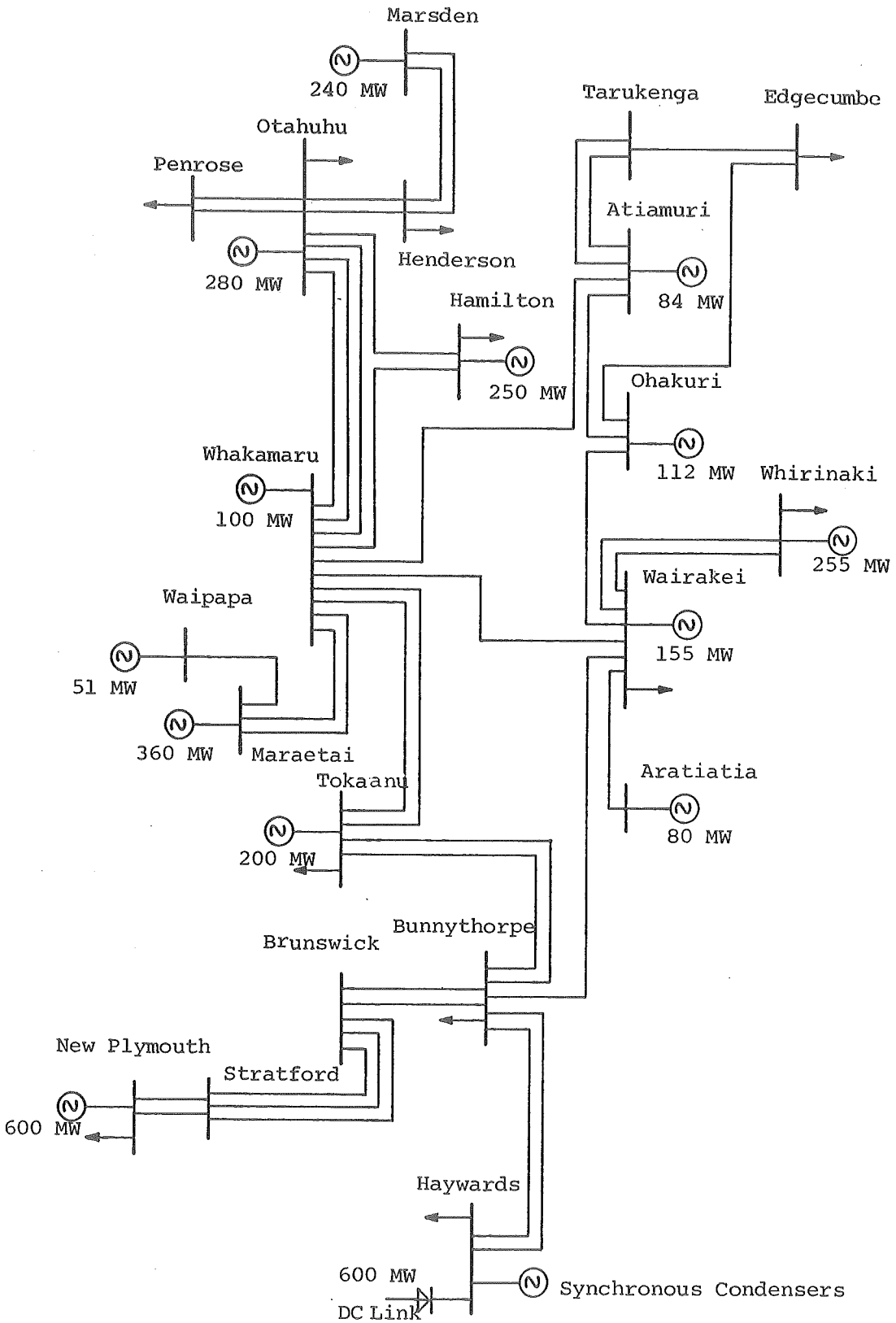

Fig. 6.1 NZ North Island Primary System.

undersea cable and a short length (35 km) of overhead line to the northern terminal at Haywards. Each pole converter has two mercury arc 6 pulse bridges in series.

For the purpose of the QSS model the link is modelled as a single bridge. For transient converter simulation the DC link is represented using a 12 pulse configuration as illustrated in Fig. 6.2

In this representation the transient stability programme, using a QSS DC link model, provides the time variant system equivalents for the TCS. In turn the instantaneous values of I_1, I_2, E_1 and E_2 of Fig. 6.2 are obtained from the TCS to provide rms power and fundamental frequency voltage at the converter terminal bus, for use in the transient stability programme.

6.0.2 Disturbances Examined

Because of the time consuming and expensive nature of TCS it is not possible to perform large numbers of such simulations. It was thus necessary to choose carefully the cases for which TCS would be of maximum benefit. Three cases were chosen:

i) Rectifier AC System Fault: This study was performed as an initial test of the coordination between the two programmes. It is intended to provide a disturbance during which the DC link behaviour remains within the range of applicability of the QSS equations so that the accuracy of the QSS model can be assessed. It was also used to provide detailed information on AC faults. (Arrillaga et al 1980).

ii) Inverter AC System Fault: This study was performed as a case for which there would be a maximum difference between the TCS and QSS model performance. A depressed AC voltage at the inverter terminals provides conditions for commutation failure and the QSS model is unable to detect or model this type of link behaviour.

iii) DC Line Fault: The DC line fault differs from its AC counterpart in the clearance time and its effects on the AC system. The DC fault case was studied to obtain a detailed analysis of the DC link performance and recovery. (Heffernan

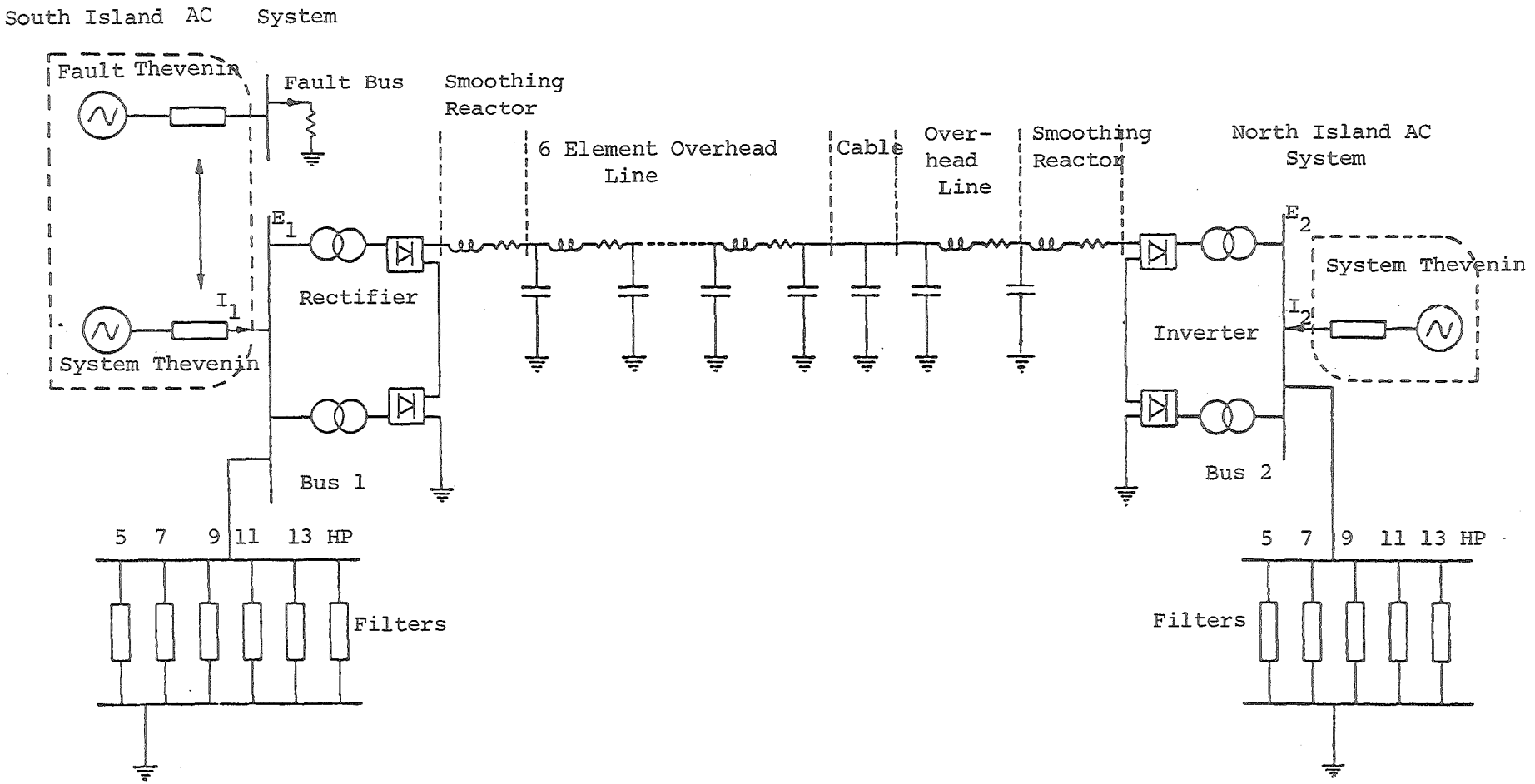

Fig. 6.2 DC Link Representation for Transient Converter Simulation.

et al 1980). The QSS model in this case was matched as closely as possible to improve the correspondence between the two models.

6.1 RECTIFIER AC SYSTEM FAULT

A three-phase fault of 5 cycle duration was applied at the Twizel bus of the SI system (see Fig. 3.1). The fault produced a 25% drop in AC voltage at the rectifier terminal immediately after fault application but represents a severe disturbance to the SI AC system because of its position. This case study is coded 2321.

6.1.1 The Effect of Time Variant Equivalents

The initial approach to combining the TCS and TS programmes was to use a fixed system equivalent obtained from an AC-DC faults programme, as discussed in section 5.2.3. The first combined TS analysis used this approach and showed up an immediate problem.

As a result of specifying voltage and real power at the converter node, the power factor of the injected current was forced to change from lagging to leading in order to satisfy the state of the node as defined by the TCS results. As shown in curve 2 of Fig. 6.4, this results in the impossible condition of the converter supplying reactive power to the system.

The condition arises because the fixed equivalent used for TCS does not match the time variant response of the AC system. With the fixed network equivalent, the AC rectifier terminal voltage remains relatively constant during the fault period, as illustrated in curve 2 of Fig. 6.3, while the source voltage (with a QSS model, curve 1 of Fig. 6.3) decays due to the dynamic response of the generators nearby. The voltages cross over approximately 2 cycles after fault inception and this coincides with the change in power factor illustrated by curve 2 of Fig. 6.4. This demonstrates that the solution of the faults programme, using the transient reactance of the machine, is valid only at a single point in time, in this case at 2 cycles after fault inception.

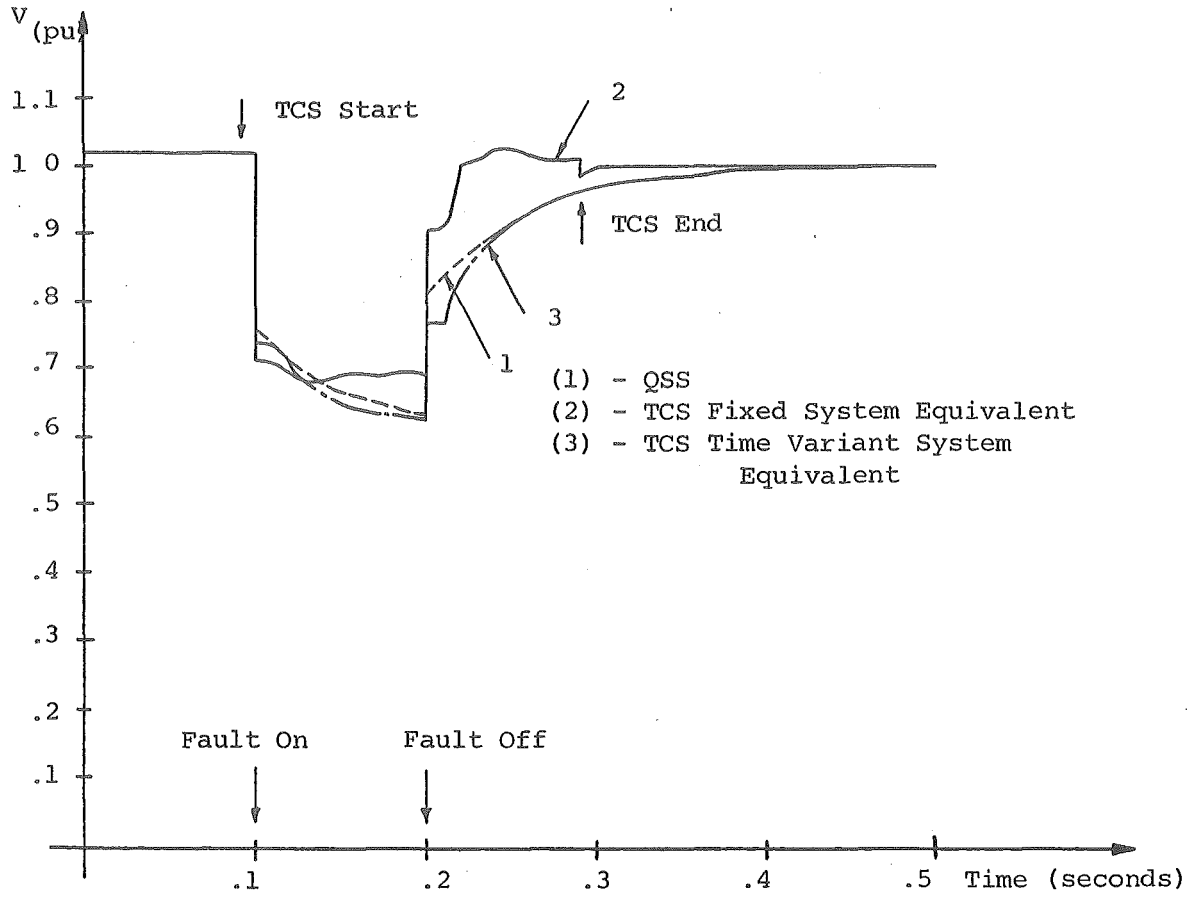

Fig. 6.3 Rectifier Terminal AC Voltage - Case 2321.

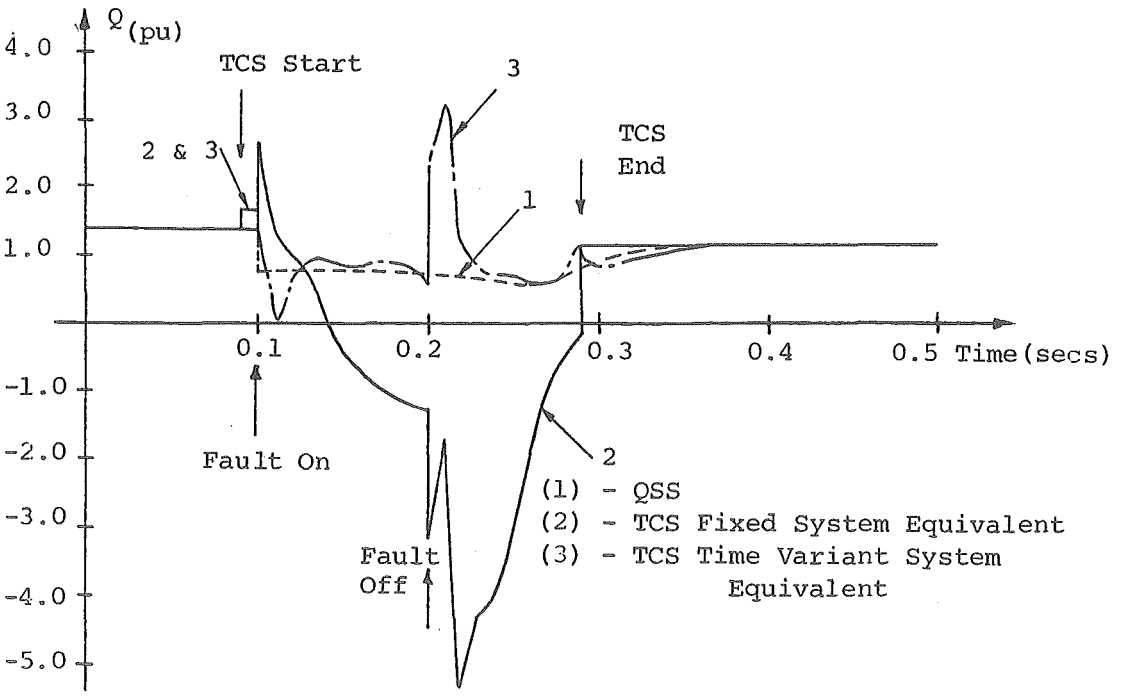

Fig. 6.4 Rectifier Reactive Power - Case 2321.

It is clear from these initial results that fixed equivalent modelling of the AC system during disturbances, is not acceptable. This is further emphasised during the post fault period where the TCS recovery voltage considerably exceeds that of the dynamically responsive system. (Curves 1 and 2 of Fig. 6.3). This is also supported by the post fault reactive power response of curve 2 in Fig. 6.4.

A new approach to obtaining a system equivalent for TCS has been developed. An equivalent is obtained directly from the transient stability study at each integration step of the study. This simplifies the degree of coordination required between different programmes and the dotted part of Fig. 5.9 is invoked. With the AC fault bus represented explictly (as described in section 5.2.4) and no other topology changes, the Thevenin impedance remains constant and the time variant nature of the network is observed in the changing Thevenin voltage. The time variant Thevenin voltage is interpreted by the TCS programme, to provide it with an instantaneous source voltage at each integration step. An example of the time variant Thevenin voltages for the rectifier AC system fault, is illustrated in Fig. 6.5. The voltages reflect the dynamic behaviour of the network and also provide a basis for a more detailed analysis of fault development using the TCS programme.

6.1.2 Comparison of Results

6.1.2.1 Differences in voltage and reactive power -

A second simulation was performed using the time variant system equivalent. The results of this simulation are included in Figs. 6.3 and 6.4, as curve 3. These figures illustrate that a much better match between the QSS model performance and the TCS results is achieved. The voltages of Fig. 6.3 exhibit small differences, particularly after fault removal. The requirement to match the TCS results with the TS integration steps, at the disturbance times (refer to Fig. 5.8), distorts the behaviour of the TCS results immediately after fault removal.

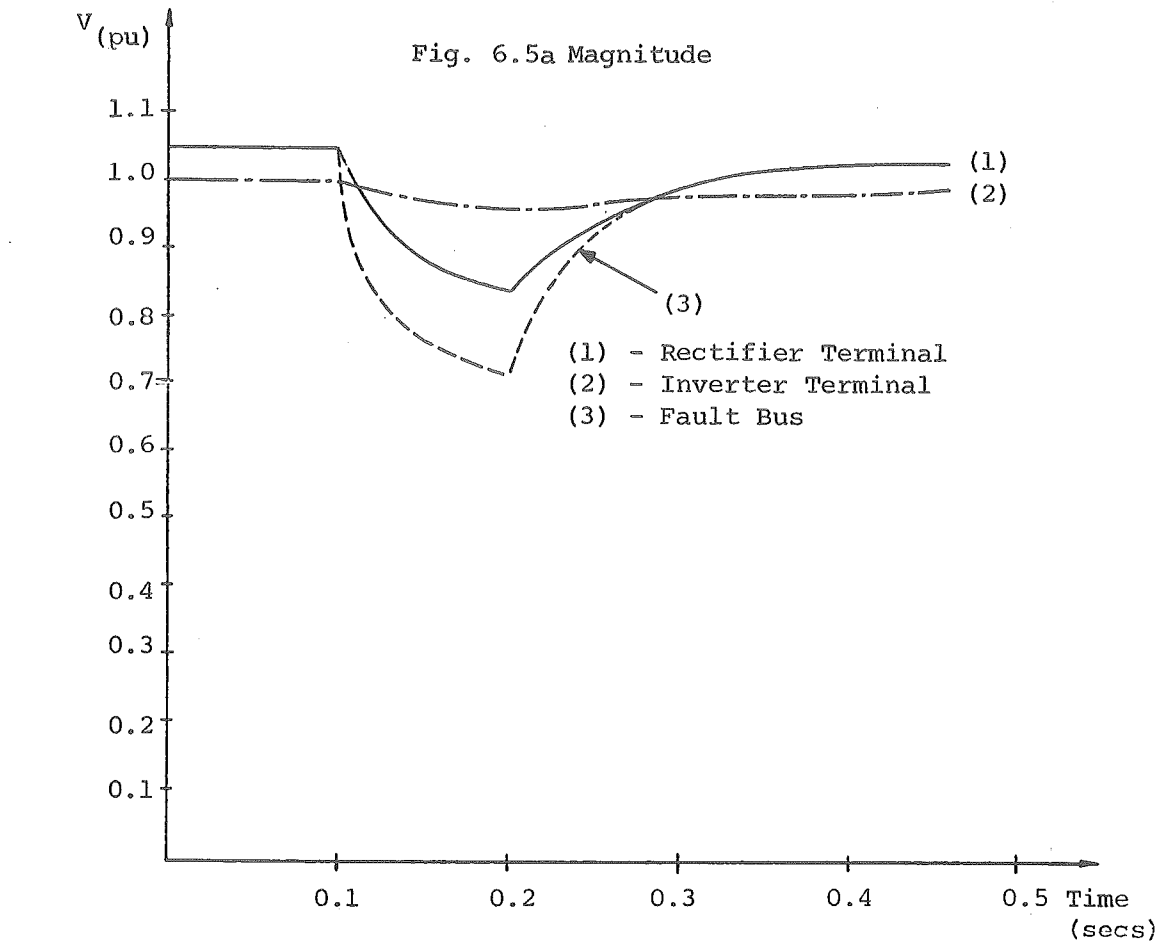

(a) Fig. 6.5a Magnitude

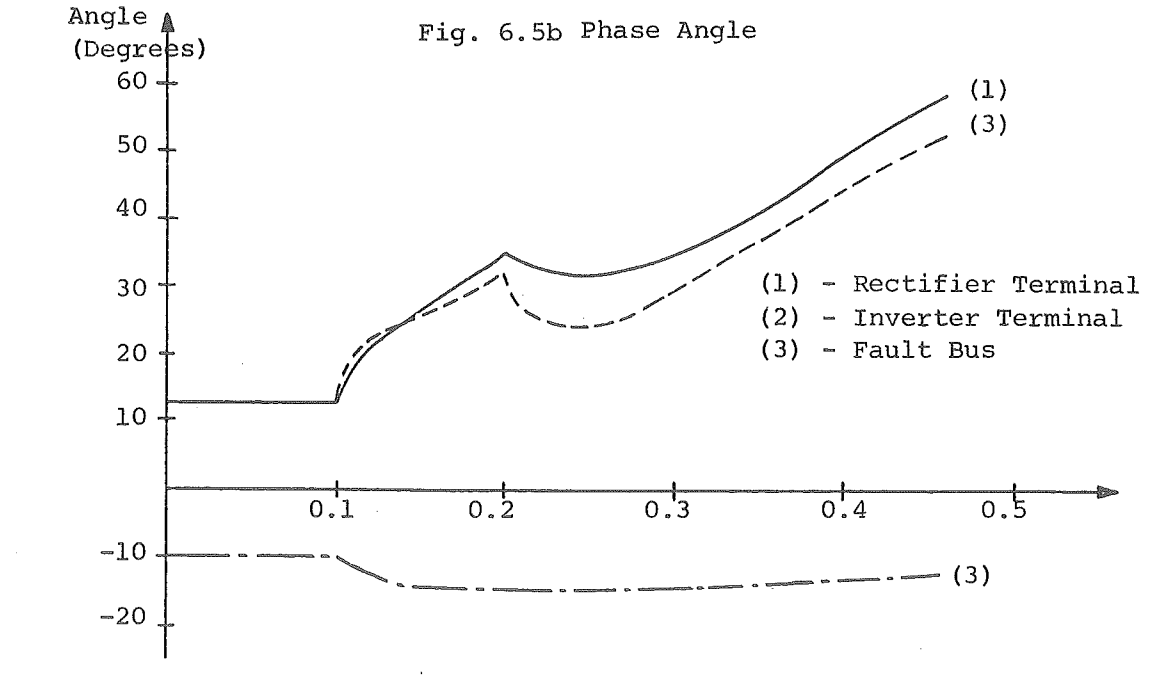

(b) Fig. 6.5b Phase Angle

Fig. 6.5 Magnitude and Phase of Time Variant Thevenin Voltage - Case 2321.

The small voltage differences are amplified in the reactive power profile of Fig. 6.4 which shows up one of the significant differences between the two models. In the QSS model, filter representation is included by introducing shunt admittance while the TCS reflects the full dynamic response of the filters. The departure between the two models immediately after fault inception and fault removal is due to the different filter models. For the TCS representation, the combination of the dynamic filter response and control action results in an initial drop in reactive power demand from the AC system. The mismatch is more pronounced following fault clearance.

6.1.2.2 Differences in real power - Although the reactive power profile is useful in indicating the accuracy of matching between the two programmes, it is the real power transferred by the DC link which affects transient stability analysis. Figure 6.6 shows the real power flow to the link terminals. The inverter power (Fig. 6.6b) is plotted for positive power flow out of the link terminal to facilitate a comparison between the two ends of the link.

In the post fault period in particular, the fixed equivalent simulation (curve 2), departs considerably from the time variant case (curve 3).

Immediately after fault inception the TCS indicates that the rectifier DC power flow is less than the level predicted by the QSS model. (Curve 3 of Fig. 6.6a). This is caused by the sudden drop in the rectifier DC voltage, giving rise to a drop in DC current as illustrated in Fig. 6.7. Control response at the inverter restores the DC current and the link recovers from the initial disturbance quickly.

At the inverter end the immediate power response predicted by the QSS model (curve 1 of Fig. 6.6) deviates considerably from the TCS solution (curve 3), which reflects the delay effect caused by the DC line.

Although instantaneous power differences are observed, the nett energy transfer as calculated by the TCS and QSS models

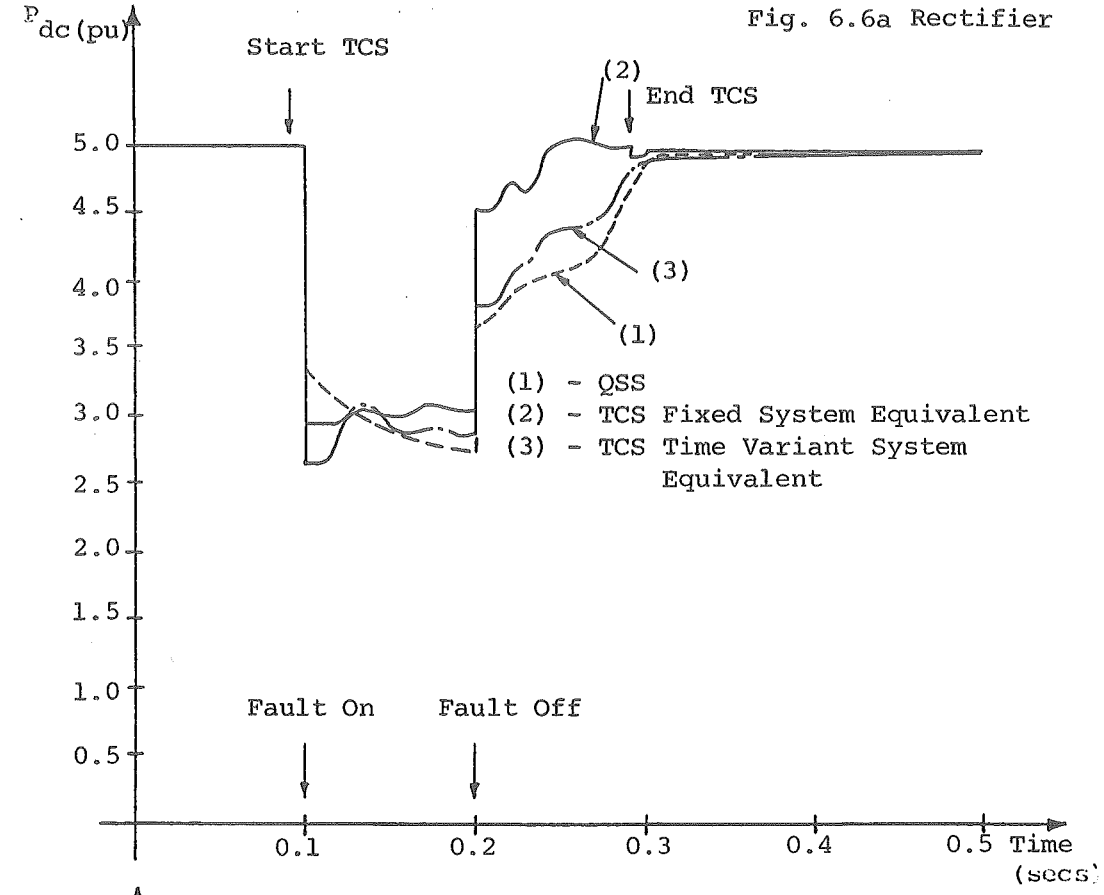

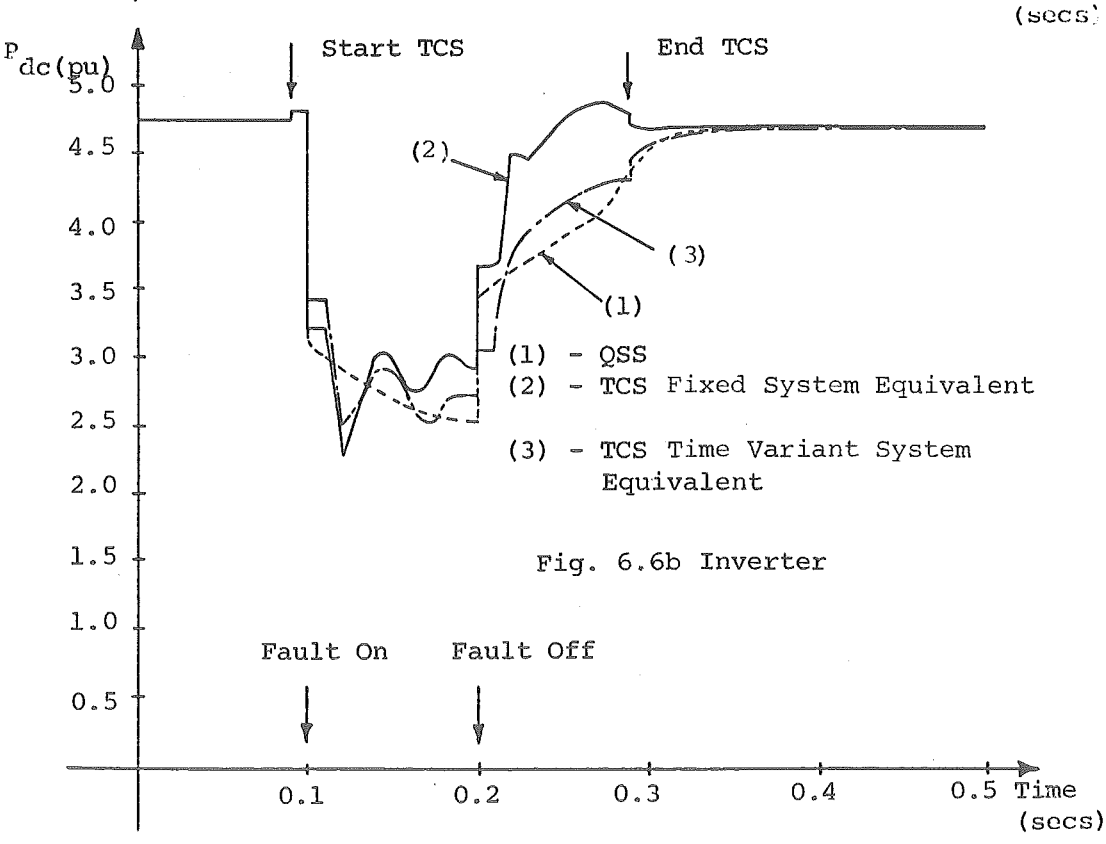

Fig. 6.6b Inverter

Fig. 6.6 Real Power Flows at DC Link Terminals - Case 2321.

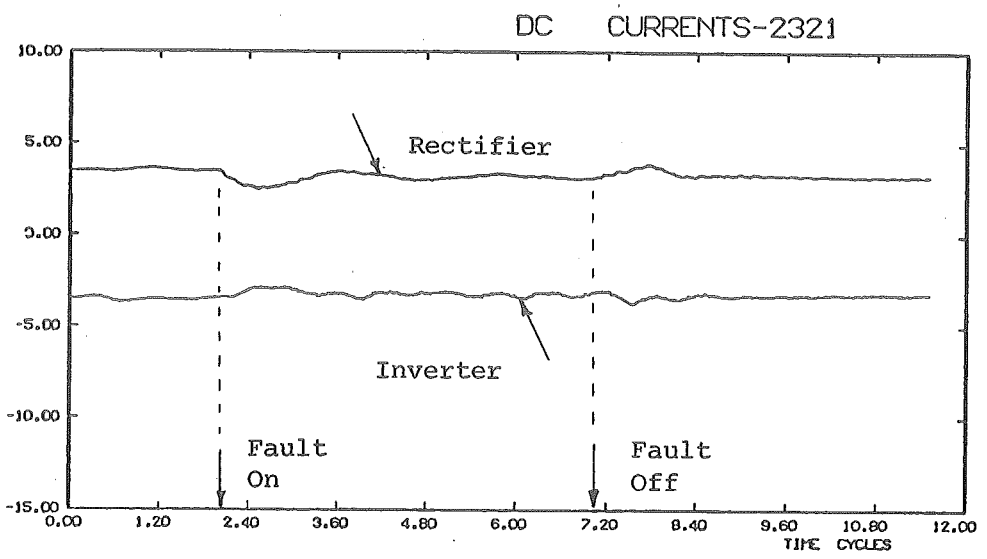

Fig. 6.7 Converter DC Currents - Case 2321.

are similar, thus causing relatively small first swing maximum angle differences. For the high inertia machines at the rectifier terminals the difference is 3%, while for the low inertia synchronous condensers at the inverter, the difference is 12%. At both terminals the QSS model gives the larger maximum angles, and thus provides pessimistic but safe results.

TABLE 6.1 SWING ANGLES FOR LINK TERMINAL MACHINES - CASE 2321

Case	Maximum Swing Angle	
	Benmore	Haywards
QSS	16.9°	- 8.1°
TCS Fixed Equivalent	14.7°	- 5.9°
TCS Variant Equivalent	16.4°	- 7.1°

6.1.2.3 Coincidence at TCS end points - The purpose of using the TCS in TS analysis is to accurately model the DC link behaviour during the disturbance period until the time that link response and control has settled sufficiently to allow the QSS model to take over. In addition there is little point in continuing TCS beyond the first swing maximum, unless subsequent swings are critical to the stability of the system.

The return to quasi-steady state behaviour of the TCS can be evaluated by monitoring control action and DC current variations. Once control action has settled and firing instants become equally spaced, non characteristic harmonics cease to be produced by the converter and the link terminal AC voltage waveforms lose their distortion. These effects are illustrated in Fig. 6.8.

In the case of the rectifier, Fig. 6.8a, the fault causes the rectifier delay angle to reach its minimum. Since the AC voltage remains below nominal, there is no control action at this terminal and the waveforms are essentially undistorted. At the inverter end control action settles at about 10 cycles (Fig. 6.8b), and waveforms from this point are essentially undistorted, indicating that the TCS can be terminated.

The solutions of the TCS and QSS models are not exactly coincident at the termination of the TCS study. Table 6.2 records the respective differences at the start and end of the TCS study period.

The results in Table 6.2 are obtained at the last integration step of the TS programme for which a TCS data point is available. A QSS solution of the link is obtained at this step but the injected AC currents are derived from the final TCS data point (refer Fig. 5.8). In this case the mismatches are small and maximum mismatch occurs for the inverter power and is approximately 3% of the QSS value.

Fig. 6.8a RECTIFIER VOLTAGES-2321

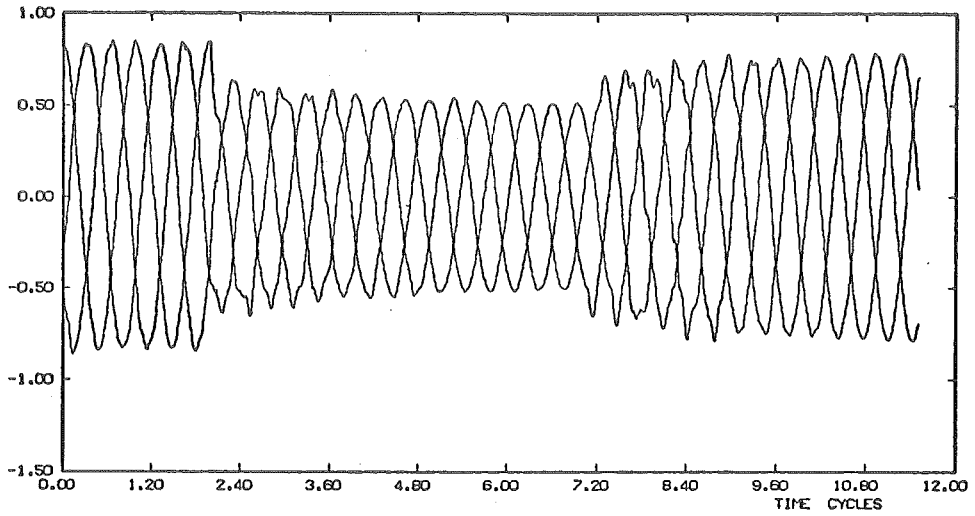

Fig. 6.8b INVERTER VOLTAGES-2321

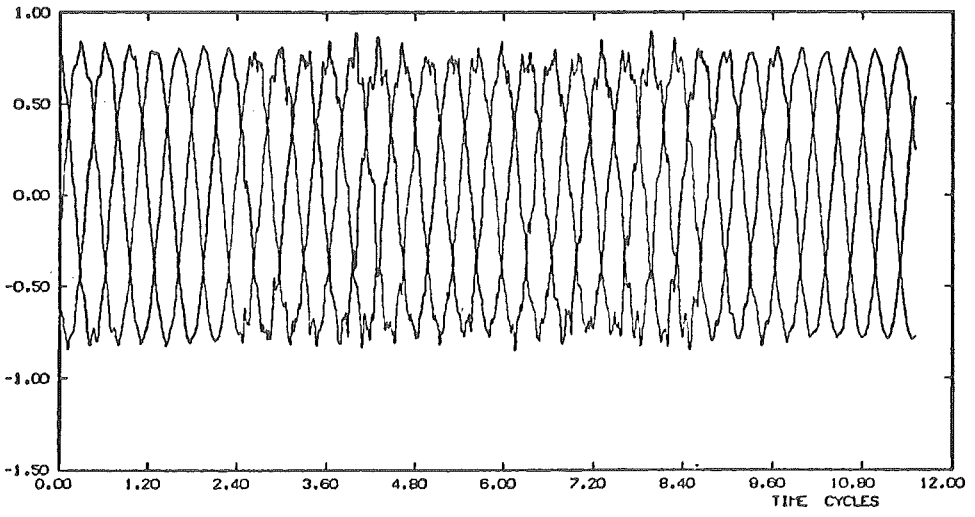

Fig. 6.8 Transient Converter Simulation AC Terminal Voltages - Case 2321.

TABLE 6.2 COINCIDENCE OF SOLUTIONS AT START AND END OF TCS - CASE 2321

		Power (pu)		Voltage (pu)	
		Rectifier	Inverter	Rectifier	Inverter
Start	QSS	5.00	- 4.76	1.025	0.980
	TCS	4.99	- 4.78	1.022	0.979
End	QSS	4.63	- 4.42	0.964	0.965
	TCS	4.51	- 4.28	0.955	0.963

6.1.3 Approximations for TCS Equivalents

In section 4.4 a number of approximations were discussed to reduce the computational effort required in processing TCS results for TS analysis. These approximations are evaluated for this case and the results appear in Figs. 6.9 and 6.10.

It is clear from these results that the approximations are excellent. The maximum difference between rms and fundamental voltage for the inverter occurs at 4.0 cycles and is only 0.5%. The accuracy of the approximations is to be expected because of the minimal distortion of waveforms, particularly those at the rectifier terminals. (Refer to Fig. 6.8a).

6.2 INVERTER AC SYSTEM FAULT

Faults at inverter terminals provide a severe test for the DC link controls and often result in repeated commutation failures causing considerable disruption to the normal valve firing sequence at the inverter. This form of converter malfunction is of particular importance because it cannot be represented by the QSS model and a transient converter simulation is essential.

To make the study a worst case one, a 3 phase fault of 5 cycles duration was applied very close to the inverter

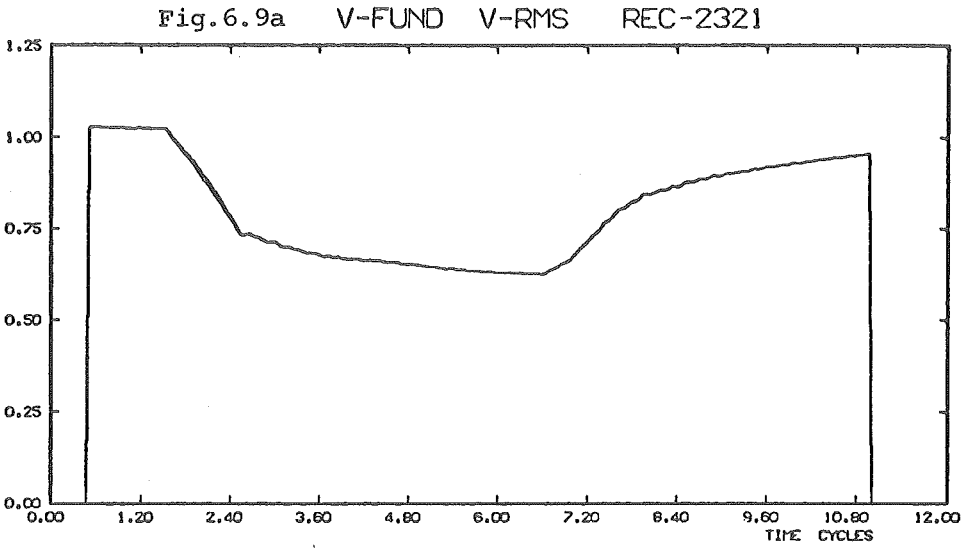

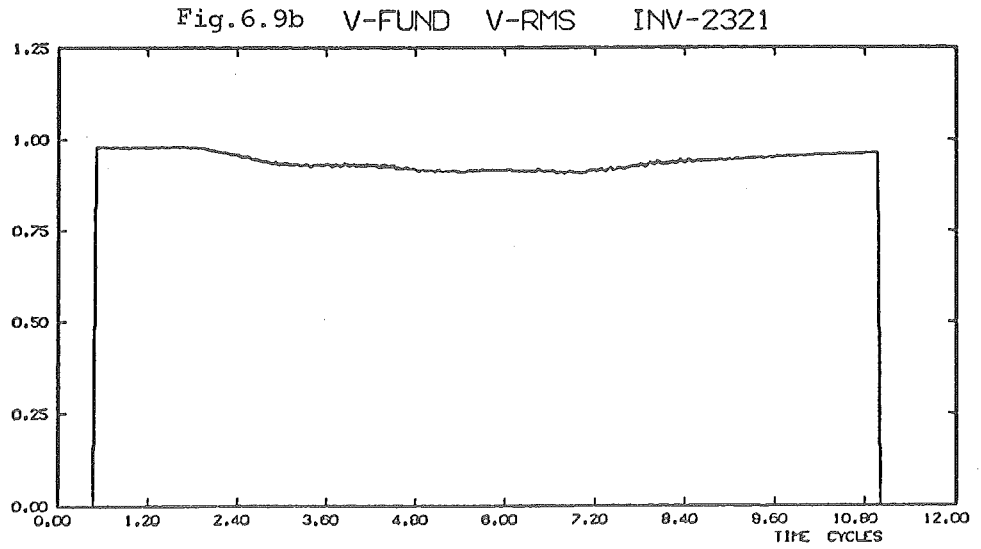

Fig. 6.9 Voltage Approximations at Link Terminals - Case 2321.

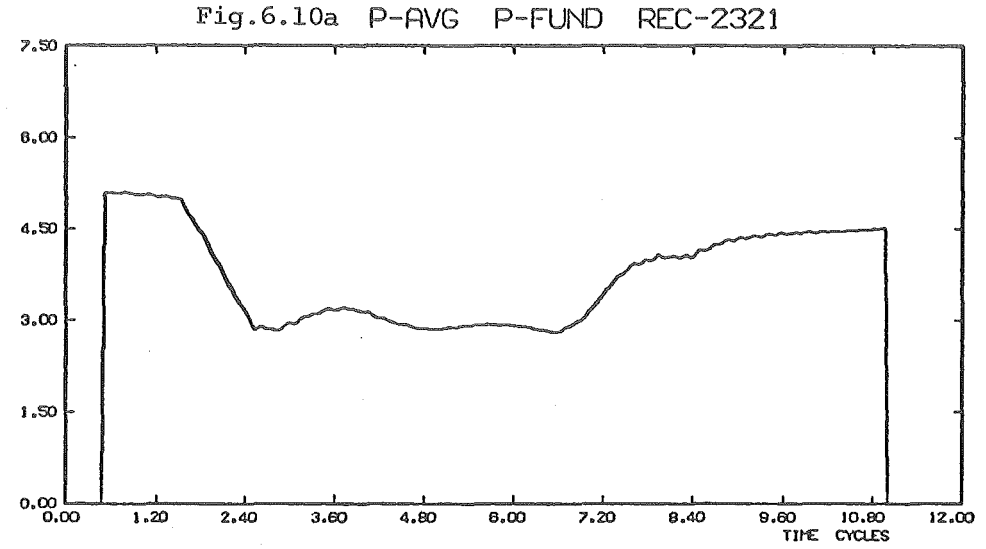

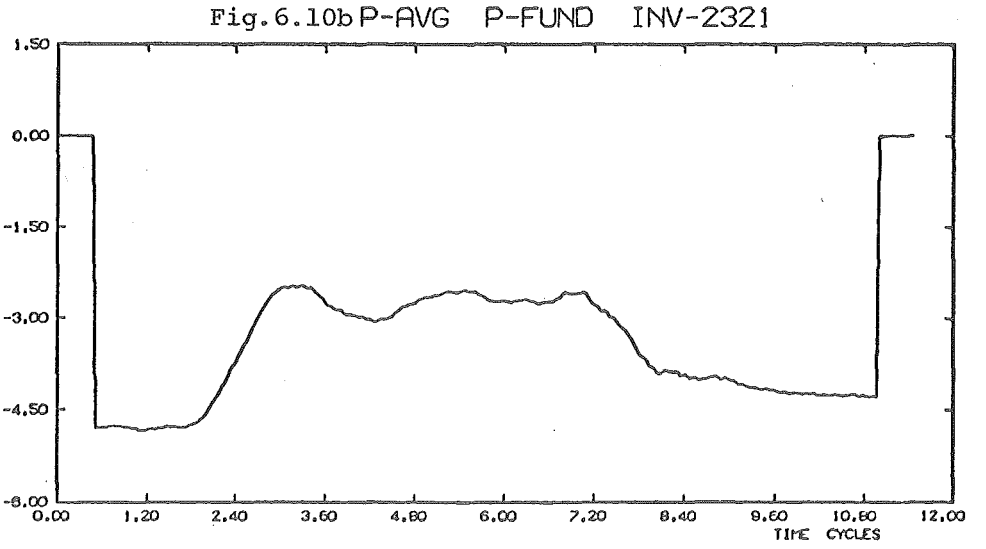

Fig. 6.10 Power Approximations at Link Terminals - Case 2321.

terminals. Referring to Fig. 6.2, the fault was applied to Bus 2 and a small fault resistance (1 ohm) was included to provide sufficient source voltage for commutation to be maintained. The fault caused an 80% drop in voltage at Bus 2 immediately after fault inception. This case study is coded 2311.

6.2.1 Fault Representation Using TCS Equivalents

Referring to the rectifier AC system fault case, during the period when the TCS equivalents replace the QSS model, fault application at the Twizel bus was made in the normal way, i.e. the admittance matrix of the TS network was modified at fault inception and removal, to account for the fault admittance.

It is possible to use the same approach for this case. However this required modification of the TCS equivalents. Since the fault is applied at Bus 2, and the transient converter simulation models it explicitly, the TCS currents (I_2 of Fig. 6.2), include the fault current as shown in Fig. 6.11.

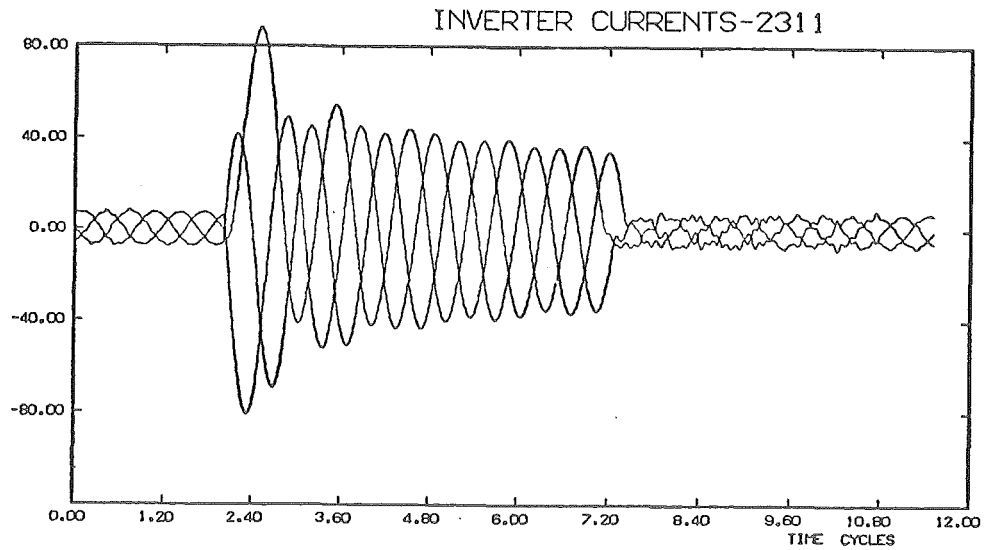

Fig. 6.11 AC Currents (I_2) at Inverter Bus - Case 2311.

Because the fault is resistive, the real power obtained in deriving the TCS equivalents, includes real power flowing in the fault. The difference between the AC power flowing into Bus 2, and the DC power flow at the inverter is illustrated in Fig. 6.12.

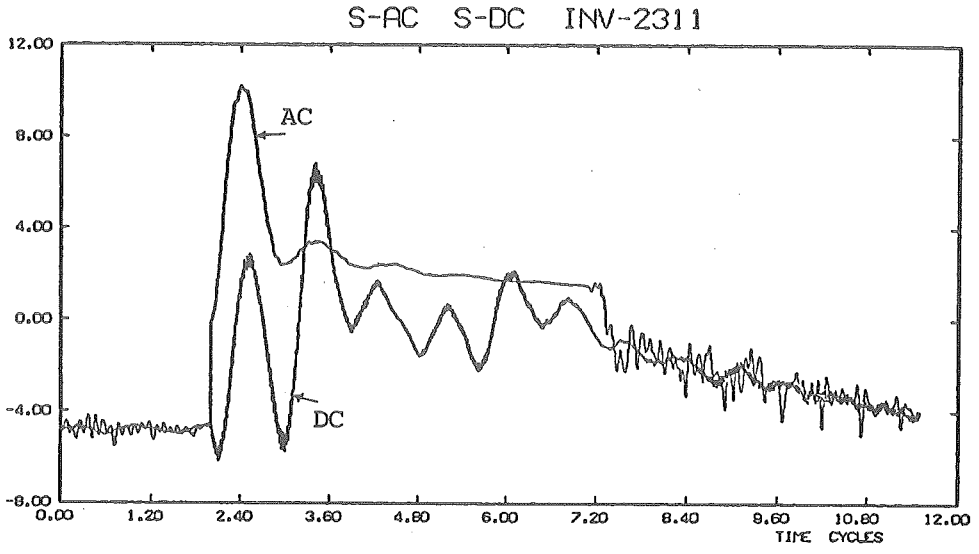

Fig. 6.12 AC and DC Apparent Power at Inverter Terminal - Case 2311.

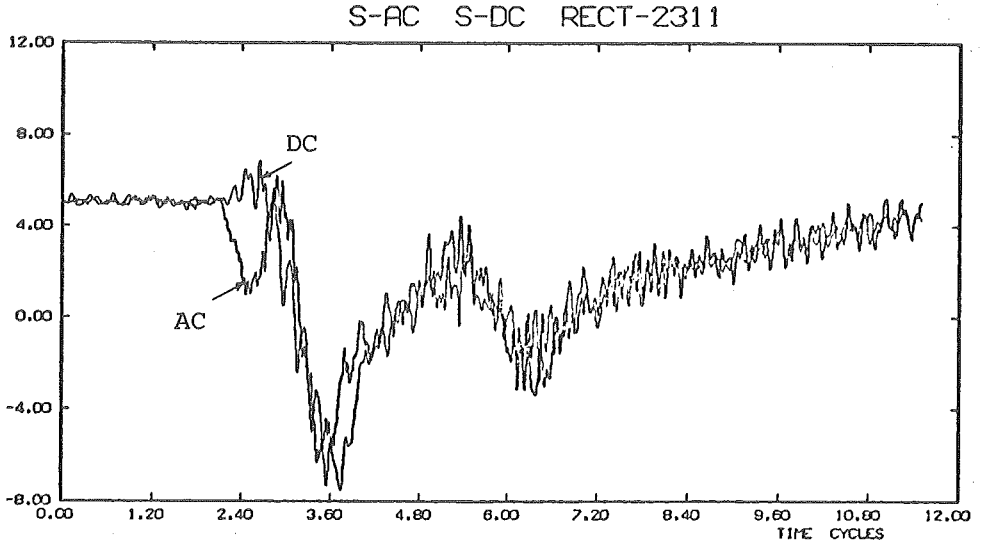

Fig. 6.13 AC and DC Apparent Power at Rectifier Terminal - Case 2311.

The fault power can be removed, leaving only the real power flow to the converter using:

$$P_{dc} = P_{ac} - (E_2)^2 / R_{fault} \qquad (6.1)$$

where P_{ac} is the real power flow into Bus 2 .

An alternative and simplified approach is to use the TCS equivalents, unmodified by equation 6.1, to specify the fault for the TS network and thereby eliminate the fault application via a modified matrix. This method is only applicable for the special case where the fault is

introduced at the converter bus, and cannot be generalised.

Both methods were used in separate TS runs and the results compared at each integration step were identical.

6.2.2 Low Voltage Mismatch

A difficulty was experienced during the fault period of this case study when the TCS was used in the TS analysis. This problem was manifested by the argument of the inverse cosine, of equation 5.33, exceeding unity. This occurred for only a few integration steps during the fault period. It is caused by a mismatch between the TCS power and voltage due to the limitations of processing TCS results with very low voltages (or currents).

With a very low voltage, the first term in the argument of equation 5.33 becomes very much larger and any mismatch between E_{dyn} and P_{dyn} can result in an argument exceeding unity.

This difficult was overcome by releasing the power specification and allowing it to change until equation 5.33 could be solved. This resulted in a different power to that obtained from transient converter simulation.

Table 6.3 shows the simulation power and the modified power to allow solution of equation 5.33. The results in this table were independent of the method of fault application discussed in section 6.2.1. Because the absolute magnitude of the powers is small, the adjustment of P_{dyn}, to allow solution of equation 5.33, has a negligible effect on the stability analysis. This problem was not experienced in any of the other case studies carried out.

6.2.2.1 Second iteration - To check that the mismatch between E_{dyn} and P_{dyn} was not due to poor convergence between the TCS and TS programmes, a second iteration in the outer loop of Fig. 5.10 was performed. This was done using the unmodified results from the first TCS to produce a new network equivalent for a second TCS.

TABLE 6.3 MISMATCH OF INVERTER POWER DURING FAULT PERIOD.

Integration Step During Fault	1	2	3	4	5	6	7	8	9	10
DC Power by TCS (Pu)	-0.752	0.244	0.002	0.043	0.024	0.015	0.009	0.006	0.005	0.005
DC Power to Satisfy Eq. (5.34) (Pu)	-0.869	-0.128	-	0.037	-	-	-	-	-	0.035

TABLE 6.4 POWER AND VOLTAGE DIFFERENCES BETWEEN FIRST AND SECOND ITERATIONS OF TCS AND TS PROGRAMMES.

Integration Step During Fault.		1	2	3
Inverter Power	1st	-0.752	0.244	0.002
	2nd	-0.777	0.223	0.006
Inverter AC Voltage	1st	0.125	0.098	0.085
	2nd	0.126	0.099	0.084

The second simulation was performed for the 2 cycles after fault inception and the differences between the first and second TCS equivalents are given in Table 6.4.

Table 6.4 shows that the results from the first and second iterations of the two programmes are very close and little benefit is gained by performing the second iteration.

The results from the second iteration did not alter the mismatch problem. For example, at step 1, the power required to allow solution of equation 5.33 changed from 0.869 Pu to 0.894 Pu. Although the occurrence of the mismatch problem is significant in itself, it was not considered further because of the very small powers involved when it occurs.

6.2.3 Comparison of Results

Immediately after the fault is applied, the inverter experiences repeated commutation failures which persist during the fault period. The AC current waveforms in Fig. 6.11 do not show these disturbances because of the large fault current flowing. The commutation failures produce oscillations in DC power (Fig. 6.12) at the inverter terminal illustrating the effect which they have on the DC link performance. A comparison between Figs. 6.12 and 6.13 shows that the DC power at the rectifier terminal is smoothed by the DC line response and the oscillations in Fig. 6.12 are therefore not due to the line.

6.2.3.1 Differences in voltage and reactive power -

Figures 6.14 and 6.15 illustrate the differences between the QSS and TCS AC voltage and reactive power at the inverter terminals. This case has a similar filter response to that discussed in section 6.1.2.1. In the post fault period the reactive power demands of the link are lower in the TCS because of the slower link recovery for this model.

A good match is obtained for the voltages, (Fig. 6.14), during the fault period because of the dominance of the fault in the TCS results. In the post fault period the

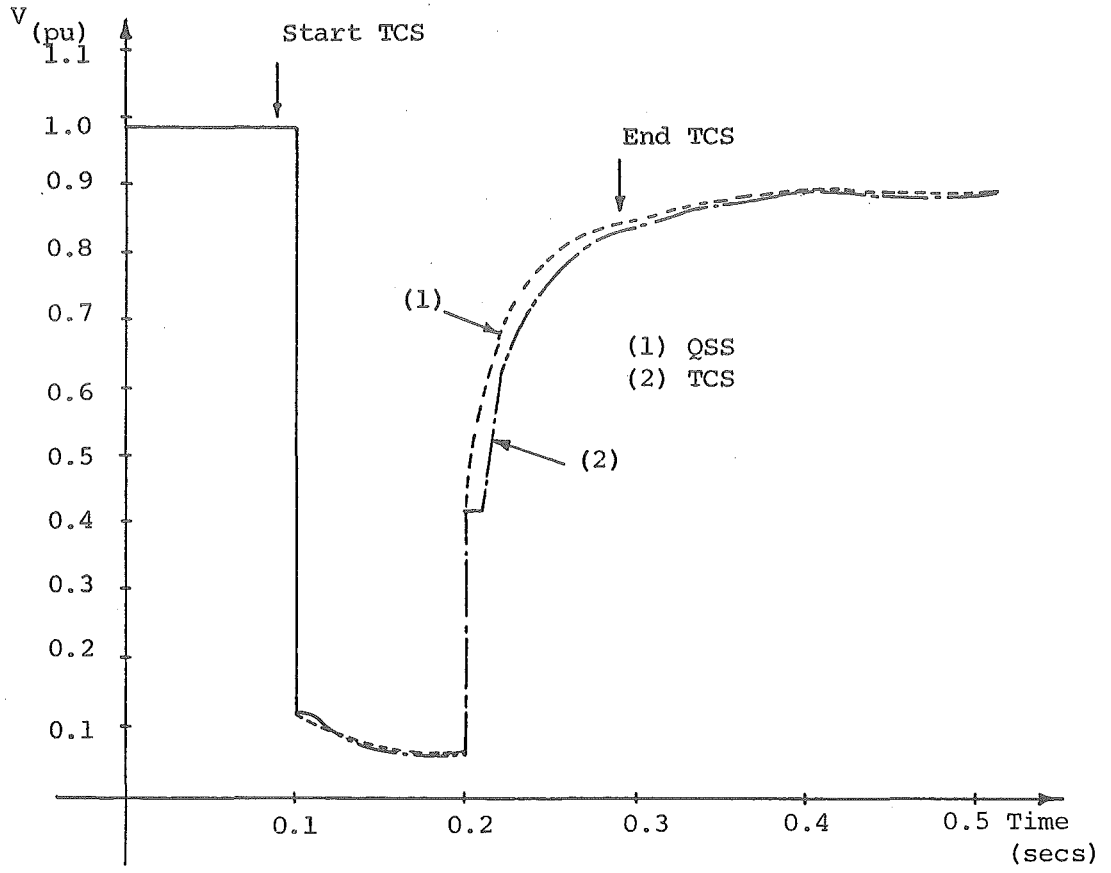

Fig. 6.14 Inverter AC Terminal Voltage - Case 2311.

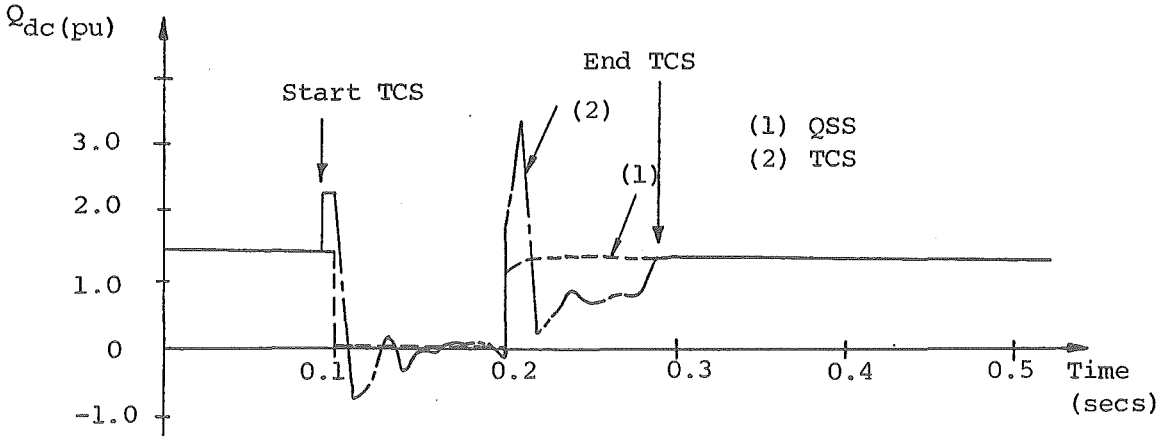

Fig. 6.15 Reactive Power Flow to Inverter Terminal - Case 2311.

match is not so accurate because of the slower link response determined by transient converter simulation.

6.2.3.2 Differences in real power - The DC power flows at the two terminals of the link are given in Fig. 6.16.

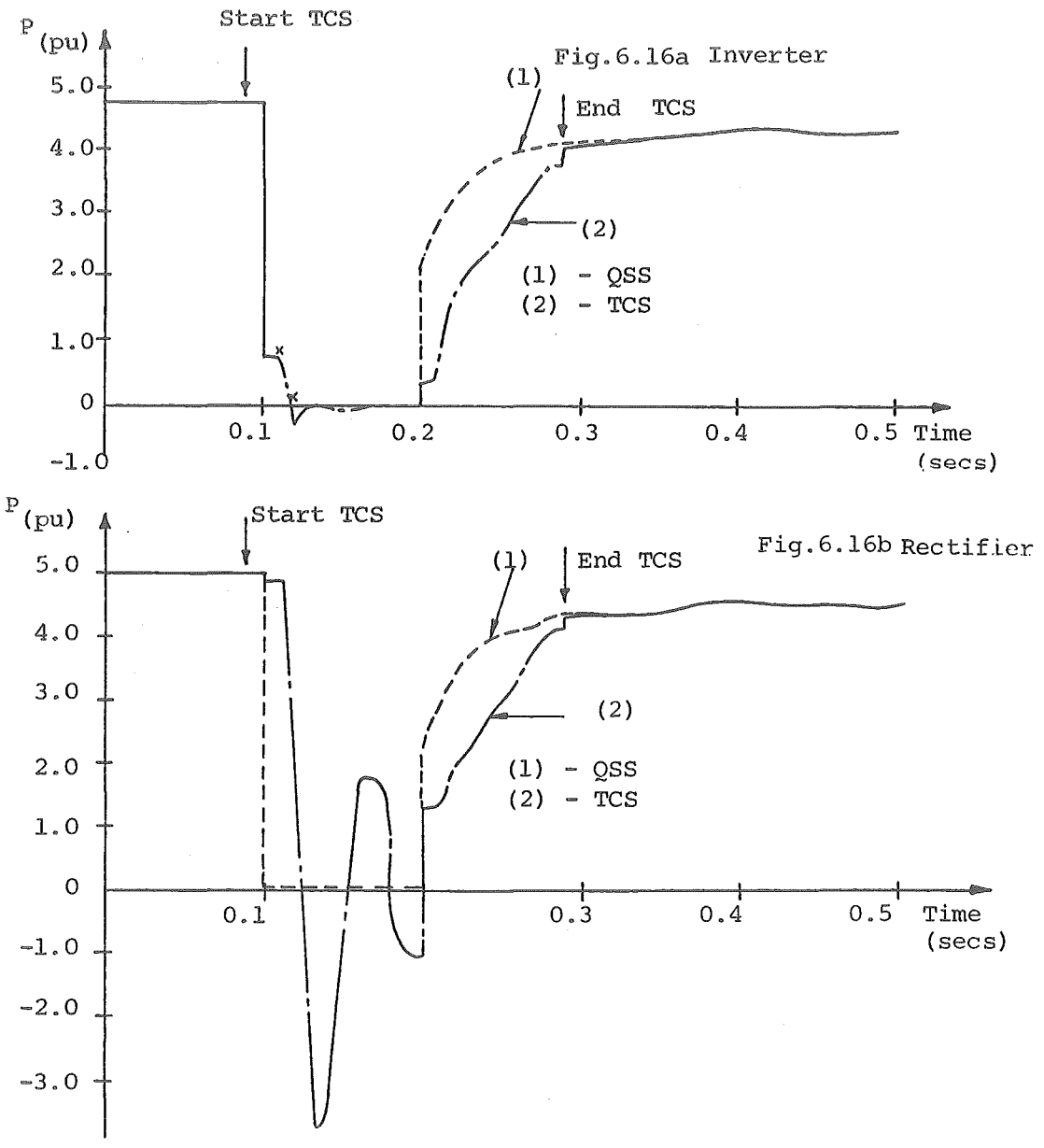

Fig. 6.16 Real Power Flows at DC Link Terminals - Case 2311.

For the inverter terminal (Fig. 6.16a) the power plotted is that obtained from TCS with the fault power removed. The two crosses on this figure indicate the powers obtained in the TS analysis so that equation 5.34

could be solved and as the figure shows, they are close to those obtained by TCS.

The QSS model shows significant departures from the results obtained using TCS. The differences between the results are caused by a number of factors:

a) Due to the DC line response, power continues to be fed into the rectifier end of the line for one cycle after the fault occurs at the inverter bus.

b) At the inverter terminal, immediately before fault clearance takes place, (i.e. the first detected current zero after breaker operation), a commutation failure occurs. This converter disturbance delays the clearance time of the fault. It is impossible for a QSS model to detect this sequence of events.

c) In addition to the delay due to the commutation failure, inverter recovery is also affected by the response of the DC line and the controller at the rectifier end. As shown in Fig. 6.16b the TCS rectifier response is slower than the QSS response.

The accurate response obtained from the transient converter simulation affects the results of the TS analysis to a greater degree than for the rectifier AC system fault case, as shown by the swing curves in Fig. 6.17. In this case, the maximum swing angle obtained using the QSS model is less than that obtained using the TCS model (i.e. optimistic) and this is especially noticeable for the low inertia machines at the inverter terminal.

The QSS model would have to be modified to match the response rate determined from the TCS before it could produce more accurate results. However accurate matching of the QSS and TCS responses cannot be generally applied to this disturbance because of the indeterminate nature of consequential converter disturbances and their effect on normal valve firing sequences. In addition the QSS model cannot predict the oscillatory response at the rectifier terminal, illustrated in Fig. 6.16b during the fault period. This is due to the rapid rise in DC current in response to the

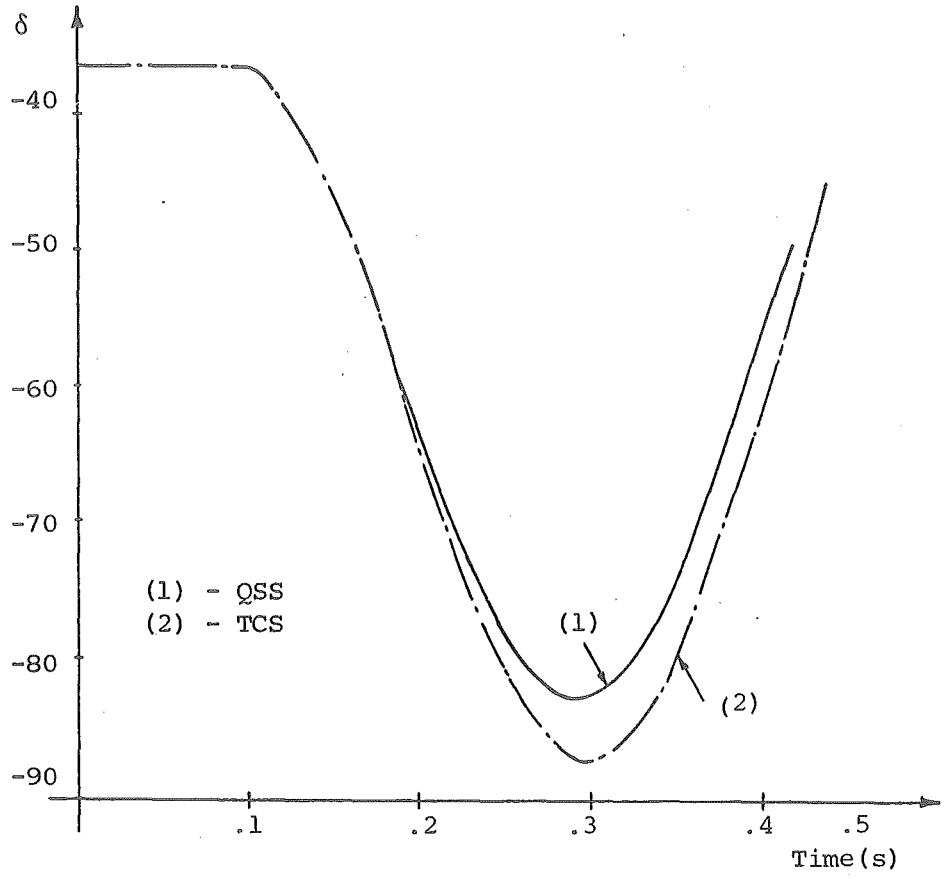

Fig. 6.17 Inverter AC System Fault - North Island Swing Curves.

collapse of DC voltage at the rectifier terminal. The oscillation does not involve any nett energy transfer and does not affect the swing angle at the Benmore generator significantly.

6.2.3.3 Coincidence at TCS end points - For this case the peak swing angle at Haywards occurs at 0.29 secs and it was considered unnecessary to continue the simulation beyond this point. An examination of the waveforms at this time showed the voltages to be close to sinusoidal. The maximum difference at the termination of this run was in the inverter power which differed by 7% from the QSS value. (See Fig. 6.16a). Table 6.5 records the differences between the TCS and QSS variables.

6.2.4 Approximations for TCS Equivalents

As shown in Fig. 6.11 the sudden change in AC current highlights the difficulty of interpreting a fundamental

TABLE 6.5 COINCIDENCE OF SOLUTIONS AT START AND END OF TCS - CASE 2311

		Power (Pu)		Voltage (Pu)	
		Rectifier	Inverter	Rectifier	Inverter
Start	QSS	5.00	- 4.76	1.025	0.980
	TCS	5.02	- 4.79	1.024	0.979
End	QSS	4.27	- 4.04	0.981	0.840
	TCS	4.12	- 3.76	0.990	0.838

component over the cycle spanning the fault time and emphasises the reason for extrapolation to achieve data alignment at the fault times. This difficulty is illustrated in Fig. 6.18 where a comparison between fundamental and rms power is given. The period spanning 1.5 to 2.5 cycles shows considerable differences between the two variables. The first data point after fault application is obtained at 2.5 cycles (point (b) of Fig. 6.18). At this point the fundamental power is 20% less than the rms power. An examination of the inverter AC currents in Fig. 6.11 shows that two

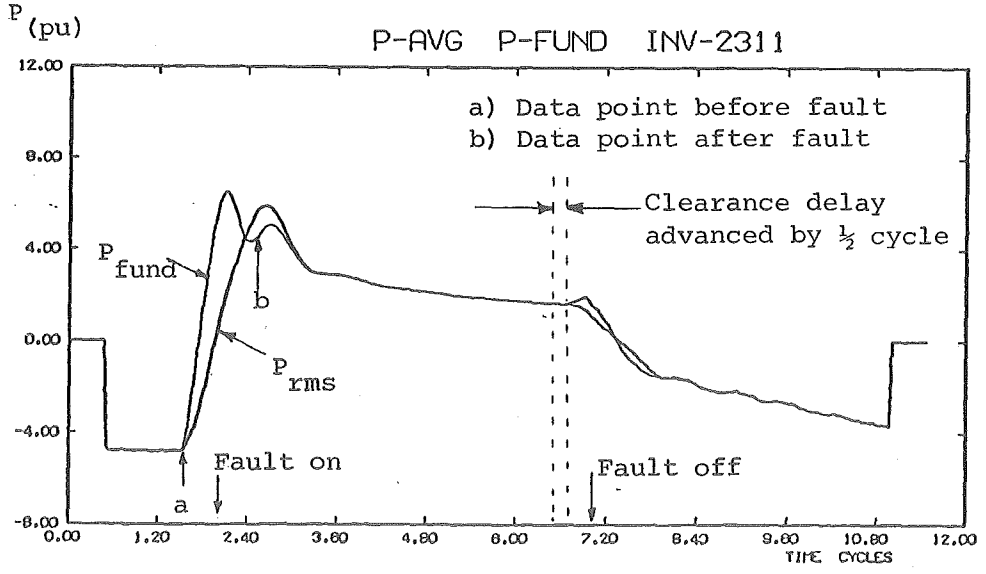

Fig. 6.18 Power Approximation at Inverter - Case 2311.

phases have a large DC offset which decays rapidly over the first 2 cycles of the fault period. The offset is a function of both the fault application time and magnitude of the reactive components of the AC source impedance, (Heffernan 1980), and is responsible for the differences between the rms and fundamental powers.

Figure 6.18 also illustrates the effect of the delayed fault clearance. The fault was intended to clear at 7.0 cycles but the effective clearance time is delayed 0.2 cycles.

Because of control action at the rectifier terminal, the rectifier voltages exhibit some harmonic distortion during the fault period. This affects the voltage approximation at the rectifier (Fig. 6.19),although the maximum deviation of the fundamental component from the rms voltage is only 2%, occurring at cycle 6.

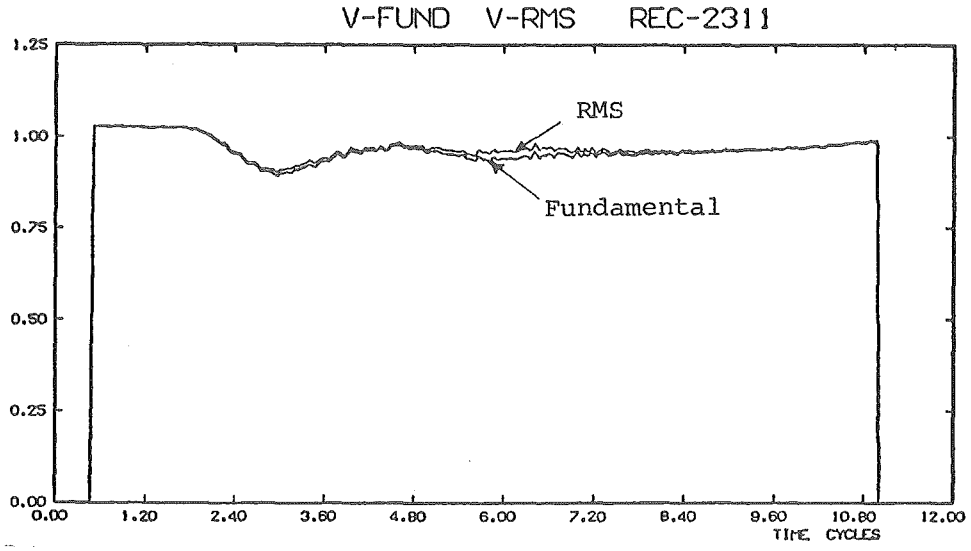

Fig. 6.19 Voltage Approximation at Rectifier - Case 2311.

6.3 DC FAULT STUDY

The QSS DC link model has severe limitations in its ability to represent the behaviour of a DC link during a DC line fault disturbance. It yields unrealistic current peaks as it cannot accurately represent the timing of valve firings in relation to the fault occurrence, or the subsequent effects of rapid control action. It is also inadequate in

representing the transient imbalance of harmonic currents between the converters and the AC system caused by the sudden fault current and subsequent control action.

A DC fault study was performed to evaluate the dynamic performance of the DC link for the purposes of transient stability analysis. In this case a DC fault was applied on the DC line just beyond the rectifier smoothing reactor and was initiated immediately after a valve firing. This provides a worst case study since control action influence is delayed for 30° until the next firing. The case is coded 1301.

6.3.1 Link Performance During Fault

A DC fault, using the QSS model, is represented by instantaneous shutdown of the link at the prescribed time followed by restarting at the end of the specified fault period. Transient converter simulation of a DC fault provides much more detailed information of the link behaviour, as illustrated in Figs. 6.20 and 6.21.

Fault initiation took place at cycle 2 and, as shown in Fig. 6.20, AC fault current flows for half a cycle after fault initiation. During this period the rectifier delay angle is retarded into the inverting region (between 120°and

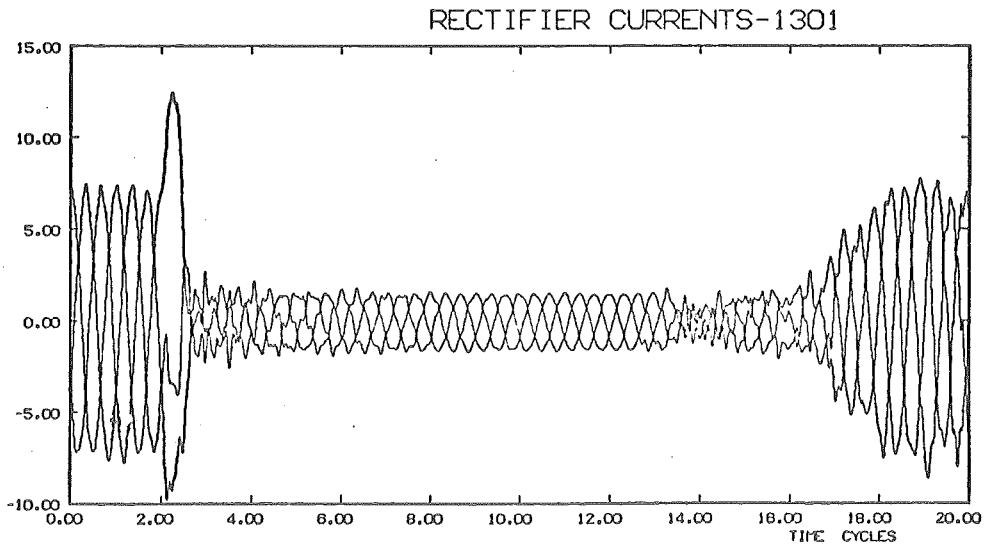

Fig. 6.20 AC Currents at Rectifier Terminal - Case 1301.

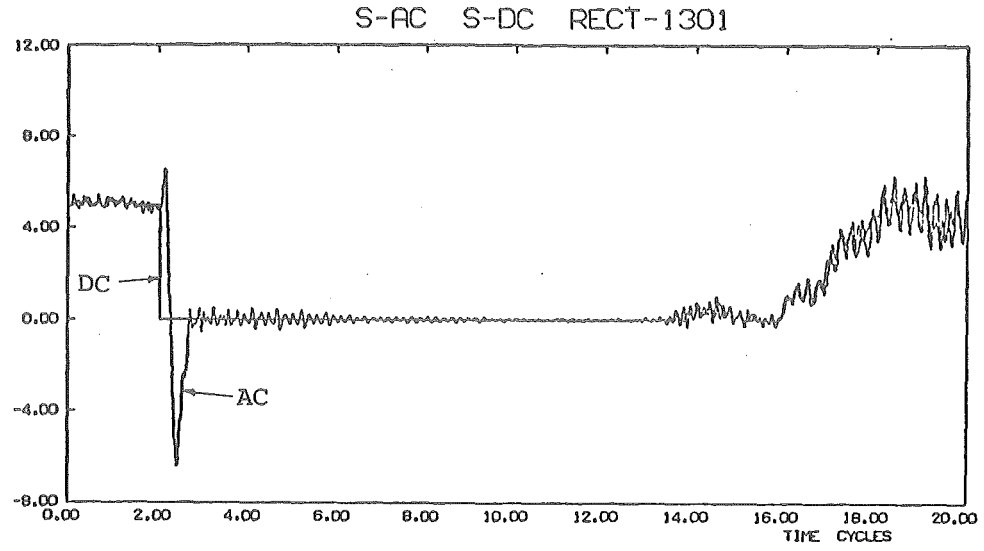

Fig. 6.21 AC and DC Apparent Power at Rectifier Terminal - Case 1301.

130°) to accelerate the DC line discharge. Since the fault is close to the rectifier this effect is not observable on the DC power trace of Fig. 6.21 but is clearly shown in the AC power response. The power response in Fig. 6.21 illustrates the rapid fault clearance achieved by converter control action.

Once control action has isolated the DC line, fault arc extinction is dependent on the natural oscillatory response of the DC line itself. This period combined with that required for deionisation gives a minimum shutdown time of 220 msecs or 11 cycles. (Heffernan, Arrillaga et al 1980). In Fig. 6.21 line recharging is initiated at cycle 13 and once full line voltage is obtained (at cycle 16) transmission can be reestablished. The reference above gives a more detailed analysis of the link response during a DC fault.

6.3.2 Matching QSS Restart With TCS

At the end of the extinction and deionisation period, transmission recovery begins and in the absence of prior knowledge of the TCS response, the QSS model produces instantaneous power recovery at this time, as illustrated by curve 1 of Fig. 6.22.

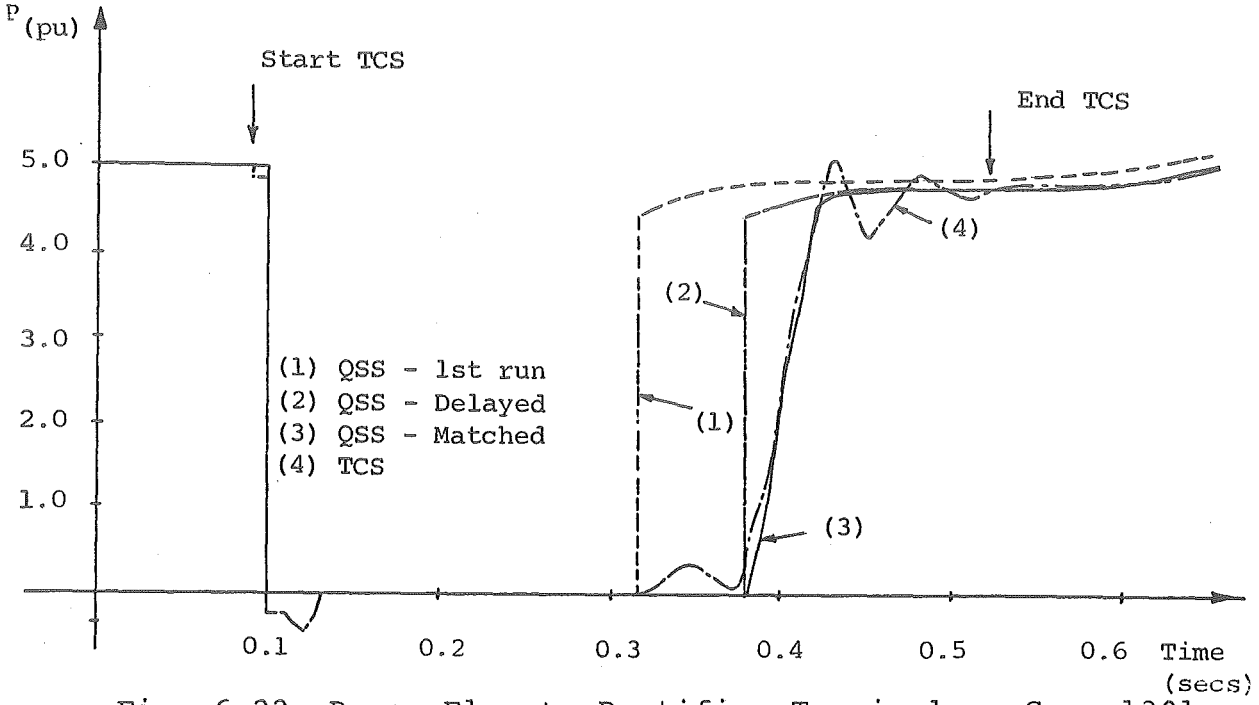

Fig. 6.22 Power Flow to Rectifier Terminal - Case 1301.

However as the TCS progressed it became clear that transmission would not be established from this time and matching between the two programmes would be poor. A number of subsequent equivalents were obtained, the final one adopted having the restart delayed to cycle 16 and ramped to nominal DC current linearly over the next 2 cycles. This equivalent provided excellent matching between the two models as illustrated by curve 3 in Fig. 6.22.

This method of interactive coordination utilises the inner loop of Fig. 5.10 and reduces what normally would be an iterative procedure to a single iteration. Maximum cost effectiveness is therefore obtained from a single TCS run by avoiding repeated simulations of the same case.

Although the differences observed in the second iteration of case 2311 (section 6.2), were not large, the above approach reduces these differences still further without the cost of a second simulation.

6.3.3 Termination of TCS

As shown in Fig. 6.22 there is a 7% overshoot in the TCS link power at full recovery. This is due to the finite

rate of response of the controller. The simulation was continued after recovery for a further 4 cycles to ensure that the oscillation is damped and converges to the same conditions as the QSS model.

6.3.4 Comparison of Results

Throughout the DC fault there were no consequential converter disturbances and because of this, and the accurate matching achieved with the QSS model, the differences between the QSS and the TCS models can be minimised.

6.3.4.1 Rectifier reactive power response - Referring to Fig. 6.23, extra reactive power is required immediately after fault application due to the half cycle of fault current and associated commutation angle increase. This causes a small depression of voltage at the rectifier terminals, which is illustrated in Fig. 6.24.

Once the fault current is cleared by control action this depression changes to a rise in voltage due to the

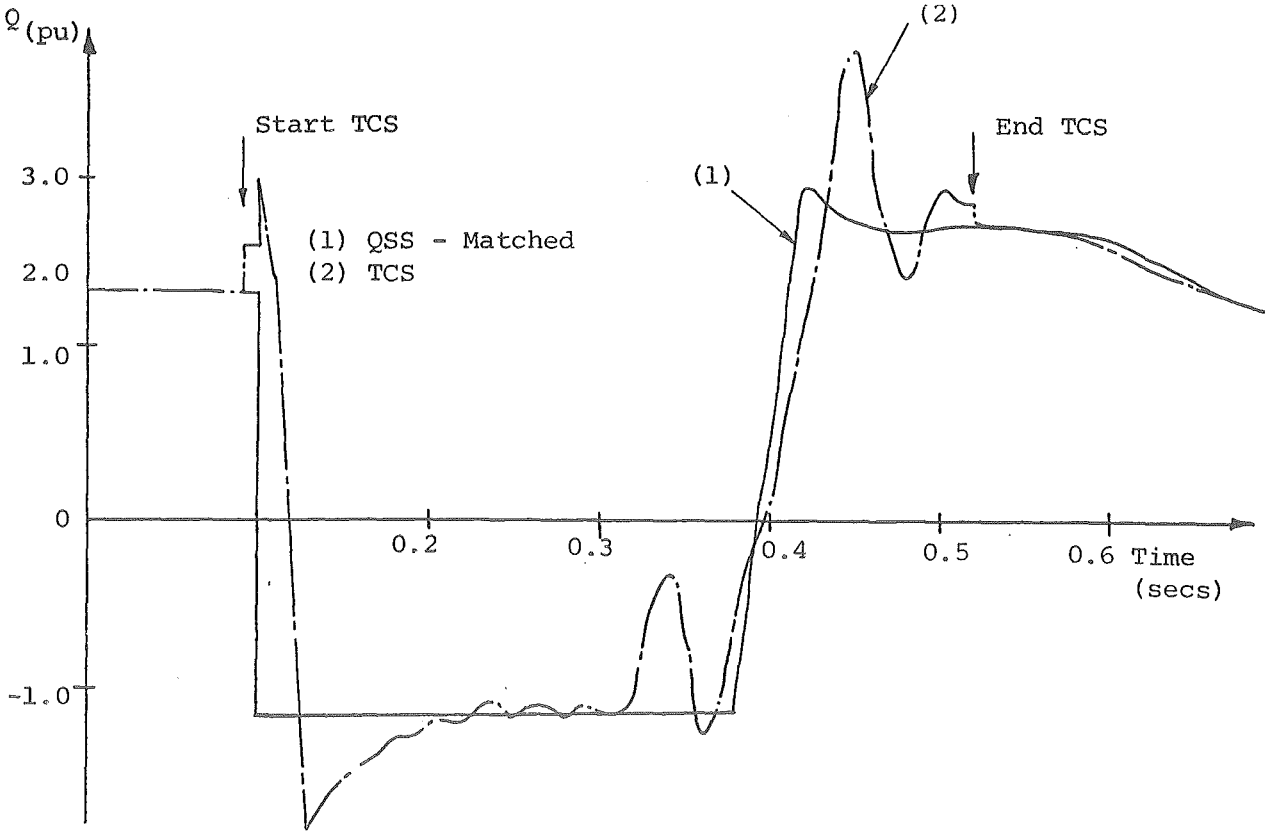

Fig. 6.23 Reactive Power Flow to Rectifier - Case 1301.

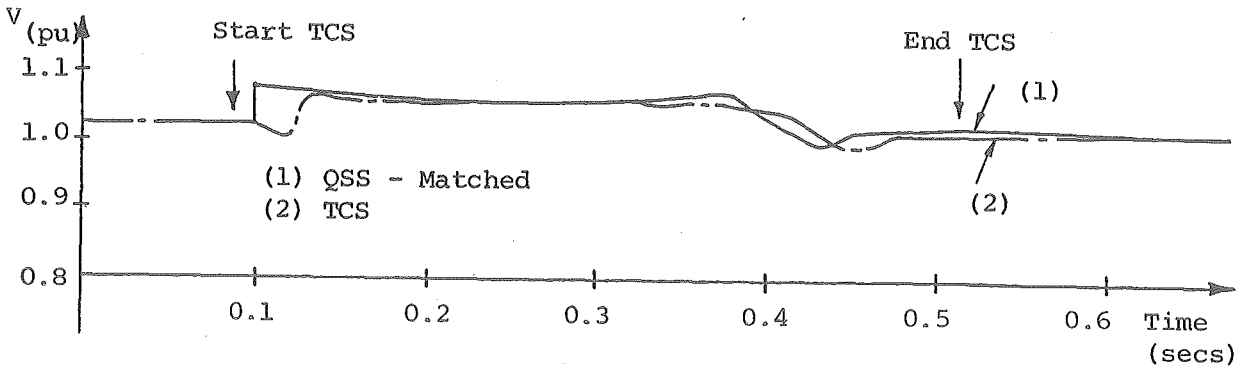

Fig. 6.24 Rectifier AC Terminal Voltage - Case 1301.

extra reactive power available to the network from the filters.

Towards the end of the fault period, the link draws reactive power from the filters as the line is recharged. The oscillatory response after fault recovery rapidly decays as control action settles. Differences at the inverter terminal are minor.

6.3.4.2 Differences in real power - Figure 6.25 illustrates the difference in swing angles of the two machines near the DC link terminals for the two models corresponding to curves 1 and 4 of Fig. 6.22. In this case there is a considerable error in the TS assessment with a 16% error in the SI machine first swing peak of the QSS model.

However, as the matching between the QSS and TCS models is improved, the differences in peak swing angle are reduced. For curve 2 of Fig. 6.22 the difference is 2% and for curve 3 it is less than 1%. The maximum swing angles for these cases are included in Table 6.6. These differences are particularly small and are due in part to the improved matching between models and also to the fact that the peak swing of both machines occurs very close to the DC fault clearance time, (0.43 secs and 0.41 secs respectively). Hence any differences during the link restart period, i.e. ramped or instantaneous in the case of the QSS model, have little effect on the peak swing angle.

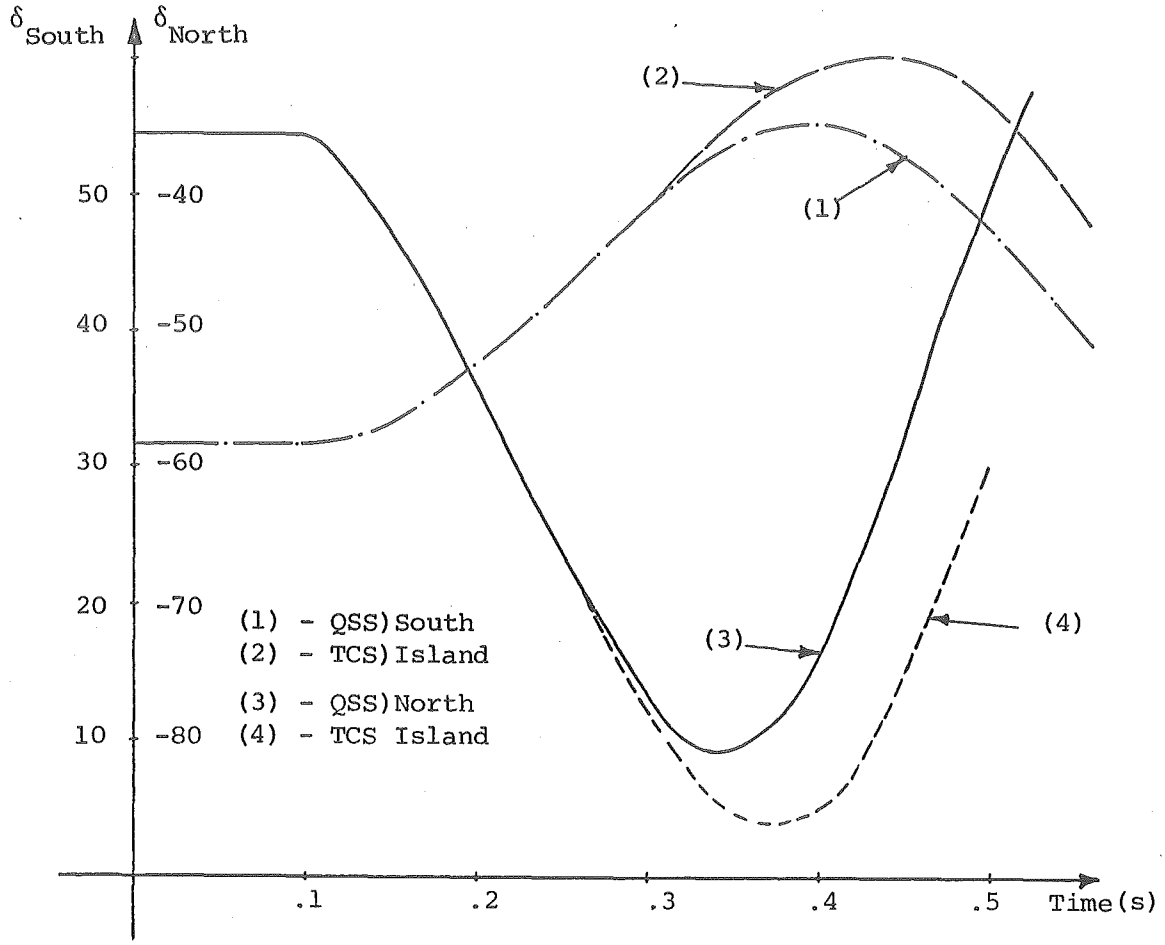

Fig. 6.25 D.C. Line Fault - Swing Curves.

TABLE 6.6 FIRST SWING MAXIMUM ANGLES FOR DC LINE FAULT - CASE 1301

	First Swing Maximum Angle	
	South Island	North Island
QSS (1st Run)	24.1°	45°
QSS (Delayed)	29.1°	50.0°
QSS (Matched)	29.0°	49.7°
TCS	28.7°	49.2°

6.3.5 Approximations for TCS Equivalents

In this study the differences between fundamental and rms values for all the TCS equivalents was less than 0.7%. The maximum error occurs in the inverter AC voltages during the periods of control action.

The AC voltages are not subject to sudden steps, as in the case for AC faults, and the analayis for fundamental components across the fault switching times is not affected by the fault. This improves the evaluation of fundamental variables over this period and the rms and fundamental components are indistinguishable when plotted.

6.4 CONCLUSION

The case studies presented in this chapter demonstrate the feasibility and effectiveness of combining both the TCS and TS programmes. Together they provide more accurate modelling of AC-DC systems than either programme can provide on its own. The introduction of a time variant Thevenin equivalent for the transient converter simulation provides an AC system representation technique for TCS which supersedes any previous approach to this problem. In using this approach, more detailed information can be obtained from the TCS regarding fault development, DC link response, converter performance, over voltages, over currents, etc. (Heffernan, Arrillaga et al 1980,Arrillaga et al 1980).

The combination of the two programmes has been successfully demonstrated and techniques developed to allow a case study to be performed in a single iteration. This may require several runs of the TS programme to improve the system equivalent as TCS trends become apparent but these are relatively inexpensive in comparison to the single TCS run. Matching of the two programmes at the end point of the TCS can easily be monitored by observing waveform distortion or control actions. Good matching was obtained for all cases.

The different results obtained from the TS analysis of the three cases investigated, indicates that a QSS model cannot be classified as giving either pessimistic or

optimistic results for peak swing angles. This emphasises the need to perform worst case transient converter simulations during investigations of a system so that the QSS link model performance can be modified to more accurately represent DC link performance for further studies. The system used for these case studies is relatively strong and a weaker system, where stability is more marginal, may produce much greater differences between the two models.

The conclusions drawn in Chapter 4, on the derivation of TCS equivalents, are supported by the results presented for these cases. The differences between rms and fundamental quantities are generally small. In the inverter AC system fault case, a DC offset caused a considerable difference between fundamental and rms power. However since the real power must come from the AC network, whether fundamental or otherwise, the rms power is considered to be the best reflection of the effect of the link on machine response.

CHAPTER 7

TRANSIENT STABILITY IMPROVEMENT USING DC LINK CURRENT SETTING CONTROL

7.0 INTRODUCTION

Early in the development of DC links it was recognised that, apart from their attributes for bulk energy transmission, they could also be extremely useful elements for improving the stability of AC power systems (Uhlmann 1964, Machida 1966, Peterson et al 1966, Kauferle et al 1970, Dougherty et al 1970). In contrast to AC transmission, DC link power is directly and easily controllable independently of the phase of its AC terminal voltages. Its speed of response is several orders faster than the natural response speed of the AC system controllers.

Many of the modern DC link schemes have special purpose controllers which respond to the power-frequency dynamics of the AC system. In synchronous links the DC power may be modulated by AC tie line power flow to provide system damping and avoid overload. (Pacific Intertie, CU Project). The main consideration for stability in synchronous links is to control the frequency of an isolated system. (Sardinia, Vancouver IS, Gotland). In these examples the capacity of the controlled system is of the same order as the capacity of the DC link. However, stability can be improved in large systems by monitoring the line power flows and frequency to aid damping following large disturbances. (Nelson River, Eel River).

Some consideration has been given to using the DC link for improving 1st swing transient stability (Arrillaga and Elamin 1976). Its fast controllability lends itself to rapid power changes which could contribute to synchronising power flows between machines in a disturbed system.

The work in this chapter extends that of Arrillaga and Elamin by investigating aspects of first swing stability improvement related to realistic models and systems. A number of aspects of TS improvement, using DC links, are

examined, using the QSS, DC link model discussed in Chapter 5, and representative cases are chosen for detailed investigation using transient converter simulation. The effects of differences in the models on system responses are described and with the aid of interactive coordination of the TCS and QSS models, the feasibility of the proposal is established. The development of a generalised control system is beyond the scope of this work as each control system must be designed for the characteristics and dynamics of the particular AC system for which it will be used.

7.1 BASIC PROPOSAL FOR TRANSIENT STABILITY IMPROVEMENT

7.1.1 First Swing Stability Improvement

The simple case of a generator connected to an infinite bus is illustrated in Fig. 7.1.

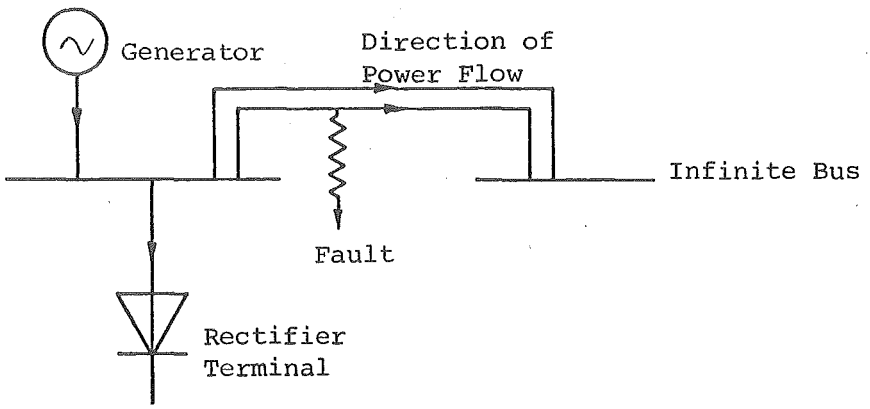

Fig. 7.1 Generator and DC Link Terminal.

If a fault occurs close to the terminals of the generator the electrical power output from it is considerably reduced during the fault period while the prime mover, which is slow to respond, continues to deliver pre-fault power to the generator shaft. Due to the excess of mechanical power the generator accelerates and the rotor angle increases, resulting in an increased power flow to the system. Any method whereby the synchronising power coming from the generator, immediately after the fault, can be increased will decrease the power available for acceleration. This will reduce the maximum swing angle of the generator and reduce the possibility of losing synchronism. When a DC link is

close to the terminals of the generator, rapid control of the link can provide an increased power demand at the generator terminals, drawing extra power from it and improving the transient stability of the machine. A sudden increase in DC power can be obtained by an increase in DC current setting.

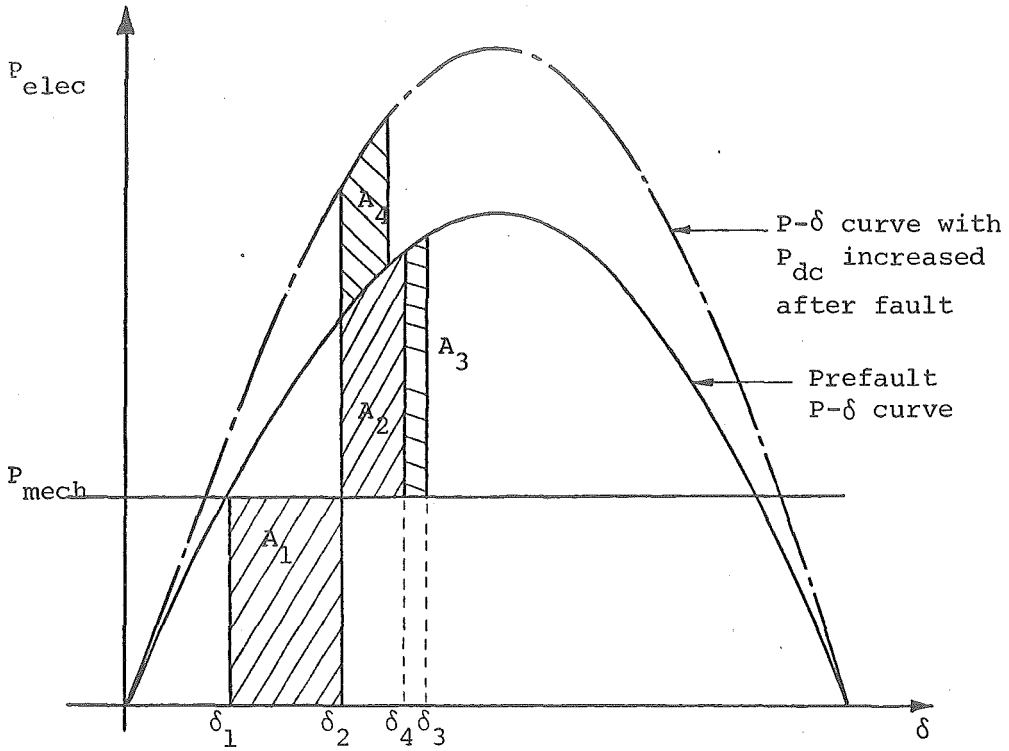

Fig. 7.2 P-δ Curve With Post Fault I_d Increase.

The simple power angle curve of Fig. 7.2 demonstrates, in principle, the effect of a sudden DC power increase. The figure is a very simplified case of a much more complex situation and applies only to a generator modelled as a voltage behind reactance and connected to an infinite bus. During a 3 phase terminal fault the generator experiences accelerating energy proportional to area A1. Without any change in DC current setting, after the fault, the machine experiences a deceleration energy proportional to areas A2 plus A3 before peak swing angle δ_3 is reached.

However if the DC current setting is raised so that the DC power is increased this can be considered as raising the electrical output curve (although it is no longer part of a sine curve) and a new power angle curve is invoked for the period that the DC current is raised. This is demonstrated in concept by the two P-δ curves of Fig. 7.2.

The energy now available for deceleration after the fault is proportional to A2 plus A4 and the peak swing angle is reduced to δ_4. For the illustration of Fig.7.2 the DC current is restored to its nominal value before the peak swing angle is reached.

7.1.2 Full Damping Control

Simple first swing stability improvement can be extended to demonstrate full damping in which the DC power is increased during periods of rotor acceleration and decreased during periods of rotor deceleration. This is illustrated in Fig. 7.3 which, for clarity, assumes changes in DC power take place at maximum or minimum swing angles.

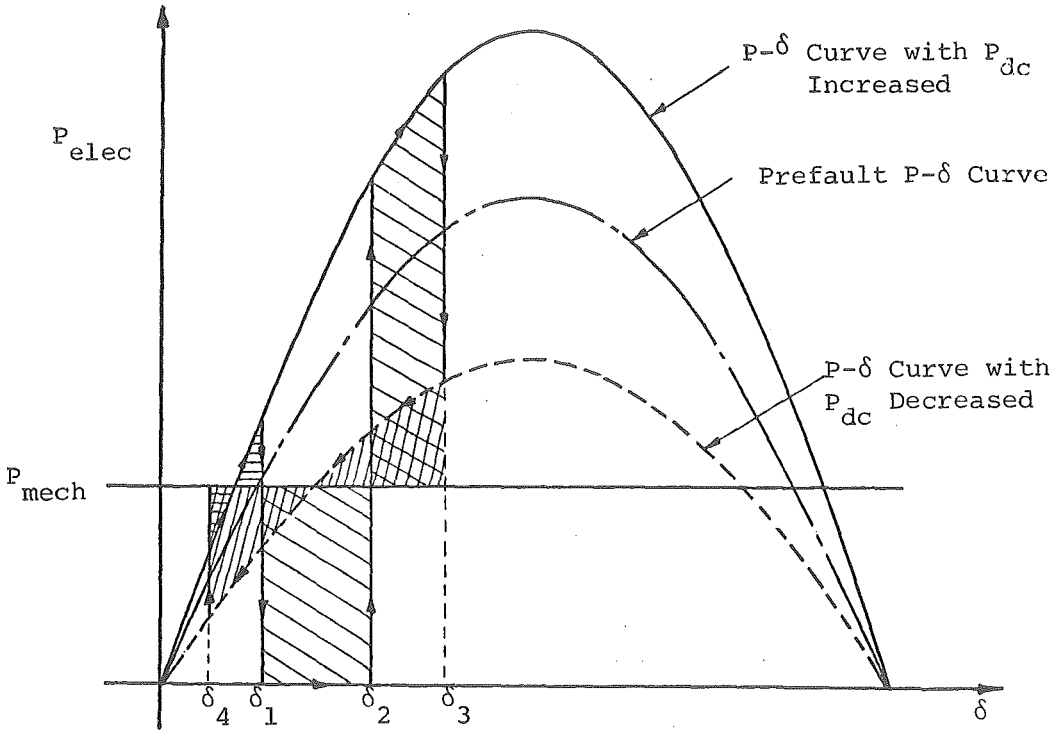

Fig. 7.3 P-δ Curve With Damping Control.

In this idealised case, by the use of sudden DC power changes it is possible to damp the swing of a faulted machine very rapidly.

7.1.3 Short Term DC Current Overload

This proposed TS improvement method relies on the ability of the DC link to change its current setting, from its pre-fault value, for a short period of time. Work by

Haywood et al 1976, Uhlmann 1970 shows that considerable damping of post disturbance swings can be achieved with short DC current setting decreases. However first swing stability improvement in many practical systems requires DC current increase. If the pre-fault DC current is at maximum link rating then a short term overload is required. Some DC links are now being designed to withstand such short term overloads. (Danfors 1976, Bergstrom 1977). In addition, tests on thyristor valves have shown that they can stand quite high short term over currents. (Fotin et al 1976, Hensberger 1978). In the Russian tests a 100% overload DC current was withstood for 8 cycles without valve malfunction.

7.2 POSSIBILITIES FOR TRANSIENT STABILITY IMPROVEMENT

7.2.1 Classification of Systems

There are a number of possibilities for transient stability improvement by either DC current (power) increase or decrease, depending on the machine to be stabilised and the direction of DC power flow. These possibilities are summarised in Table 7.1.

The work by Arrillaga and Elamin 1976 covers case 1 only with a specialised formulation for that case. Cases 1, 2 and 4 of Table 7.1 are situations which are found in practical systems while case 3 would be very unusual.

Case 1 is the type of system which would occur where remote generation capacity is being transmitted long distances to local load centres, i.e. (Nelson River, Ingha Shaba, Cabora Bassa). In this case there is a considerable incentive to ensure that the transient stability of the sending system is not marginal to avoid loss of generating capacity which would result in a drop in transmitted power. In this case the improved security of the generation system justifies the added disturbance at the healthy end.

Case 2 applies to a system where the DC link power is used to reinforce local generation in meeting the load demand. (Sardinia). Stability of the local generation is important to ensure voltage stability for continued inverter

TABLE 7.1 CLASSIFICATION OF SYSTEMS FOR STABILITY IMPROVEMENT USING A DC LINK

Case	System	Stabilised M/c	DC Terminal	Stabilising Control
1	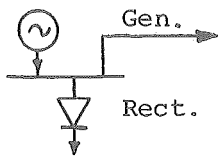	Generator	Rectifier	I_d Increase
2	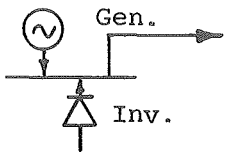	Generator	Inverter	I_d Decrease or DC Link Reversal
3	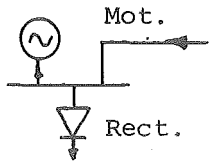	Motor	Rectifier	I_d Decrease or DC Link Reversal
4	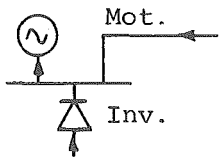	Motor	Inverter	I_d Increase

operation. Where the generator is used for reactive power supply for the inverter, a loss of synchronism of the generator could leave a severe reactive power deficiency at the inverter terminals. This may make inverter operation impossible thereby compounding the power loss of the receiving system.

Case 4 could represent several situations:

i) A DC link terminated close to a large load centre which has a high content of inertia load.

ii) A DC link in a similar situation to case 2 where the local generation is hydro pumped storage and representing the pumping phase in the hydro plant cycle.

iii) A DC link which has a number of synchronous condensers at its terminal to provide reactive power compensation for the inverter. During and after a fault,

the energy loss is compensated, to some degree, by inertial energy from the condensers resulting in deceleration in a similar way to a motor.

This case is of particular interest because a DC current increase at an inverter exhibits a potential for commutation failure.

7.2.2 System for Study

The simpl system of Fig.7.4 was used for transient stability improvement investigations for a number of reasons:

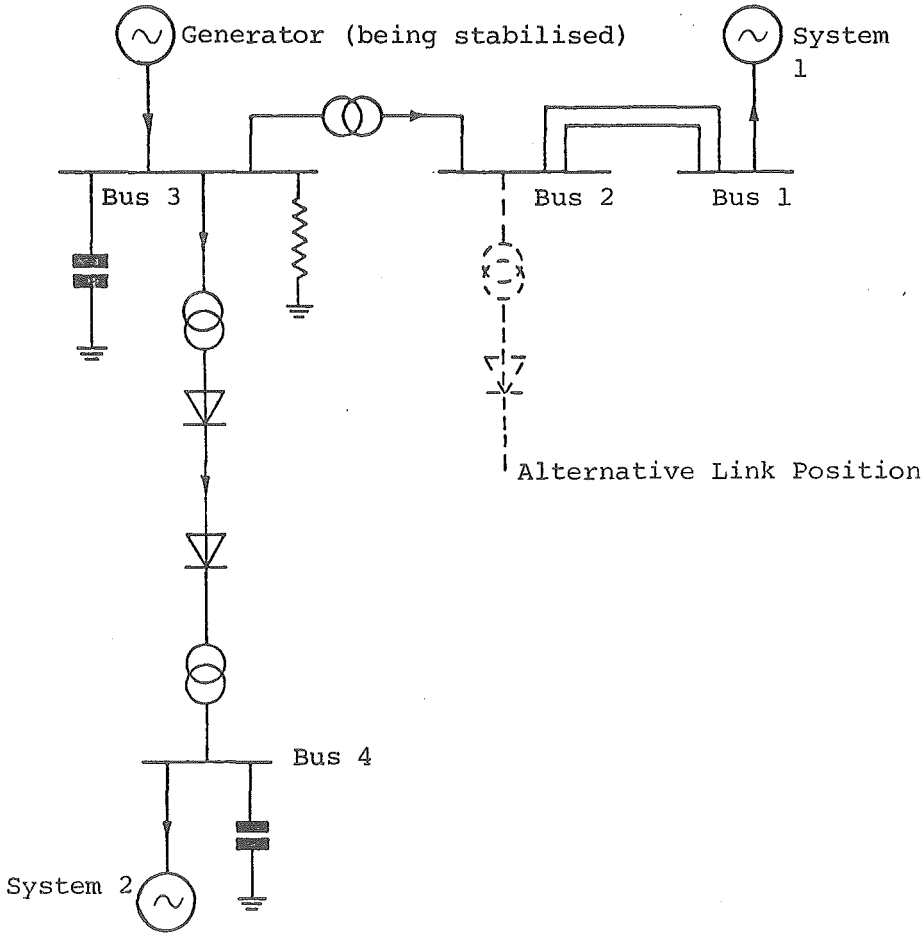

Fig. 7.4 System for Stability Improvement Investigations.

i) The effects of the DC link are not obscured by a complicated system.

ii) The behaviour of the system can be approximated by the P-δ curves of Figs. 7.2 and 7.3.

iii) The system is similar in concept to the S.I. terminal of the N.Z. DC link.

iv) The system is small and hence computational speed and costs are low allowing a large number of studies to be performed.

v) The same basic system can be used for cases 1, 2 and 4 of Table 7.1.

The data for the DC link and network of Fig. 7.4 was derived from the N.Z. system and is given in Appendix A7.

The system is disturbed with a low impedance fault very close to the generator terminals to simulate a worst case study. The fault impedance is sufficiently low so that the DC link shuts down during the fault. A 7 cycle fault is used to bring the system close to its stability margin so that effects of DC power injection can be clearly observed.

It was not intended that this system be used to evaluate the effects of TS improvement at the remote end of the link. This requires a more complete representation of the total system under study and therefore a simple infinite bus was used for system 2. Effects at the remote terminal are considered when the full N.Z. system is used in section 7.5.3. To observe TS improvement the DC link is given an increased current setting after fault clearance. Where not otherwise explicitly referred to, the setting was increased to twice nominal setting (or 1.6 times rated maximum) for a period of 6 cycles.

7.3 THE EFFECT OF REALISTIC MACHINE MODELS

7.3.1 Summary of Results

The work of Elamin 1975 uses a simple voltage behind reactance model of the generators for TS improvement investigations. This model, for most simple stability calculations, gives a good first approximation to the peak swing angle of a machine. However when faults are close to the terminals of a machine, this model is not accurate. Table 7.2 shows the results of a comparison between simple and detailed machine models for the study system. The simple machine model is the same as that used by Elamin and the

TABLE 7.2 EFFECT OF MACHINE MODELS ON TS IMPROVEMENT

CASE		δ_{max}	IMMEDIATE POST FAULT SOLUTION			
Machine Model	I_d Setting		P_{dc} (pu)	$\frac{\Delta P_{gen}}{\Delta P_{dc}}$	$V_{term(gen)}$	$V_{term(sys)}$
Simple Generator	Const.	74.9°	4.32		0.97	0.95
Simple System 1	100% Increase	64.9°	8.13	0.70	0.92	0.95
Detailed Generator	Const.	Unstable	2.53		0.59	0.89
Simple System 1	100% Increase	89.2°	4.37	0.55	0.55	0.8
Detailed Generator	Const.	108.0°	2.49		0.58	0.88
Detailed System 1	100% Increase	89.4°	4.27	0.53	0.54	0.88
Both Detailed	Impedance Model of DC Link	Unstable				

Note: $\Delta P_{gen}/\Delta P_{dc}$ represents the proportion of extra DC power (due to the increase in I_d) which is being taken by the generator (i.e. stabilising power).

detailed model includes transient and subtransient effects.

Table 7.2 makes a comparison between each case by taking the results of the TS solution step immediately after fault clearance so that relevant differences in system states can be observed, indicating the trends for each case.

7.3.2 Discussion

The tabulated results establish a number of points:

i) The simple machine model yields extremely optimistic results. The use of a detailed model for the system machine does show a small effect and this is exaggerated a little by the marginal stability of the case. Swing curves for the different models are presented in Fig. 7.5. For the purposes of comparison, these curves show deviation from initial state.

ii) The modelling of transient and subtransient effects means that, during the fault, the collapse of

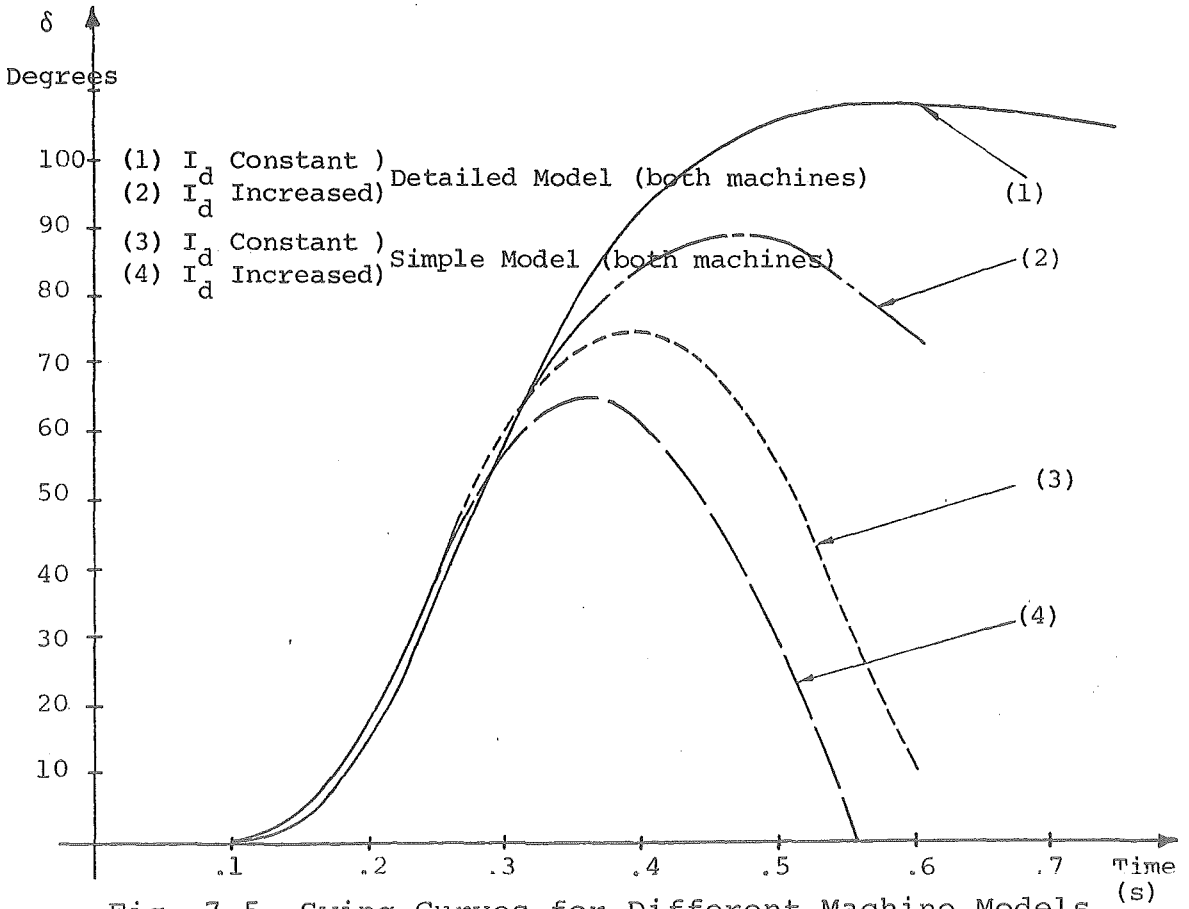

Fig. 7.5 Swing Curves for Different Machine Models.

internal emf in the machine produces a much lower recovery voltage after fault clearance. The machine voltages are illustrated in Fig. 7.6. The primary effect of this voltage reduction is to reduce the transmission capability of the link as shown in Fig. 7.7. The post fault DC power, with detailed modelling and constant current setting, is 50% less than the prefault value and 40% less than the post fault power of the simple model. Figure 7.7 shows that the synchronising powers drawn by the link are very different for the cases illustrated.

iii) The swing curves of Fig. 7.5 demonstrate the effectiveness of a sudden DC current increase for improving TS. For the simple machine model an improvement of 14% is achieved while for the detailed model a 17% improvement is observed. The improvement is due to the extra energy absorbed by the DC link. Referring to Fig. 7.7, the simple model case shows that the DC power in the post fault period exceeds the pre-fault value by 50%.

However with the detailed model the current increase only restores the link power to approximately the pre-fault

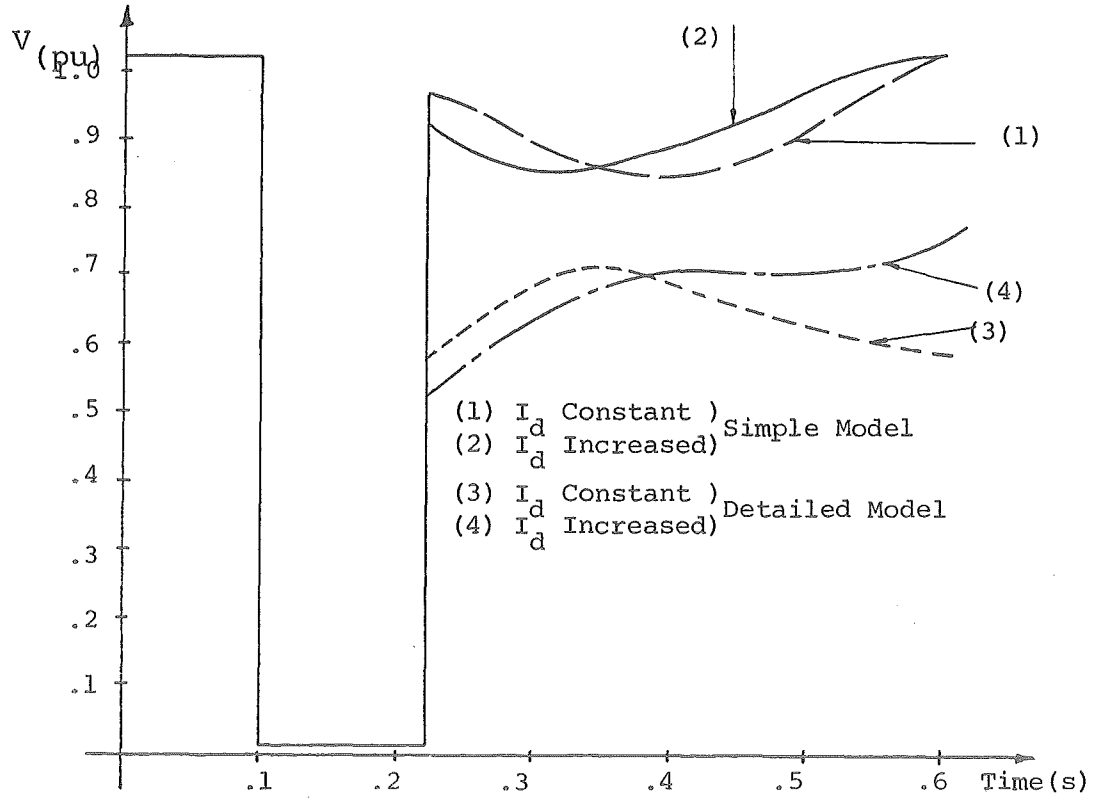

Fig. 7.6 Generator Terminal Voltages for Different Machine Models.

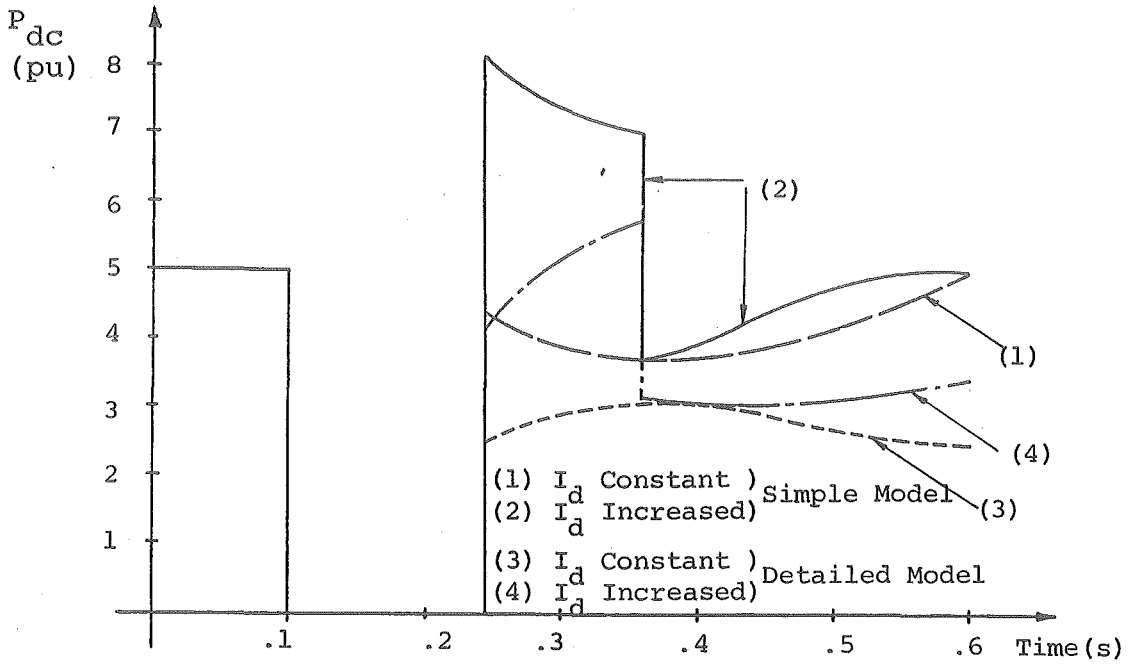

Fig. 7.7 DC Link Powers for Different Machine Models.

value. As well as this reduction in DC power, there is a reduction in the proportion of extra power coming from the generator. The effectiveness of the link in drawing extra synchronising power from the generator is decreased when correct modelling of the generator is used.

iv) Figure 7.8 demonstrates the extra reactive power demand required for the increased DC current at a lower AC terminal voltage. This is due to a considerable increase in commutation angle at the converter from 33° (at recovery) for constant current, to 53° for current increase. A comparison between Fig. 7.6 and Fig. 7.8 shows that the extra reactive power demand causes a 6% drop in recovery voltage at the generator terminals. This is a relatively minor sacrifice for the considerable gain in TS improvement.

v) If the DC link is not properly represented and is replaced by its equivalent impedance load then the resulting network is unstable. This demonstrates the need for a proper DC link model for TS studies.

7.3.3 Effect on P-δ Curve

To demonstrate the effect of the detailed generator model on stability improvement using the power angle curve,

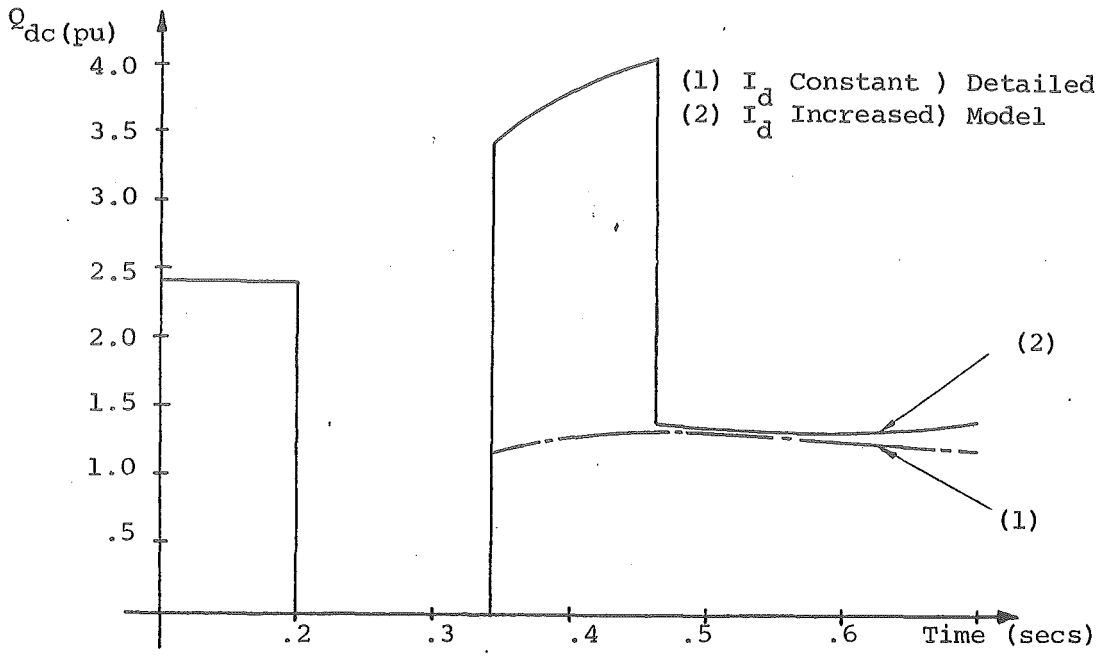

Fig. 7.8 DC Link Reactive Power Demand for DC Current Increase.

Fig. 7.2 has to be modified significantly.

Fig. 7.9 demonstrates the effect of the reduced DC transmission capacity combined with a drop in machine internal voltage. In this case the true post fault P-δ trajectory is a family of curves tending towards the pre-fault P-δ curve as the generator voltage and DC power recover. Hence the case where DC current is increased is not as optimistic as Fig. 7.2 demonstrated and tends to only approach the pre-fault P-δ curve, because of the extra DC power demand.

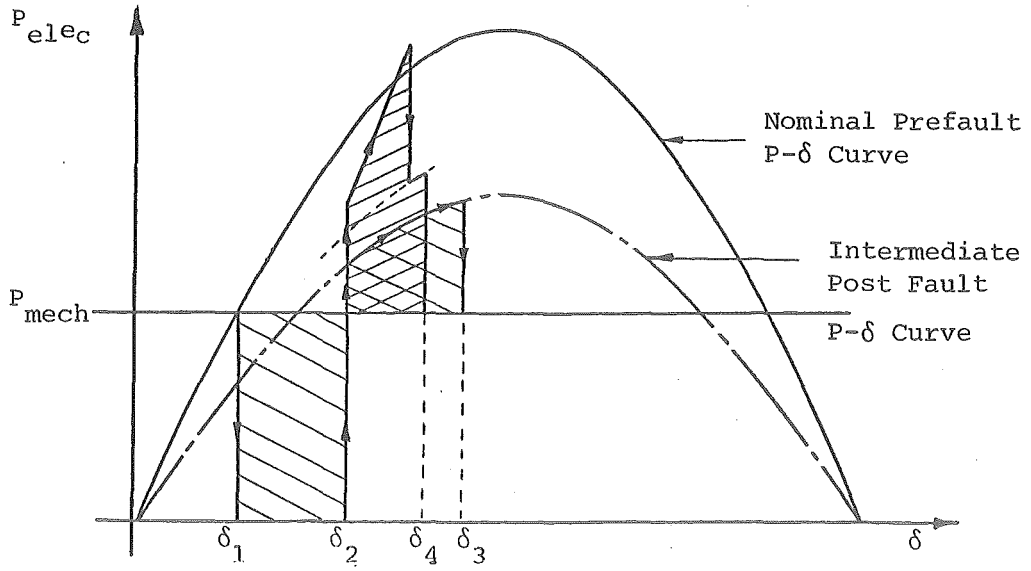

Fig. 7.9 Modified P-δ Curve for Detailed Generator Model.

Figure 7.9 is essentially a static representation of dynamically changing P-δ curves.

7.3.4 The Influence of Fault Position

Results for a low resistance fault applied at Bus 2 of Fig. 7.4, mid-way between the generator and system 1 machines, are presented in Table 7.3.

With the fault position moved away from the generator the disturbance to the generator is decreased and an increased effect is observed at the system 1 machine terminals. This results in an improved recovery voltage at the DC link terminal allowing greater DC power flow when the current setting is increased. With a detailed machine model, the recovery DC power, with constant I_d, only drops 30% on its pre-fault value and, with current increase, it achieves a 28% improvement. Consequently the maximum swing angle is reduced by 14% with current increase. Maximum swing angles are also reduced considerably because, for this fault, the DC link is able to keep operating during the fault period. Fig. 7.10 shows the effect on DC power for a remote fault.

With the fault shifted to Bus 2 a higher proportion of DC power is supplied from the generator when the DC current is increased. In the generator fault case (Table 7.2) only 53% of the increased DC power came from the generator but in this case 74% comes from the generator. This can be attributed to the more even balance of voltage between the generator and the system during and after the fault. Significant differences still exist between the simple and detailed machine models and hence simple models cannot be considered acceptable.

7.4 FACTORS AFFECTING TRANSIENT STABILITY IMPROVEMENT

There are a number of factors to be considered when evaluating the response of a DC link for the purpose of stability improvement:

TABLE 7.3 INFLUENCE OF FAULT POSIITON ON TS IMPROVEMENT.

CASE		δ_{max}	IMMEDIATE POST FAULT SOLUTION			
Model	I_d Setting		P_{dc} (pu)	$\frac{\Delta P_{gen}}{\Delta P_{dc}}$	$V_{term(gen)}$	$V_{term(sys)}$
Simple Generator	Const.	58.7°	4.75		0.98	0.96
Simple System	100% Increase	51.4°	8.29	0.70	0.94	0.96
Detailed Generator	Const.	64.4°	3.46		0.79	0.84
Detailed System	100% Increase	55.4°	6.42	0.74	0.75	0.84

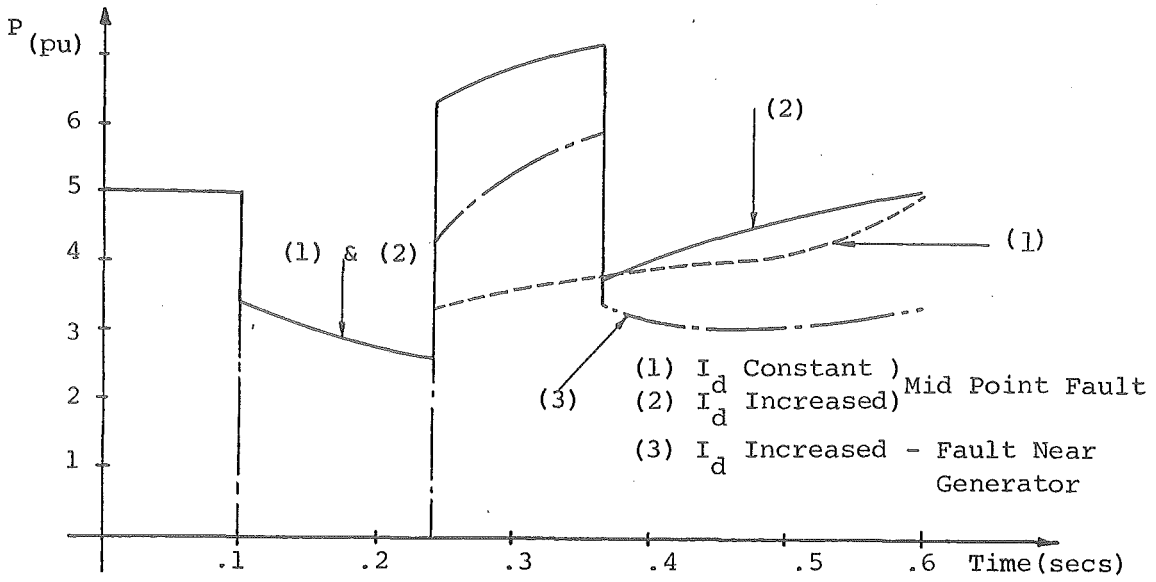

Fig. 7.10 DC Power for Different Fault Positions.

1) Magnitude of DC current increase.

2) Period of DC current increase.

3) DC link position in the network.

4) Fault resistance.

5) Rate at which DC current can be changed.

7.4.1 Magnitude of DC Current Increase

Figures 7.11 to 7.13 illustrate results from a number of studies in which the magnitude of DC current is varied, up to a 350% increase on the pre-fault value. Figure 7.11 shows that there is a maximum DC power injection which can be achieved, i.e. with a 175% increase in I_d for a generator fault and 250% for a mid-point fault. This limit is reached because the increased reactive power demand of the link depresses the AC voltage to an extent where the reduction of DC voltage outweighs the increase in DC current. However Fig. 7.13 demonstrates maximum improvement to swing angle occurs at 100% and 150% for the two cases, respectively. The rate of fall off in the extra DC power coming from the generator, illustrated in Fig. 7.12, accounts for the difference between maximum DC power and minimum peak swing angle.

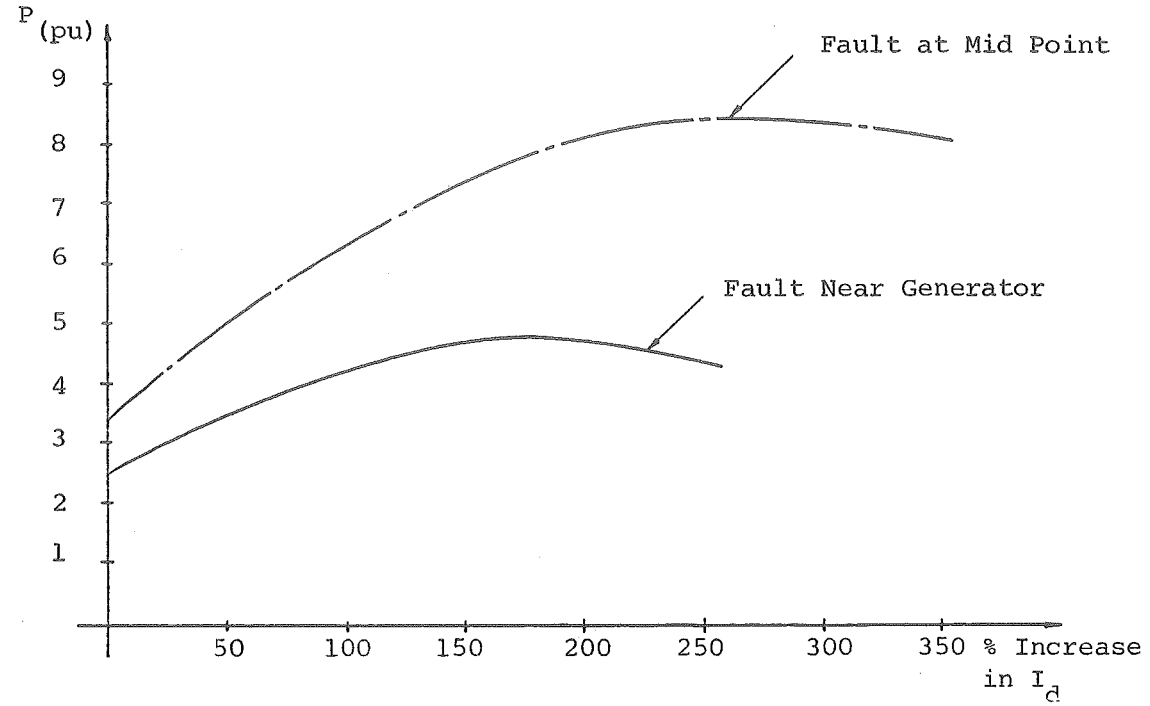

Fig. 7.11 DC Power Increase Against % Increase in I_d.

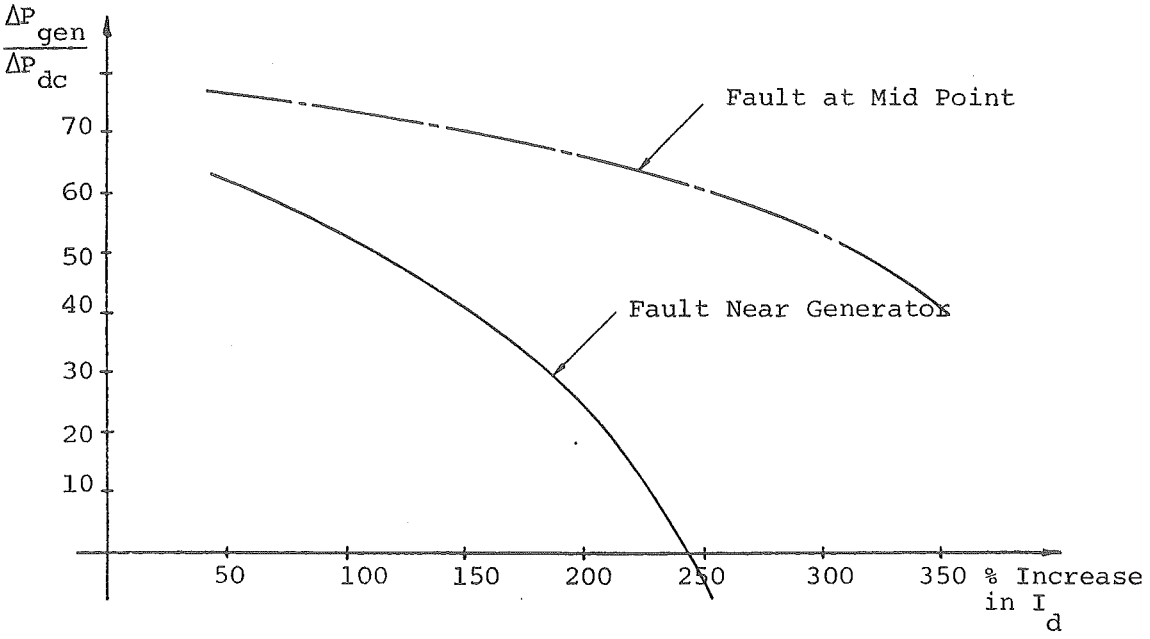

Fig. 7.12 Proportion of Increased DC Power Taken By Generator Against % Increase in I_d.

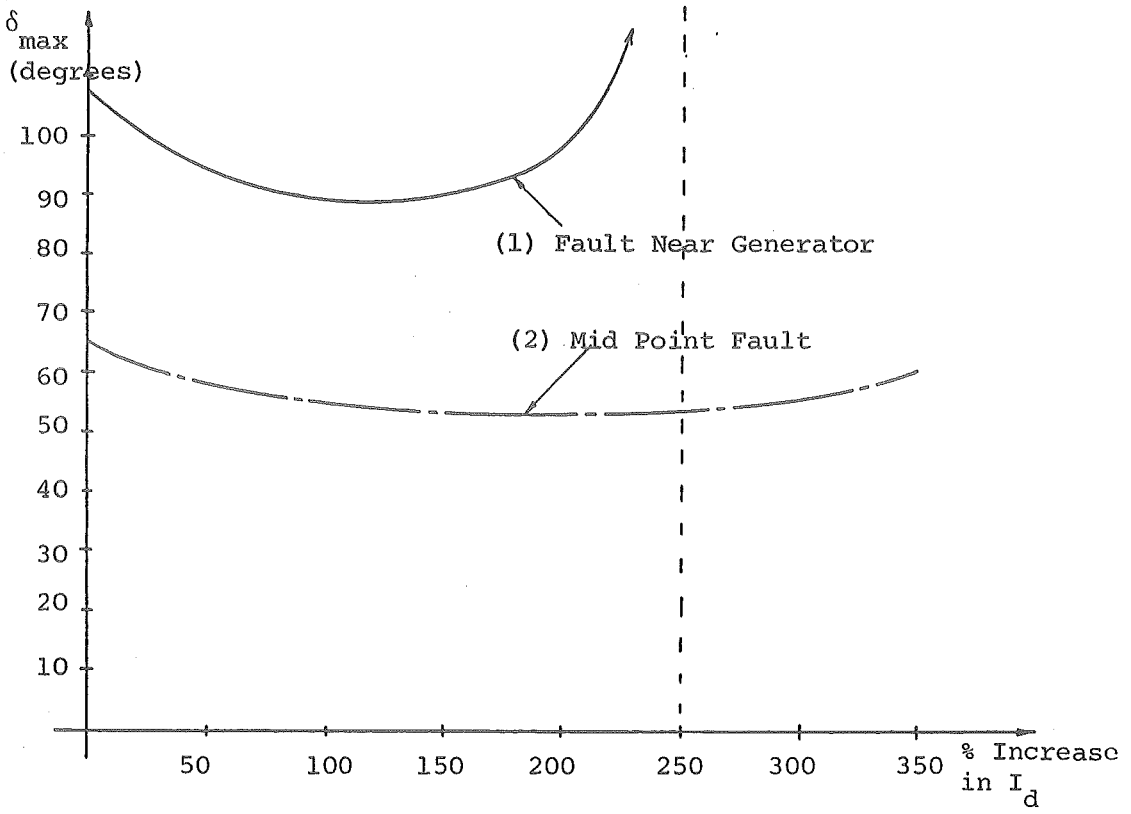

Fig. 7.13 Maximum Swing Angle Against % Increase in I_d.

These results illustrate that, without any special means for extra voltage support at the DC link terminals, optimum stability improvement can be achieved with a feasible and easily obtainable DC current overload. Any benefits of higher DC currents are lost by the dropping proportion of power actually being taken from the generator.

Special methods for voltage support using switched static VAR systems, overexcited machines and high rectifier delay angles have been proposed (Grund et al 1979) and in this way the recovery DC power may be improved. These techniques are most effective for faults close to the generator and in Fig. 7.13, curve 1 would tend towards curve 2. However any method of voltage support for stability improvement has to be a practical and economically viable mode for continuous operation of the converter. It would be uneconomic and unsatisfactory to consider operating a DC link on large delay angles continuously just for the purposes of TS improvement, as proposed by Grund et al. Extra equipment for reactive power injection would have to be carefully justified. Results presented in Figs. 7.11 to 7.13 show that

a useful decrease in maximum swing angle can be obtained, without such sophisticated voltage support schemes.

7.4.2 Period of DC Current Increase

So far the results presented have been based on a current increase period of 6 cycles. Figure 7.14 illustrates the improvement in maximum swing angle as the period varies from 1 to 9 cycles. This result shows that even quite short periods (2-3 cycles provide a significant reduction in peak swing angle (11% - 13%). The improvement begins to

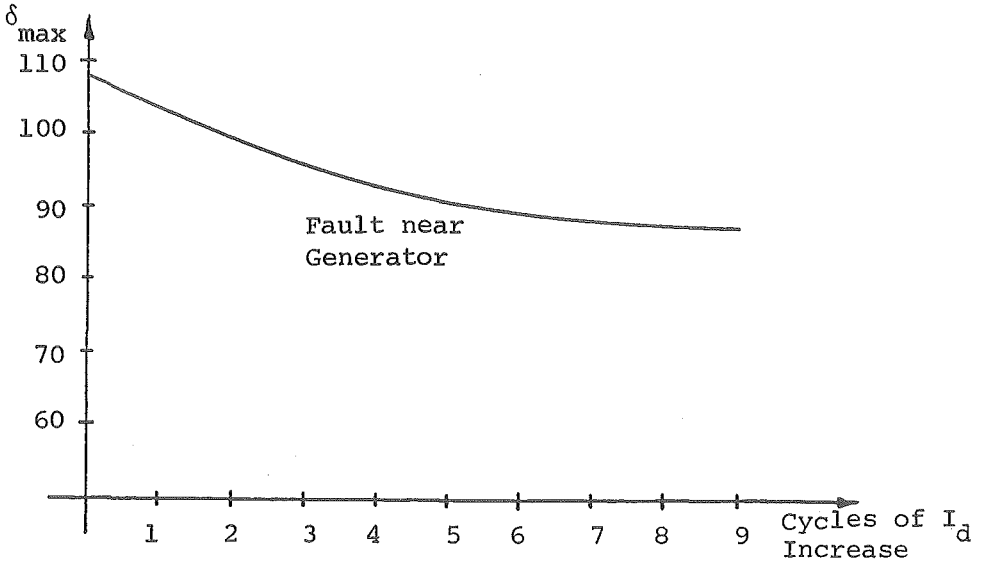

Fig. 7.14 Maximum Swing Angle Against Period of I_d Increase.

diminish for periods greater than 6 cycles and this is dependent on the natural frequency of the system under study. In these studies the peak swing angle occurs 10.5 cycles after fault clearance. For systems with a higher natural frequency the optimum period would be less while the reverse would be true for systems with a lower natural frequency. In this latter case the period for which over-rating of the DC link could occur, without damage to its components, could limit the maximum period of I_d increase. The tests performed by Fotin et al (1976) indicate that thyristors can tolerate a period of 8 cycles at twice rated current without any adverse effects on them.

7.4.3 DC Link Position in the Network

The position of the DC link in the network affects its ability to increase the synchronising power drawn from the machine being stabilised. This effect was studied by shifting the connection point of the rectifier to a point midway between the generator and system (dotted in Fig. 7.4). To maintain the same initial angle between machines the transformer impedance was reduced. The results for a fault close to the generator terminals are summarised in Figs. 7.15 and 7.16.

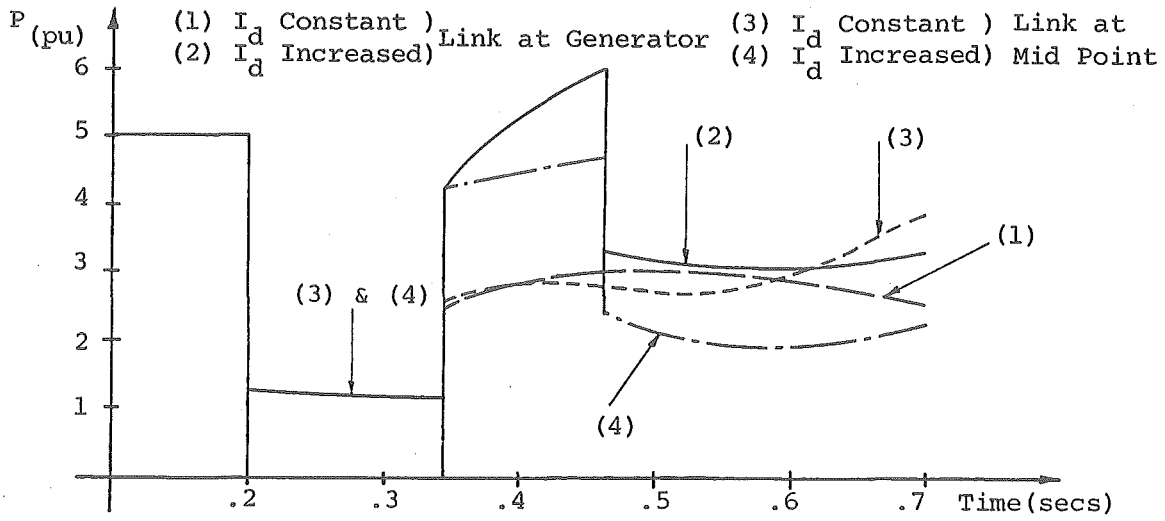

Fig. 7.15 DC Powers for Different Link Positions.

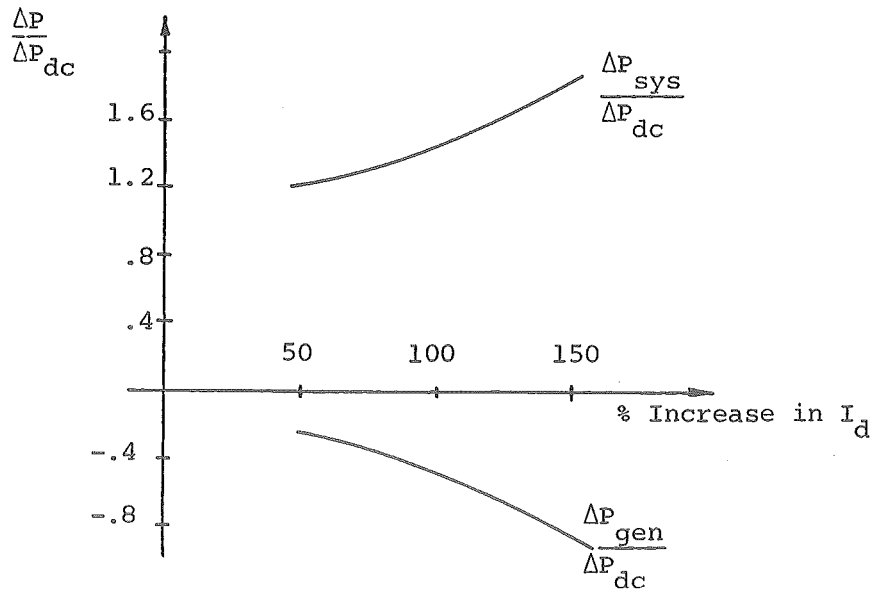

Fig. 7.16 Distribution of Increased DC Power for DC Link at Mid Point.

Figure 7.15 compares the DC powers for the two link positions and shows that the lack of strong voltage support at the link terminals reduces the effectiveness of the increased DC current. Coupled with this effect is a decrease in post fault synchronising power when DC current increase is introduced. Figure 7.16 contrasts with Fig. 7.12 in demonstrating that the extra post fault power drawn by the link is taken preferentially from the system at the expense of synchonising power from the machine being stabilised. This situation does not provide stability improvement and the maximum swing angle increases with DC current increase as shown in Table 7.4.

TABLE 7.4 MAXIMUM SWING ANGLES FOR A DC LINK REMOTE FROM THE GENERATOR BEING STABILISED

Case	I_d Const.	50% Increase	100% Increase	150% Increase
δ_{max}	82.9°	85.9°	95.7°	Unstable

The onset of instability occurred suddenly, as the maximum swing angle increased. At maximum angle between the two machines the voltage at the link terminal is lowered considerably and consequently the DC link power is reduced, as illustrated by curve 4 of Fig. 7.15 at 0.5 secs. In the unstable case, link shutdown took place at 0.48 secs, accelerating instability.

In a system where the link position is between two finite generators, TS deterioration may not occur. In this case the extra DC link power would come from one or other generator and this would represent a greater synchronising power flow between the two, decreasing their maximum swing angle.

7.4.4 Fault Resistance

Some consideration has to be given to the effect of fault resistance on TS improvement. For 3 phase faults,

the fault resistance can normally be considered as negligible since the worst case is being considered. However if it were necessary to include resistance in the fault path, the stabilising controls of Table 7.1 need to be altered. With a high fault resistance considerable real power is absorbed by the fault and this is supplied from the machines. Instead of a generator accelerating during the fault period, deceleration may take place due to the fault power exceeding the turbine power. Any TS improvement controls would need to decrease the generator power in the post fault period.

7.4.5 Rate of DC Current Increase

For simplicity, studies so far have assumed that the DC link start up can take place instantaneously. Results from transient converter simulation of a DC line fault (Chapter 6) show that DC link start up is a gradual response so that voltage and current overswing are avoided. Hence the results so far tend to be optimistic as there will be some loss in transmitted DC energy due to gradual link startup. The experience with the DC fault case enables a restart time constant to be calculated. Using this, the current setting of the QSS model, during startup, can be ramped to provide a gradual startup similar to that obtained by TCS. Figure 7.17 illustrates the two current setting characteristics used. The effect of this ramped start on results is given in Table 7.5.

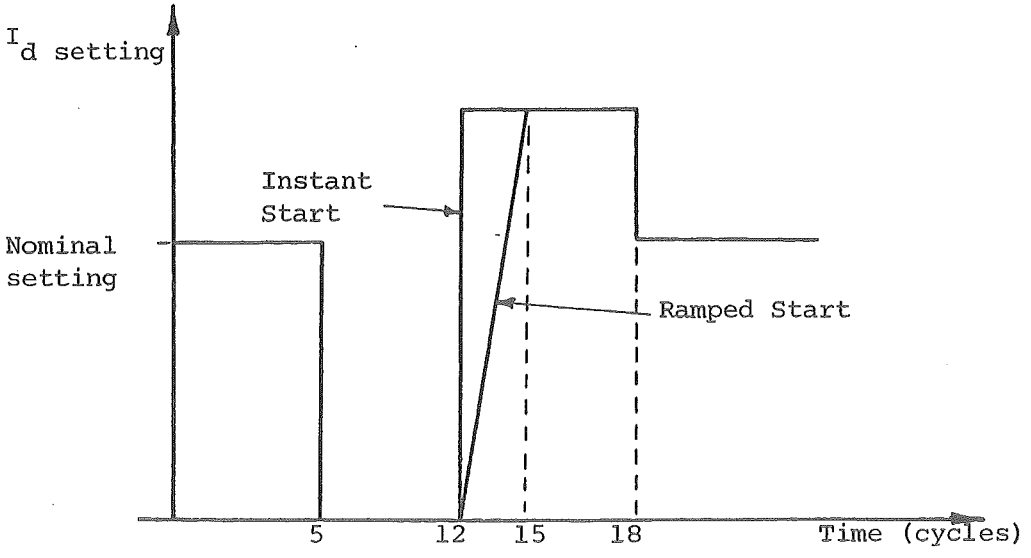

Fig. 7.17 Current Setting Characteristics for Stability Improvement Using QSS Model.

TABLE 7.5 EFFECT OF RAMPED DC LINK STARTUP ON MAXIMUM SWING ANGLES

Case	I_d Setting	Startup Time (cycles)	δ_{max}
1	Const.	0	108.4°
2		2	Unstable
3	100% Increase	0	89.4°
4		3	95.4°

The effect of the ramped DC link start is to reduce the improvement in δ_{max} from 18% to 12%. However the maximum DC current overload condition exists for only 4 cycles, reducing the overload duty on the converter valves.

7.4.6 Summary of Results

i) A comparison of simple and detailed machine models shows that the simple model yields unrealistic results.

ii) With detailed generator models significant improvements in first swing stability can be obtained for relatively short periods of DC current increase.

iii) For severe faults in a system with the DC link terminating at the machine to be stabilised, excessive DC current increases can lead to instability. For any given system an optimum current setting increase can be determined beyond which first swing stability will not be improved.

iv) For the system investigated, the optimum improvement in first swing stability is obtained for feasible periods and magnitudes of DC current overload.

v) A significant improvement in TS can be achieved without the need for special voltage support equipment.

vi) When DC link response rate is accounted for, the effectiveness of a post fault current setting increase is reduced and the period of DC current overload is also reduced.

7.5 RESULTS WITH REALISTIC SYSTEMS

The results so far have been obtained with the simple system of Fig. 7.4. Although a generator connected to a large system provides a clear and unobscured view of the effect of DC current increases, DC links do not operate in such ideal systems. The NZ system is used to extend the results of section 7.4 to a real system. The area of interest is principally focused on the rectifier end (SI system) of the link but the final part in this section looks at the response of the undisturbed NI system to a DC current increase.

7.5.1 Two Generator SI System Equivalent

The simple system of Fig. 7.18 was used as a first approximation to the NZ SI system to illustrate the effect of a second generator near to the DC link. In this case the system is marginally stable for a 7 cycle fault near the rectifier bus. The results of this case are summarised in the curves of Fig. 7.19 and illustrate some important differences from earlier results. The maximum reduction in peak swing angle with a current increase is only 5.5%. This is due to two effects:

i) For a 100% increase in current setting the proportion of extra DC power taken by machine 1 is reduced from 60-70% to 50%. This effect is produced because each machine in the system takes some proportion of the extra DC power.

ii) With a fault close to generator 1, this machine experiences acceleration during the fault period. However generator 2 experiences deceleration due to the resistive

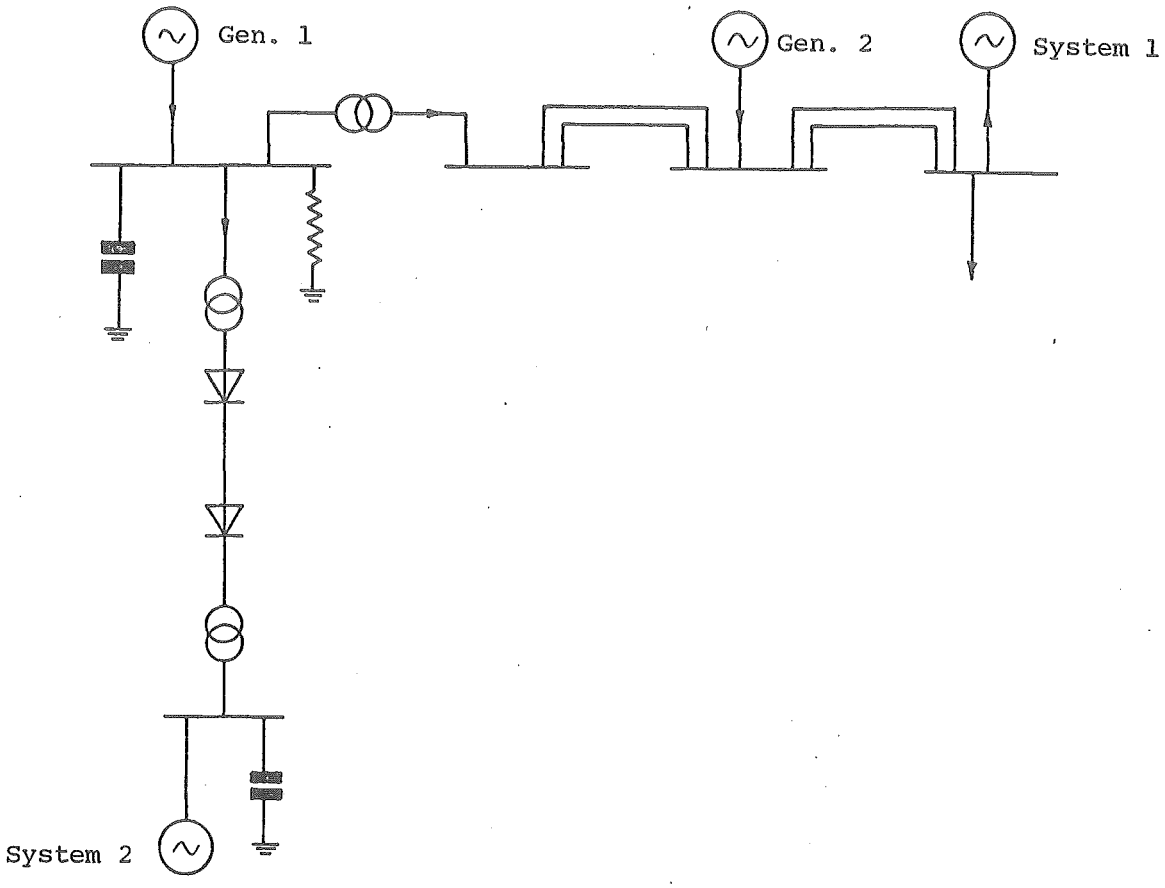

Fig. 7.18 Simplified South Island System for Stability Improvement.

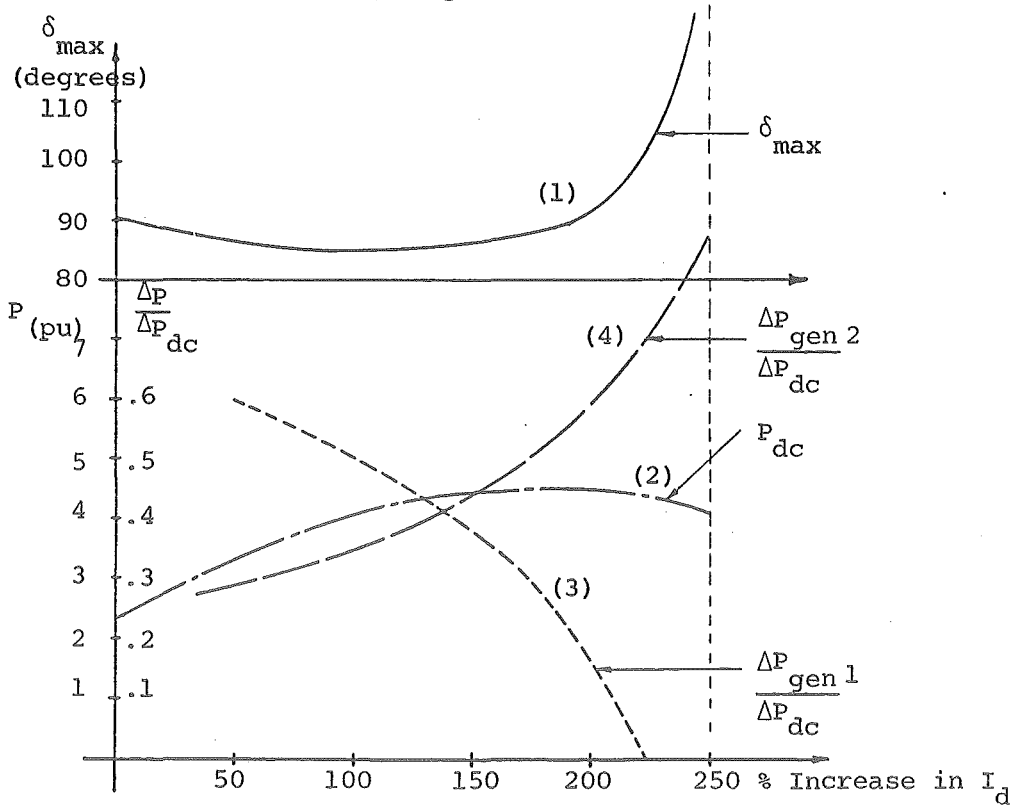

Fig. 7.19 Results for Simplified South Island System of Fig. 7.18.

power loss from the fault current feeding through the transmission network. An increase in DC power demand after the fault tends to stabilise generator 1 but has the opposite effect on generator 2. The swing of generator 1 is reduced but the swing of generator 2 is increased and this effect becomes more noticeable as $\Delta P_{gen\,1} / \Delta P_{dc}$ drops and $\Delta P_{gen\,2} / \Delta P_{dc}$ rises (curves 3 and 4 of Fig. 7.19).

Curve 1 illustrates that a 100% increase in DC current is the optimum increase even though peak DC power is obtained with a 200% increase.

7.5.2 Full SI System

In this case the full SI system was used as the study system and generators close to the DC link were on their rated loadings. Data for this system is a subset of the data presented in Appendix A6. A 7 cycle fault disturbance was applied and the results are given in Table 7.6 for two fault positions.

With the fault close to the Benmore generator terminals a high proportion of the increased DC power is lost to the rest of the system and only 10% is taken by the machine being stabilised. The peak swing angle is reduced by 5.5% with a current setting increase. This improvement reflects the increased synchronising power flowing from other disturbed generators in the system apart from the Benmore machine.

When the fault is moved to a point some distance away from the Benmore generator it takes a much greater proportion of the extra DC power and the reduction in peak swing angle is 13%. This result shows that methods used to improve the recovery voltage of the stabilised generator will benefit transient stability improvement.

7.5.3 Full NZ System

Consideration must be given to the influence that a sudden DC power increase, requested in one system, may have on the system at the other end of a DC link. In the NZ system there are a number of synchronous condensers close

TABLE 7.6 TS IMPROVEMENT RESULTS FOR FULL SOUTH ISLAND SYSTEM.

CASE		δ_{max}	IMMEDIATE POST FAULT SOLUTION		
Fault Position	I_d Setting		P_{dc}(pu)	$\frac{\Delta P_{Ben}}{\Delta P_{dc}}$	V_t Benmore (pu)
Close to Benmore Generator Terminals	Constant	49.5°	2.94		0.67
	100% Increase	46.9°	4.64	0.10	0.57
Close to Benmore 220 kV Bus	Constant	37.6°	3.34		0.75
	100% Increase	32.8°	5.55	0.45	0.67

to the inverter terminal. Because of their relatively low inertia, these machines are susceptible to sudden power changes. Figure 7.20 presents the swing curves of the machines at either end of the DC link for a 3 phase fault near the Benmore machine with and without a post fault current setting increase.

The effect of a DC current increase at the Haywards machine is to reduce the first swing excursion and increase the backswing with following swings being slightly greater than without DC current increase. There is an 11% reduction in the first swing peak.

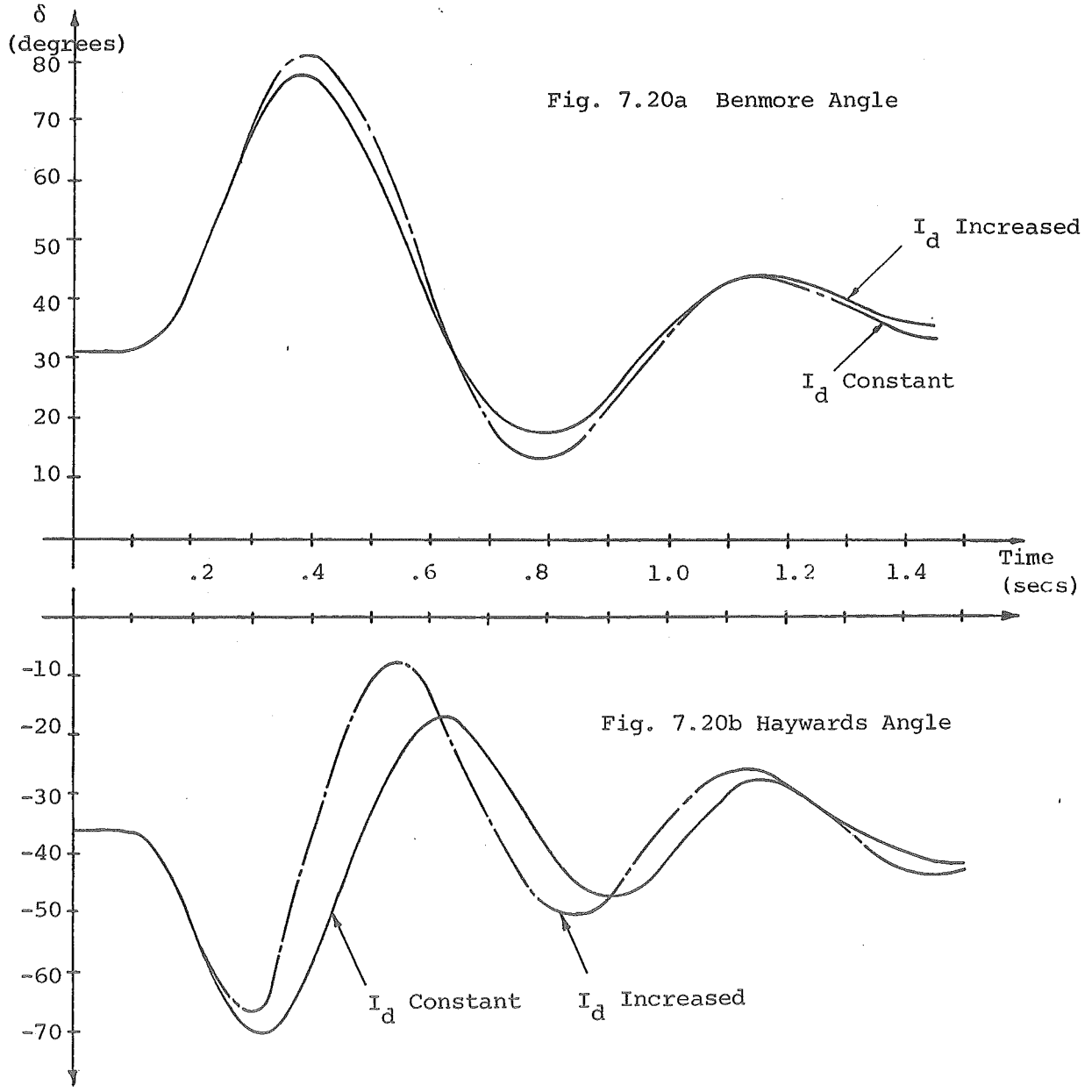

Fig. 7.20 Swing Curves for NZ System with Stability Improvement.

Although the DC current increase was intended for stability improvement at the Benmore machine, some first swing stability improvement has also been observed at the inverter end. If generation had been present at the inverter this would not be the case. The extra disturbance at the inverter end is not great and this is because the effect of the increased current setting is small when compared to the original fault, which causes total DC transmission loss during the fault period. The beneficial improvement at the rectifier has been obtained with little extra disturbance in the inverter system.

7.6 CONSIDERATION OF FULL DAMPING CONTROL

7.6.1 Discussion of Controller

A number of special purpose controllers have been designed for DC links,to solve power frequency problems in both synchronous and asynchronous links. (Hayward and Patterson 1976,Cresap and Mittelstadt 1976). It is beyond the scope of this work to design such a controller for TS improvement and damping. The purpose of this section is to demonstrate, using a simple control strategy, the rapid damping a DC link can apply to an AC system when its DC current is adjusted in response to machine swing.

For this purpose the DC current setting is controlled by a simple switched controller responding to generator slip and is a derivative switched controller for rotor position. Some deadzone is included so that the DC link is restored to its nominal current setting once the system is settled. The simple controller characteristic is illustrated in Fig. 7.21a and can be modified to include frequency control if a characteristic, in the form of Fig. 7.21b, is used.

In the TS programme, slip is computed as the rate of deviation from nominal frequency. If a simple two machine system is used then both TS improvement and frequency control can be achieved with the same control signal. In a real system the TS improvement control signal will need to be obtained from absolute machine acceleration and deadzone

Fig.7.21a

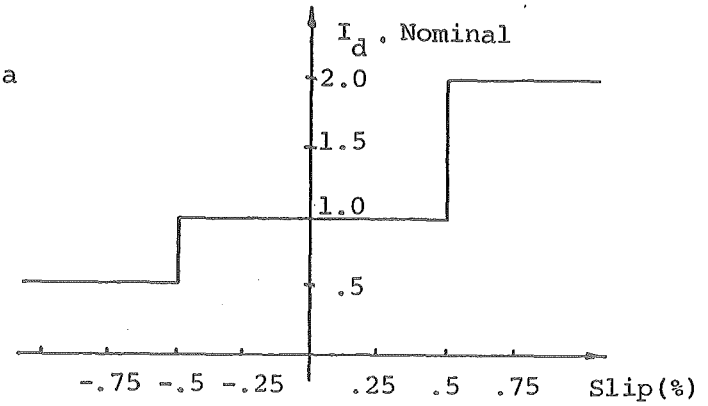

Fig. 7.21b

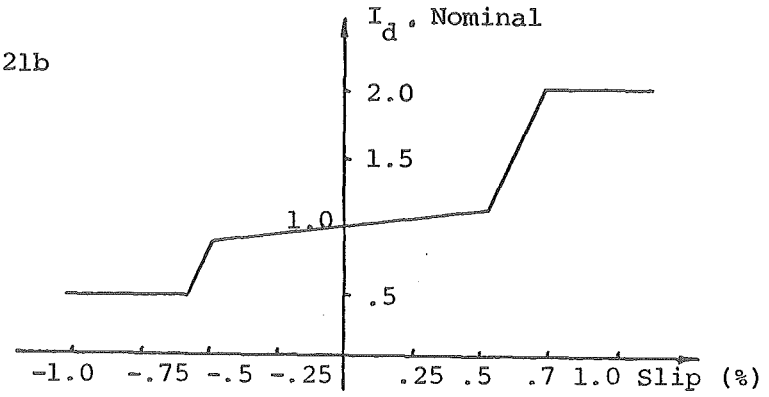

Fig. 7.21 Switched Controller Characteristics.

in this control will allow the system frequency to drift without continually invoking the stability improvement controls.

Some capability limit will need to be included to avoid an excessive period of overload operation. It is likely that a period of increased current setting will be followed by a period of reduced DC current to counteract the negative swing. In this way the increased energy dissipation in the converters will be balanced by a period of reduced dissipation allowing a number of subsequent DC current steps to take place.

7.6.2 Results

The simple controller of Fig. 7.21a was used with the system of Fig. 7.18 and the resulting swing angle of the rectifier machine is presented in Fig. 7.22. These swing curves demonstrate the very effective damping to be obtained

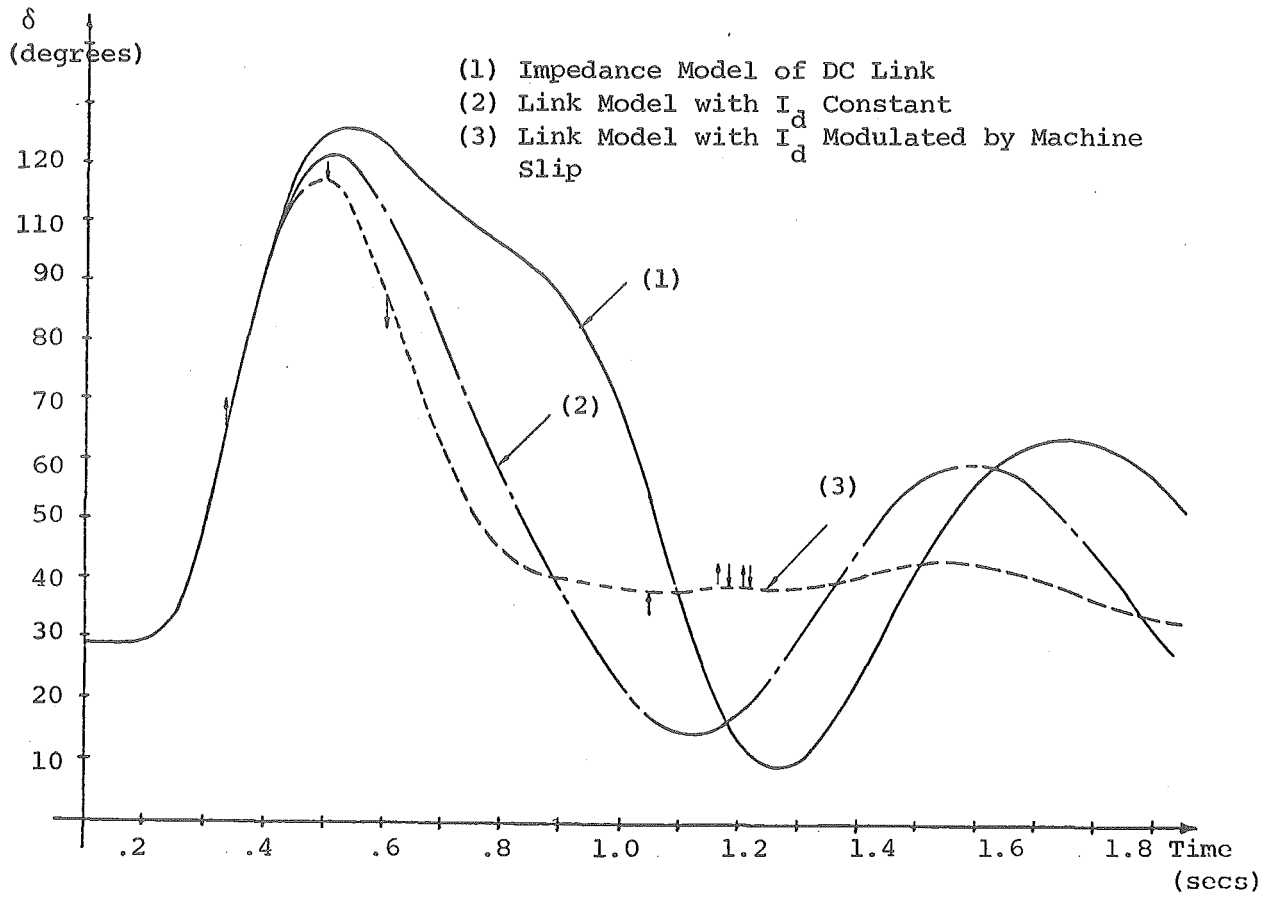

Fig. 7.22 Effect of Full Damping Control on Swing Angle.

using the DC link for transient stability improvement. Not only is the first swing reduced but the system is restored to almost a steady state condition. The arrows associated with curve 3 indicate the times at which the DC current settings deviated from nominal, those above indicating current increase and those below indicating a current decrease. It can be seen from these that the period of increased setting lasts for 8 cycles and is followed shortly after by a period of 22.5 cycles when the link is operating at half nominal current setting. This period allows nominal operating conditions to be restored in the converters. Some chatter is observed as the system approaches steady state. This problem could be avoided with proper controller design (i.e. adding some hysteresis to the control characteristic).

As a further illustration of the need for a DC link model, curve 1 of Fig. 7.22 is the swing curve of the

system with the link modelled as an impedance. With this model the system is only marginally stable.

7.7 ALTERNATIVE TS IMPROVEMENT SYSTEMS

The systems investigated so far have focussed on TS improvement at a rectifier terminal, these being categorised by case 1 of Table 7.1. Because of the large number of case studies required for these investigations, the QSS link model was used for TS assessment. It is therefore necessary to perform a TCS of the stability improvement proposal to validate, or otherwise, the results of the QSS studies, and to check their accuracy. This simulation is discussed in section 7.8.1. However the results from a TCS of case 1 (of Table 7.1) cannot be extrapolated to cases 4 and 2 of the table and it is necessary to perform separate simulations for these cases. These simulations are included in sections 7.8.2 and 7.8.3. For completeness the results of the QSS modelling of these two cases are presented here.

7.7.1 Inverter End TS Improvement

The system used for this study is similar to that shown in Fig. 7.4 but with the DC power flow in the opposite direction and the generator operating as a motor. The data for this system is included in Appendix A8. This system is less stable than for the equivalent rectifier case so the fault period was reduced to 5 cycles to give a reasonably marginal case for study.

The results are summarised in Fig. 7.23 and are little different from those of the rectifier system. This is to be expected because of the limitations of the QSS DC link model.

7.7.2 DC Link Power Reversal

One of the difficulties in considering power reversal is the time which such a reversal takes (Arrillaga et al 1972, Milias-Argitis et al 1977, Cahen et al 1966). If a power reversal is to be of use for first swing

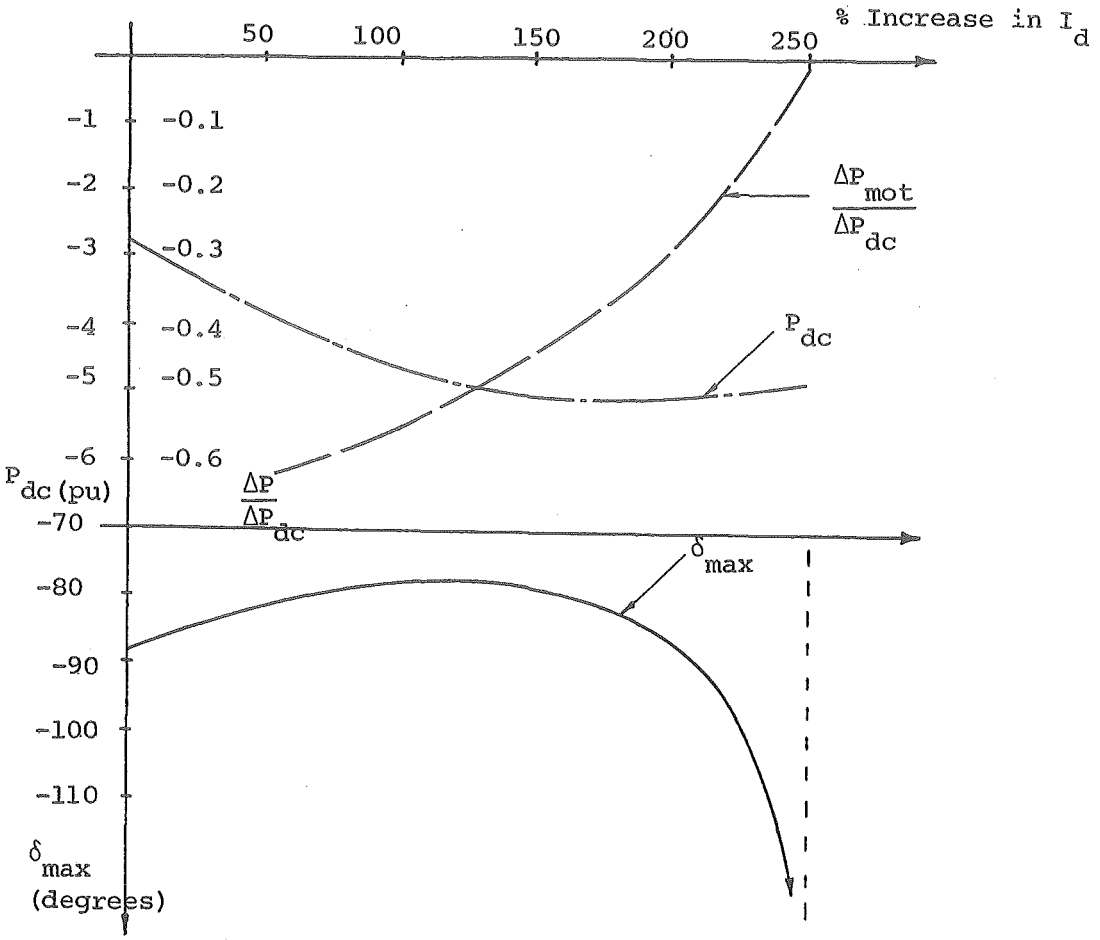

Fig. 7.23 Inverter End TS Improvement.

stability improvement, there has to be a clearly defined need for it before reversal is activated. In the case of severe faults, where TS improvement is of prime importance, the DC link would normally be shutdown during the fault period. This means that a decision for reversal may be made during the fault period and can be acted upon when the DC link restarts after fault clearance. After a number of cycles of reversed operation a transfer to normal operation will be required. This power flow change can take place without shutdown or extinction of the DC current. A typical profile of power flow is given in Fig. 7.24.

The system used for this study is similar to that illustrated in Fig. 7.4 but with the DC power flow reversed. The transmission parameters are reduced to compensate for the increased ratings and the system data is presented in Appendix A9.

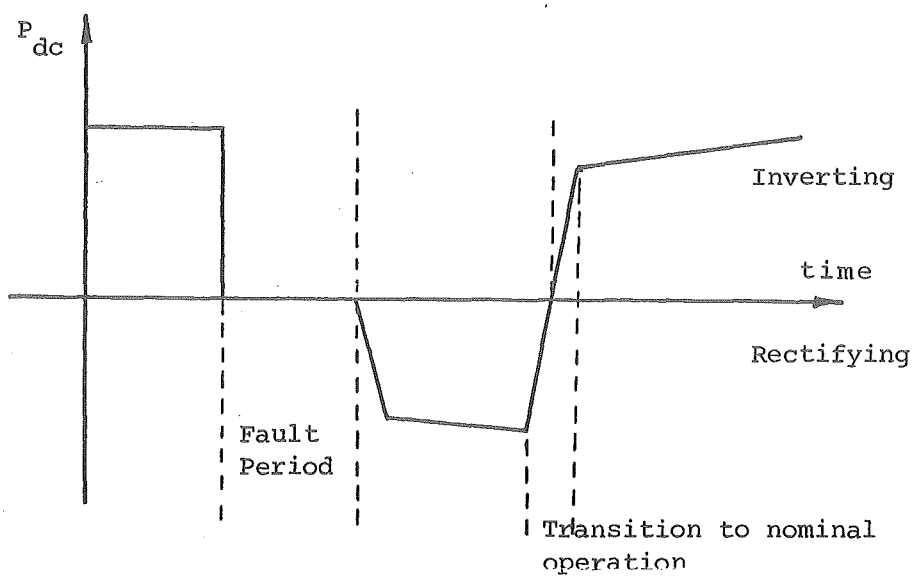

Fig. 7.24 DC Power Flow With Link Reversal.

The outlined power reversal algorithm was implemented with the QSS model and the results appear in Table 7.7.

It is noticeable that a considerable peak swing reduction can be achieved merely by a reduction in DC current setting or a delay in startup. This form of link performance would be easy to implement in practice and hence system stability would have to be very marginal before a fast power reversal would become a consideration. The feasibility of power reversal is next examined by TCS.

7.8 TRANSIENT CONVERTER SIMULATION RESULTS

Three transient converter simulations were performed to investigate in detail, each of cases 1, 2 and 4 of Table 7.1, to compare the system performance with that predicted by the QSS model of the DC link.

In each of these cases a severe fault is considered, which results in DC link shutdown. The results of Chapter 6 show that DC power flow decays very rapidly at fault onset which, for these cases, allows simulation to begin at fault removal without any effect on transient stability. This saves a considerable amount of computation time and expense by eliminating the need for an initial condition run and the simulation during the fault period.

TABLE 7.7 TS IMPROVEMENT BY DC LINK POWER REVERSAL

Post Fault DC Current Change	Constant	50% Reduction 6 Cycles	6 Cycle Shutdown	50% Setting in Reverse for 6 Cycles	100% Setting in Reverse for 6 Cycles
δ_{max}	74.3°	66.3°	66.3°	59.8°	58.8°
% Improvement		10.8%	17.5%	19.5%	20.8%

Initial delay angles at fault clearance are calculated assuming complete link shutdown and depend on which end of the link is disturbed. For example, in a rectifier end fault, α_r will remain on its minimum while α_i will be 90°. The simulation period includes post fault DC link startup, (Restart), with increased DC link current (or DC power reversal) for 6 cycles followed by restoration of the link to its prefault settings. The simulations were performed by M.D. Heffernan (1980).

7.8.1 Rectifier End Fault Case

Using the DC line fault (section 6.3) as a guide, the system equivalent for TCS was obtained using a ramped DC current over a period of 3 cycles (0.06 secs) for the DC link restart. The use of the relatively slow startup is supported by the fact that the rectifier is restarting under low voltage conditions. Because of this, all control activity will be at the inverter end which is operating with full AC voltage and link response at the rectifier, following control action, will be delayed by the line time constant. The results of the study (coded 1321R) are illustrated in Fig. 7.25. The rectifier voltage shows little distortion during the period of DC current increase emphasising minimum rectifier control action. Fig. 7.25b illustrates that the restart is slower than the 3 cycles used for the QSS run and the rectifier currents reach a steady state after 4 cycles. The rectifier is well behaved without any malfunctions. The inverter waveforms show that the inverter takes control of the DC current at 16 cycles and remains in control for the rest of the study. This means that a current setting change, 6 cycles after fault clearance, would have to be transferred to the inverter to be effective, and extra delays in communication may extend the period of increased current setting. A comparison of the QSS and TCS results is given in Fig. 7.26 and Table 7.8.

While the trends in DC power are similar for both models, the TCS results show a more delayed response, both at restart and restoration of nominal DC current setting.

Fig. 7.25a RECTIFIER VOLTAGES-1321R

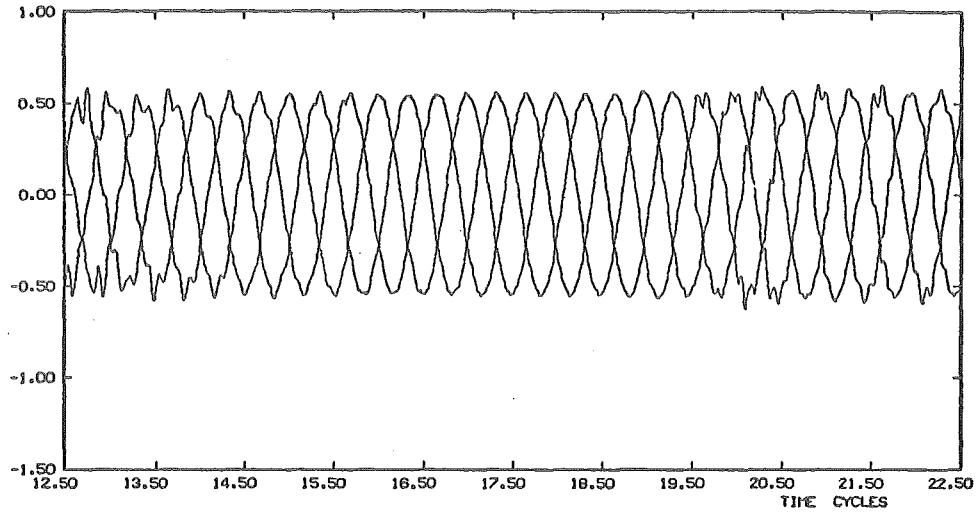

Fig. 7.25b RECTIFIER CURRENTS-1321R

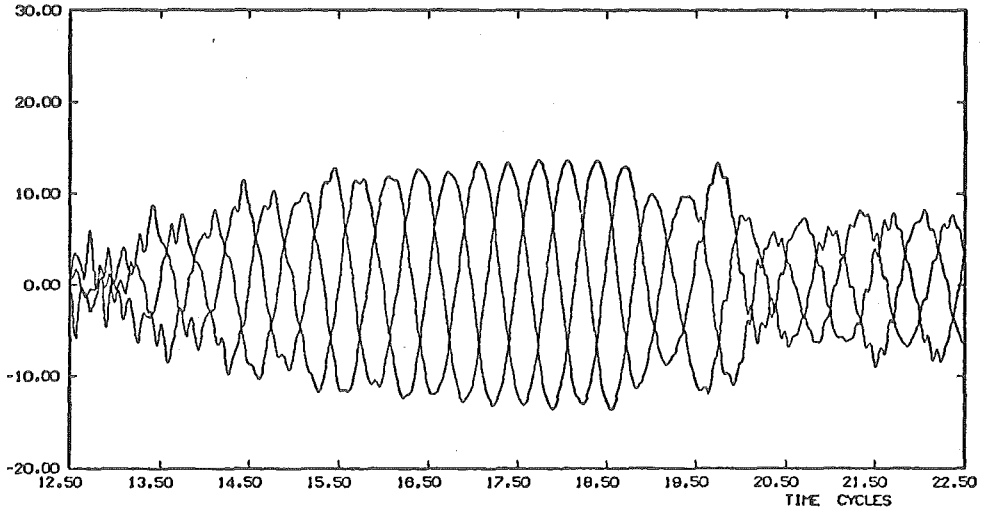

Fig. 7.25c INVERTER CURRENTS-1321R

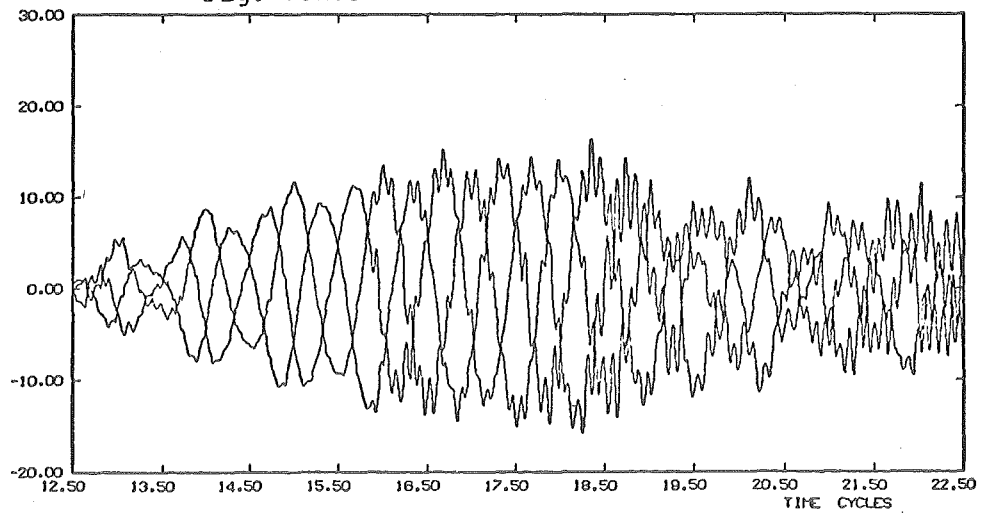

Fig. 7.25 Simulation Results for TS Improvement at a Rectifier Terminal.
(Restart at 12.0 Cycles).

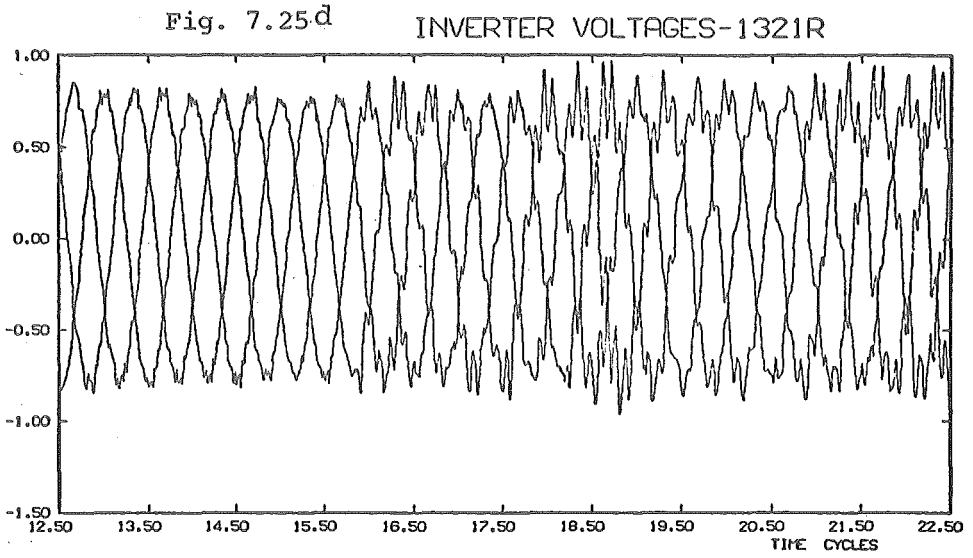

Fig. 7. 25 Simulation Results for TS Improvement at a Rectifier Terminal. (Restart at 12.0 Cycles).

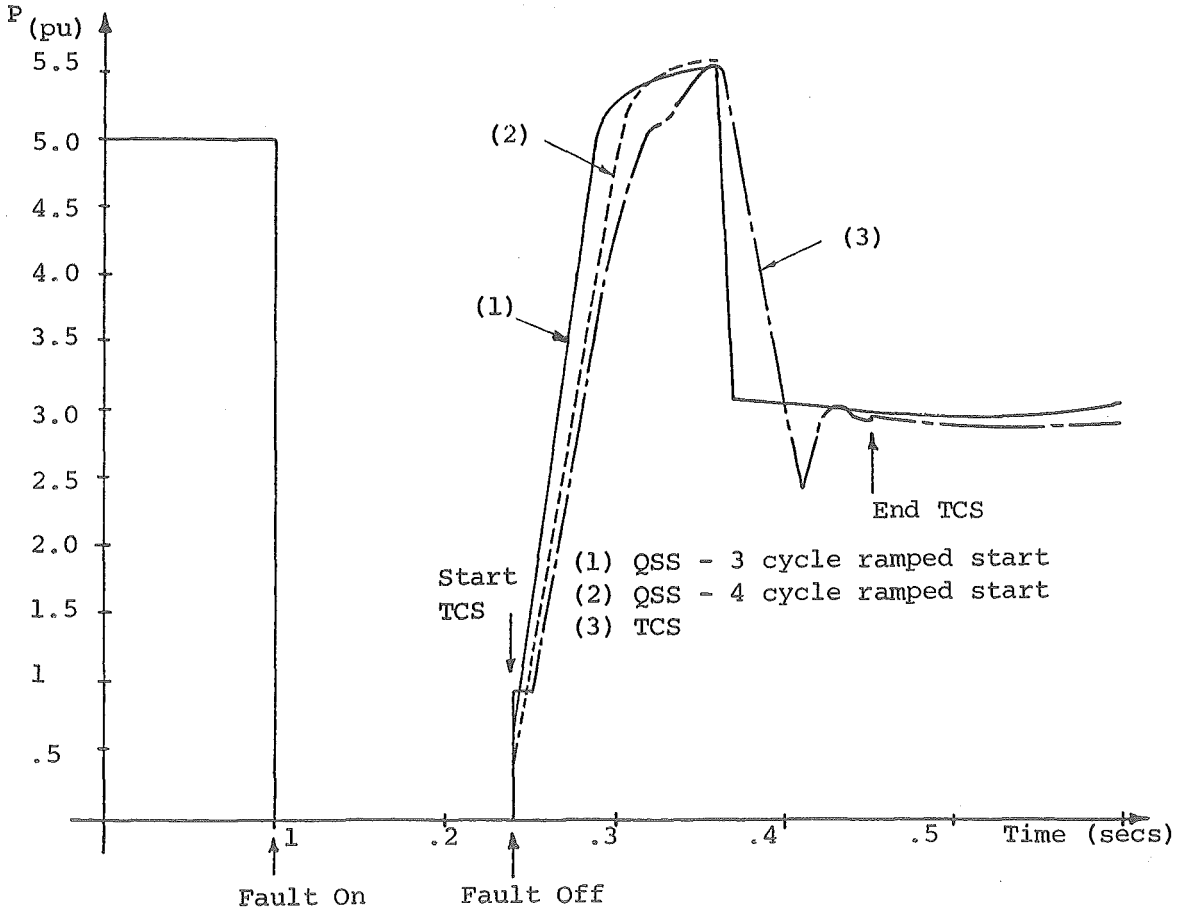

Fig. 7.26 Comparison of QSS and TCS Powers at Rectifier Terminal.

TABLE 7.8 MAXIMUM SWING ANGLES OF QSS AND TCS MODELS

Case	QSS - Instant Start	QSS - 3 Cycle Start	QSS - 4 Cycle Start	TCS
δ_{max}	89.5°	95.5°	98.5°	101.5°

This delay influences the peak swing angle since less synchronising power is taken by the rectifier and the system becomes marginally stable. However, with the experience gained from the TCS, the QSS run can be modified to match closely the correct DC link behaviour, especially by including a half cycle delay before restart. Carter et al (1977) and Grund et al (1979) refer to delays of 2-6 cycles before restarting of the DC link. The results of TCS illustrate that immediate restart is practical and the only delay is due to the natural response rate of the DC link.

7.8.2 Inverter End Fault Case

In this case the rectifier is restarting with full AC voltage, while the inverter is operating under a reduced voltage. The early stages of TCS showed the restart to be much faster than for the rectifier end fault. In order to match, more closely, the QSS run with the TCS (and make the first iteration between programmes nearly convergent), the 3 cycle ramped restart used for the first system equivalent was modified to become a half cycle delay followed by a 1½ cycle ramped restart. A comparison between the QSS and TCS models is presented in Fig. 7.27. Figure 7.27a illustrates that a very accurate match can be achieved for the link restart. However restart at the inverter, (Fig. 7.27b), is delayed by DC line response and is nearly a cycle behind the QSS restart. The timing difference could be modified so that the QSS model matches at the link terminal of the disturbed system since it is here that the transient behaviour is of most importance for stabilising

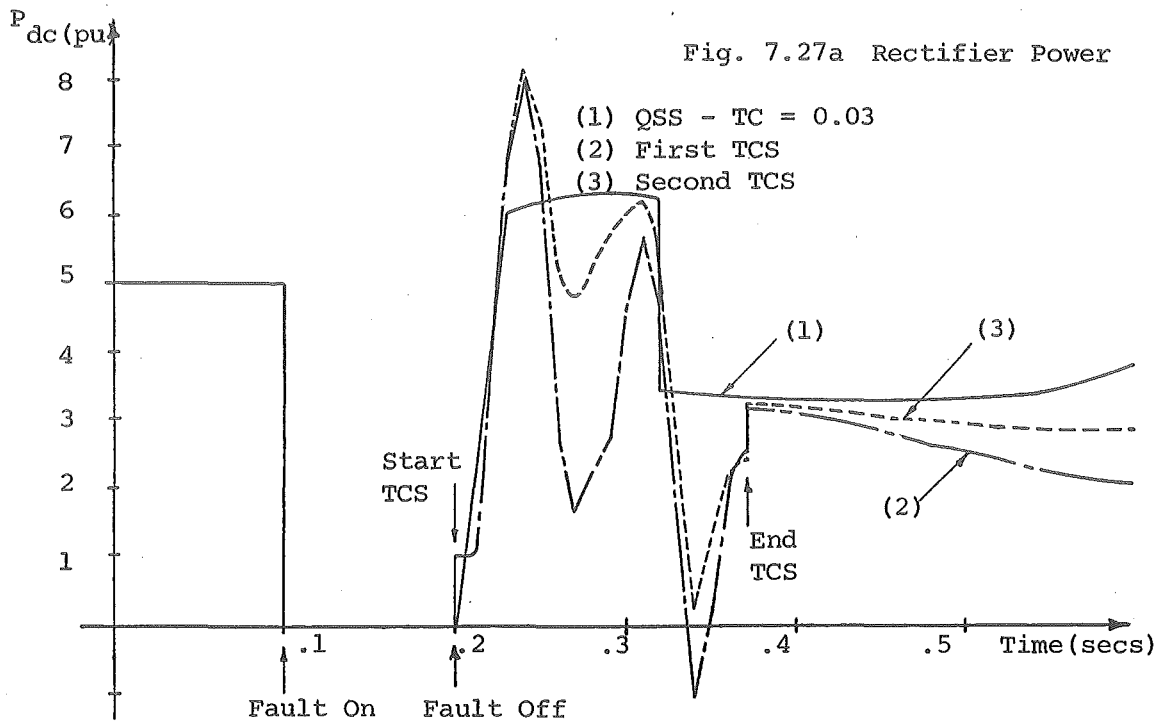

Fig. 7.27a Rectifier Power

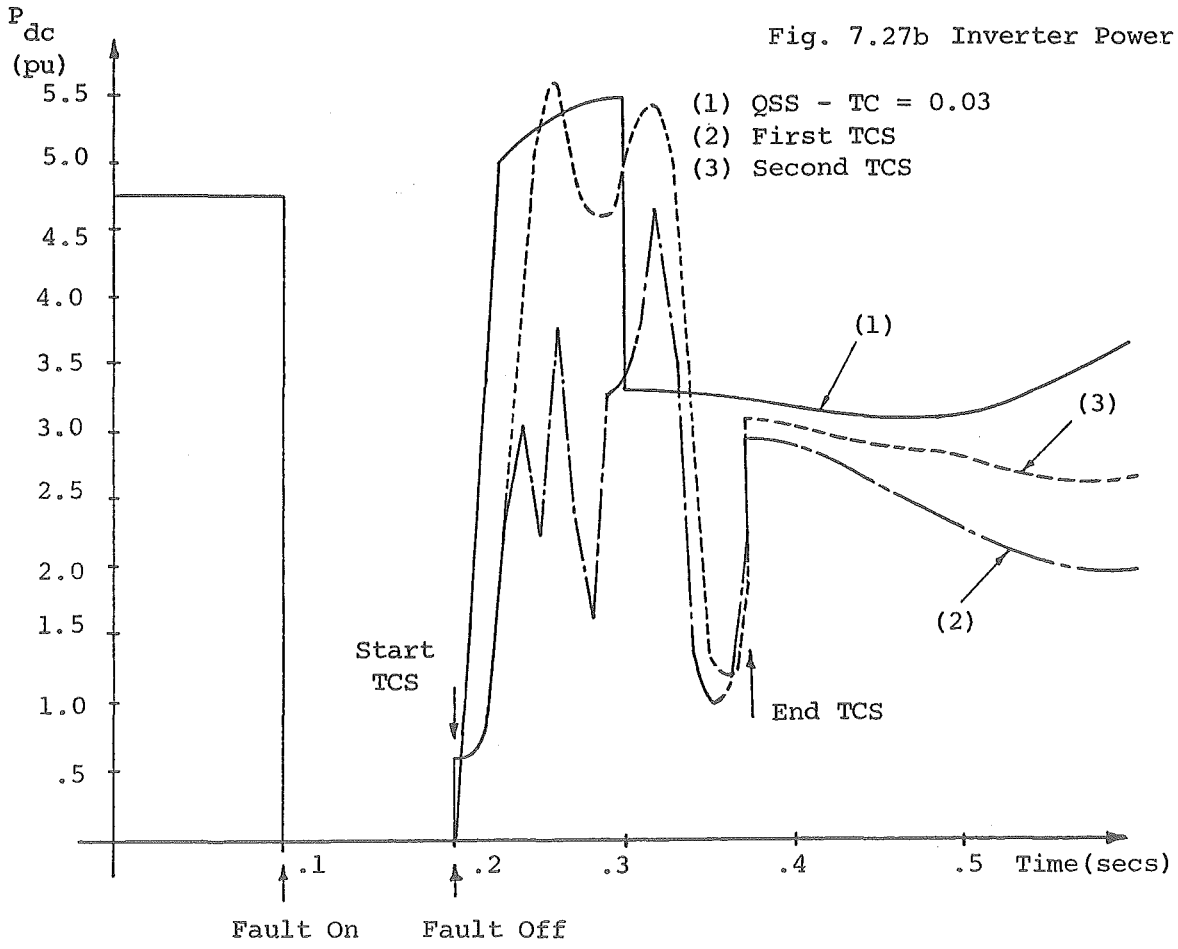

Fig. 7.27b Inverter Power

Fig. 7.27 Comparison of QSS and TCS Results-Inverter End Stability Improvement.

the disturbed machine.

Two simulations were performed for this study. The results of the first study (curve 2 of Fig. 7.27 and coded 2313R) differ markedly from both the QSS and the second simulation (curve 3 of Fig. 7.27 and coded 2313R2).

7.8.2.1 First simulation - The first simulation was performed with the inverter controls set to minimise the extinction angle. As a result of the low inverter AC voltage and increased current setting this type of control is unable to prevent commutation failures which occur at cycles 12.5, 13.5 and 16.5 of Fig. 7.28a. The commutation failures created additional disturbances which would not have occurred without the step up in current setting and the DC power during this period is severely reduced. In this case the attempt at stability improvement results in a destabilising influence, as Fig. 7.29 illustrates, the system is unstable.

7.8.2.2 Second simulation - The commutation failures of the first TCS were caused by the optimising function of the extinction angle control and, since this control is intended for steady state conditions, the controller can be modified to decrease the gain of the optimising control during the transient period.

The improvement in the link response is clearly illustrated in Fig. 7.28b in which the inverter currents are undisturbed. Much greater synchronising power can be transmitted for TS improvement as shown by curve 3 of Fig. 7.27, with the result that the system is marginally stable, as illustrated by curve 3 of Fig. 7.29.

The lack of matching between the QSS and TCS restart at the inverter means that the QSS swing angle is extremely optimistic. In addition there is a considerable delay before simulation shows a drop in inverter power after the current setting reduction. For this study the current setting reduction was implemented at the rectifier and the delay could be reduced by implementing the change at the inverter as well.

Fig. 7.28a

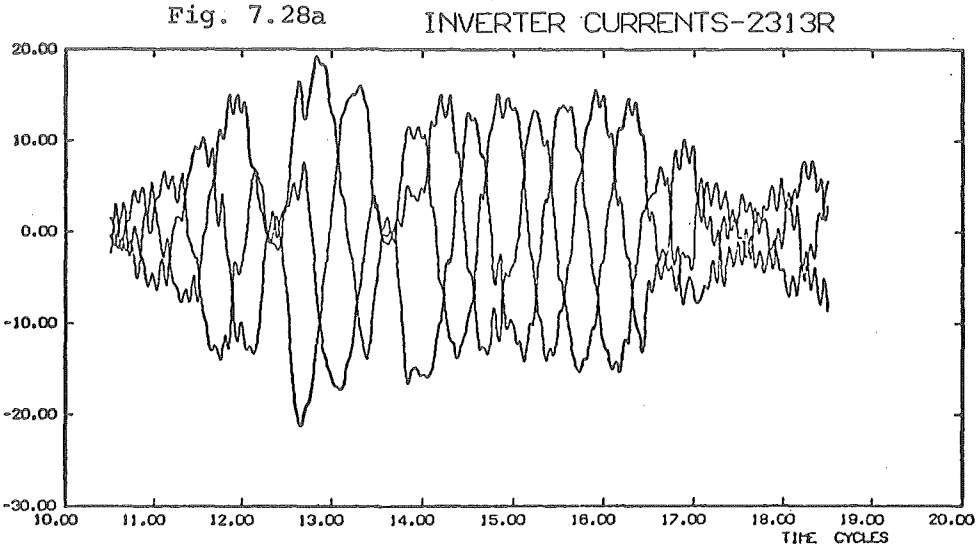

Fig. 7.28b

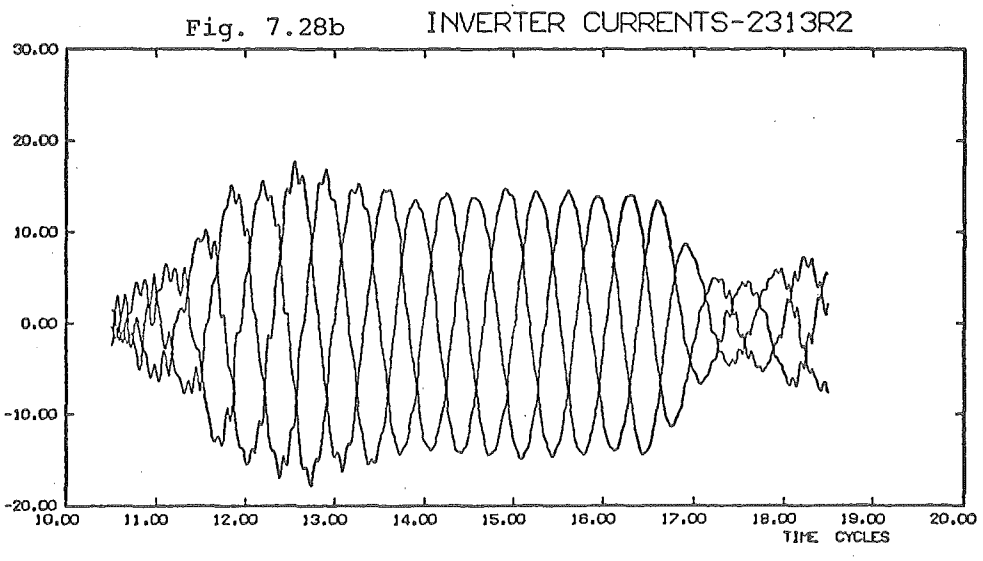

Fig. 7.28 Simulation Results for TS Improvement at Inverter End.

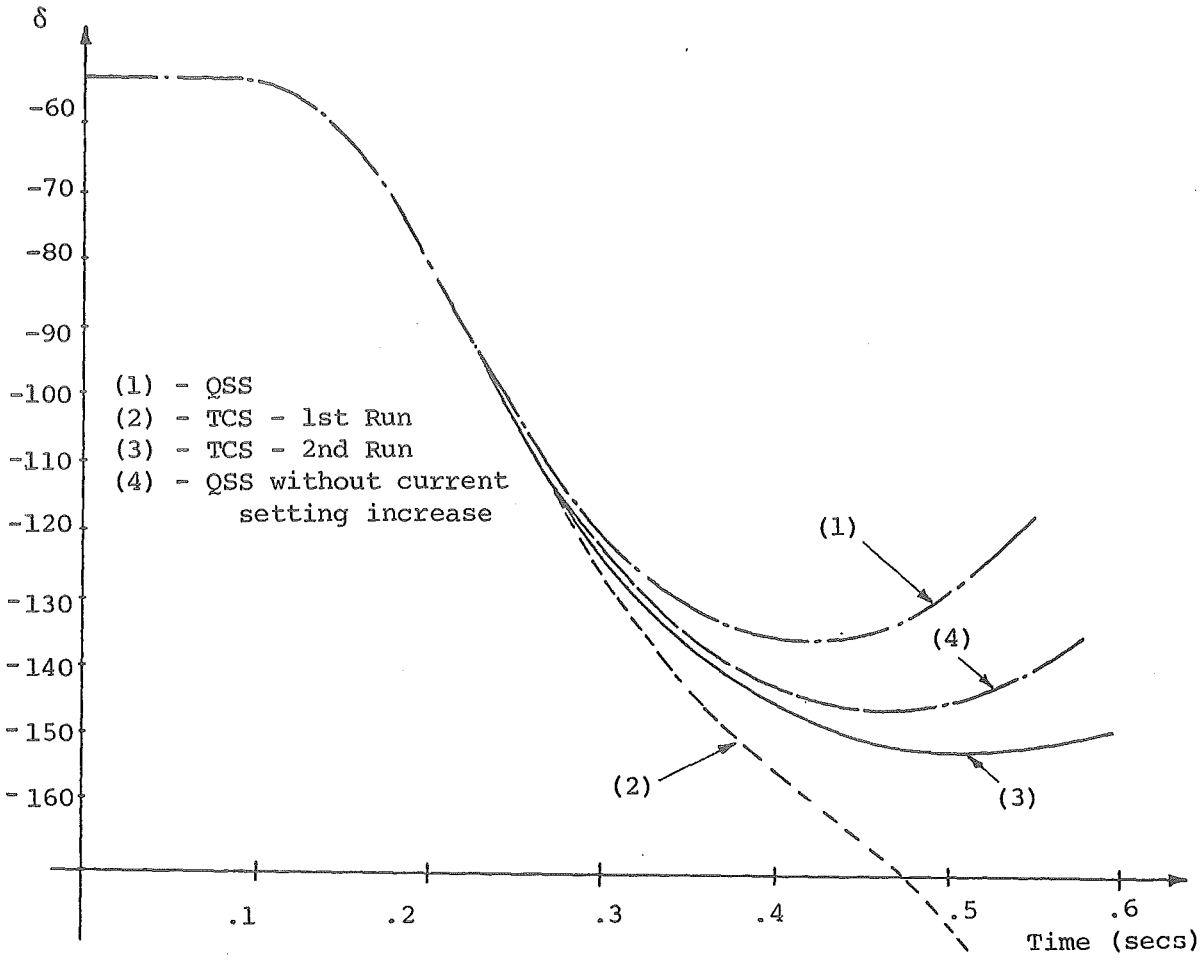

Fig. 7.29 Swing Curves for Inverter End Stability Improvement.

7.8.3 DC Link Reversal

Significant stability improvement can be obtained by a reduction in DC power demand in the post fault period, as discussed in section 7.7.2. However a transient converter simulation of DC link power reversal was performed to examine the feasibility of this control strategy and to determine the accuracy of the QSS model for this case.

The link restart, after fault clearance, is with the normal inverter terminal operating as a rectifier with a reduced terminal voltage. The current setting during reversed operation of the link is 50% of its pre-fault value and this corresponds to the 4th case in Table 7.7.

Results of the simulations are illustrated in Fig. 7.30. Figure 7.30 shows that the restart takes 2 cycles before full current is established and a 70% overswing in

Fig. 7.30a INVERTER CURRENTS-2314

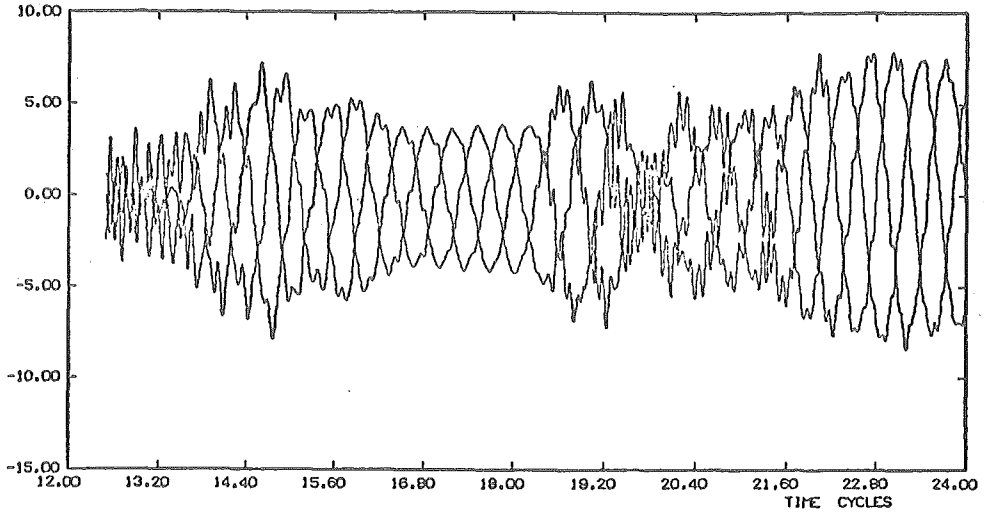

Fig. 7.30b DC CURRENTS-2314

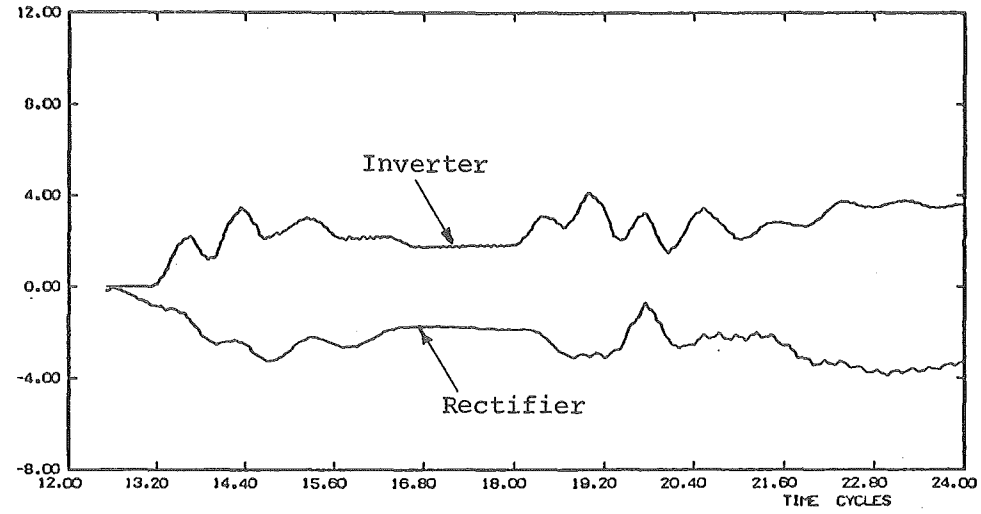

Fig.7.30c DC VOLTAGES-2314

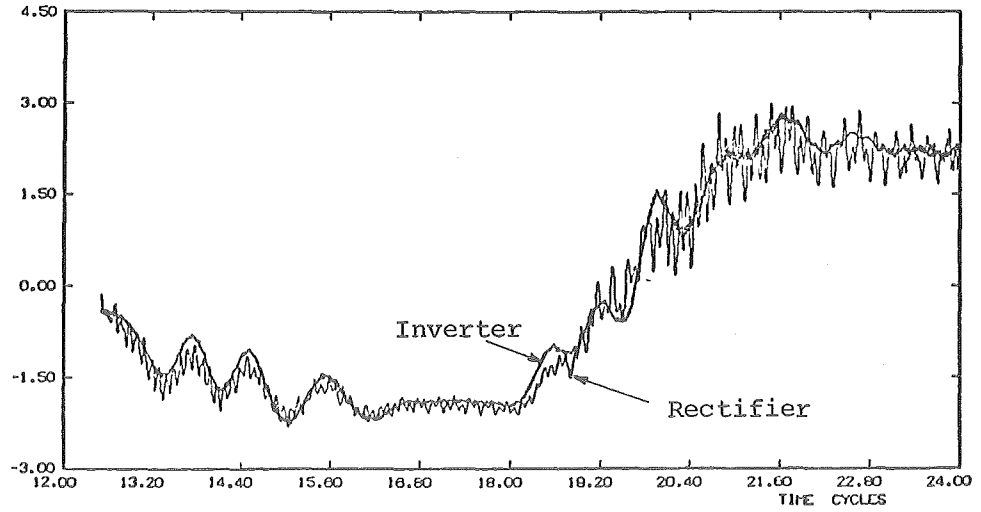

Fig. 7.30 Simulation Results for TS Improvement Using DC Link Reversal.

current occurs (at cycle 14.5 of Fig. 7.30a), before the transmission settles in the reversed mode. During the transition back to inverter operation DC current oscillations occur and the current drops towards extinction as illustrated in Figs. 7.30a and 7.30b. However the DC voltage transition is smooth as shown by Fig. 7.30c. No consequential converter disturbances occur throughout the study and the reversal is well controlled with the transition to normal power flow taking 3 cycles.

Figure 7.31 illustrates a comparison between the TCS and QSS models. At both link terminals the TCS predicts a greater power flow than the QSS model during the reversed period. This is due to the overswing in current following the restart. However the peak swing angle of 60.4° for the

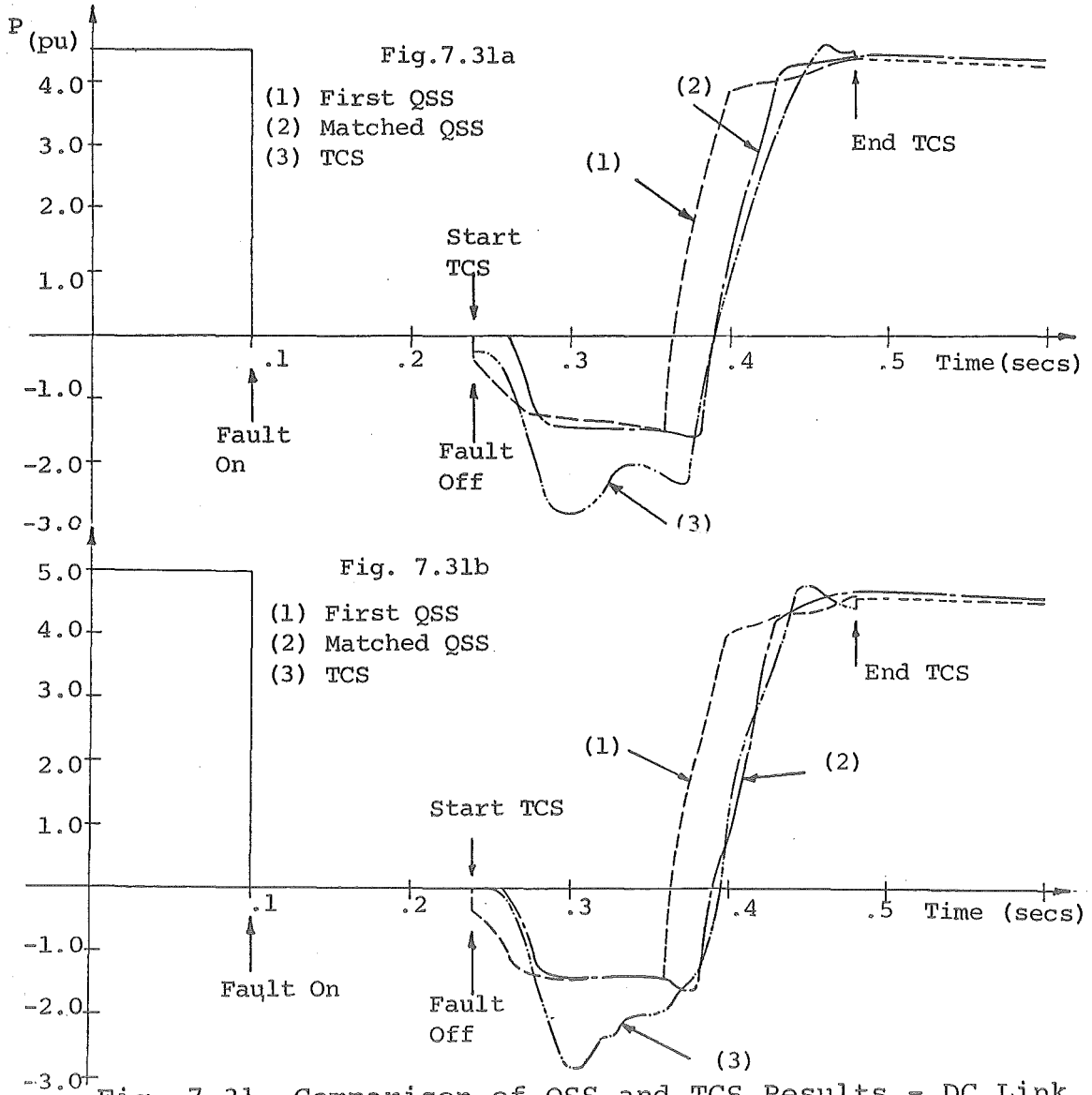

Fig. 7.31 Comparison of QSS and TCS Results - DC Link Reversal for Stability Improvement.

TS study, with TCS results, is slightly greater than for the QSS model (59.8°). This unexpected result is due to the lower terminal AC voltage, immediately after fault clearance, obtained by TCS. This reduces the synchronising power flow from the Benmore generator even though link power is drawn from the machine bus instead of injected into it.

Curves 1 and 2 of Fig. 7.31 illustrate the correspondence between the initial QSS, matched QSS and the TCS models. They show that it is not possible for the QSS model to predict the current overswing during reversal and therefore the greater DC power transferred. However the matching at both terminals during and after the transition to normal power flow, is good for curve 2.

7.9 CONCLUSION

Earlier investigations into TS improvement (Elamin 1975) have been extended to cover a number of aspects of TS improvement using DC current setting control. The importance of realistic modelling has been demonstrated and the results show that for feasible values of DC current increase and no special methods of reactive power support, a useful decrease in peak swing angle can be obtained. The extra disturbance, transmitted to the healthy system, can in some cases be beneficial. The ability to provide rapid damping to post fault swings is illustrated.

The transient converter simulations performed have supported the QSS results showing that current setting control for stability improvement is feasible. For the systems in cases 1 and 2 of Table 7.1, the differences in peak swing angle are small when the QSS model is matched to the TCS. However TCS is essential for these cases to establish the performance parameters of the QSS model. In addition the TCS of case 2 shows that a link reversal is possible for periods of 6 cycles (or more), and the transition in power flow from one direction to the other can be achieved, without converter disturbances, in 3 cycles.

For the system of case 4, (Table 7.1), in which stability improvement is being applied at an inverter terminal, the QSS model fails to predict correct link performance. This result duplicates the finding of section 6.3 and emphasises the necessity to use TCS for inverter terminal disturbances. As a consequence of the final TCS of case 4, stable inverter response was obtained in a second TCS with a transiently modified controller.

By performing several worst case transient converter simulations the performance parameters of the QSS model can be set and this model can then be used for many more TS studies. A large number of inexpensive TS studies may be performed with a minimised TCS cost. This is an efficient, accurate and economical approach to TS studies of integrated AC and DC systems and is quicker than full TCS for every case (Vovos and Galanos 1979).

CHAPTER 8

CONCLUSION

This thesis has investigated the modelling of converter loads and DC links for transient stability analysis of integrated AC and DC systems. It has shown that simple models of converters provide inadequate load models for TS studies and new and more accurate models have been proposed.

In the case of large rectifier loads, the effects of modelling the dynamics of the DC load are significant. A simple QSS model using normal mode equations is not valid throughout the disturbance period and an alternative model, which can be used for all modes of operation, is developed. Convergence difficulties caused by rectifier operation in abnormal modes, is overcome by the introduction of a unified solution algorithm which is subsequently used for the QSS DC link model. The results obtained show that the detailed rectifier model is necessary if the influence of rectifier loads in transient stability analysis is to be correctly assessed. This work has been reported in two recent publications (Appendices A10 and A11).

The difficulties of interpreting TCS waveforms for TS analysis have been discussed. Two variables are used to specify the link behaviour at each terminal. From the analysis of many TCS waveforms it is found that Fourier processing is required only for the voltage variable while the rms approximation for real power is sufficiently accurate for TS analysis.

The interactive coordination of both TS and TCS programmes is demonstrated to be feasible and practical. The TS programme provides an exact and time variant AC representation for the TCS and this eliminates the computational problem of representing large AC networks in transient converter simulations. As well, the TCS provides an exact representation of the DC link reponse and replaces the QSS model, and its inherent assumptions, during the

transient period when its applicability is questionable. This innovative solution eliminates the limitations of both TS and TCS models used separately in AC/DC analysis, provides a flexible and economical alternative to the use of expensive physical simulators for HVDC links and allows accurate transient stability analysis of integrated AC and DC systems.

This work, together with the development of the TCS programme (Heffernan 1980), has formed the basis of a three part publication currently under consideration (see Appendices A12, A13 and A14).

The results of typical case studies of AC faults, DC faults and TS improvement applications show that, except for inverter AC system disturbances, the QSS DC link model can be matched closely to the TCS to provide nearly identical first swing maximum angles. In this way a few TCS studies may be performed to provide parameters for modifying the QSS model performance so that it may then be used for many subsequent studies in the same system. This approach makes efficient use of the computationally expensive converter simulations.

In the case of inverter AC system faults, the QSS model cannot predict the behaviour of the DC link because of the indeterminate nature of consequential converter disturbances. To obtain accurate TS assessment in such cases it is essential that a converter simulation be performed.

The investigation of first swing stability improvement illustrates that short term current overload or DC power reversal are feasible control strategies and they provide significant reductions in peak swing angle. Implementation of this type of control in real systems will require a detailed representation of the controller design for accurate simulation and further effort could be profitably spent in this area.

REFERENCES

ADAMSON, C. and HINGORANI, N.G. "High Voltage Direct Current Power Transmission", 1st Ed., Garraway Ltd, London, 1960 (Book), 284pp.

AINSWORTH, J.D. Discussion on "The Dynamics of AC/DC Systems with Controlled Multiterminal HVDC Transmission" by Carter et al. Trans. IEEE, Vol. PAS-96, No. 2, March/April 1977, pp.411-412.

AL-KHASHALI, H.J. "Generalised Dynamic Modelling of High Voltage AC-DC Transmission Systems", University of Manchester Institute of Science and Technology, 1976, 103pp. (THesis: Ph.D. : Engineering).

ARNOLD, C.P. "Solution of the Multimachine Power System Stability Problem", University of Manchester Institute of Science and Technology, 1976. (Thesis: Ph.D. : Engineering).

ARNOLD, C.P. and PUCHECO, E.J.P. "Modelling Induction Motor Start Up in a Multi-Machine Transient Stability Programme", Conference Paper A79 492-0, IEEE Summer Power Meeting, July, 1979.

ARRILLAGA, J., ERINMEZ, A. and GIESNER, D.B. "Power-Reversal Control of HVDC Interconnectors", Proc. IEE, Vol. 119, No. 9, September 1972, pp.1345-1350.

ARRILLAGA, J. and ELAMIN, I.M. "Transient Stability Performance of a 3 Machine System Including an HVDC Link", Proc. IEE, Vol. 123, No. 11, November 1976, pp.1239-1244.

ARRILLAGA, J., AL-KHASHALI, H.J. and CAMPOS BARROS, J.G. "General Formulation for Dynamic Studies in Power Systems Including Static Converters", Proc. IEE, Vol. 124, No. 11, November 1977, pp.1047-1052.

ARRILLAGA, J., ARNOLD, C.P., HEFFERNAN, M.D. and CAMPOS BARROS, J.G. "Stability of Isolated Generator-HVDC Converter Units", IEEE Summer Power Meeting, Mexico City, July 1977, A77-508-5.

ARRILLAGA, J. and BODGER, P.S. "Integration of HVDC Links with Fast Decoupled Load Flow Solutions", Proc. IEE, Vol. 124, No. 5, May 1977, pp.463-468.

ARRILLAGA, J., CAMPOS BARROS, J.G. and AL-KHASHALI, H.J. "Dynamic Modelling of Single Generators Connected to HVDC Converters", Trans. IEEE, Vol. PAS-97, No. 4, July-August 1978, pp. 1018-1029.

ARRILLAGA, J., HEFFERNAN, M.D., LAKE, C.B. and ARNOLD, C.P. "Fault Studies in AC Systems Interconnected by HVDC Links", Proc. IEE, Vol. 127, Part C, No. 1, January 1980, pp.15-19.

BERGSTROM, L., MAGLOF, L., MEISER, R.J. and NELSON, J.M. "The CU HVDC Transmission System", Paper presented to Cigré SC14 Meeting and Colloquim, Winnipeg, Canada, June 1977, 16pp.

BRAMELLER, A., YACAMINI, R., ELAMIN, I.M. and LYNCH, C.A. "Transient Stability of AC-HVDC Systems Using a Direct Solution", Conference Paper A79 074-6, IEEE Winter Power Meeting, February 1979.

BRERETON, D.S., LEWIS, D.G. and YOUNG, C.C. "Representation of Induction Motor Loads During Power System Stability Studies", Trans. AIEE, Vol. PAS-76, Part III, August 1957, pp.451-461.

CAHEN, F.M., DI PERNA, A. and GAVRILOVIC, A. "The Sardinia-Italian Mainland HVDC Transmission Scheme - Frequency Control of Sardinian System", IEE Conference Publication No. 22, 1966, pp.50-55.

CAPS (Computer Analysis of Power Systems Working Group of the Computer and Analytical Methods Subcommittee - Power System Engineering Committee), "System Load Dynamics - Simulation Effects and Determination of Load Constants", Trans. IEEE, Vol.PAS-92, No. 2, March-April 1973, pp.600-609.

CARTER, C.K., GRUND, C.E., HAPP, H.H. and POHL, R.V. "The Dynamics of AC/DC Systems with Controlled Multiterminal HVDC Transmission", Trans. IEEE, Vol. PAS-96, No. 2, March-April 1977, pp.402-413.

COCHRAN, W.T. et al. "What is the Fast Fourier Transform?". Proc. IEEE, Vol. 55, No. 10, October 1977, pp.1664-1674.

CONCORDIA, C. "Representation of Loads", IEEE Symposium on the Adequacy and Philosophy of Modelling - Dynamic System Performance, February 1975,pp.41-45.

CRESAP, R.L. and MITTELSTADT, W.A. "Small Signal Modulation of the Pacific HVDC Intertie", Trans. IEEE, Vol. PAS-95, No. 2, March-April 1976, pp.536-541.

DANFORS, P. "Inga Shaba EHVDC Transmission", Discussion of Group 14, Question 2.3, Cigré 1976 Session, pp.25-26.

DOMMEL, H.W. and SATO, N. "Fast Transient Stability Solutions", Trans. IEEE, Vol. PAS-91, No. 4, July-August 1972, pp.1643-1650.

DOUGHERTY, J.J. and HILLESLAND, T. Jr. "Power System Stability Considerations with Dynamically Responsive DC Transmission Lines", Trans. IEEE, Power Apparatus and Systems, Vol. PAS-89, No. 1, January 1970, pp.34-45.

DUKE, R.M. "A Thyristor-Controller Regulating Transformer", University of Canterbury, Christchurch, N.Z., 1979, (Thesis: Ph.D. : Engineering) 245pp.

ELAMIN, I.M. "Basic Aspects of Transient Stability in AC-DC Power Systems, University of Manchester Institute of Science and Technology, 1975. (Thesis: M.Sc. : Engineering).

ELGERD, O.I. "Electric Energy Systems Theory", McGraw-Hill, New York, 1971 (Book), 564pp.

FOTIN, F.P. et al. "Tests of Powerful High Voltage Thyristor Valves on a Test Plant in the Town of Togliatt", Cigré Conference, Paris, 1976, Paper 14-1, 6pp.

FUJI ELECTRIC. "Instruction Manual for Tiwai Aluminium Smelter Current Controller", 1972.

GIESNER, D.B. "The Dynamic Behaviour of AC/DC Power Systems Under AC Fault Conditions", University of Manchester Institute of Science and Technology, 1971, 163pp. (Thesis: Ph.D. : Engineering).

GIESNER, D.B. and ARRILLAGA, J. "Operating Modes of the 3-Phase Bridge Converter", Int. Journal Electrical Engineering Education, Vol. 8, 1970, pp.373-388.

GRUND, C.E., BREUER, G.D. and PETERSON, R.P. "AC/DC System Dynamic Performance - Transient Stability Augmentation with Dynamic Reactive Power Compensation", Conference Paper F79 655-2, IEEE Summer Power Meeting, July 1979.

HAKIM, M.M.A. and BERG, C.J. "Dynamic Single Unit Representation of Induction Motor Groups", Trans. IEEE, Vol. PAS-95, No. 1, January-February 1976, pp.155-165.

HARKER, B.J. "Steady State Analysis of Integrated AC and DC Systems", University of Canterbury, Christchurch, N.Z., 1980. (Thesis: Ph.D. : Engineering).

HARRIS, F.J. "On the Use of Windows for Harmonic Analysis with the Discrete Fourier Transform", Proc. IEEE, Vol. 66, No. 1, January 1978.

HAYWOOD, R.W. and PATTERSON, W.A. "Applications of Control on the Eel River and Nelson River HVDC Schemes to Enhance Operation of Interconnected Systems", Cigré Conference, Paris, 1976, Paper 14-04, 12pp.

HEFFERNAN, M.D. "Stability of Hydrogenerators Connected to HVDC Converters", University of Canterbury, Christchurch, N.Z., 1977, 90pp. (Report: M.E. in Engineering).

HEFFERNAN, M.D. "Analysis of AC/DC System Disturbances", University of Canterbury, Christchurch, N.Z., 1980, 315pp. (Thesis: Ph.D. : Engineering).

HEFFERNAN, M.D., ARRILLAGA, J., TURNER, K.S. and ARNOLD, C.P. "Recovery from Temporary HVDC Line Faults", Conference Paper 80 SM 675-9, IEEE Summer Power Meeting, July 1980.

HENSBERGER, J., ROTH, K. and THIELE, G. "Testing of Thyristor Valves for Bipole 2 of Manitoba HVDC System", Paper 14-03, Cigré, August 30-September 7, 27th Session, 1978.

HINGORANI, N.G. and HAY, J.L. "Dynamic Simulation of an HVDC System on a Digital Computer", Proc. IEE International Conference (No. 22) on HVDC, 1966, pp.119-124.

HINGORANI, N.G. and HAY, J.L. "Representation of Faults in the Dynamic Simulation of HVDC Systems by Digital Computer", Proc. IEE, Vol. 114, No. 5, May 1967, pp.629-638.

IEEE COMMITTEE REPORT "Excitation System Dynamic Characteristics", Trans. IEEE, Vol. PAS-92, No. 1, January 1973, pp.64-75.

IEEE COMMITTEE REPORT "Dynamic Models for Steam and Hydro Turbines in Power System Studies", Conference Paper T73 089-0, IEEE Winter Power Meeting, February 1973.

ILICETO, F. and CAPASSO, A. "Dynamic Equivalents of Asynchronous Motor Loads in System Stability Studies", Trans. IEEE, Vol. PAS-93, No. 5, 1974, pp.1650-1659.

KAUFERLE, J. and RUMPF, E. "The Influence of HVDC Transmission Systems and their Control on the Stability of Associated AC Networks", Paper 32-15, Cigré 23rd Session, 1970.

KIMBARK, E.W. "Power System Stability - Vol. I:Elements of Stability Calculations", Wiley and Sons, New York, (Book), 1948, 355pp.

KIMBARK, E.W. "Power System Stability - Vol. III: Synchronous Machines", Dover Publications Inc., New York,(Book), 1956, 322pp.

KIMBARK, E.W. "Direct Current Transmission, Vol. I", Wiley Interscience (Book), 1971, 508pp.

LAKE, C.B., "A Computer Programme for AC Fault Studies in a.c./d.c. Systems", University of Canterbury, Christchurch, New Zealand, 1977, (Report: M.E. : Engineering).

LATHI, B.P. "Communication Systems", Wiley and Sons, New York (Book), 1968, 431pp.

LAW, C.K. "A Fast Transient Stability Programme", University of Manchester Institute of Science and Technology, 1972. (Thesis: M.Sc. : Engineering).

MACHIDA, T. "Improving Transient Stability of AC System by Joint Usage of DC System", Trans. IEEE, Vol. PAS-85, No. 3, March 1966, pp.226-232.

MARSHALL, W.K., et al. "A Simplified HVDC Link for System Stability Studies", Conference Paper C74 434-7, IEEE Summer Power Meeting, July 1974.

MICU, E. "Suggested Definition of Reactive Power for Non-sinusoidal Systems", Proc. IEE, Vol. 120, No. 7, July 1973, pp.796-797.

MILIAS-ARGITIS, J. and GALANOS, G. "Dynamic Simulation of HVDC Transmission Systems", Paper presented at IEEE PES Winter Meeting, New York, January 1976, A76-118-0, 4pp.

MILIAS-ARGITIS, J., GALANOS, G. and GIANNAKOPOULOS, G. "A Digital Method for the Control of Power Flow in HVDC Interconnections", Paper presented at IEEE PES Winter Meeting, New York, January-February 1977, A77-024-3, 7pp.

OLIVE, D.W. "New Techniques for the Calculation of Dynamic Stability", Trans. IEEE, Vol. PAS-85, No. 7, July 1966, pp.767-777.

PENNINGTON, R.H. "Introductory Computer Methods and Numerical Analysis", 2nd Edition, Collier MacMillan Ltd, London, (Book), 1970.

PETERSON, M.A. and KRAUSE, P.C. "Damping of Power Swings in a Parallel AC and DC System", Trans. IEEE, Vol. PAS-85, No. 3, March 1966, pp.226-232.

REEVE, J., FAHMY, G. and STOTT, B. "Versatile Load Flow Method for Multiterminal HVDC Systems", Conference Paper F76 354-1, IEEE Summer Power Meeting, July 1976.

SHARON, D. "Reactive Power Definitions and Power Factor Improvement in Non-Linear Systems", Proc. IEE, Vol. 120, No. 6, June 1973, pp.704-706.

SHEPHERD, W. and ZAKIKHANI, P. "Suggested Definition of Reactive Power for Nonsinusoidal Systems", Proc. IEE, Vol. 119, No. 9, September 1972, pp.1361-1362.

SKILLING, H.M. "Electrical Engineering Circuits", 2nd Edition, Wiley and Sons, New York, (Book), 1965, 783pp.

STOTT, B. "Loadflows for AC and Integrated AC/DC Systems", University of Manchester Institute of Science and Technology, 1971. (Thesis: Ph.D. : Engineering).

STOTT, B. "Review of Loadflow Calculation Methods", Proc. IEEE, Vol. 62, No. 7, July 1974, pp.916-929.

STOTT, B. "Power System Dynamic Response Calculations", Proc. IEEE, Vol. 67, No. 2, February 1979, pp.219-241.

UHLMANN, E. "Stabilisation of an AC Link by a Parallel DC Link", Direct Current, August 1964, pp.89-94.

UHLMANN, E. "AC Network Stabilisation by DC Links", Cigré Conference, Paris, 1970, Paper 32-01, 12pp.

UHLMANN, E. "Power Transmission by Direct Current", Springer-Verlag, Berlin/Heidelberg, 1975, 389pp.

VOVOS, M.A. and GALANOS, G.D. "Transient Stability of AC-DC Systems", Conference Paper F79 158-7, IEEE Winter Power Meeting, February 1979,

WONG, K.P. "Comparison of Fault Levels in AC and AC/DC Systems", University of Manchester Institute of Science and Technology, 1972. (Thesis: M.Sc. : Engineering).

ZOLENKOPF, K. "Bi-Factorisation - Basic Computational Algorithm and Programming Techniques", Conference on Large Sets of Sparse Linear Equations, Oxford, 1970, pp.75-96.

APPENDIX A1

RELATIONSHIP BETWEEN AC AND DC CURRENTS IN ABNORMAL MODES

The fundamental amplitude and phase of a current $i(\theta)$ which is half wave symmetrical is given by a Fourier integral of the form:

$$\sqrt{2}I_L = \frac{2}{\pi} \int_0^{\pi} i(\theta) e^{-j\theta} d\theta \qquad (A1)$$

where

$$\theta = \omega t$$

and

I_L = rms line current.

For the case of an overlap angle greater than 60°, during the first half cycle $i(\theta)$ is described piece-wise by the following equations (where $\theta = 0$ at the peak of commutating line to neutral voltage).

$$i = I[\cos\alpha' + \frac{1}{2}\cos\delta' - \frac{\sqrt{3}}{2}\cos(\theta+60°)] \qquad (A2)$$

where

$$\delta' - 150° \leqslant \theta < \alpha' + 30°$$

$$i = I[\frac{1}{2}\cos\alpha' + \frac{1}{2}\cos\delta' - \cos(\theta+90°)] \qquad (A3)$$

where

$$\alpha' + 30° \leqslant \theta < \delta' - 90°$$

$$i = I[\frac{1}{2}\cos\alpha' - \frac{1}{2}\cos\delta'] \qquad (A4)$$

where

$$\delta' - 90° \leqslant \theta < \alpha' + 90°$$

$$i = I[\cos(\theta-90°) - \frac{1}{2}\cos\alpha' - \frac{1}{2}\cos\delta'] \qquad (A5)$$

where

$$\alpha' + 90° \leqslant \theta < \delta' - 30°$$

$$i = I[\frac{\sqrt{3}}{2}\cos(\theta-60°) - \cos\delta - \frac{1}{2}\cos\alpha'] \qquad (A6)$$

where

$$\delta' - 30° \leqslant \theta < \alpha' + 150°$$

$$i = I[\cos(\theta-30°) + \cos(\theta-150°) - \cos\alpha' - \cos\delta'] \quad (A7)$$

where

$$\alpha' + 150° \leqslant \theta < \delta' + 30°$$

and where

$$I = \frac{2I_d}{(\cos\alpha' - \cos\delta')}$$

Using identities

$$2\cos\theta = e^{j\theta} + e^{-j\theta} \quad (A8)$$

$$\int e^{-ja\theta} = j\,\frac{1}{a}\,e^{-ja\theta} \quad (A9)$$

and equations (A2) to (A7), the equation (A1) can be reduced to the following form:

$$\frac{\pi I_L}{\sqrt{2}I_d}(\cos\alpha' - \cos\delta') = \frac{1}{2}j\,(\angle{-30°} - \angle{30°})(\angle{-2\alpha'} - \angle{-2\delta'}) + \frac{\sqrt{3}}{4}j\,(\angle{60°} - \angle{-60°})(-\angle{2\alpha'} - \angle{-2\delta'}) + \angle{-2\alpha'} - \angle{-2\delta'} - j\,\frac{3}{2}u \quad (A10)$$

or

$$I_L = \frac{\sqrt{6}}{\pi} \cdot I_d \frac{\sqrt{3}}{4(\cos\alpha' - \cos\delta')}[\angle{-2\alpha'} - \angle{-2\delta'} - j2u] \quad (A11)$$

APPENDIX A2

NEWTON-RAPHSON SOLUTION METHOD

This solution method is an iterative procedure which enables a vector, $\bar{x}$, to be found which satisfies the equation:

$$F(\bar{x}) = 0 \tag{A2.1}$$

Considering the single variable case of:

$$f(x) = 0 \tag{A2.2}$$

then from an approximation x_i, at any iteration i, which is in error Δx_i from the true solution, we can say:

$$f(x_i + \Delta x_i) = 0 \tag{A2.3}$$

Using Taylors theorem to expand A2.3 yields:

$$f(x_i+\Delta x_i) = f(x_i) + \frac{(\Delta x_i)^1}{1!} f(\dot{x}_i) + \frac{(\Delta x_i)^2}{2!} f(\ddot{x}_i) + \ldots. \tag{A2.4}$$

If the error Δx_i is small then terms in $(\Delta x_i)^n$, where $n > 1$ and integer, can be neglected. Thus:

$$f(x_i) + (\Delta x_i) f(\dot{x}_i) = 0 \tag{A2.5}$$

$$\text{or} \quad \Delta x_i = - f(\dot{x}_i) \frac{1}{f(x_i)} \tag{A2.6}$$

A new estimate for variable x_i can be obtained from:

$$x_{i+1} = x_i + \Delta x_i \tag{A2.7}$$

Equation A2.5 is usually written as

$$f(x_i) = -J \Delta x_i \tag{A2.8}$$

In the multi-variable case with N equations in N unknowns, $\bar{x}$ is a vector dimension N and J, the Jacobian, is a

square matrix $N \times N$ of first order partial differentials of the functions $F(\bar{x})$. The Jacobian represents the slopes of the tangent hyperplanes which approximate the function $F(\bar{x})$ at each iteration (Stott 1974) and its elements are defined by:

$$J_{km} = \frac{\partial F_k}{\partial x_m} \qquad \text{(A2.9)}$$

The method works by estimating values of $\bar{x}_i$, calculating $\bar{F}(\bar{x}_i)$ and $[J]$ from these estimates, solving for $[\Delta\bar{x}_i]$ by:

$$[\Delta\bar{x}_i] = - [J]^{-1} F(\bar{x}_i) \qquad \text{(A2.10)}$$

and using $[\Delta\bar{x}_i]$ to obtain a better estimate of $[\bar{x}_i]$. This process is iterated to convergence which is determined when $[\Delta\bar{x}_i]$ is less than a given tolerance.

APPENDIX A3

FUNDAMENTAL EQUATIONS OF FOURIER ANALYSIS AND CONVOLUTION

For any function, finite in time and energy, it is possible to transform between the time and frequency domains using the Fourier transform pair (Lathi 1968):

$$f(t) = \frac{1}{2\pi} \int_{-\infty}^{\infty} F(\omega)\ e^{j\omega t}\ d\omega \qquad \text{(A3.1)}$$

$$F(\omega) = \int_{-\infty}^{\infty} f(t)\ e^{-j\omega t}\ dt \qquad \text{(A3.2)}$$

$F(\omega)$, the spectral density of $f(t)$, is the forward Fourier transform of $f(t)$ and is a continuous function in the frequency domain.

Periodic functions, $f_T(t)$, require special treatment since they are assumed infinite in time and therefore (A3.2) would yield a non-finite result. To make equation A3.2 finite integral limits are restricted to the period of $f_T(t)$ and $F(\omega)$ becomes a discrete frequency spectrum (i.e. $F(n\omega_1)$). For periodic functions A3.1 and A3.2 become:

$$f_T(t) = \sum_{n=-\infty}^{\infty} F(n\omega_1)\ e^{jn\omega_1 t} \qquad \text{(A3.3)}$$

$$F(n\omega_1) = \frac{1}{T} \int_{-\frac{T}{2}}^{\frac{T}{2}} f_T(t)\ e^{-jn\omega_1 t} \qquad \text{(A3.4)}$$

where $\omega_1 = \frac{2\pi}{T}$

Expressing these in terms of the familiar trignometric form:

$$f_T(t) = \sum_{n=o}^{\infty} C_n \cos(n\omega_1 t + \phi_n) \qquad \text{(A3.5)}$$

$$a_o = \frac{1}{T} \int_{-\frac{T}{2}}^{\frac{T}{2}} f_T(t)\ dt \qquad \text{(A3.6)}$$

$$a_n = \frac{2}{T} \int_{-\frac{T}{2}}^{\frac{T}{2}} f_T(t) \cos n\omega_1 t \, dt \qquad \text{(A3.7)}$$

$$b_n = \frac{2}{T} \int_{-\frac{T}{2}}^{\frac{T}{2}} f_T(t) \sin n\omega_1 t \, dt \qquad \text{(A3.8)}$$

$$C_n = \sqrt{a_n^2 + b_n^2} \qquad \text{(A3.9)}$$

$$\phi_n = - \tan^{-1}(b_n/a_n) \qquad \text{(A3.10)}$$

When processing $f_T(t)$ by digital computer to obtain a_n, b_n etc, $f_T(t)$ consists of a set of equally spaced samples. Provided $f_T(t)$ is band limited and there are at least 2 samples/cycle of the highest frequency present, then the spectral components can be computed by the fast Fourier transform algorithm (Cochran et al 1967). For 2 m samples per period T:

$$f_T(t) = \sum_{n=o}^{m} C_n \cos(n\omega_1 t + \phi_n) \qquad \text{(A3.11)}$$

and for the qth sample

$$a_o = \frac{1}{T} \sum_q f(q\Delta T) \, \Delta T \qquad \text{(A3.12)}$$

$$a_n = \frac{2}{T} \sum_q f(q\Delta T) \cos[n\omega(q\Delta T)] \, \Delta T \qquad \text{(A3.13)}$$

$$b_n = \frac{2}{T} \sum_q f(q\Delta T) \sin[n\omega(q\Delta T)] . \Delta T \qquad \text{(A3.14)}$$

CONVOLUTION

For two functions $f_1(t)$ and $f_2(t)$ the convolution of $f_1(t)$ with $f_2(t)$ is defined as:

$$f(t) = \int_{-\infty}^{\infty} f_1(\tau) . f_2(t - \tau) d\tau \qquad \text{(A3.15)}$$

$$\text{or } f(t) = f_1(t) \otimes f_2(t) \qquad \text{(A3.16)}$$

The convolution theorem leads to the following result:

$$f_1(t) \leftrightarrow F_1(\omega) \tag{A3.17}$$

$$f_2(t) \leftrightarrow F_2(\omega) \tag{A3.18}$$

$$f_1(t).f_2(t) \leftrightarrow \frac{1}{2\pi} F_1(\omega) \otimes F_2(\omega) \tag{A3.19}$$

$$f_2(t) \otimes f_2(t) \leftrightarrow F_1(\omega).F_2(\omega) \tag{A3.20}$$

where $\leftrightarrow$ denotes Fourier transformation.

Graphically A3.15 represents $f_2(t)$ folded about the $\tau = 0$ axis and moved in the positive t direction along the τ axis. The value of $f(t)$ is the area under the product of $f_1(\tau)$ and $f_2(t - \tau)$ for each t.

APPENDIX A4

EFFECT OF FREQUENCY MISMATCH BETWEEN TCS AND TS PROGRAMMES

Using the results of Appendix A3 the effect of frequency mismatch can be evaluated.

Given a small deviation from nominal frequency $\omega_1' = \omega_1 + \Delta\omega_1$ then

$$a_1 = \frac{2}{T} \int_{-\frac{T}{2}}^{\frac{T}{2}} \cos\omega_1' t \ \cos\omega_1 t \ dt \qquad \text{(A4.1)}$$

$$a_1 = \frac{2}{T(\omega_1' - \omega_1)} \sin \frac{(\omega_1' - \omega_1)T}{2} + \frac{2}{(T(\omega_1' + \omega_1)} \sin \frac{(\omega_1' + \omega_1)T}{2} \qquad \text{(A4.2)}$$

For a fundamental frequency of 50 Hz (i.e. T = 20 ms)

$$\omega_1 = 314.16$$

With a deviation of 0.25 ms in the period T

$$\omega_1' = 310.28$$

Hence $a_1 = 0.9935$

The true amplitude of a_1 is 1.0 and therefore the error in identifying ω_1' at a frequency ω_1 is 0.65%

APPENDIX A5

CONVERSION OF TCS SAMPLES TO A FORM SUITABLE FOR USE IN AN FFT

The discrete fast Fourier transform can only be applied to sampled data for which there are 2^n samples, (where n is integer), and where the samples are equally spaced. (Cochran et al 1967). TCS waveforms consist of approximately 300 samples of data per fundamental cycle of waveform and these samples are not equally spaced. Investigations were carried out to determine the best method for generating equally spaced samples and the minimum number required.

Both spline, (Pennington 1970), and linear interpolation were used for generating equally spaced samples. However the differences in the harmonic coefficients obtained, after application of an FFT to equally spaced data, were indiscernible between the two methods. This is due to the relatively close spacing of the original data with respect to the highest frequencies of interest. Spline interpolation was discarded since the computational effort required for its use exceeded that of linear interpolation by a factor approaching 100.

Several TCS waveforms were investigated with the number of equally spaced samples ranging from 32 to 512. However since the only harmonic used by the TS study is the fundamental, large numbers of samples increased the computational effort with no change to the accuracy of the fundamental. It was found that in practice 32 samples were sufficient for evaluating the fundamental without the fold down effects of the sampling theorem, (Lathi 1968), affecting the accuracy.

APPENDIX A6

DATA FOR THE NEW ZEALAND PRIMARY GENERATION AND 220KV TRANSMISSION NETWORK

ELECTRICAL POWER-SYSTEM TRANSIENT-STABILITY STUDY

DEPARTMENT OF ELECTRICAL ENGINEERING - UNIVERSITY OF CANTERBURY
CHRISTCHURCH, NEW ZEALAND.

15/05/80

SYSTEM NO. 5

NZ 220KV SYSTEM NO 222
63 BUSBARS,92 LINES,24 MACHINES
LOAD FLOW INITIAL CONDITIONS BY BRUCE HARKER

SYSTEM FREQUENCY = 50.0 HERTZ
M.V.A. BASE = 100.0 M.V.A.

NO SYNCHRONOUS MACHINE CONTROLLER DATA INPUT
NO INDUCTION MOTOR DATA INPUT

STEADY-STATE SYSTEM DATA

BUSBAR DATA INPUT

BUSBAR	VOLTAGE	ANGLE	GEN MW	GEN MVAR	LOAD MW	LOAD MVAR
AVIEMORE--11	1.04000	12.8670	220.00000	-1.70000	0.00000	0.00000
AVIEMORE-220	1.04200	7.6590	0.00000	0.00000	0.00000	0.00000
BENMORE---16	1.02500	8.1430	540.00000	92.51000	0.00000	0.00000
BENMORE---DC	1.02500	8.1430	0.00000	0.00000	0.00000	0.00000
BENMORE--220	1.04000	7.4020	0.00000	0.00000	0.00000	0.00000
BROMLEY--220	1.00100	-9.8410	0.00000	0.00000	129.60000	38.30000
HALFWAYBU220	1.02600	-3.7230	0.00000	0.00000	95.30000	40.40000
INVERCARG220	1.00800	-7.7490	0.00000	0.00000	183.20000	20.00000
ISLINGTON220	1.00500	-10.5180	0.00000	159.45000	504.10000	124.30000
KINWA---220	1.00400	-24.0660	0.00000	0.00000	59.20000	9.20000
LIVINGSTN220	1.03800	3.6920	0.00000	0.00000	0.00000	0.00000
MANAPOURI-14	1.06000	0.9230	400.00000	91.33000	0.00000	0.00000
MANAPOURI220	1.04300	-2.9890	0.00000	0.00000	0.00000	0.00000
OHAU-A---11	1.05000	9.8630	214.00000	11.92000	0.00000	0.00000
OHAU-A---220	1.04500	6.0600	0.00000	0.00000	0.00000	0.00000
OHAU-B---11	1.04900	9.6920	175.00000	9.25000	0.00000	0.00000
OHAU-B---220	1.04400	5.8090	0.00000	0.00000	0.00000	0.00000
OHAU-C---11	1.05000	9.8880	175.00000	10.56000	0.00000	0.00000
OHAU-C---220	1.04500	6.0110	0.00000	0.00000	0.00000	0.00000
ROXBURGH--11	1.05500	0.0000	82.80000	36.52000	0.00000	0.00000
ROXBURGH-220	1.04300	-1.3630	0.00000	0.00000	0.00000	0.00000
SOUTHDUN-220	1.02700	-3.5900	0.00000	0.00000	34.20000	12.50000
STOKE---220	1.01000	-25.4830	0.00000	0.00000	53.20000	-20.26000
TEKAPO-B--11	1.04600	8.3050	160.00000	5.96000	0.00000	0.00000
TEKAPO-B-220	1.04200	5.3590	0.00000	0.00000	0.00000	0.00000
TIWAI----220	1.00000	8.6200	0.00000	0.00000	420.00000	157.42000
TWIZEL---220	1.04400	5.6880	0.00000	0.00000	0.00000	0.00000
WAITAKI--11	1.05200	9.8010	70.00000	9.52000	0.00000	0.00000
WAITAKI--220	1.04200	7.0500	0.00000	0.00000	0.00000	0.00000
ARATIATIA-11	1.03200	29.8880	70.00000	2.23000	0.00000	0.00000
ARATIATIA220	1.03200	29.8880	0.00000	0.00000	0.00000	0.00000
ATIAMURI--11	1.05000	30.0720	50.00000	13.08000	0.00000	0.00000
ATIAMURI-220	1.05000	30.0720	0.00000	0.00000	0.00000	0.00000
BRUNSWICK220	1.03600	4.7880	0.00000	0.00000	0.00000	0.00000
BUNTHORPE220	1.02500	2.8260	0.00000	0.00000	66.90000	16.80000
EDGECUMBE220	1.00400	21.2020	0.00000	0.00000	135.50000	11.70000
HAMILTON--11	1.04000	0.0320	150.00000	6.33000	0.00000	0.00000
HAMILTON-220	1.04000	-8.1580	0.00000	0.00000	120.00000	40.00000
HAYWARDS-220	0.98000	-4.2490	0.00000	183.12000	716.80000	73.54000
HAYWARDS--DC	0.98000	-4.2490	0.00000	0.00000	0.00000	0.00000
HENDERSON220	0.99200	-15.0880	0.00000	0.00000	160.00000	40.00000
MARKETAI--11	1.06500	-1.0558	210.00000	75.55000	0.00000	0.00000
MARKETAI-220	1.04500	-3.6670	0.00000	0.00000	0.00000	0.00000
MARSDEN--11	1.07000	-7.2260	150.00000	67.40000	0.00000	0.00000
MARSDEN--220	1.03300	-11.5320	0.00000	0.00000	0.00000	0.00000
NEWPLYMTH-11	1.06500	12.0480	400.00000	103.60000	0.00000	0.00000
NEWPLYMTH220	1.05000	8.9780	0.00000	0.00000	200.00000	100.00000
OHAKURI--11	1.03300	33.7990	170.00000	8.64000	0.00000	0.00000
OHAKURI--220	1.03300	27.3440	0.00000	0.00000	0.00000	0.00000
OTAHUHU--11	1.02500	-11.1000	200.00000	106.92000	0.00000	0.00000
OTAHUHU--220	0.98800	-14.9900	0.00000	0.00000	500.00000	100.00000
PENROSE--220	0.98200	-15.6890	0.00000	0.00000	300.00000	98.00000
STRATFORD220	1.04900	7.6730	0.00000	0.00000	0.00000	0.00000
TARUKENGA220	1.03700	27.4690	0.00000	0.00000	0.00000	0.00000
TOKAANU--11	1.06000	3.0300	180.00000	27.95000	0.00000	0.00000
TOKAANU--220	1.04800	-1.1380	0.00000	0.00000	2.50000	0.80000
WAIPAPA--11	1.06100	-0.2240	40.00000	8.74000	0.00000	0.00000
WAIPAPA--220	1.04600	-3.4660	0.00000	0.00000	0.00000	0.00000
WAIRAKEI--11	1.03000	31.1760	140.00000	2.14000	0.00000	0.00000
WAIRAKEI-220	1.02900	26.3300	0.00000	0.00000	19.20000	6.30000
WHIRINAKI-11	1.03000	28.2860	160.00000	20.26000	0.00000	0.00000
WHIRINAKI220	1.02300	25.5600	0.00000	0.00000	200.00000	50.00000
WHAKAMARU-11	1.05500	0.0000	91.30000	13.93000	0.00000	0.00000
WHAKAMARU220	1.04000	-4.1630	0.00000	0.00000	0.00000	0.00000

BRANCH DATA INPUT

SENDING BUSBAR	RECEIVING BUSBAR	RESISTANCE P.U.	REACTANCE P.U.	SUSCEPTANCE P.U.	TAP P.C.
BENMORE---16	BENMORE---DC	0.00001	0.00001	0.00000	0.00
HAYWARDS--DC	HAYWARDS-220	0.00001	0.00001	0.00000	0.00
AVIEMORE-220	BENMORE--220	0.00325	0.01509	0.02304	0.00
AVIEMORE-220	AVIEMORE--11	0.00150	0.04470	0.00000	0.00
AVIEMORE-220	BENMORE--220	0.00330	0.01530	0.02298	0.00
AVIEMORE-220	WAITAKI--220	0.00153	0.00723	0.01062	0.00
BENMORE--220	TWIZEL---220	0.00429	0.02930	0.08201	0.00
BENMORE--220	BENMORE---16	0.00095	0.03300	0.00000	0.00
BROMLEY--220	ISLINGTON220	0.00203	0.01651	0.05364	0.00
BROMLEY--220	TWIZEL---220	0.01714	0.13990	0.45460	0.00
HALFWAYBU220	ROXBURGH-220	0.00768	0.06592	0.19082	0.00
HALFWAYBU220	SOUTHDUN-220	0.00175	0.01010	0.01665	0.00
INVERCARG220	MANAPOURI220	0.01338	0.09178	0.25996	0.00
INVERCARG220	MANAPOURI220	0.01338	0.09178	0.25996	0.00
INVERCARG220	ROXBURGH-220	0.01880	0.11223	0.17208	0.00
INVERCARG220	ROXBURGH-220	0.01915	0.11252	0.17814	0.00
INVERCARG220	TIWAI----220	0.00226	0.01456	0.04596	0.00
INVERCARG220	TIWAI----220	0.00226	0.01456	0.04596	0.00
ISLINGTON220	KIKIWA---220	0.03326	0.20030	0.30182	0.00
ISLINGTON220	LIVINGSTN220	0.03230	0.17662	0.35841	0.00
ISLINGTON220	TEKAPO-B-220	0.02112	0.14576	0.39973	0.00
ISLINGTON220	TWIZEL---220	0.01630	0.13037	0.44180	0.00
KIKIWA---220	STOKE----220	0.00762	0.04370	0.07278	0.00
LIVINGSTN220	ROXBURGH-220	0.02649	0.12951	0.16426	0.00
LIVINGSTN220	WAITAKI--220	0.00588	0.02767	0.04092	0.00
MANAPOURI220	TIWAI----220	0.01549	0.10734	0.29780	0.00
MANAPOURI220	TIWAI----220	0.01549	0.10734	0.29780	0.00
MANAPOURI220	MANAPOURI-14	0.00068	0.01902	0.00000	0.00
OHAUWA---220	TWIZEL---220	0.00115	0.00662	0.00109	0.00
OHAUWA---220	TWIZEL---220	0.00115	0.00662	0.00109	0.00
OHAUWA---220	OHAU-A----11	0.00170	0.03410	0.00000	0.00
OHAUWB---220	TWIZEL---220	0.00024	0.00179	0.00057	0.00
OHAUWB---220	TWIZEL---220	0.00024	0.00179	0.00057	0.00
OHAUWB---220	OHAU-C----220	0.00064	0.00477	0.00152	0.00
OHAUWB---220	OHAU-B----11	0.00210	0.04250	0.00000	0.00
OHAU-C---220	OHAU-C----11	0.00210	0.04250	0.00000	0.00
OHAU-C---220	TWIZEL---220	0.00088	0.00656	0.00209	0.00
ROXBURGH-220	SOUTHDUN-220	0.00849	0.07059	0.19654	0.00
ROXBURGH-220	TWIZEL---220	0.01590	0.13710	0.43180	0.00
ROXBURGH-220	TWIZEL---220	0.01590	0.13710	0.43180	0.00
ROXBURGH-220	ROXBURGH--11	0.00160	0.03230	0.00000	0.00
TWIZEL---220	TEKAPO-B-220	0.00230	0.01554	0.04860	0.00
TEKAPO-B--11	TEKAPO-B-220	0.00190	0.03510	0.00000	0.00
WAITAKI---11	WAITAKI--220	0.00668	0.07605	0.00000	0.00
ARATIATIA220	WAIRAKEI-220	0.00060	0.00340	0.00532	0.00
ATIAMURI-220	OHAKURI--220	0.00120	0.00570	0.00832	0.00
ATIAMURI-220	TARUKENGA220	0.00650	0.03750	0.06152	0.00
ATIAMURI-220	TARUKENGA220	0.00650	0.03750	0.06152	0.00
BRUNSWICK220	BUNTHORPE220	0.00460	0.03790	0.11985	0.00
BRUNSWICK220	BUNTHORPE220	0.00460	0.03790	0.11985	0.00
BRUNSWICK220	STRATFORD220	0.01450	0.08470	0.13470	0.00
BRUNSWICK220	STRATFORD220	0.01440	0.08330	0.13565	0.00
BRUNSWICK220	STRATFORD220	0.01440	0.08330	0.13565	0.00
BUNTHORPE220	HAYWARDS-220	0.02210	0.10490	0.15180	0.00
BUNTHORPE220	HAYWARDS-220	0.02210	0.10490	0.15180	0.00
BUNTHORPE220	TOKAANU--220	0.02900	0.13800	0.20000	0.00
BUNTHORPE220	TOKAANU--220	0.02900	0.13800	0.20000	0.00
BUNTHORPE220	WAIRAKEI-220	0.03120	0.18440	0.26490	0.00
EDGECUMBE220	OHAKURI--220	0.01390	0.08250	0.12750	0.00
HAMILTON-220	OTAHUHU--220	0.01040	0.06960	0.19960	0.00
HAMILTON-220	WHAKAMARU220	0.00860	0.05130	0.17320	0.00
HENDERSON220	MARSDEN--220	0.01490	0.09240	0.17560	0.00
HENDERSON220	MARSDEN--220	0.01490	0.09240	0.17560	0.00
HENDERSON220	OTAHUHU--220	0.00220	0.01880	0.05767	0.00
HENDERSON220	OTAHUHU--220	0.00220	0.01880	0.05767	0.00
MARAETAI-220	WAIPAPA--220	0.00210	0.01000	0.01441	0.00
MARAETAI-220	WHAKAMARU220	0.00170	0.00810	0.01171	0.00
MARAETAI-220	WHAKAMARU220	0.00170	0.00810	0.01171	0.00
NEWPLYMTH220	STRATFORD220	0.00300	0.02500	0.07886	0.00
NEWPLYMTH220	STRATFORD220	0.00300	0.02500	0.07886	0.00
OHAKURI--220	WAIRAKEI-220	0.00490	0.02350	0.03396	0.00
OTAHUHU--220	PENROSE--220	0.00140	0.00830	0.01282	0.00
OTAHUHU--220	PENROSE--220	0.00140	0.00830	0.01282	0.00
OTAHUHU--220	WHAKAMARU220	0.03550	0.16850	0.24390	0.00
OTAHUHU--220	WHAKAMARU220	0.01780	0.11710	0.34860	0.00
OTAHUHU--220	WHAKAMARU220	0.01780	0.11710	0.34860	0.00
TOKAANU--220	WHAKAMARU220	0.01300	0.06300	0.09200	0.00
TOKAANU--220	WHAKAMARU220	0.01300	0.06300	0.09200	0.00
TOKAANU--220	WHAKAMARU220	0.01300	0.06300	0.09200	0.00
WAIRAKEI-220	WHIRINAKI220	0.00880	0.07300	0.23060	0.00
WAIRAKEI-220	WHIRINAKI220	0.00880	0.07300	0.23060	0.00
ARATIATIA-11	ARATIATIA220	0.00340	0.09090	0.00000	0.00
ATIAMURI--11	ATIAMURI-220	0.00680	0.10010	0.00000	0.00
HAMILTON--11	HAMILTON-220	0.02420	0.10070	0.00000	0.00
MARAETAI--11	MARAETAI-220	0.00180	0.02480	0.00000	0.00
MARSDEN---11	MARSDEN--220	0.00280	0.05660	0.00000	0.00
NEWPLYMTH-11	NEWPLYMTH220	0.00050	0.01510	0.00000	0.00
OHAKURI---11	OHAKURI--220	0.00440	0.07130	0.00000	0.00
OTAHUHU---11	OTAHUHU--220	0.00140	0.03510	0.00000	0.00
TOKAANU---11	TOKAANU--220	0.00150	0.04510	0.00000	0.00
WAIPAPA---11	WAIPAPA--220	0.00840	0.15880	0.00000	0.00
WAIRAKEI--11	WAIRAKEI-220	0.00230	0.06400	0.00000	0.00
WHIRINAKI-11	WHIRINAKI220	0.00150	0.03150	0.00000	0.00
WHAKAMARU-11	WHAKAMARU220	0.00690	0.08830	0.00000	0.00

SHUNT IMPEDANCE DENOTED BY - *

SYNCHRONOUS MACHINE DATA

M/C PARAMETERS

BUSBAR NAME	MACHINE NO	MODEL	DATA BASE MVA	INERT. CONST. MJ/MVA	REACTANCES (P.U.) TRANSIENT D-AXIS	TRANSIENT Q-AXIS	SYNCHRONOUS D-AXIS	SYNCHRONOUS Q-AXIS	SUB-TRANSIENT D-AXIS	SUB-TRANSIENT Q-AXIS	POT-TIER	ARM. RESIST (P.U.)	O/C TCS (SECS) TRANSIENT D-AXIS	TRANSIENT Q-AXIS	SUB-TRANSIENT D-AXIS	SUB-TRANSIENT Q-AXIS	SATN. FACT.	RTR. TYPE
AVIEMORE--11	1		100.00	8.838	0.0990	0.0990	0.2990	0.2990	0.0660	0.0660	0.000	0.0018	4.07	0.050	0.0530	0.0530	0.000	SAL
BENMORE---16	1		100.00	18.506	0.0390	0.0390	0.1900	0.1900	0.0290	0.0290	0.000	0.0003	6.00	0.080	0.0800	0.0800	0.000	SAL
ISLINGTON220	1	1	100.00	1.082	0.3350	0.3350	0.3350	0.3350	0.3350	0.3350	0.000	0.0047	99.99	99.99	0.0000	0.0000	0.000	-
MANAPOURI-14	1		100.00	24.540	0.0390	0.0390	0.1510	0.1510	0.0240	0.0240	0.000	0.0005	6.00	0.080	0.0800	0.0800	0.000	SAL
OHAU-A----11	1		100.00	8.751	0.0940	0.0940	0.4110	0.4110	0.0470	0.0470	0.000	0.0015	5.00	0.043	0.0430	0.0430	0.000	SAL
OHAU-B----11	1		100.00	7.421	0.0920	0.0920	0.4810	0.4810	0.0550	0.0550	0.000	0.0016	5.00	0.043	0.0430	0.0430	0.000	SAL
OHAU-C----11	1		100.00	7.421	0.0920	0.0920	0.4810	0.4810	0.0550	0.0550	0.000	0.0016	5.00	0.043	0.0430	0.0430	0.000	SAL
ROXBURGH--11	1		100.00	7.950	0.0860	0.0860	0.4500	0.4500	0.0520	0.0520	0.000	0.0017	7.16	0.055	0.0550	0.0550	0.000	SAL
TEKAPO-B--11	1		100.00	3.770	0.0990	0.0990	0.4909	0.4909	0.0760	0.0760	0.000	0.0011	6.68	0.013	0.0130	0.0130	0.000	SAL
WAITAKI---11	1		100.00	3.718	0.1900	0.1900	0.5000	0.5000	0.1540	0.1540	0.000	0.0056	3.94	0.044	0.0440	0.0440	0.000	SAL
ARATIATIA-11	1		100.00	3.062	0.2400	0.2400	0.9400	0.9400	0.1800	0.1800	0.000	0.0076	5.00	0.050	0.0500	0.0500	0.000	SAL
ATIAMURI--11	1		100.00	3.060	0.2350	0.2350	0.9100	0.9100	0.1690	0.1690	0.000	0.0070	5.00	0.050	0.0500	0.0500	0.000	SAL
HAMILTON--11	1		100.00	10.650	0.1240	0.1240	0.4560	0.4560	0.1070	0.1070	0.000	0.0016	5.00	0.050	0.0500	0.0500	0.000	SAL
HAYWARDS-220	1		100.00	3.280	0.0520	0.0520	0.3440	0.3440	0.0250	0.0250	0.000	0.0006	5.00	0.050	0.0500	0.0500	0.000	SAL
MARAETAI--11	1		100.00	11.850	0.0650	0.0650	0.2700	0.2700	0.0430	0.0430	0.000	0.0065	5.00	0.050	0.0500	0.0500	0.000	SAL
MANSDEN---11	1		100.00	16.400	0.0630	0.0630	0.4830	0.4830	0.0530	0.0530	0.000	0.0005	6.90	0.050	0.0500	0.0500	0.000	SAL
NEWPLYMTH-11	1		100.00	24.050	0.0380	0.0380	0.2620	0.2620	0.0220	0.0220	0.000	0.0002	6.70	0.050	0.0800	0.0800	0.000	SAL
OHAKURI---11	1		100.00	9.035	0.1850	0.1850	0.6830	0.6830	0.1290	0.1290	0.000	0.0039	5.00	0.050	0.0500	0.0500	0.000	SAL
OTAMUHU---11	1		100.00	13.480	0.0520	0.0520	0.3430	0.3430	0.0120	0.0120	0.000	0.0010	8.50	0.075	0.0750	0.0750	0.000	SAL
TOKAANU---11	1		100.00	9.220	0.1090	0.1090	0.3290	0.3290	0.0730	0.0730	0.000	0.0020	2.84	0.060	0.0600	0.0600	0.000	SAL
WAIPAPA---11	1		100.00	4.527	0.4400	0.4400	1.5700	1.5700	0.3170	0.3170	0.000	0.0185	5.00	0.050	0.0500	0.0500	0.000	SAL
WAIRAKEI--11	1		100.00	6.483	0.1120	0.1120	0.5800	0.5800	0.0728	0.0728	0.000	0.0050	5.00	0.050	0.0500	0.0500	0.000	SAL
WHIRINAKI-11	1		100.00	7.520	0.0580	0.0580	0.4730	0.4730	0.0337	0.0337	0.000	0.0050	5.00	0.050	0.0500	0.0500	0.000	SAL
WHAKAMARU-11	1		100.00	2.590	0.2250	0.2250	0.8550	0.8550	0.1530	0.1530	0.000	0.0038	5.04	0.059	0.0590	0.0590	0.000	SAL

M/C LOADINGS

BUSBAR NAME	M/C NO.	M/C POWER OUTPUT MW	MVAR	DAMPING FACTOR	
AVIEMORE--11	1	220.00000	-1.70000	0.00	
BENMORE---16	1	540.00000	92.51000	0.00	
ISLINGTON220	1	0.00000	159.43000	0.00	
MANAPOURI-14	1	400.00000	91.33000	0.00	
OHAU-A----11	1	214.00000	11.92000	0.00	
OHAU-B----11	1	175.00000	9.25000	0.00	
OHAU-C----11	1	175.00000	10.56000	0.00	
ROXBURGH--11	1	82.80000	36.52000	0.00	
TEKAPO-B--11	1	160.00000	5.90000	0.00	
WAITAKI---11	1	70.00000	9.52000	0.00	
ARATIATIA-11	1	70.00000	2.23000	0.00	A
ATIAMURI--11	1	50.00000	13.08000	0.00	A
HAMILTON--11	1	150.00000	6.33000	0.00	A
HAYWARDS-220	1	0.00000	183.12000	0.00	A
MARAETAI--11	1	210.00000	75.55000	0.00	A
MANSDEN---11	1	150.00000	67.40000	0.00	A
NEWPLYMTH-11	1	400.00000	103.80000	0.00	A
OHAKURI---11	1	170.00000	8.64000	0.00	A
OTAMUHU---11	1	200.00000	106.92000	0.00	A
TOKAANU---11	1	180.00000	27.95000	0.00	A
WAIPAPA---11	1	40.00000	8.74000	0.00	A
WAIRAKEI--11	1	140.00000	2.14000	0.00	A
WHIRINAKI-11	1	160.00000	20.26000	0.00	A
WHAKAMARU-11	1	91.30000	13.93000	0.00	A

M/C USING ALTERNATIVE REF. M/C DENOTED BY - A

DC LINK PARAMETERS

BUS NAME	ANGLE LIMITS MAX	MIN	SERIES BRIDGES	VOLTAGE BASE(KV)	CURRENT MARGIN(A)	LINE RESIS (OHMS)	REACTANCE(PU) COM	TRAN	FILTER	TAP %
BENMORE---DC	90.00	3.00	1.00	420.00	0.00	25.560	0.02243	0.02243	0.99200	0.000
MAYWARDS--DC	90.00	18.00	1.00	420.00	120.00	25.560	0.01905	0.01905	1.03250	0.000

SHUNT LOADS

BUSBAR NAME	MEGAWATTS	MEGAVARS	NON-IMPEDANCE TYPE LOAD (PC) VARYING WITH V P	Q	FIXED P	Q
BROMLEY--220	129.60000	38.30000	0.	0.	0.	0.
HALFWAYBU220	95.30000	40.40000	0.	0.	0.	0.
HAVERCAMG220	183.20000	20.00000	0.	0.	0.	0.
ISLINGTON220	504.10000	124.30000	0.	0.	0.	0.
KIKIWA---220	59.20000	9.20000	0.	0.	0.	0.
SOUTHDUN-220	34.20000	12.90000	0.	0.	0.	0.
STOKE----220	53.20000	-20.26000	0.	0.	0.	0.
TIWAI----220	420.00000	157.42000	0.	0.	0.	0.
BUNTHORPE220	66.90000	16.80000	0.	0.	0.	0.
EDGECUMBE220	135.50000	11.70000	0.	0.	0.	0.
HAMILTON-220	120.00000	20.00000	0.	0.	0.	0.
HAYWARDS-220	716.60000	73.54000	0.	0.	0.	0.
HENDERSON220	160.00000	40.00000	0.	0.	0.	0.
NEWPLYMTH220	200.00000	100.00000	0.	0.	0.	0.
OTAHUHU--220	500.00000	100.00000	0.	0.	0.	0.
PENROSE--220	300.00000	90.00000	0.	0.	0.	0.
TOKAANU--220	2.50000	0.80000	0.	0.	0.	0.
WAIRAKEI-220	19.20000	6.30000	0.	0.	0.	0.
WHIRINAKI220	200.00000	50.00000	0.	0.	0.	0.

NOTE - ANY NON-ESSENTIAL PARAMETERS MISSING FROM THE INPUT DATA HAVE BEEN ASSIGNED APPROPRIATE VALUES IN THE CALCULATION PROCESS, AS SHOWN ABOVE. A VALUE INDICATED AS A SERIES OF 9S IS ACTUALLY VERY LARGE.

APPENDIX A7

DATA FOR TS IMPROVEMENT IN A RECTIFIER AC SYSTEM - CASE 1 OF TABLE 7.1

STEADY-STATE SYSTEM DATA

BUSBAR DATA INPUT

BUSBAR	VOLTAGE	ANGLE	GEN MW	GEN MVAR	LOAD MW	LOAD MVAR
BENMORE---16	1.02500	15.4300	1000.00000	225.00000	0.00000	0.00000
BENMORE---DC	1.02500	15.4000	0.00000	0.00000	0.00000	0.00000
SYSTEM---220	1.00000	0.0000	-493.90000	30.05000	0.00000	0.00000
BENMORE--220	1.00800	7.0800	0.00000	0.00000	0.00000	0.00000
HAYWARDS-220	0.98000	0.0000	-476.56000	143.44000	0.00000	0.00000
HAYWARDS--DC	0.98000	0.0000	0.00000	0.00000	0.00000	0.00000

BRANCH DATA INPUT

SENDING BUSBAR	RECEIVING BUSBAR	RESISTANCE P.U.	REACTANCE P.U.	SUSCEPTANCE P.U.	TAP P.C.
BENMORE---16	BENMORE---DC	0.00001	0.00001	0.00000	0.00
HAYWARDS-220	HAYWARDS--DC	0.00001	0.00001	0.00000	0.00
BENMORE--220	SYSTEM---220	0.00400	0.05000	0.09000	0.00
BENMORE--220	SYSTEM---220	0.00400	0.05000	0.09000	0.00
BENMORE--220	BENMORE---16	0.00050	0.03000	0.00000	0.00

SHUNT IMPEDANCE DENOTED BY - *

SYNCHRONOUS MACHINE DATA

M/C PARAMETERS

BUSBAR NAME	MACHINE NO	MODEL	DATA MVA BASE	INERT. CONST. KWSKVA	REACTANCES (P.U.) TRANSIENT D-AXIS	TRANSIENT Q-AXIS	SYNCHRONOUS D-AXIS	SYNCHRONOUS Q-AXIS	SUB-TRANSIENT D-AXIS	SUB-TRANSIENT Q-AXIS	POT-IER	ARM. RESIST (P.U.)	O/C TCS (SECS) TRANSIENT D-AXIS	TRANSIENT Q-AXIS	SUB-TRANSIENT D-AXIS	SUB-TRANSIENT Q-AXIS	SATN. FACT.	RTR. TYPE
BENMORE---16	1	5	100.00	20.000	0.0150	0.0150	0.0750	0.0750	0.0100	0.0100	0.000	0.0003	6.00	0.100	0.1000	0.1000	0.000	SAL
SYSTEM---220	1	5	100.00	999.900	0.0100	0.0100	0.0200	0.0200	0.0050	0.0050	0.000	0.0003	6.00	0.100	0.1000	0.1000	0.000	SAL
HAYWARDS-220	1	1	100.00	999.900	0.0100	0.0100	0.0100	0.0100	0.0100	0.0100	0.000	0.0000	99.99	9.999	0.0000	0.0000	0.000	-

M/C LOADINGS

BUSBAR NAME	M/C NO.	M/C POWER OUTPUT MW	MVAR	DAMPING FACTOR
BENMORE---16	1	1000.00000	225.00000	0.00
SYSTEM---220	1	-493.90000	30.05000	0.00
HAYWARDS-220	1	-476.56000	143.44000	0.00

DC LINK PARAMETERS

BUS NAME	ANGLE LIMITS MAX	MIN	SERIES BRIDGES	VOLTAGE BASE(KV)	CURRENT MARGIN(A)	LINE RESIS (OHMS)	REACTANCE(PU) COM	TRAN	FILTER	TAP %	
BENMORE---DC	90.00	3.00	1.00	420.00	0.00	25.560	0.02243	0.02243	0.99200	0.000	RECTIFIER
HAYWARDS--DC	90.00	18.00	1.00	420.00	120.00	25.560	0.01905	0.01905	1.03250	0.000	INVERTER

RESTART T.C.= 0.0600

100.00%AGE INCREASE IN CURRENT SETTING ON AT 0.240 SECS AND OFF AT 0.360 SECS

****
* NOTE - ANY NON-ESSENTIAL PARAMETERS MISSING FROM THE INPUT DATA HAVE BEEN ASSIGNED APPROPRIATE VALUES *
* IN THE CALCULATION PROCESS, AS SHOWN ABOVE. A VALUE INDICATED AS A SERIES OF 9S IS ACTUALLY VERY LARGE. *
****

APPENDIX A8

DATA FOR TS IMPROVEMENT IN AN INVERTER AC SYSTEM - CASE 4 OF TABLE 7.1

STEADY-STATE SYSTEM DATA

BUSBAR DATA INPUT

BUSBAR	VOLTAGE	ANGLE	GEN MW	GEN MVAR	LOAD MW	LOAD MVAR
BENMORE---16	1.00000	-15.2870	-1000.00000	238.77000	0.00000	0.00000
BENMORE---DC	1.00000	-15.2870	0.00000	0.00000	0.00000	0.00000
SYSTEM---220	1.00000	0.0000	529.99000	30.89000	0.00000	0.00000
BENMORE--220	0.98800	-7.6580	0.00000	0.00000	0.00000	0.00000
HAYWARDS-220	1.02500	0.0000	500.00000	129.03000	0.00000	0.00000
HAYWARDS--DC	1.02500	0.0000	0.00000	0.00000	0.00000	0.00000

BRANCH DATA INPUT

SENDING BUSBAR	RECEIVING BUSBAR	RESISTANCE P.U.	REACTANCE P.U.	SUSCEPTANCE P.U.	TAP P.C.	
BENMORE---16	BENMORE---DC	0.00001	0.00001	0.00000	0.00	M
HAYWARDS-220	HAYWARDS--DC	0.00001	0.00001	0.00000	0.00	M
BENMORE--220	SYSTEM---220	0.00400	0.05000	0.09000	0.00	
BENMORE--220	SYSTEM---220	0.00400	0.05000	0.09000	0.00	
BENMORE--220	BENMORE---16	0.00050	0.02500	0.00000	0.00	

SHUNT IMPEDANCE DENOTED BY - *
MONITORED BRANCH DENOTED BY - M

SYNCHRONOUS MACHINE DATA

M/C PARAMETERS

BUSBAR NAME	MACHINE NO	MODEL	DATA MVA BASE	INERT. CONST. KWSKVA	REACTANCES (P.U.) TRANSIENT D-AXIS	TRANSIENT Q-AXIS	SYNCHRONOUS D-AXIS	SYNCHRONOUS Q-AXIS	SUB-TRANSIENT D-AXIS	SUB-TRANSIENT Q-AXIS	POT-IER	ARM. RESIST (P.U.)	O/C TCS (SECS) TRANSIENT D-AXIS	TRANSIENT Q-AXIS	SUB-TRANSIENT D-AXIS	SUB-TRANSIENT Q-AXIS	SATN. FACT.	RTR. TYPE
BENMORE---16	1	5	100.00	20.000	0.0150	0.0150	0.0750	0.0750	0.0100	0.0100	0.000	0.0003	6.00	0.100	0.1000	0.1000	0.000	SAL
SYSTEM---220	1	5	100.00	999.900	0.0100	0.0100	0.0200	0.0200	0.0050	0.0050	0.000	0.0003	6.00	0.100	0.1000	0.1000	0.000	SAL
HAYWARDS-220	1	1	100.00	999.900	0.0100	0.0100	0.0100	0.0100	0.0100	0.0100	0.000	0.0000	99.99	9.999	0.0000	0.0000	0.000	-

M/C LOADINGS

BUSBAR NAME	M/C NO.	M/C POWER OUTPUT MW	MVAR	DAMPING FACTOR
BENMORE---16	1	-1000.00000	238.77000	0.00
SYSTEM---220	1	529.99000	30.89000	0.00
HAYWARDS-220	1	500.00000	129.03000	0.00

DC LINK PARAMETERS

BUS NAME	ANGLE LIMITS MAX	MIN	SERIES BRIDGES	VOLTAGE BASE(KV)	CURRENT MARGIN(A)	LINE RESIS (OHMS)	REACTANCE(PU) COM	TRAN	FILTER	TAP %	
HAYWARDS--DC	90.00	3.00	1.00	420.00	0.00	25.560	0.01905	0.01905	1.03250	0.000	RECTIFIER
BENMORE---DC	90.00	18.00	1.00	420.00	120.00	25.560	0.02243	0.02243	0.99200	0.000	INVERTER

DC LINE FAULT TIMES--ON AT 0.2000 SECS OFF AT 0.2100 SECS
RESTART T.C.= 0.0300
100.00%AGE INCREASE IN CURRENT SETTING ON AT 0.210 SECS AND OFF AT 0.320 SECS

****
* NOTE - ANY NON-ESSENTIAL PARAMETERS MISSING FROM THE INPUT DATA HAVE BEEN ASSIGNED APPROPRIATE VALUES *
* IN THE CALCULATION PROCESS, AS SHOWN ABOVE. A VALUE INDICATED AS A SERIES OF 9S IS ACTUALLY VERY LARGE. *
****

APPENDIX A9

DATA FOR TS IMPROVEMENT USING DC LINK POWER REVERSAL - CASE 2 OF TABLE 7.1

NO INDUCTION MOTOR DATA INPUT

STEADY-STATE SYSTEM DATA

BUSBAR DATA INPUT

BUSBAR	VOLTAGE	ANGLE	GEN MW	GEN MVAR	LOAD MW	LOAD MVAR
BENMORE---16	1.00000	26.0300	1000.00000	404.13000	0.00000	0.00000
BENMORE---DC	1.00000	26.0300	0.00000	0.00000	0.00000	0.00000
BENMORE--220	0.97800	17.4200	0.00000	0.00000	0.00000	0.00000
SYSTEM---220	1.00000	0.0000	-1443.33000	397.13000	0.00000	0.00000
HAYWARDS-220	1.02500	0.0000	500.10000	129.21000	0.00000	0.00000
HAYWARDS--DC	1.02500	0.0000	0.00000	0.00000	0.00000	0.00000

BRANCH DATA INPUT

SENDING BUSBAR	RECEIVING BUSBAR	RESISTANCE P.U.	REACTANCE P.U.	SUSCEPTANCE P.U.	TAP P.C.
BENMORE---16	BENMORE---DC	0.00001	0.00001	0.00000	0.00
HAYWARDS-220	HAYWARDS--DC	0.00001	0.00001	0.00000	0.00
BENMORE--220	BENMORE---16	0.00050	0.01000	0.00000	0.00
SYSTEM---220	BENMORE--220	0.00200	0.04000	0.10000	0.00
SYSTEM---220	BENMORE--220	0.00200	0.04000	0.10000	0.00

SHUNT IMPEDANCE DENOTED BY - *

SYNCHRONOUS MACHINE DATA

M/C PARAMETERS

BUSBAR NAME	MACHINE NO	MODEL	DATA MVA BASE	DATA KWSKVA	INERT. CONST.	REACTANCES (P.U.) TRANSIENT D-AXIS	TRANSIENT Q-AXIS	SYNCHRONOUS D-AXIS	SYNCHRONOUS Q-AXIS	SUB-TRANSIENT D-AXIS	SUB-TRANSIENT Q-AXIS	POT-IER	ARM. RESIST (P.U.)	O/C TCS (SECS) TRANSIENT D-AXIS	TRANSIENT Q-AXIS	SUB-TRANSIENT D-AXIS	SUB-TRANSIENT Q-AXIS	SATN. FACT.	RTR. TYPE
BENMORE---16	1	5	100.00	20.000	0.0150	0.0150	0.0750	0.0750	0.0100	0.0100	0.000	0.0003	6.00	0.100	0.1000	0.1000	0.000	SAL
SYSTEM---220	1	5	100.00	999.900	0.0010	0.0010	0.0020	0.0020	0.0010	0.0010	0.000	0.0003	6.00	0.100	0.1000	0.1000	0.000	SAL
HAYWARDS-220	1	1	100.00	999.900	0.0100	0.0100	0.0100	0.0100	0.0100	0.0100	0.000	0.0000	99.99	9.999	0.0000	0.0000	0.000	-

M/C LOADINGS

BUSBAR NAME	M/C NO.	M/C POWER OUTPUT MW	M/C POWER OUTPUT MVAR	DAMPING FACTOR
BENMORE---16	1	1000.00000	404.13000	0.00
SYSTEM---220	1	-1443.33000	397.13000	0.00
HAYWARDS-220	1	500.10000	129.21000	0.00

DC LINK PARAMETERS

BUS NAME	ANGLE LIMITS MAX	ANGLE LIMITS MIN	SERIES BRIDGES	VOLTAGE BASE(KV)	CURRENT MARGIN(A)	LINE RESIS (OHMS)	REACTANCE(PU) COM	REACTANCE(PU) TRAN	FILTER	TAP %	
HAYWARDS--DC	90.00	3.00	1.00	420.00	0.00	25.560	0.01905	0.01905	1.03250	0.000	RECTIFIER
BENMORE---DC	90.00	18.00	1.00	420.00	120.00	25.560	0.02243	0.02243	0.99200	0.000	INVERTER

DC LINK REVERSAL WITH CURRENT SETTING OF 473.60 REVERSED AT 0.24 SECS AND RESTORED AT 0.36 SECS
RESTART T.C.= 0.0400

****
* NOTE - ANY NON-ESSENTIAL PARAMETERS MISSING FROM THE INPUT DATA HAVE BEEN ASSIGNED APPROPRIATE VALUES *
* IN THE CALCULATION PROCESS, AS SHOWN ABOVE. A VALUE INDICATED AS A SERIES OF 9S IS ACTUALLY VERY LARGE. *
****

APPENDIX A10

PAPER PUBLISHED IN TRANS. IEEE, VOL. PAS-99, NO. 1, JANUARY/FEBRUARY 1980

F 79 662-8

MODELLING RECTIFIER LOADS FOR A MULTI-MACHINE TRANSIENT-STABILITY PROGRAMME

C. P. Arnold, Member I.E.E.E.
University of Canterbury
Christchurch
New Zealand

K. S. Turner, Student Member I.E.E.E.
New Zealand Electricity
Christchurch
New Zealand

J. Arrillaga, Non Member
University of Canterbury
Christchurch
New Zealand

Abstract - An improved rectifier load model for use in transient-stability studies is developed. The model, which simulates abnormal modes of operation and the dynamics of the d.c. load, is used to investigate the stability of a power-system where the rectifier can represent a large percentage of load.

INTRODUCTION

Rectifier loads with large power ratings and sophisticated power electronic control have become common in power-systems. Figure 1 illustrates the primary transmission system of the South Island of New Zealand, which includes an aluminium smelter load. This represents some 15% of the total installed capacity. Since this load is constant, it can represent up to 50% of the load during periods of low power demand,

When the transient-stability of power-systems is being investigated, considerable error can occur with inaccurate representation of the rectifier load.

An accurate representation of rectifier loads is developed in this paper. Although the model described has been specifically developed for an aluminium smelter load, it is also applicable to other types of large rectifier loads such as chlorine plants. The model includes the dynamic effects of the d.c. side of the rectifier and also includes abnormal operation during large disturbances. This extended model is thus accurate for a wide range of conditions observed during transient-stability studies.

The usual purpose of load modelling in multi-machine transient-stability studies is to provide the programme with updated instantaneous values of real and reactive power absorption. This allows overall system stability to be evaluated and provides information on the operating characteristics of the load during large disturbances.

This paper describes various rectifier load models, discusses their effect on transient-stability and proposes a unified algorithm of superior convergence properties, than the conventional sequential algorithm.

BASIC RECTIFIER MODEL

Large rectifier loads generally consist of a number of series and/or parallel connected bridges, each bridge being phase shifted relative to the others. With these configurations high pulse numbers can be achieved resulting in minimal distortion of the supply voltage without filtering. Rectifier loads can therefore be modelled as a single equivalent bridge with a sinusoidal supply voltage at the terminals but without representation of passive filters. This model is shown in figure 2.

Rectifier loads can utilise a number of control methods. They can use diode and thyristor elements in full or half bridge configurations. In the case of the aluminium smelter in New Zealand diode bridges are used with tap changer and saturable reactor control. The effect of the saturable reactors on diode conduction is identical to delay angle control of a thyristor over a limited range of delay angles [1]. All these different control methods can be modelled using a controlled rectifier with suitable limits imposed on the delay angle (α).

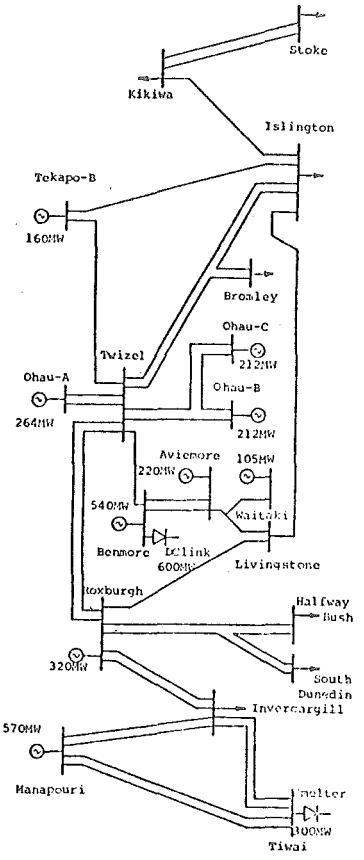

Figure 1. New Zealand South Island Primary System.

The main assumptions made in the development of the basic rectifier model are:

- control action on delay angle is considered to be instantaneous,
- no tap changing takes place during or after the disturbance,
- the d.c. current (I_d) is smooth,
- there are no losses associated with either the

F 79 662-8 A paper recommended and approved by the IEEE Power System Engineering Committee of the IEEE Power Engineering Society for presentation at the IEEE PES Summer Meeting, Vancouver, British Columbia, Canada, July 15-20, 1979. Manuscript submitted February 1, 1979; made available for printing May 1, 1979.

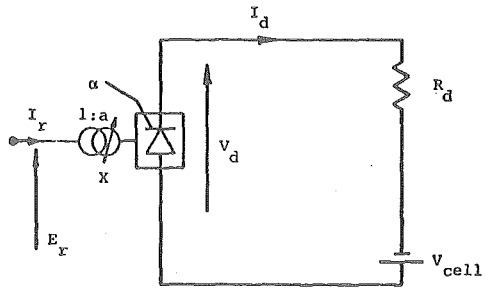

Fig. 2. Simple Rectifier Load Equivalent.

convertor transformer or the switching devices,
- rectangular current waveforms occur at the rectifier terminals,
- there is no harmonic distortion.

With an assumed a.c. terminal voltage (E_r), and operating under constant current control, a simple rectifier can be solved directly without iteration. In the case of aluminium smelters, effects such as cell counter voltage (V_{cell}) can be included in the d.c. load. The following equations may be used to describe the action of the rectifier [2][3].

$$I_d = \frac{aE_r}{\sqrt{2}X_c}(\cos\alpha - \cos\delta) \quad (1)$$

$$V_d = \frac{3aE_r}{\sqrt{2}\pi}(\cos\alpha + \cos\delta) \quad (2)$$

$$I_d = (AI_d - V_{cell})/(A + R_d) \quad (3)$$

$$V_d = I_dR_d + V_{cell} \quad (4)$$

From these equations the following may be established:-

$$\cos\alpha = \frac{\pi}{3\sqrt{2}aE_r}\left(V_d + \frac{3X_cI_d}{\pi}\right) \quad (5)$$

$$\cos\delta = \frac{\sqrt{2}\pi V_d}{3aE_r} - \cos\alpha \quad (6)$$

$$\cos\phi = (\cos\alpha + \cos\delta)/2 \quad (7)$$

Constant current cannot be maintained during a large disturbance as a limit or delay angle will be reached. In this event the rectifier control specification will become one of constant delay angle and equation (3) becomes:-

$$I_d = \frac{\frac{3\sqrt{2}}{\pi}aE_r\cos\alpha_{min} - V_{cell}}{\left(R_d + \frac{3X_c}{\pi}\right)} \quad (8)$$

Protection limits and disturbance severity determines the rectifier operating characteristics during the disturbance. Shutdown occurs if I_d reaches a set minimum or zero and cell counter voltage will cause shutdown before the a.c. terminal voltage reaches zero.

The real and reactive power flowing into the rectifier can be obtained by:

$$P = V_dI_d \quad (9)$$

$$Q = P\tan\phi \quad (10)$$

DYNAMIC D.C. LOADS

The basic rectifier model assumes that current on the d.c. side of the bridge can change instantaneously. For some types of rectifier loads this may be a valid assumption, but data for the New Zealand aluminium smelter shows that the d.c. load has a time constant of 113 ms. This is a significant delay with respect to fault clearing times of 100 to 140 ms. In order to realistically examine the effects which rectifiers have on the transient-stability of the system, this time constant must be taken into account. This requires a more complex model to account for extended overlap angles due to a low commutating voltage.

Modes of Operation

The full range of rectifier operation can be classified into four modes [4].

Mode 1 - Normal operation.

Mode 2 - Enforced delay. This is imposed on the firing angle as the forward voltage across the incoming thyristor is negative until the previous commutation is complete or until the firing angle exceeds 30^o.

Mode 3 - Periods of three-phase and d.c. short-circuit which exist when 4 valves are conducting. (Two commutations overlap).

Mode 4 - Continuous three-phase and d.c. short-circuit, caused by two commutations taking place continuously. The a.c. and d.c. current paths are independent.

Table 1 gives a brief summary of the four modes.

Mode	Firing Angle	Overlap Angle u
1	$0^o \leq \alpha \leq 90^o$	$0^o \leq u \leq 60^o$
2	$0^o \leq \alpha \leq 30^o$	60^o
3	$30^o \leq \alpha \leq 90^o$	$60^o \leq u < 120^o$
4	$30^o \leq \alpha \leq 90^o$	120^o

Table 1 - Rectifier Modes of Operation

When the rectifier is operating in modes 3 and 4 equations (1) and (2) are replaced by:-

$$I_d = \frac{aE_r}{\sqrt{6}X_c}(\cos\alpha' - \cos\delta') \quad (11)$$

$$V_d = \frac{3\sqrt{3}}{\sqrt{2}\pi}aE_r(\cos\alpha' + \cos\delta') \quad (12)$$

where

$$\alpha' = \alpha - 30^o \quad (13)$$

$$\delta' = \delta + 30^o \quad (14)$$

Relationship between AC and DC Currents

For small overlap angles and on the basis of a 120^o rectangular current pulse, the fundamental r.m.s. a.c. line and d.c. currents are normally related by:

$$I_r = k\frac{\sqrt{6}}{\pi}I_d \quad (15)$$

where k is unity.

For overlap angles exceeding 30^o an exact expression obtained by Fourier analysis should be used [2], that is:

$$k = \frac{(\angle -2\alpha - \angle -2\delta - j2u)}{4(\cos\alpha - \cos\delta)} \quad (16)$$

This expression is only valid for mode 1 and 2 operation.

A new expression has been derived (appendix A) which can be used for the other abnormal modes of operation:

$$k = \frac{\sqrt{3}(\angle -2\alpha' - \angle -2\delta' - j2u)}{4(\cos\alpha' - \cos\delta')} \qquad (17)$$

A graph of the error between the approximation (equation (15)) and the exact expression of equations (16) and (17) for a number of delay angles is shown in figure 3.

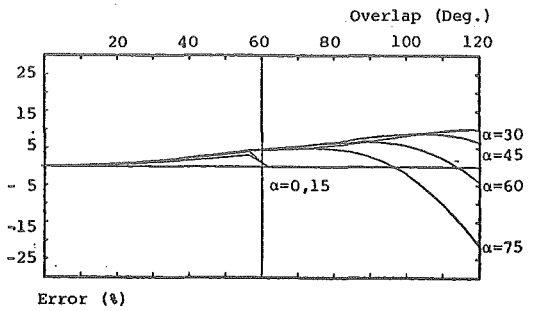

Figure 3. Percentage deviation of k from unity.

STABILITY STUDIES: SEQUENTIAL ALGORITHM

The basic rectifier model has been included in a transient-stability programme in a similar manner as the generator and non-impedance load models [5].

From an initial load-flow a nominal bus shunt admittance (y_o) can be calculated for the rectifier. This is included directly into the network admittance matrix [Y]. Thus the injected current into the network in the initial steady-state is zero. During the stability run the rectifier is solved sequentially, along with the generator and load differential equations, to obtain an injected current which accounts for the difference between the actual characteristics and the shunt admittance characteristic [6]. That is:

$$\bar{I}_{inj} = (\bar{y}_o - \bar{y})\bar{V} \qquad (18)$$

where

$$\bar{y}_o = \frac{\bar{s}_o^*}{\bar{V}_o^2} \qquad (19)$$

$$\bar{y} = \frac{s^*}{\bar{V}^2} \qquad (20)$$

A vector of nodal injected currents is thus obtained which is used to solve the network equation:

$$[\bar{I}_{inj}] = [\bar{Y}]\,[\bar{V}] \qquad (21)$$

Equation (21) is solved directly for $[\bar{V}]$, an updated vector of network nodal voltages, using sparsity-programmed ordered triangular factorization for minimal storage and high efficiency. The new value of nodal voltage at each node is used for an updated solution of all dynamic equipment and the process iterated to convergence.

Limitations of the Sequential Method

The basic rectifier model does not depart greatly from an impedance characteristic and is well behaved for low terminal voltages, the injected current tending to zero as the voltage approaches zero. Figure 4 compares the current due to a rectifier with that due to a constant impedance load. As the injected current is never large the iterative solution for all a.c. conditions is stable.

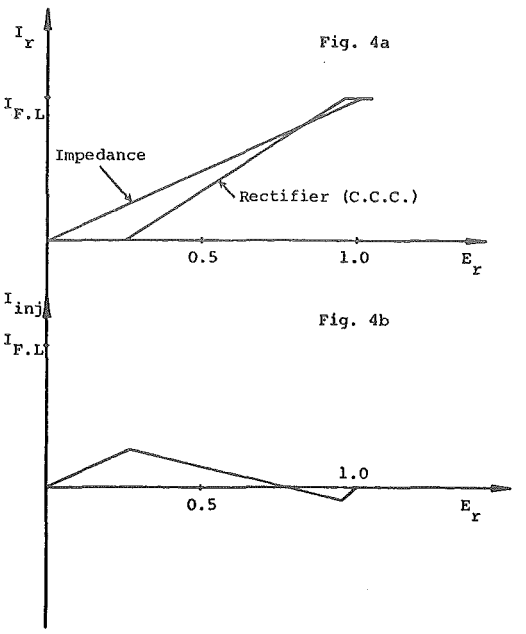

Fig. 4. Difference between Impedance and Simple Rectifier Characteristic (for $V_{cell} \neq 0$)

When the rectifier model is modified to account for the dynamic behaviour of the d.c. load its characteristic departs widely from that of an impedance. Immediately after a fault application the voltage drops to a low value but the injected current magnitude does not change significantly. Similarly on fault clearing, the voltage recovers instantaneously to some higher value while the current remains low.

When the load characteristic differs greatly from that of an impedance, the sequential solution technique can exhibit convergence problems [5][6], especially when the voltage is low. With small terminal voltages the a.c. current magnitude of the rectifier load is related to the d.c. current but the current phase is greatly affected by the terminal voltage. Small voltage changes in the complex plane can result in large variations of the voltage and current phase angles.

STABILITY STUDIES: UNIFIED ALGORITHM

To avoid the convergence problems of the sequential solution, an alternative algorithm has been developed. This combines the rectifier and network solutions into a unified process. It however does not affect the sequential solution of the other components of the power-system with the network.

The basis of this approach is to reduce the a.c. network, excluding the rectifier, to an equivalent Thevenin source voltage and impedance as viewed from the primary side of the rectifier transformer terminals. This equivalent of the system, along with the rectifier, can be described by a set of non-linear simultaneous equations which can be solved by a standard Newton-Raphson algorithm. The solution of the reduced-system yields the fundamental a.c. current at the rectifier terminals.

To obtain the network equivalent impedance it is only necessary to inject 1 pu current into the network at the rectifier terminals while all other nodal injected currents are zero. With an injected current vector of this form, a solution of equation (21) gives the driving point and transfer impedances in the resulting voltage vector.

$$[\bar{Z}] \equiv [\bar{V}'] = [\bar{Y}]^{-1}[\bar{I}'_{inj}] \quad (22)$$

where

$$[\bar{I}'_{inj}] = \begin{vmatrix} o \\ o \\ \bar{I}_r' \\ o \\ o \end{vmatrix} \text{ and } \bar{I}_r' = 1+j0 \quad (23)$$

The equivalent circuit shown in figure 5 can now be applied to find the rectifier current ($\bar{I}_r$) by using the Newton-Raphson technique.

The effect of the rectifier on the rest of the system can be determined by superposition:

$$[\bar{V}] = [\bar{V}^o] + [\bar{Z}]\,\bar{I}_r \quad (24)$$

where

$$[\bar{V}^o] = [\bar{Y}]^{-1}[\bar{I}^o_{inj}] \quad (25)$$

and $[I^o_{inj}]$ are the injected currents due to all other generation and loads in the system.

If the network remains constant, vector $[\bar{Z}]$ is also constant and thus only needs re-evaluation on the occurrence of a discontinuity such as line switching, fault application or removal, or motor switching.

Thus the advantages of the unified and sequential methods are combined. That is, good convergence for a difficult element in the system is achieved while the programming for the rest of the systems remains simple and storage requirements are kept low.

Equations for Normal Operation

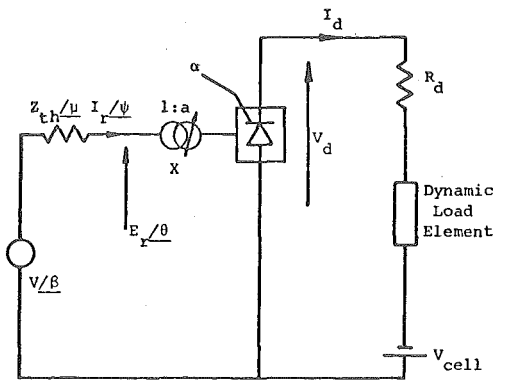

Fig. 5. Equivalent System for Newton-Raphson Solution.

The equivalent-system of figure 5 can be described by a set of five independent equations. Under constant current control these are:-

$$V\underline{/\beta} - E_r\underline{/\theta} - Z_{th}\underline{/\mu}\ I_r\underline{/\psi} = 0 \quad (26)$$

$$V_d - k_1 a E_r \cos\alpha + k_2 X_c I_d = 0 \quad (27)$$

$$V_d - k_3 a E_r \cos(\theta-\psi) = 0 \quad (28)$$

$$I_d - I_{dsp} = 0 \quad (29)$$

Substituting

$$V_d = I_d R_d + V_{cell} \quad (30)$$

$$I_r = k\frac{\sqrt{6}}{\pi} I_d \quad (31)$$

into equations (26) to (28) reduces the number of variables to five, that is E_r, θ, ψ, α and I_d. In the normal mode, the constant k of equation (31) is close to unity and can be calculated at the beginning of each iteration using information from the previous iteration.

When the delay angle α reaches a specified lower limit (α_{min}), the control specification given by equation (29) changes to

$$\alpha - \alpha_{min} = 0 \quad (32)$$

and equation (27) is replaced by an algebraic form of the differential equation for I_d, obtained using the trapezoidal rule (see Appendix B):

$$I_d - k_a E_r \cos\alpha - k_b = 0 \quad (33)$$

Equations for Abnormal Operation

In mode 3, account has to be taken of the effect of the periods of three-phase short-circuit on the a.c. voltage at the rectifier terminals. These periods reduce the fundamental voltage at the rectifier to zero when the overlap reaches 120°. In addition, the relationship between I_r and I_d, given by equation (17), can have a significant effect on the fundamental of a.c. current. To account for this, a linearised form of the curve for α=30° in figure 3 is included explicitly in the formulation:

$$V\underline{/\beta} - E_r\underline{/\theta} - Z\underline{/\mu}\ k I_d (f_1(u))\underline{/\psi} = 0 \quad (34)$$

$$k_5 a E_r \cos(\theta-\psi)(f_1(u)) - k_6 a E_r \cos(\alpha-30^o) + k_7 X_c I_d = 0 \quad (35)$$

$$I_d - k_a E_r \cos(\alpha-30^o) - k_b = 0 \quad (36)$$

$$\cos(\alpha+u+30^o) - \cos(\alpha-30^o) + \frac{k_4 X_c I_d}{a E_r} = 0 \quad (37)$$

$$\alpha - \alpha_{min} = 0 \quad (38)$$

where $f_1(u)$ is a linear function of u. The variables in this formulation are E_r, θ, ψ, α, u and I_d.

In mode 4, the rectifier and the a.c. system are independent and the fundamental a.c. current is no longer related to the d.c. current. The a.c. current is a function of the network equivalent source and the d.c. current is obtained from the differential equation describing the d.c. load. The solution of the system in mode 4 is direct.

Programme Aspects

Good starting values are important to ensure convergence of the Newton-Raphson algorithm. The load-flow provides initial conditions and during normal running of the transient-stability programme, values from the end of the previous step are used as initial conditions for the next step. With step lengths of between 10 ms and 25 ms, the Newton-Raphson algorithm converges in 2 or 3 iterations.

Discontinuities during the stability study require a special calculation of the initial condition as the network change can be large. A new network equivalent impedance and voltage is obtained immediately after a discontinuity and, since I_d does not change instantaneously, an estimate of E_r can be made using equation (31) and

$$E_r = V - I_r Z_{th} \quad (39)$$

Evaluation of other variables can be made using the values of V, β, E_r and I_d. The initial conditions so obtained give convergence in 2 to 5 iterations for the first overall iteration of the whole system and only 1

or 2 iterations on successive system iterations. Reconvergence of the a.c. system is unaltered by the rectifier.

Choice of operating mode after a discontinuity is just as important as good initial conditions. The incorrect choice can lead to an attempt to solve the wrong set of equations for the prevailing conditions. This can lead to failure of the algorithm and study termination. Mode choice is made using a factor k_m [4] where:

$$k_m = \frac{\sqrt{2} X_c I_d}{a E_r} \qquad (40)$$

The range of k_m for each mode is as follows:-

Mode 1 - $k_m < \cos(60-\alpha)$
Mode 2 - $\cos(60-\alpha) < k_m < 0.8660$
Mode 3 - $0.8660 < k_m < 1.1547$
Mode 4 - $1.1547 < k_m$

Immediately after a discontinuity, the choice of mode is influenced by the estimate made for E_r. If the value of k_m indicates mode 4, iterations are made in mode 3, to check that the overlap angle will in fact reach 120°. This test is repeated at the beginning of each time step so that reversion to mode 3 can be determined correctly. This can be justified as, in fact, mode 4 is merely a boundary condition of mode 3.

A particular advantage of the Newton-Raphson formulation is the flexibility it affords to the setting of control specifications. The normal specifications are either constant current or constant delay angle. During the transition through mode 2,the overlap angle is fixed at 60° and the enforced delay angle is calculated. This can be easily accomplished by replacing equation (29) by:

$$\cos^{-1}\left(\cos\alpha - \frac{\sqrt{2} X_c I_d}{a E_r}\right) - \alpha - u_{sp} = 0 \qquad (41)$$

where $u_{sp} = 60^\circ$

Equation (33), the algebraic form of the defferential equation for I_d, also becomes a control specification when reconverging after a discontinuity. This equation reduces to:

$$I_d - k_b = 0 \qquad (42)$$

for zero step length, holding I_d at its previous value.

COMPARISON OF SEQUENTIAL AND UNIFIED ALGORITHMS

The network shown in figure 1 was used as a test system to examine the convergence properties of the sequential and unified algorithms. The disturbance applied to the network was a three-phase line fault located at various points in the system. Line switching and fault clearance occurred 140 mS later, this being the normal primary protection fault clearing time for the system. For longer studies auto-reclosure of lines took place 360 mS after line opening. In all studies the rectifier steady-state load was constant at 288 MW and 100MVAR and generators were modelled to include transient and subtransient effects and automatic voltage regulators and speed governors were included. All other loads were of the impedance type.

The most difficult computational problem occurred when re-converging after a discontinuity. Once recovergence had been achieved and the first integration step following this had been successfully solved, the solution was normally numerically well behaved.

Table 2 presents a comparison of the convergence properties of the two algorithms. In cases 1, 2 and 4, the number of iterations required to reconverge after three different discontinuities during each study was used as the basis for comparison. Cases 1, 3 & 4 were more severe faults than case 2 when observed from the rectifier terminals.

In case 1, the unified algorithm showed a slight advantage when reconverging following a discontinuity. However the number of iterations required during the integration procedure was almost identical. The slight increase in the time-step iterations using the unified method was due to a tighter tolerance being set for convergence of the rectifier variables of the Newton-Raphson process in all the studies.

Considering case 2, it can be seen that the rate of reconvergence after a discontinuity using the sequential method was slow. This was so, even though the rectifier model operated in mode 1 throughout the study, with a maximum overlap angle of 35°. However once reconvergence had been achieved then the number of time-step iterations compared favourably with the unified method.

The unified algorithm was clearly superior in case 3 as divergence occurred when the sequential method was used. Case 4 demonstrated that convergence problems also occur using the sequential method during the time-step iterations, but these difficult cases do not cause problems to the unified method. The unified method consistently gave reconvergence after a discontinuity within 5 iterations and the number of time-step iterations was

Case	Fault Position	Rectifier Model	Algorithm	Iterations to Reconverge			Total Iterations For 1 second Study
				Fault On	Fault Off	Auto Reclose	
1	Manapouri	Basic	Sequential	5	5	4	324
			Unified	2	4	3	332
2	Roxburgh	Dynamic	Sequential	27	6	6	346
			Unified	3	5	3	364
3	Manapouri fault X=0.0060	Dynamic	Sequential	Failed	-	-	-
			Unified	3	3	3	302
4	Manapouri fault X=0.0065	Dynamic	Sequential	8	Failed at first Time Step after Fault Application		
			Unified	3	3	3	298

Table 2. Comparison of Sequential and Unified Algorithms.

also small provided that the step length was suitable for the system as a whole.

EFFECTS OF RECTIFIER LOADS ON TRANSIENT-STABILITY

In order that the effects of rectifier loads on transient-stability could be examined the two systems of figure 6 were used. These are sub-systems of figure 1, with high and low short-circuit ratios. The disturbance to the network was a three-phase line fault applied at either Manapouri or Invercargill. This permitted specific rectifier effects to be observed. The studies were continued only long enough to record first swing stability and the results are presented in table 3.

Fig. 6a

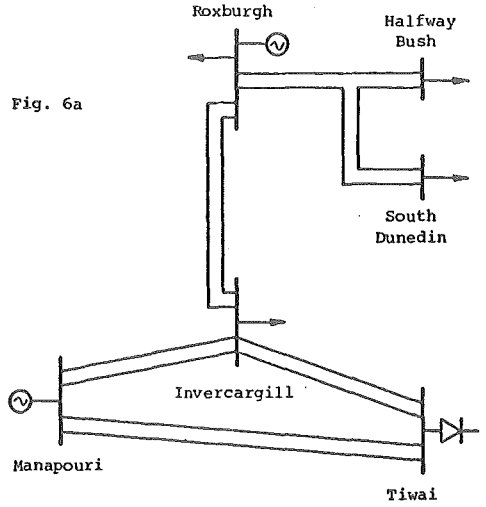

Fig. 6b

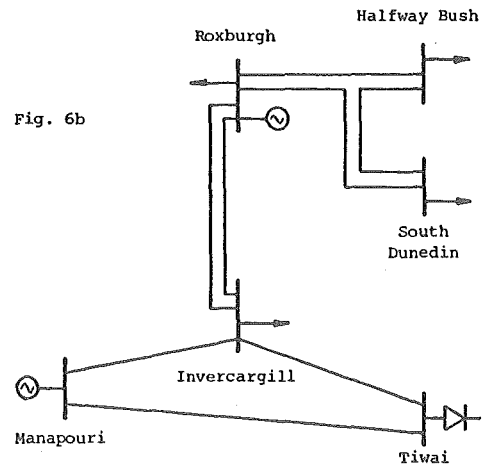

Fig. 6. Sub-systems used for results in Table 3.

With the stronger system (Network A) the difference between the alternative rectifier models are small. The rectifier is seen to have much more influence when the system is weaker (Network B). This is clearly shown by the results of corresponding cases, like A2 and B2 where the differences between the impedance and dynamic models are 2% and 14.8% respectively.

A comparison between cases B1 and B2 illustrates the importance of accurate rectifier representation. As the fault gets closer, the rectifier is forced into increasingly non-linear operating modes.

Fig. 7 illustrates the differences in power and voltage behaviour for case B3 under the three alternative rectifier models. With the dynamic rectifier model the power demand during and immediately after the fault is seen to be substantially reduced and the voltage recovery throughout the system is improved. Although the governor action was adequately represented, the mechanical power input for the three cases is almost constant during the period up to the first swing.

In case B4, fault clearance was delayed by one cycle and the impedance representation led to instability, while under the Basic and Dynamic rectifier models marginal stability was observed.

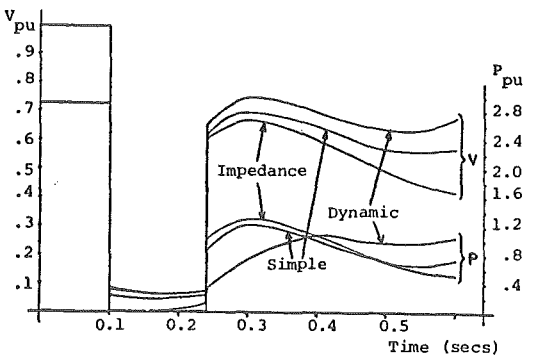

Fig. 7. Voltage and Power at Rectifier Bus for case B3.

Rectifier behaviour during the fault is influenced by the proximity of the fault, the system short-circuit capacity and the d.c. load time constant. For close-in faults in weak systems with dynamic d.c. loads, the rectifier is forced into mode 4 operation. As the d.c. current decays, the operation changes to modes 3, 2, and then 1. Figure 8 shows the rectifier operation in all four modes for case B3.

For very short d.c. load time constants, the period in which the rectifier will be in the abnormal modes will be small and the simple impedance or rectifier model will provide a sufficiently accurate representation.

During the fault the rectifier will be operating at a very low power factor due to the abnormally large overlap angle. The rate of change of the power factor is determined by the d.c. load time constant. As soon as the fault clears, the sudden increase in a.c. terminal voltage results in a very low overlap angle and a power factor close to unity. As an example of the rectifier behaviour table 4 shows the ratio of MW/MVAR during various stages of the study in case B3.

The reduction of MVAR demand during the post fault period helps to give rise to a greater recovery of system voltages.

Along with factors discussed previously, the topology of the system, proximity of fault and the rectifier protection limits are also factors in determining the extent of the rectifier effect on transient-stability. If the fault is distant from the rectifier in a system with a high short-circuit capacity, then the impedance type representation of the rectifier gives somewhat conservative results. For systems with low short-circuit capacities, however, the results with impedance type representation are too conservative to be practical and full rectifier representation is essential.

Network	Case	Manapouri Generation (MW)	Impedance Load (MW)	Fault Position	First Swing Maximum - Manapouri			Difference between Impedance and Dynamic Model
					Impedance Model	Basic Model	Dynamic Model	
A	1	450	260	Manapouri	40.6°	38.9° (1)	40.3° (4)	0.7%
	2	450	260	Invercargill	25.1°	25.0° (1)	24.6° (3)	2.0%
	3	570	340	Manapouri	75.2°	73.1° (1)	73.2° (4)	2.7%
	4	570	340	Invercargill	53.4°	53.0° (1)	57.4° (3)	3.7%
B	1	450	260	Manapouri	66.0°	60.1° (2)	62.6° (4)	5.1%
	2	450	260	Invercargill	37.2°	36.4° (1)	31.7° (4)	14.8%
	3	570	340	Invercargill	92.0°	82.0° (1)	72.0° (3)	21.7%
	4	570	340	Invercargill (5)	Unstable	98.0° (1)	84.0° (3)	-

(1) Rectifier Shutdown during fault
(2) No Rectifier Shutdown during fault
(3) Short Circuit at Rectifier Terminals after Fault Application
(4) No Short Circuit at Rectifier Terminals after Fault Application
(5) Fault Period Increased by One Cycle

Table 3. Effects of Rectifier Models on Transient-Stability.

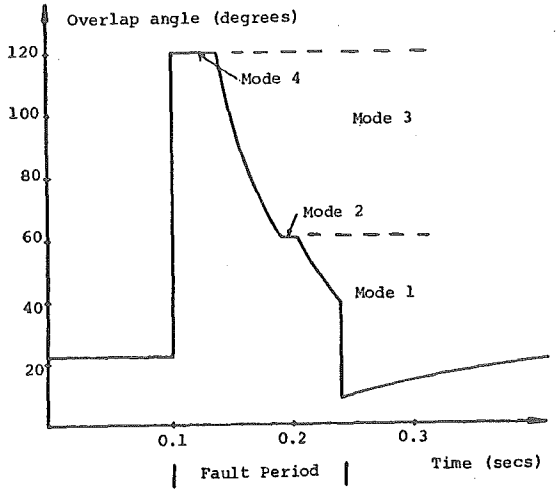

Fig. 8. Rectifier Overlap Angle vs. time for case B3.

Run Time	MW/MVAR	P.F.
Pre Fault	3.0	0.95
During Fault	0.0-1.5	0.0 -0.83
Early Post Fault	6.5-4.5	0.98-0.97
At Swing Maximum	3.9	0.97

Table 4. Ratio of MW/MVAR of Rectifier for Case B3.

CONCLUSIONS

Three different methods of representing a rectifier load have been investigated. It has been demonstrated that a detailed rectifier model, which includes the dynamic effect of the d.c. loads, and abnormal modes of operation, is necessary to correctly assess the influence of the rectifier in transient-stability studies.

Two algorithms for including non-impedance type loads have been evaluated. Although the specific model relates to rectifier loads, the two methods are equally applicable to other non-impedance types of load. While the sequential method is simple and easy to programme the unified technique is capable of handling the non-impedance load characteristic without any deterioration of convergence.

ACKNOWLEDGEMENTS

The authors are grateful to P.W. Blakeley, General Manager of New Zealand Electricity and to the computer Centre of the University of Canterbury for their help.

LIST OF SYMBOLS

I_d	- direct current
V_d	- direct voltage
α	- firing angle
u	- overlap angle
δ	- $\alpha+u$
X_c	- commutation reactance
R_d	- d.c. resistance
V_{cell}	- d.c. residual voltage at no load
ϕ	- power factor at rectifier terminals
$\bar{I}_r$ or $I\angle\psi$	- fundamental line current at rectifier terminals
$\bar{E}_r$ or $E_r\angle\theta$	- fundamental a.c. phase to phase voltage at rectifier transformer terminals
A	- constant current controller gain
P	- rectifier real power
Q	- rectifier reactive power
$\bar{I}_{inj}$	- complex nodal injected current
$\bar{Y}$	- complex nodal shunt admittance
$\bar{S}$	- complex power
$\bar{Z}$	- driving point or transfer impedance
$\bar{Z}_{th}$ or $Z_{th}\angle\mu$	- system equivalent Thevenin impedance as seen from the rectifier
a	- rectifier transformer tap
$\bar{V}$ or $V\angle\beta$	- system equivalent Thevenin voltage as seen from the rectifier
*	- complex conjugate

APPENDICES

Appendix A. Relationship between AC and DC currents in Abnormal Modes

The fundamental amplitude and phase of a current i(θ) which is half wave symmetrical is given by a Fourier integral of the form:

$$\sqrt{2}I_L = \frac{2}{\pi}\int_0^{\pi} i(\theta)e^{-j\theta}d\theta \qquad (A1)$$

where

$\theta = \omega t$

and

I_L = r.m.s. line current.

For the case of an overlap angle greater than 60°, during the first half cycle i(θ) is described piece-wise by the following equations (where θ=0 at the peak of commutating line to neutral voltage).

$$i = I\left[\cos\alpha' + \frac{1}{2}\cos\delta' - \frac{\sqrt{3}}{2}\cos(\theta+60^\circ)\right] \qquad (A2)$$

where

$\delta'-150^\circ<\theta<\alpha'+30^\circ$

$$i = I\left[\frac{1}{2}\cos\alpha' + \frac{1}{2}\cos\delta' - \cos(\theta+90^\circ)\right] \qquad (A3)$$

where

$\alpha'+30^\circ<\theta<\delta'-90^\circ$

$$i = I\left[\frac{1}{2}\cos\alpha' - \frac{1}{2}\cos\delta'\right] \qquad (A4)$$

where

$\delta'-90^\circ<\theta<\alpha'+90^\circ$

$$i = I\left[\cos(\theta-90^\circ) - \frac{1}{2}\cos\alpha' - \frac{1}{2}\cos\delta'\right] \qquad (A5)$$

where

$\alpha'+90^\circ<\theta<\delta'-30^\circ$

$$i = I\left[\frac{\sqrt{3}}{2}\cos(\theta-60^\circ) - \cos\delta' - \frac{1}{2}\cos\alpha'\right] \qquad (A6)$$

where

$\delta'-30^\circ<\theta<\alpha'+150^\circ$

$$i = I\left[\cos(\theta-30^\circ) + \cos(\theta-150^\circ) - \cos\alpha' - \cos\delta'\right] \qquad (A7)$$

where

$\alpha'+150^\circ<\theta<\delta'+30^\circ$

and where

$$I = \frac{2I_d}{(\cos\alpha'-\cos\delta')}$$

Using identities:

$$2\cos\theta = e^{j\theta} + e^{-j\theta} \qquad (A8)$$

$$\int e^{-ja\theta} = j\frac{1}{a}e^{-ja\theta} \qquad (A9)$$

and equations (A2) to (A7), the equation (A1) can be reduced to the following form:

$$\frac{\pi I_L}{\sqrt{2}I_d}(\cos\alpha' - \cos\delta') = \frac{1}{2}j\,(\angle{-30^\circ}-\angle{30^\circ})(\angle{-2\alpha'}-\angle{-2\delta'}) + \frac{\sqrt{3}}{4}\,j\,(\angle{60^\circ}-\angle{-60^\circ})(-\angle{2\alpha'}-\angle{-2\delta'}) + \angle{-2\alpha'}-\angle{-2\delta'}-j\,\frac{3}{2}\,u \qquad (A10)$$

or

$$I_L = \frac{\sqrt{6}.I_d}{\pi}\,\frac{\sqrt{3}}{4(\cos\alpha'-\cos\delta')}\left[\angle{-2\alpha'}-\angle{-2\delta'}-j2u\right] \qquad (A11)$$

Appendix B. Algebraic Form of the Differential Equation for Direct Current

When dynamic loads exist on the d.c. side of the rectifier, the following equations apply:

$$V_d = I_d R_d + V_{cell} + L\frac{dI_d}{dt} \qquad (B1)$$

$$V_d = \frac{3\sqrt{2}}{\pi}aE_r\cos\alpha - 3X_c I_d \qquad (B2)$$

where L is the equivalent inductance in the d.c. load. Therefore:

$$\frac{dI_d}{dt} = \frac{1}{TR_d}\left(\frac{3\sqrt{2}}{\pi}aE_r\cos\alpha - V_{cell}\right) \div \left(\frac{I_d}{T}\,\frac{3X_c}{R_d} + 1\right) \qquad (B3)$$

E_r, I_d and cosα are functions of time, and hence,

$$\frac{dI_d(t)}{dt} = pE_r(t)\cos\alpha(t) - qI_d(t) + g \qquad (B4)$$

where

$$p = \frac{1}{TR_d}\,\frac{3\sqrt{2}}{\pi}a$$

$$q = \frac{1}{T}\left(\frac{3X_c}{\pi R_d} + 1\right)$$

$$g = V_{cell}/TR_d$$

From the trapezoidal rule, any function of time x(t) is given by

$$x(t+h) = x(t) + \frac{h}{2}\left(\frac{d}{dt}x(t) + \frac{d}{dt}x(t+h)\right) \qquad (B5)$$

where h is the integration step length.

Applying equation (B5) to (B4) gives:

$$I_d(t+h) = I_d(t) + \frac{h}{2}\left(pE_r(t)\cos\alpha(t) - qI_d(t) + g + pE_r(t+h)\cos\alpha(t+h) - qI_d(t+h) + g\right)$$

or (B6)

$$I_d(t+h) = k_a E_r(t+h)\cos\alpha(t+h) + k_b \qquad (B7)$$

where

$k_a = h/(2+qh)$

$k_b = (1-2qk_a)I_d(t) + pk_a E_r(t)\cos\alpha(t) + 2k_a g$

REFERENCES

[1] Fuji Electric, Instruction Manual for Tiwai Aluminium Smelter Current Controller, 1972.

[2] E. W. Kimbark "Direct Current Transmission", Vol.1 Wiley, 1971.

[3] M. D. Heffernan "Stability of Hydrogenerators connected to HVDC Convertors", M.E.Report, University of Canterbury, New Zealand, 1977.

[4] D. B. Giesner and J. Arrillaga "Operating Modes of the 3-phase Bridge Convertor", Int. J. Elect. Engng. Educ., Vol. 8, pp. 373-388, 1970.

[5] C. P. Arnold, "Solutions of the Multi-Machine Power System Stability Problem". Ph.D. Thesis, University of Manchester Institute of Science and Technology, 1976.

[6] H. W. Dommel and N. Sato,"Fast Transient Stability Solution", IEEE Transactions on Power Apparatus and Systems, vol. PAS-91, pp. 1643-1650, 1972

APPENDIX A11

PAPER PUBLISHED IN PROC. IEE, VOL. 127, PT.C, NO. 5, SEPTEMBER 1980

TECHNICAL NOTE

Clarifying an ambiguity in recent a.c.-d.c. load-flow formulations

Prof. J. Arrillaga, M.Sc.Tech., Ph.D., C.Eng., F.I.E.E., B.J. Harker and K.S. Turner

Indexing terms: Power conversion, Load and voltage regulation

Abstract: The note presents a formulation for a.c.–d.c. load flow that is far simpler in use than former methods described in the literature. Voltage ambiguity which is present in the authors' and other earlier papers, is removed.

1 Formulation

The following expression, derived from the current flow across the convertor transformer, is used in recent a.c.-d.c. load flow models[1–4]

$$0 = k_1 I_d - Y_t E \sin\phi + a Y_t V \sin\psi \quad (1)$$

The voltage variables used in the above equation (with reference to Fig. 1), are the fundamental components of the actual primary V and secondary E voltages, respectively.

Moreover, the basic a.c.-d.c. voltage relationship used in these references is also expressed in terms of the variable E, i.e.

$$0 = V_d - k_1 E \cos\alpha - k_2 X_c I_d \quad (2)$$

However, the effect of the a.c. system reactance is already taken into account as commutation reactance X_c and therefore the commutating voltage to be used in eqn. 2 should be the open circuit secondary voltage. In practice, because of the presence of filters on the primary side, the a.c. system impedance has very little effect on the commutation and the commutating voltage is normally approximated to the actual primary voltage referred to the secondary (or convertor side) of the transformer.

While this anomaly appears to have no effect on the algorithmic behaviour, the accuracy of the a.c. and d.c. variables around the convertor terminals is reduced. An alternative, unambiguous formulation is described here. The following relationships (in per unit)[1] are derived for the variables defined in Fig. 1.

(*a*) The fundamental current magnitude on the convertor side is related to the direct current by the equation

$$I_s = \frac{3\sqrt{2}}{\pi} I_d \quad (3)$$

(*b*) The fundamental current magnitudes on both sides of the assumed lossless transformer are related by the off-nominal tap, i.e.

$$I_p = a I_s \quad (4)$$

Paper 925C, received 16th June 1980
Prof. Arrillaga is with the Department of Electrical Engineering, University of Canterbury, Christchurch 1, New Zealand, and the other two authors are with New Zealand Electricity, Private Bag, Wellington, New Zealand.

(*c*) The direct voltage may be expressed in terms of the a.c. source commutating voltage referred to the transformer secondary, i.e.

$$V_d = \frac{3\sqrt{2}}{\pi} a V \cos\alpha - \frac{3}{\pi} I_d X_c \quad (5)$$

The convertor a.c. source commutating voltage is the busbar voltage on the system side of the convertor transformer, V.

(*d*) The direct current and voltage are related by the d.c. system configuration,

$$f(V_d, I_d) = 0 \quad (6)$$

e.g. for a simple rectifier supplying a passive load,

$$V_d - I_d R_d = 0$$

(*e*) With a lossless transformer and perfect filtering on the primary side the real power equation relates the d.c. power to the transformer secondary power in terms of fundamental components only, i.e.

$$V_d I_d = E I_s \cos\phi \quad (7)$$

(*f*) Similarly, the primary real power may be equated to the d.c. power, i.e.

$$V_d I_d = V I_p \cos\psi \quad (8)$$

(*g*) The fundamental component of current flow across the convertor transformer can be expressed as

$$I_s = B_t E \sin\phi - B_t a V \sin\psi \quad (9)$$

where $jB_t = Y_t$ is the transformer leakage admittance.

So far a total of seven equations have been derived and no other independent equation may be written relating the

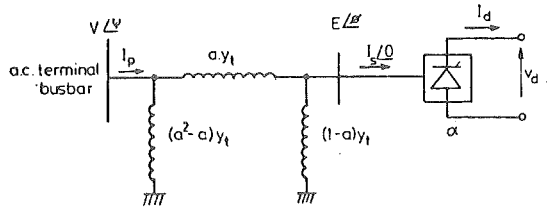

Fig. 1 *Model for load-flow analysis*

0143-7046/80/05294 + $01·50/0

total set of nine convertor variables, i.e. $E, \phi, \psi, I_p, I_s, \alpha, a, V_d, I_d$.

In theory, two independent variables are sufficient to model a d.c. convertor, operating under balanced conditions, from a known terminal voltage source. However, the control requirements of h.v.d.c. convertors are such that a range of variables, or functions of them (e.g. constant power), are the specified conditions. If the minimum number of variables are used then the control specifications must be translated into equations in terms of these two variables. These equations will often contain complex nonlinearities, and present difficulties in their derivation and program implementation. In addition, the expressions used for the active and reactive power at the convertor nodes may be rather complex and this will make the programming of a unified solution more difficult.

For these reasons a nonminimal set of variables is recommended, i.e. all variables which are influenced by control action are retained in the model. This is in contrast to a.c. loadflows where, because of the restricted nature of control specifications, the minimum set is normally used.

Variables I_p, I_s, E and ϕ can be eliminated as they play no part in defining control specifications.

Thus eqns. 3, 4, 7 and 8 can be combined into

$$V_d - k_1 a V \cos\psi = 0 \tag{10}$$

where $k_1 = \frac{3\sqrt{2}}{\pi}$

The final two independent equations required are derived from the specified control mode.

2 D.C. model summary

The d.c. model may thus be summarised as follows:

$$\bar{R}(\bar{x}, V)_k = 0 \tag{11}$$

where

$$R(1) = V_d - \mathrm{K}_1 a V \cos\psi$$

$$R(2) = V_d - \mathrm{K}_1 a V \cos\alpha + \frac{3}{\pi} I_d X_c$$

$$R(3) = f(V_d, I_d)$$

$R(4)$ = control equation

$R(5)$ = control equation

and

$$\bar{x} = [V_d, I_d, a, \cos\alpha, \psi]^{\mathrm{T}}$$

V can either be a specified quantity or an a.c. system variable. The equations for P_{dc} and Q_{dc} may now be written as

$$Q_{dc} = V I_p \sin\psi$$

$$= V K_1 a I_d \sin\psi \tag{12}$$

and $P_{dc} = V I_p \cos\psi$

$$= V K_1 a I_d \cos\psi \tag{13}$$

or $P_{dc} = V_d I_d$ (14)

3 References

1 ARRILLAGA, J., and BODGER, P.: 'Integration of h.v.d.c. links with fast-decoupled load-flow solutions', *Proc. IEE*, 1977, 124, (5), pp.463-468

2 ARRILLAGA, J., and BODGER, P.: 'A.C.-D.C. load flows with realistic representation of the convertor plant', *ibid.*, 1978, 125, (1), pp.41-46

3 EL-MARSAFAWY, M.M. and MATHUR, R.M.: 'A new fast technique for load-flow solutions of integrated multiterminal d.c./a.c. systems', *Trans. IEEE*, 1979, Winter meeting, Paper F79 174-4

4 ARRILLAGA, J., HARKER, B.J., and BODGER, P.: 'Unified and sequential load flows for a.c. systems containing static convertors', *PSCC*, 1978, (Darmstadt), pp.719-729

APPENDIX A12

COMPUTATION OF AC-DC SYSTEM DISTURBANCES - PART I INTERACTIVE COORDINATION OF GENERATOR AND CONVERTER TRANSIENT MODELS

COMPUTATION OF A.C.-D.C. SYSTEM DISTURBANCES - PART I. INTERACTIVE COORDINATION OF GENERATOR AND CONVERTOR TRANSIENT MODELS

M.D. Heffernan — New Zealand Electricity

K.S. Turner — Student Mem., IEEE

J. Arrillaga — University of Canterbury (N.Z.)

C.P. Arnold — Mem., IEEE

Abstract - In the presence of h.v.d.c. links the conventional quasi-steady state simulation of power system disturbances is not justifiable. This paper describes a realistic solution which combines the efficiency of single-phase multimachine transient stability analysis and the accuracy of detailed transient convertor simulation. Versatility and moderate computing requirements establish the proposed solution as a viable alternative to the use of analogue simulators.

INTRODUCTION

Traditionally the analysis of a.c. power system disturbances involves the use of two separate programmes. A quasi-steady state, linearized, fault study is carried out to obtain information of the fault current and voltage levels at a discrete instant. A dynamic study is also carried out to assess the stability of the system following the disturbance.

However the highly non-linear behaviour of h.v.d.c. transmission systems can only be predicted with reasonable confidence under clearly defined steady state operating conditions. During disturbances there is no guarantee that normal convertor operation will remain within the region of applicability of the steady state equations, or that the convertors will retain controllability. Therefore in systems containing relatively large h.v.d.c. transmission schemes and with disturbances at or close by the convertor terminals, only a fully detailed elemental transient analysis can provide accurate simulation of the convertor behaviour [1].

The dynamic behaviour of the generators can be accurately predicted by means of fundamental frequency studies. This form of investigation is commonly known as Transient Stability (TS), and is primarily concerned with evaluating the ability of the system to remain in synchronism. The differential equations describing the system can be solved with sufficient accuracy using integration steps in the order of 10 to 50 ms.

On the other hand the continuously varying topology of convertor plant, with commutation discontinuities occurring every few milliseconds, requires an elemental representation of the system components, and a much shorter integration step. This type of study, defined here as Transient Convertor Simulation (TCS), provides very detailed results in the form of 3-phase waveshapes, but requires integration step lengths in the order of 50-100 μs.

There is no doubt that a transient analysis of the power system including a detailed representation of the generators' behaviour and following the topological changes of the d.c. link can provide realistic information of the disturbance. However the demands in computer storage and time are prohibitive.

An alternative to full system representation is to reduce the a.c. system to an equivalent Thevenin source and use detailed transient simulation for the areas of changing topology, i.e. the convertors. However the use of a fixed a.c. system Thevenin equivalent at the convertor terminals, even for a brief disturbance, will provide unrealistic levels of current and voltage.

Some compromise is therefore required between the accurate, but computationally prohibitive, transient convertor simulation and the computationally efficient, but less detailed, transient stability study. A compromise which exploits the advantages of both these methods is achieved by simultaneously performing transient stability and transient convertor simulations with periodic coordination of the results. In this way the detailed convertor model is provided with a time-variant Thevenin equivalent for correct a.c. system representation [2]. Similarly, from the transient convertor simulation, accurate power frequency information can be derived to represent the d.c. system behaviour at the convertor terminals. The computational requirements are minimized by restricting the use of the transient convertor simulation to the most disturbed part of the study; as the d.c. link regains normal controllability and attains predictable behaviour, this detailed simulation is replaced by a quasi-steady state (QSS) model.

COMPUTATION OF CONVERTOR TRANSIENTS

Simulation of the transient behaviour of an a.c.-d.c. interconnection requires the simultaneous solution of a set of differential equations which vary with the convertor's topology. Any a.c. system components of immediate influence on the convertor plant must be explicitly represented in detail, e.g. convertor transformer, a.c. filters, synchronous machines directly connected to the convertor terminals, etc.

Convertor transformers are represented by the coupled circuit model. In purely a.c. systems the recovery voltage is often strongly influenced by the transformer magnetizing current, particularly when switching is involved. Convertor saturation is also a feature of a.c.-d.c. interconnections following disturbances, and if switching of the convertor transformers is involved, the coupled circuit model permits representation of the non-linear magnetizing currents.

Machines are represented by their EMF behind an appropriate reactance based on a Thevenin equivalent, or if necessary by their full transient equations.

The combined effects of other a.c. system components may be represented by an equivalent Thevenin circuit which reflects the generators' and system's behaviour, and offers a realistic impedance to the lower power-frequency related harmonics. The model for Thevenin equivalent circuits permits variation of the reactance (or EMF), starting with the subtransient and changing into the transient as the study progresses. The development of a time-variant Thevenin source is described later (Interactive Coordination of Transient Equivalents).

The time-variant Thevenin equivalent of the a.c. system (or part of it) must be accurate for all harmonics of the power frequency, in order to correctly simulate possible resonances between the a.c. system and the convertor equipment. By rearranging the Thevenin impedance into a series-parallel configuration, an equivalent which maintains a constant impedance angle for the major power frequency harmonics, and provides real-

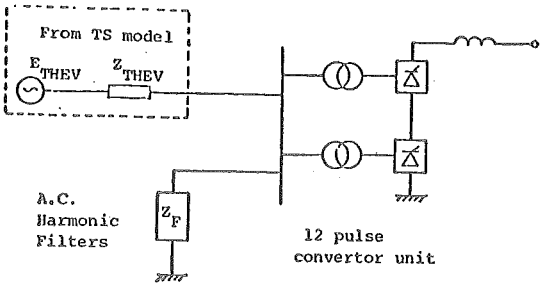

Fig. 1. Representation of each convertor and associated a.c. system.

istic damping of harmonic voltages, is obtained [3]. This representation assumes there are no a.c. network resonances, yet gives an accurate treatment to possible resonances between the a.c. network and the harmonic filters at each convertor terminal. The representation for each convertor and its associated a.c. system is depicted in Figure 1, where Z_{THEV} represents the series parallel configuration.

To determine in each case the appropriate equivalent circuit, the areas of specific interest to the particular disturbance must be identified. For a.c. fault studies the major areas of interest are the convertor terminals and the fault location. In the case of a d.c. fault study the fault is contained within the d.c. system being simulated.

For efficient computation it is convenient to segregate the system nodes according to the type of branches interconnected by them. This segregation defines α nodes (which have at least one capacitive connection), β nodes (which have at least one resistive connection but no capacitance), γ nodes (with only inductive components) and δ nodes (convertor nodes, involving only inductive components, i.e. convertor transformer and smoothing reactor). Thus the topological changes caused by valve switchings can be implemented by altering only the matrices involving convertor (k) branches and δ nodes.

A partioned state variable formulation is then developed which involves the following set of equations in terms of the state variables ψ_ℓ, ψ_k and Q_α, i.e.

$$\psi_\ell = L_\ell I_\ell \tag{1}$$

$$\psi_k = L_k I_k \tag{2}$$

$$Q_\alpha = C_\alpha V_\alpha \tag{3}$$

$$V_\beta = -R_\beta (K_{\beta\ell} I_\ell + K_{\beta k} I_k + K_{\beta r} R_r^{-1} K_{r\alpha}^t V_\alpha) \tag{4}$$

$$V_\gamma = -L_\gamma K_{\gamma\ell} L_\ell^{-1} (E_\ell - R_\ell I_\ell - pL_\ell . I_\ell + K_{\ell\alpha}^t V_\alpha + K_{\ell\beta}^t V_\beta) \tag{5}$$

$$V_\delta = -L_\delta K_{\delta k} L_k^{-1} (\quad -R_k I_k \quad + K_{k\alpha}^t V_\alpha + K_{k\beta}^t V_\beta) \tag{6}$$

$$I_r = R_r^{-1} (K_{r\alpha}^t V_\alpha + K_{r\beta}^t V_\beta) \tag{7}$$

$$p\psi_\ell = E_\ell - R_\ell I_\ell - K_{\ell\alpha}^t V_\alpha + K_{\ell\beta}^t V_\beta + K_{\ell\gamma}^t V_\gamma \tag{8}$$

$$p\psi_k = \quad -R_k I_k + K_{k\alpha}^t V_\alpha + K_{k\beta}^t V_\beta + K_{k\delta}^t V_\delta \tag{9}$$

$$pQ_\alpha = -K_{\alpha\ell} I_\ell - K_{\alpha k} I_k - K_{\alpha r} I_r \tag{10}$$

where $K_{\beta\ell}$, etc. represent branch-node incidence matrixes and suffixes ℓ and r refer to inductive and resistive branches.

A general flow diagram indicating the main steps of the basic state variable transient analysis is illustrated in Figure 2.

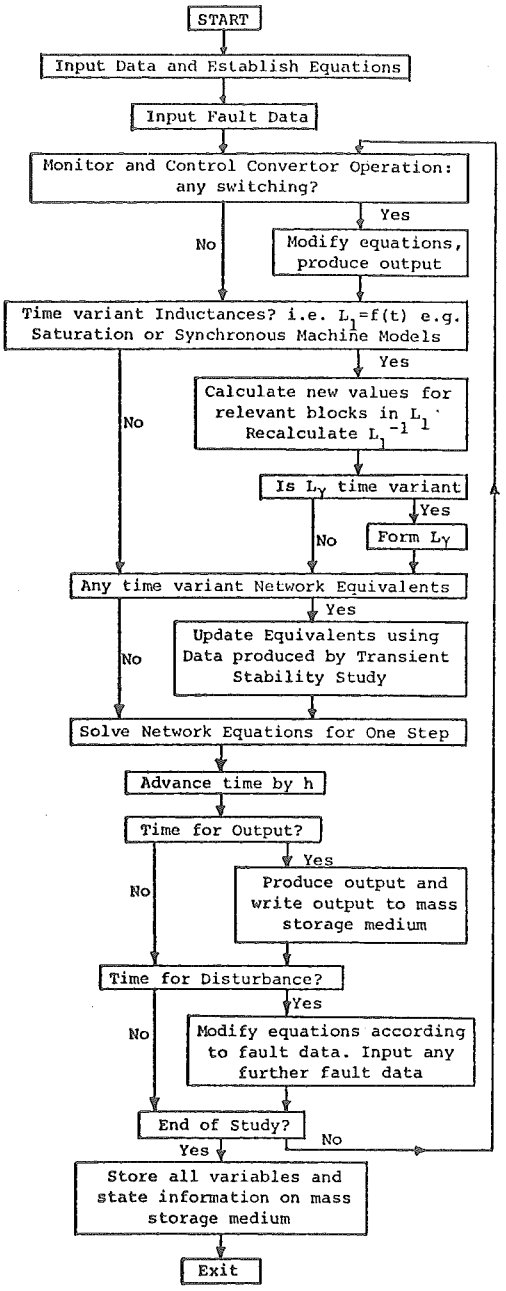

Fig. 2. General Flow Diagram for TCS.

At each step in the integration process the convertor valves are tested for current extinction, voltage cross-over and conditions for firing, based on the individual valve currents and voltages. This is illustrated in Figure 3. If indicated, changes in valve states are made and/or the control system is activated to adjust the phase of firing. When a valve switching takes place, the network equations are altered by suitable modifications of $K_{\delta k}$ and L_δ only.

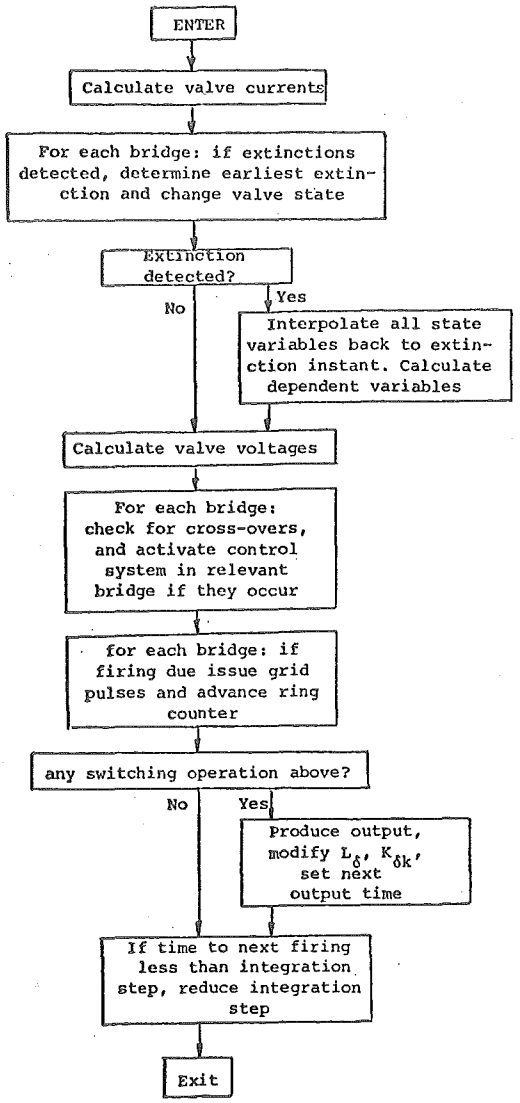

Fig. 3. Monitoring and control of h.v.d.c. convertors.

The choice of integration technique is limited to single-step methods, which are self starting. Taking into consideration the frequency of occurrence of convertor discontinuities, a multi-step method would hardly start to operate before a discontinuity occurs. Either a fourth-order Runge-Kutta or an implicit integration procedure based on a trapezoidal approximation are perfectly adequate.

Process of Establishing Initial Conditions

In the first place the three-phase real and imaginary terms of the branch impedances of the steady state equations describing the system are transferred to the topological matrices R_ℓ and L_ℓ respectively.

Conducting valves in each bridge are determined from a knowledge of the phase 'a' voltage phase angle, measured with respect to the steady-state load flow reference, and taking into consideration the inherent phase-shift in the bridge transformer (i.e. 0 or 30°) and the delay angle.

Having established the pair of conducting valves per bridge, the currents in the transformer windings must be established on both sides. In the case of a delta-connected convertor transformer initial currents must be established in the three delta windings, even though only two valves are conducting.

A steady state analysis such as a load flow, which is based on the assumption of balanced sinusoidal a.c. waveforms, cannot provide exact initial conditions for the transient analysis of a system which includes convertor models, due to the distorted wave conditions inherent in convertor operation. It is therefore necessary to perform a preliminary transient convertor simulation (equations (1) to (10)), using the load flow conditions as initial values, in order to obtain the desired steady state operating point dynamically.

To facilitate the application of a particular fault, the fault branch is previously established in the branch list. This branch impedance may then be switched in/out by modification of an element in the appropriate connection matrix. In some configurations this switching may contravene topology constraints, in which case the numerical value of the branch impedance is changed at the time for fault application from a high pre-fault value (so that the pre-fault branch current is effectively zero) to the value required to provide the appropriate faulted network.

A.C.-D.C. QUASI-STEADY STATE ANALYSIS

The QSS d.c. link model uses a Thevenin equivalent of the a.c. system at each convertor terminal and then solves the resulting network. With reference to Figure 4 a set of independent equations can be derived for the d.c. link, where j refers to a convertor terminal:

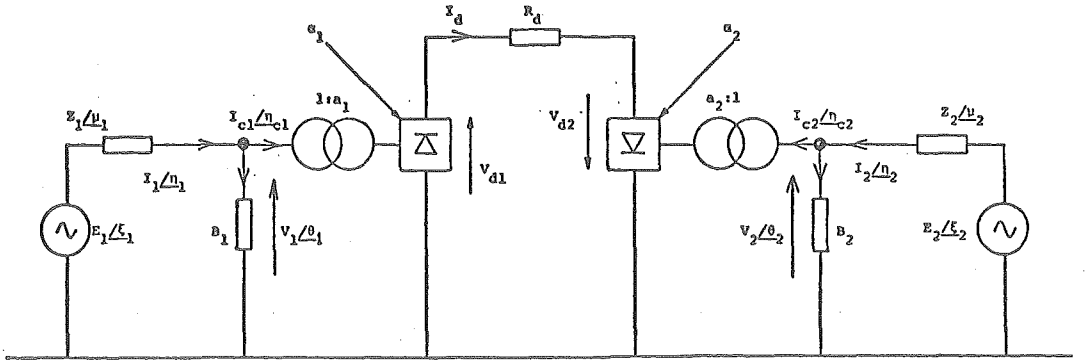

Fig. 4. A.C. and D.C. system for unified algorithm.

i) Equating voltages at the Thevenin source,

$$E_j\angle\xi_j - (Z_j\angle\mu_j)\ (I_{cj}\angle\eta_{cj} + V_j\ B_j\angle\theta_j + \pi/2)$$

$$- V_j\angle\theta_j = 0 \qquad (11)$$

The fundamental a.c. current and the d.c. current are related (in per unit) [5] by the expression

$$I_{cj} = \frac{3\sqrt{2}}{\pi}\, a_j\, I_d \qquad (12)$$

ii) Equating powers across the convertor,

$$V_{dj}\, I_d - \sqrt{3}\, V_j\, I_{cj} \cos(\theta_j - \eta_{ij}) = 0 \qquad (13)$$

The d.c. voltage can be expressed as

$$V_{dj} = \frac{3\sqrt{2}}{\pi}\, a_j\, V_j \cos\alpha_j - \frac{3}{\pi} X_{cj}\, I_d \qquad (14)$$

Combining equations (12), (13) and (14), the following results,

$$a_j\, V_j \cos\alpha_j - \frac{1}{\sqrt{2}} X_{cj}\, I_d - a_j\, V_j \cos(\theta_j - \eta_{cj}) = 0 \qquad (15)$$

iii) Applying Ohm's law across the two-terminal d.c. link,

$$V_{d1} + V_{d2} - I_d\, R_d = 0 \qquad (16)$$

or, eliminating V_{d1} and V_{d2}

$$\frac{3\sqrt{2}}{\pi}\,(a_1\, V_1 \cos\alpha_1 + a_2\, V_2 \cos\alpha_2)$$

$$- \frac{3}{\pi}\,(X_{c1} + X_{c2} + R_d)\, I_d = 0 \qquad (17)$$

For power flow from terminal 1 to terminal 2 (i.e. terminal 1 operating as rectifier and terminal 2 as invertor),

$\alpha_1 < 90^o$ and V_{d1} is positive

$\alpha_2 > 90^o$ and V_{d2} is negative

Hence these equations are general for power flow in either direction. The QSS model for a two terminal d.c. link thus consists of 7 independent equations, obtained from (11), (15) and (17), in terms of the following 9 variables:

$$I_d,\ (V_j,\ \theta_j,\ \eta_{cj},\ \alpha_j)_{j=1,2}$$

Two control equations are thus required to fully specify the system. For normal operation under constant current rectifier control, these would normally be

$$I_d - I_d^{sp} = 0 \qquad (18)$$

$$\gamma_2 - \gamma_2^{sp} = 0 \qquad (19)$$

or in terms of the variables selected, equation (19) can be written as

$$\cos\gamma_2^{sp} + \cos\alpha_2 - \frac{\sqrt{2}\, X_{c2}\, I_d}{a_2 V_2} = 0 \qquad (20)$$

The resulting QSS model represented by the above equations, and illustrated in Figure 4, is solved by the Newton-Raphson algorithm [4]. The calculation of initial conditions for the Newton-Raphson algorithm assumes special importance when it is used in conjunction with Transient Stability studies, as a result of the sudden disturbances, network topology changes and rapid variations in network variables experienced in such studies. It is essential that, during the study period, the d.c. link solution begins with good estimates for the d.c. variables. In contrast, when the Newton-Raphson algorithm is used in a loadflow study [5] it is only necessary to make one estimate for the initial conditions.

For Transient Stability, new initial conditions are calculated by a separate estimating process at the beginning of a study and immediately after a discontinuity (i.e. fault application or switching operation). The calculation of initial conditions is based on the new Thevenin voltages obtained for the convertors at the beginning of each step. Again referring to Figure 4 the following initial estimates are made for the variables involved.

- $V_j = E_j$
- $\theta_j = \xi_j$
- η_j is obtained by assuming a link terminal power factor of 0.9.
- Using equation (14), in which α_1 (or γ_2) is set to its minimum and with the d.c. current on its setting, an estimate for the maximum d.c. voltage possible at each terminal is obtained.
- By evaluating equation (16), with the estimated d.c. voltages and testing for sign, the control mode of the link is determined.
- With the control mode chosen, the value of α at the terminal controlling the current is evaluated, and the two control variables are set to their specified values.

This procedure has been successfully used for a large number of disturbances with excellent reliability.

With good starting values the Newton-Raphson algorithm converges rapidly. The results of many transient stability studies indicate that convergence takes normally 3-4 iterations after a discontinuity and 2-3 during the rest of the transient stability run.

The computation time required for a two-terminal d.c. link model is independent of the size of the a.c. system and therefore for a study involving a large a.c. system the relative requirements of the d.c. link are insignificant.

INTERACTIVE COORDINATION OF TRANSIENT EQUIVALENTS

A multimachine transient stability programme [6] is used which is capable of simulating the behaviour of large a.c.-d.c. systems under a.c. or d.c. fault conditions. At every integration step of the transient stability programme (every ½ cycle), the a.c. network is reduced to a Thevenin equivalent at each d.c. link terminal. Such equivalents at each time step constitute a reduced representation of the a.c. system as seen from the convertor terminals and they include all associated generator effects. In order to provide explicit representation of a faulted bus within the a.c. system, a third Thevenin equivalent can also be obtained, at each integration step of the transient stability study, by looking back into the a.c. network from that point. Therefore the transient stability study produces a time variant sequence of network equivalents, the variation of which will be a function of the disturbance investigated.

Initial time-variant network equivalents are obtained for a QSS solution of the d.c. link model in the transient stability study and these are also transferred to the first transient simulation of the convertor network. The results of the transient convertor simulation during the disturbed fault period are proc-

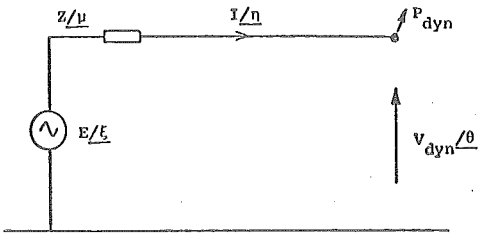

Fig. 5. Reduced system for TCS data inclusion.

essed to derive real a.c. power (P_{dyn}) and voltage (V_{dyn}) information at the convertor terminals which is compatible with the transient stability study.

The reduced system illustrated in Figure 5 can be solved directly for the a.c. currents which are then superimposed on the a.c. network in the same way as the a.c. current injections from the QSS d.c. link model.

Using $\bar{S} = \bar{V}\,\bar{I}^*$ (21)

where $\bar{V} = V_{dyn}\underline{/\theta}$ (22)

and

$$\bar{I} = (E\underline{/\xi} - V_{dyn}\underline{/\theta})\,/(Z\underline{/\mu}) \quad (23)$$

the total apparent power becomes

$$\bar{S} = (V_{dyn}.E\underline{/\theta+\mu-\xi})/Z - (V_{dyn}^2\underline{/\mu})/Z \quad (24)$$

Taking real parts of equation (24) and rearranging, θ can be solved for directly, i.e.

$$\theta = \xi - \mu + \cos^{-1}\{(P_{dyn}\,Z)/(V_{dyn}\,E) + (V_{dyn}\cos\mu)/E\} \quad (25)$$

The a.c. current is then obtained from equation (23).

An iterative process can be used, as detailed in Figure 6, to improve the interaction between the two programmes. Two such iterations were performed for a severe invertor fault case in order to determine the accuracy of the initial Thevenin equivalents, which were based on a QSS d.c. link model. Inspection of the Thevenin equivalent sequences obtained, showed differences of less than 1%.

In addition, it is possible to observe the trends as a transient convertor simulation progresses, since the simulation may be halted at any particular stage. By storing all state variable information at the last time step, the analysis may be restarted using this information for the exact initial conditions of the succeeding stage. The transient convertor simulation will thus consist of n consecutive stages, and if necessary, between any two of these stages it is possible to interactively modify the performance of the QSS d.c. link model according to the transient convertor simulation results. This provides very closely matched time-variant a.c. network equivalents for succeeding transient convertor simulation stages.

Although several short duration transient stability runs may be required with this approach, these are relatively inexpensive and they minimize the computing time of the transient convertor simulation by eliminating the need for the iterative process. Therefore for the purposes of providing accurate indication of the behaviour of the a.c. systems, in the form of time variant Thevenin equivalents, the transient stability study with a quasi-steady state d.c. link model has proved to be more than adequate.

In order to provide a time variant equivalent suitable for an a.c. fault calculation, the d.c. link model must be solved simultaneously with the fault.

By adding the fault impedance (Z^f) to the circuit of Figure 5, the fault current is obtained from:

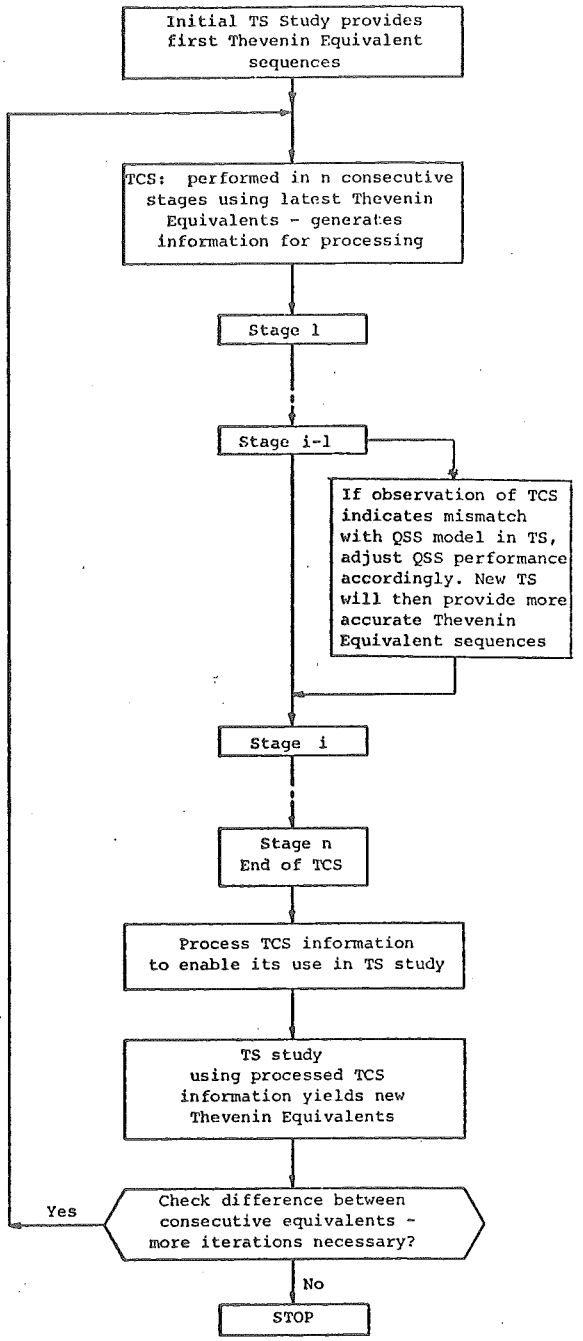

Fig. 6. Flow diagram of interaction between transient convertor simulation (TCS) and transient stability (TS) programmes.

$$\bar{I}^f = \bar{E}/(\bar{Z} + \bar{Z}^f) \quad (26)$$

For this to be a correct solution the Thevenin theorem states that all other voltages and current sources must be present, i.e. the network equivalent at the fault bus must be obtained with the d.c. link injected currents included. The converse also applies

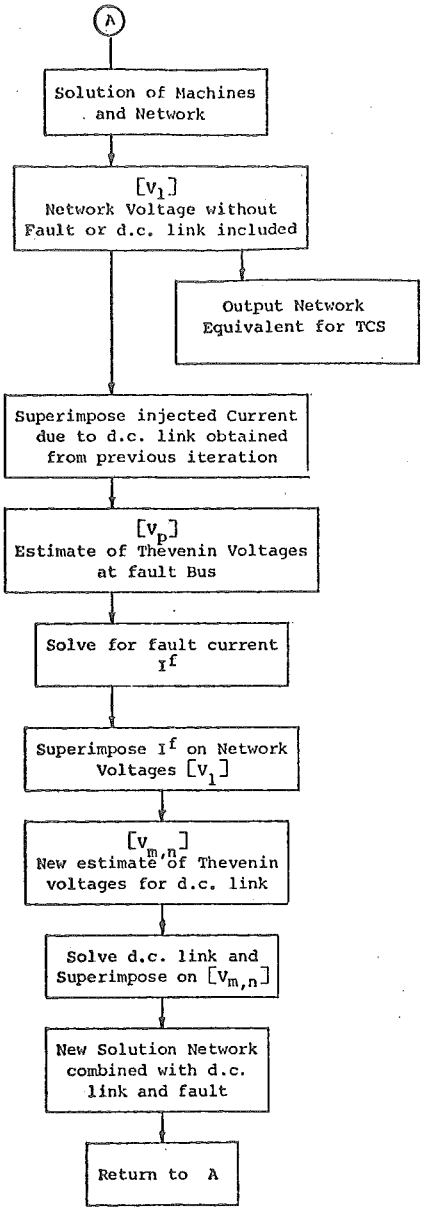

Fig. 7. Simultaneous solution at fault and d.c. link.

in obtaining the correct solution for the d.c. link. The solutions of both link and fault were thus combined in the algorithm of Figure 7.

The algorithm requires a good estimate of the d.c. injected currents at the first iteration of each step for the speed of convergence of the Transient Stability programme to be maintained. The d.c. link solution from the previous step has proved to be sufficiently accurate except for the first iteration after fault application. In this case, since the fault has a dominant effect, the fault and the network are solved without the d.c. link at the first iteration and an improved d.c. link solution is obtained for entry into the algorithm at A.

Alignment of the Two Models

The transient convertor simulation results are reduced to a sequence of data points, spaced at half cycle intervals and essentially representing the fundamental component over the cycle spaced about that point. The integration step of the Transient Stability study is fixed at half a cycle to coincide with the data points from the transient convertor simulation. In the transient stability study, at a disturbance initiation, a new solution is obtained for the system immediately after the disturbance application. However, because the transient convertor simulation results are essentially waveform orientated, a correct data point cannot be obtained at the new solution after disturbance application.

It is therefore necessary to extrapolate the transient convertor simulation data points to provide, as closely as possible, a representation of the link performance immediately before or after a disturbance application. This effect is demonstrated in Figure 8 in which the discrete integration steps of the transient stability study are related to the processed data points obtained from the transient convertor simulation.

Fault clearance requires special consideration as the mechanism differs for the two models. In the TS model the inherent assumption is made that at the time of fault clearance, T_{fc}, all three phases clear simultaneously and a new solution is obtained immediately (i.e. at T_{fc}^{+}). For the TCS, although the decision is made to clear the fault at T_{fc}, only one phase will open within 60° of T_{fc} (i.e. at the first current zero), the remaining phases opening in the following 120°. This would appear to distort the alignment of the two models for the TS solution at T_{fc}^{+}.

However the disturbance caused by the first phase clearance has the greatest influence on d.c. link control, and in spite of the TCS clearing delay, the post fault TCS data, obtained by processing one full cycle after T_{fc}, can be used to superimpose the immediate effect of the fault clearance on the TS solution at T_{fc}^{+}.

At the first and last steps of the transient simulation, the QSS model is solved as well, to provide a check on the accuracy of matching between the two link models.

RESULTS FOR A TYPICAL DISTURBANCE

The importance of coordination between the TS and TCS models of an a.c.-d.c. system is clearly demonstrated in Figure 9. These results are obtained for the New Zealand a.c.-d.c. system with a severe 3-phase fault at the invertor a.c. terminal busbar. The effect of using time invariant (case 311), and time variant (case 312), a.c. network equivalents is illustrated.

Figures 9 (a) and (b) indicate the effect of the fault on the Thevenin source voltage at the two convertors. The invertor source exhibits a considerable decay in voltage during the fault period which modifies

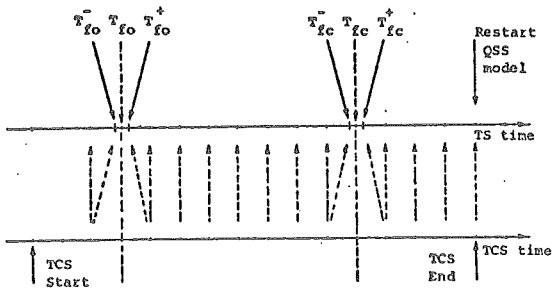

Fig. 8. Data alignment between TCS and TS models.

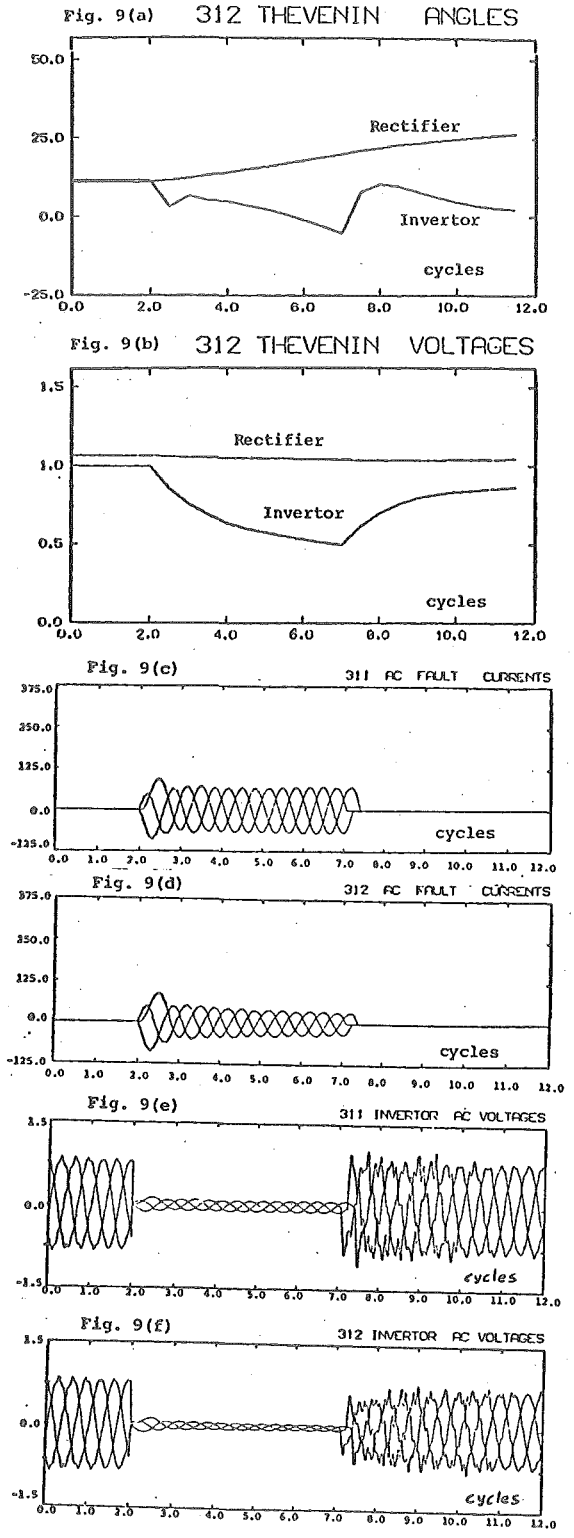

Fig. 9. Results for a 3-phase fault at the invertor terminal.

the fault current correspondingly as illustrated in Figures 9 (c) and (d). The decay in the fault current (case 312) is a direct result of providing the transient convertor simulation with a representation of the natural response of the system generators.

Figures 9(e) and (f) illustrate the recovery voltages following fault clearance. In the time invariant case (311), sharp overvoltages, with peaks of up to 130% of nominal are apparent. However, in the case using time variant a.c. system representations (312), the recovery voltages are well below the nominal voltage peaks, due to the gradual recovery of the Thevenin source voltage after the fault.

CONCLUSIONS

A general method has been developed for the computation of a.c.-d.c. system disturbances which combines the efficiency of transient stability modelling and the accuracy of transient simulation of convertor behaviour.

The transient convertor simulation uses time-variant Thevenin equivalents, formed by linear interpolation, from the discrete values obtained at every step of the transient stability study. Similarly, transient stability compatible equivalents are formed from the Transient Convertor Simulation during the disturbance. Such interaction permits the use of reduced equivalent circuits and results in moderate computing requirements. Every cycle of real-time simulation required 14 seconds of CPU time on an IBM-3033 computer. As an indication of computing cost, a complete run of a typical disturbance such as that shown in Figure 9 required 3 minutes of CPU time. Moreover, the transient convertor simulation is only required for short runs, i.e. during and immediately after the fault period. The extra computing time required for stability studies is relatively insignificant.

The use of a mass storage medium during simulations allows post-processing of results. Any variable or combination of variables can be plotted on any scale desired, without the transient convertor simulation being re-run.

The interactive model developed provides a useful tool in assessing convertor controllability during disturbances and the effect of alternative control and protection schemes. It also provides accurate information of fault current and voltage waveforms in the vicinity of large convertor plant, such information being essential for the rating of switchgear and the setting of protective relays.

Finally the accuracy of the model used to simulate the disturbance is critical in the assessment of transient stability, a subject discussed in a companion paper (Part III).

ACKNOWLEDGEMENTS

The authors wish to express their gratitude to the General Manager of New Zealand Electricity, Mr. K. D. McCool and to the staff of the Electrical Engineering Department and Computer Centre of the University of Canterbury for their help.

REFERENCES

[1] Arrillaga, J., Al-Khashali, H.J. and Campos Barros J.G. "General Formulation for Dynamic Studies in Power Systems including Static Convertors", Proceedings IEE, Vol. 124, No. 11, November 1977, pp. 1047-1052.

[2] Heffernan, M.D., Arrillaga, J., Turner, K.S. and Arnold, C.P. "Recovery from Temporary h.v.d.c. Line Faults". Paper 80 SM 675-9 presented at the IEEE PES Summer Meeting, Minneapolis, July 13-18, 1980.

[3] Bowles, J.P. "A.C. System and Transformer Representation for HVDC Transmission Studies", Trans.

IEEE, PAS 89, No. 7, 1970, pp. 1603-1607.

[4] Arnold, C.P., Turner, K.S., and Arrillaga, J. "Modelling Rectifier Loads for a Multi-machine Transient Stability Programme", Paper F79 662-8 presented at the IEEE PES Summer Meeting, Vancouver July 15-20, 1979.

[5] Harker, B.J. "Steady State Analysis of Integrated A.C. and D.C. Systems", Ph.D. Thesis, University of Canterbury, N.Z., 1980.

[6] Arnold, C.P. "Solutions of the Multi-Machine Power System Stability Problem", Ph.D. Thesis, University of Manchester Institute of Science and Technology, 1976.

NOMENCLATURE

L	-	Inductance
C	-	Capacitance
Q	-	Charge
R	-	Resistance
$E/\underline{\varepsilon}, \bar{E}$	-	Source Emf
$V/\underline{\theta}, \bar{V}$	-	Voltage
$I/\underline{\eta}, \bar{I}$	-	Current
$Z/\underline{u}, \bar{Z}$	-	Impedance
$\bar{S}$	-	Complex Power
$*$	-	Complex Conjugate
B	-	Filter Susceptance
V_d	-	Direct Voltage
I_d	-	Direct Current
R_d	-	D.C. Line Resistance
a_i	-	Convertor Transformer Tap
X_{ci}	-	Commutation Reactance
α_i	-	Convertor delay angle
γ_i	-	Convertor extinction angle
X^{sp}	-	Specified Value of Variable X
p	-	Differential Operator
TS	-	Transient Stability
TCS	-	Transient Convertor Simulation
QSS	-	Quasi-Steady State

APPENDIX A13

COMPUTATION OF AC-DC SYSTEM DISTURBANCES - PART II DERIVATION OF POWER FREQUENCY VARIABLES FROM CONVERTER TRANSIENT RESPONSE

COMPUTATION OF A.C.-D.C. SYSTEM DISTURBANCES. PT. II - DERIVATION OF POWER FREQUENCY VARIABLES FROM CONVERTOR TRANSIENT RESPONSE

K.S. Turner
Student Mem., IEEE

M.D. Heffernan

New Zealand Electricity

C.P. Arnold
Member, IEEE

J. Arrillaga

University of Canterbury (N.Z.)

Abstract - The aperiodic and distorted waveforms produced by h.v.d.c. convertors following system disturbances need to be processed in order to derive appropriate transient equivalents compatible with transient stability studies. This paper describes various techniques for the derivation of these equivalents and concludes that, while rms values provide realistic approximations for power, spectral analysis is required for the determination of voltage magnitudes.

INTRODUCTION

A comprehensive programme has been described in a companion paper (Part I) which combines two separate and distinct methods of transient analysis, i.e. Transient Stability (TS) and Transient Convertor Simulation (TCS).

Transient Stability is normally a fundamental frequency single-phase rms study and is therefore based on the assumptions of balanced and sinusoidal waveforms. In the presence of h.v.d.c. links, such assumptions are extended to the voltage and current waveforms at the convertor terminals. On the other hand, Transient Convertor Simulation is waveform orientated and exhibits the distortions and non-linearities associated with convertor operation.

The interactive coordination of the two parts of the programme requires periodic exchanges of information between them in order to achieve a realistic simulation of the behaviour of the a.c. system and the convertors. Transferring data from the Transient Convertor Simulation to the Transient Stability study is not straightforward, however, as during disturbances the convertors produce aperiodic and very distorted voltage and current waveforms. Such waveforms need to be processed in order to derive appropriate transient equivalents compatible with the TS model.

Waveform processing techniques based on spectral analysis [1] and window filtering [2] are used in this investigation to describe and justify the derivation of realistic equivalents without appreciably increasing the overall programme solution time.

REQUIREMENTS FOR TRANSIENT STABILITY

Since TS studies are carried out under balanced, single phase sinusoidal conditions it is necessary to derive this form of information from the waveforms produced by TCS. Two variables are needed to transfer the convertor information from the TCS to the TS study. A number of alternatives are available, i.e. real power, reactive power, voltage magnitude and current magnitude. Various definitions have been offered for reactive power in the presence of distorted waveforms [3][4] but a meaningful value of reactive power can only be obtained from sinusoidal components of voltage and current of the fundamental frequency. This fundamental frequency reactive power can only be derived from spectral analysis of the voltage and current waveforms and since both these variables can be used on their own, reactive power becomes redundant. The above problems do not exist in the definition of real power and further justification for its use as a variable is given later in the paper.

The choice of the second variable is between voltage and current magnitude. Since the convertor acts as a current harmonic source, the current waveform, particularly during and immediately after a disturbance, exhibits greater distortion and modulation effects than the voltage waveform. This has been tested in many TCS studies, two examples of which are illustrated in Figures 1 and 2. The spectral analysis of the voltage waveform is, therefore, less prone to error and the voltage magnitude is a better choice of variable.

The specification of voltage and real power is required at each integration step of the TS study when the Quasi-Steady State d.c. link model is replaced by the results of a TCS involving the d.c. link.

To obtain fundamental components of voltage and power, Fourier processing of the TCS waveforms is required and this must be performed over at least one fundamental cycle of the waveforms. The component of voltage and power can be obtained at any sample point using a complete cycle (period T) spanning T/2 both sides of the sample point as illustrated in Figure 3(a). The sampling points must be synchronised with the TS study

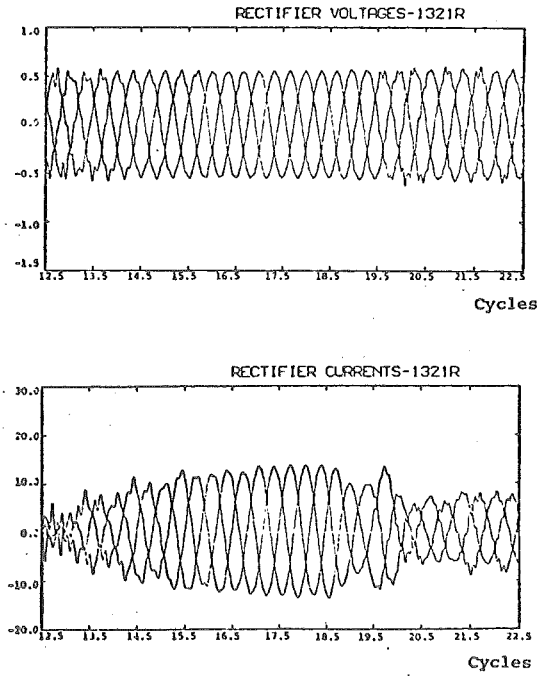

Fig. 1. Comparison between TCS waveforms at the rectifier terminal during current setting changes.

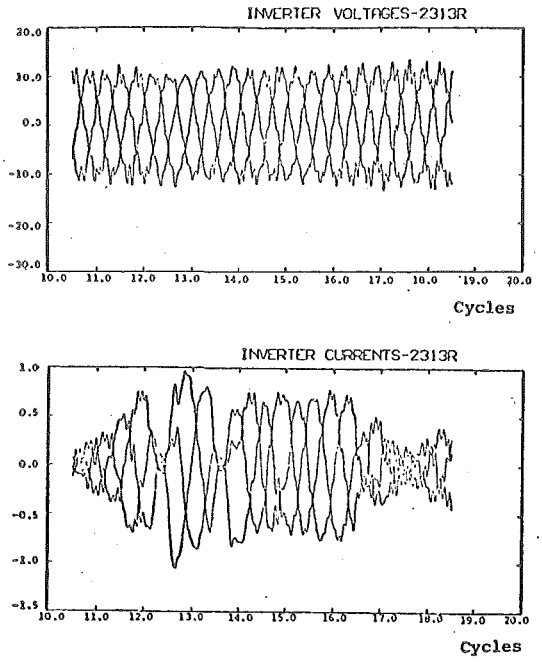

Fig. 2. Comparison between TCS waveforms at the invertor terminal during commutation failures.

integration steps and, in order to ensure that sufficient samples are used [1], the TS programme step length should not exceed half of one fundamental cycle. In the studies performed using this programme the step length and sample rate was fixed at half a cycle of the fundamental frequency as illustrated in Figure 3(b).

OBTAINING FUNDAMENTAL COMPONENTS FROM DISTORTED WAVEFORMS

The results of typical disturbances, such as those illustrated in Figures 4 and 5, cannot be interpreted in terms of simple periodic waveforms for the following reasons:

i) Convertor control action introduces deviations in the equidistant firing regime and valve firings do not necessarily occur periodically.

ii) The non-linear behaviour of the convertor excites disturbances which are not periodic in T.

iii) Disturbances to the a.c. or d.c. network introduce non-periodic responses in the system.

iv) The network equivalent source is given in a constant frequency frame of reference but the TS study deviates from constant frequency after a disturbance, effectively altering the fundamental period.

These effects can be classified in terms of modulation, frequency mismatch and non periodic noise. Their presence means that a simple fundamental component of voltage or current cannot be obtained merely by using a standard discrete Fast Fourier Transform [5] (FFT), on the samples which make up the TCS waveforms of Figures 4 and 5. The presence of non periodic frequencies contributes to the spectral component evaluated at fundamental frequency. It is therefore necessary to consider the magnitude of these contributions to assess their individual effect on the identification of a fundamental component and thus ensure that the correct values of voltage and power are available for the TS study.

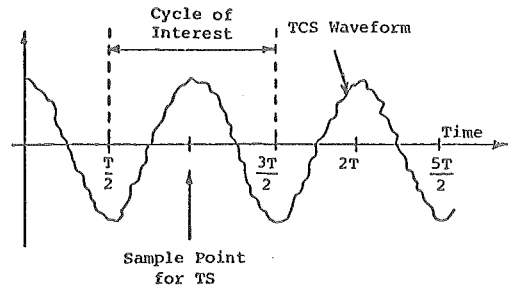

Fig. 3a

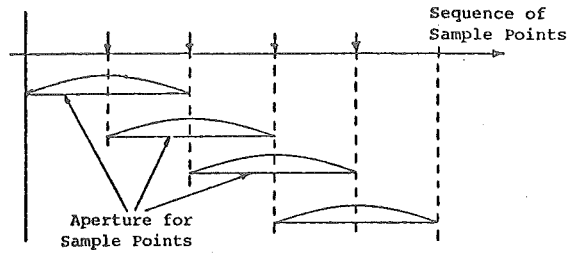

Fig. 3b

Fig. 3. Interaction between TS sample points and a TCS waveform.

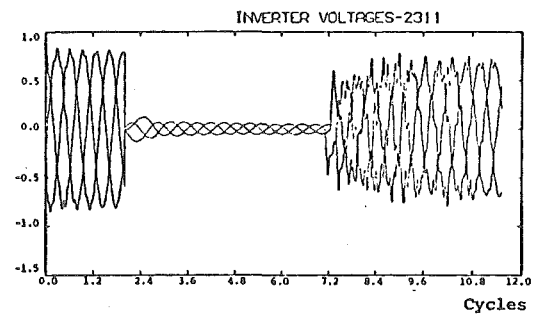

Fig. 4. TCS waveform for a 3-phase fault at the invertor terminal.

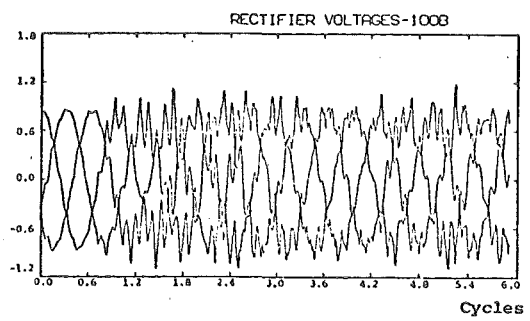

Fig. 5. Rectifier TCS waveforms for a single phase fault in the invertor a.c. system.

Modulation

Figure 4 illustrates the effect of a fault applied for a duration of 5 cycles and close to the invertor a.c. busbar of a d.c. link. There is a step change in voltage at the time of fault application and removal. In the TS study of this fault the integration step is

adjusted to obtain a solution immediately before and after a discontinuity. However, performing an FFT to obtain a fundamental component from the cycle spanning either side of the discontinuity involves a half period of pre-discontinuity and a half period of post-discontinuity. The Fourier analysis of the waveform of this cycle in effect produces an averaging of the two parts of the cycle. The existence of a fundamental component is meaningless in this case and the result is incompatible with the requirements of the TS study.

This problem is overcome by extrapolating the results of the FFT on the immediate pre-discontinuity and post-discontinuity cycles to provide a TCS data point at each respective solution in the TS study.

Apart from the discontinuities, the amplitudes of the voltages in Figure 4, in the post fault period, are modulated by the slower dynamic response of the a.c. system. This response is derived from a TS study for which the fastest oscillations are in the order of 1-5 Hz. The Fourier analysis of each fundamental cycle, at intervals of half a cycle, reflects the much lower modulating frequency in the amplitude of the fundamental component from each cycle, and no special treatment is required for these modulating effects.

Frequency Mismatch

One of the basic assumptions in TS modelling is that frequency deviations are so small that parameter values remain constant. However the Fourier analysis of the TCS waveforms, for a nominal frequency fundamental component (i.e. 50 or 60 Hz) can result in a small mismatch between the frequency of the variables at the convertor terminals and the actual system frequency in the TS study.

The TCS is only used as a substitute for the Quasi-Steady State a.c.-d.c. model during, and for a short period after, the fault. In this relatively short period (10-15 cycles) the deviation from nominal frequency is small. Typical results taken from the New Zealand system, for a fault relatively close to a convertor and a synchronous machine, show a deviation of approximately 0.25 ms (1.25%) in the period of the system frequency. If the frequency mismatch is not taken into account when processing the TCS results the error introduced into a 1 p.u. fundamental of voltage or current is 0.65% (Appendix). Since real power is obtained from both voltage and current, it may be in error by up to 1.3%. However TS data is not normally provided to an accuracy better than 5% and therefore the errors associated with frequency mismatch are not significant.

Non Periodic Noise

Figures 6(a) and 6(b) illustrate single cycles of one phase of the invertor and rectifier voltage waveforms taken from distorted periods of the results presented in Figures 4 and 5. These individual cycles show that considerable levels of non periodic frequencies exist in the waveforms due to the nonlinearities associated with control action, filter response and convertor behaviour. If these waveforms are assumed to be periodic and are subjected to Fourier transformation to obtain the spectral components of the signals (in particular the fundamental component), a phenomenon known as spectral leakage [2] occurs. Spectral leakage results in the non periodic noise contributing to each of the periodic spectral components present, introducing uncertainty in their identification by the Fourier transformation.

The phenomenon of spectral leakage is best explained with the use of the convolution theorem [1].

In order to make the Fourier Transform of a periodic signal $f_T(t)$ finite, it is necessary to multiply the periodic signal, in the time domain, by a unit gate function, g(t), where:

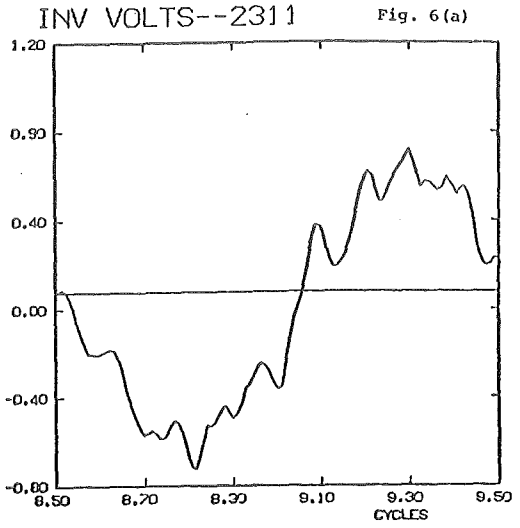

Fig. 6(a)

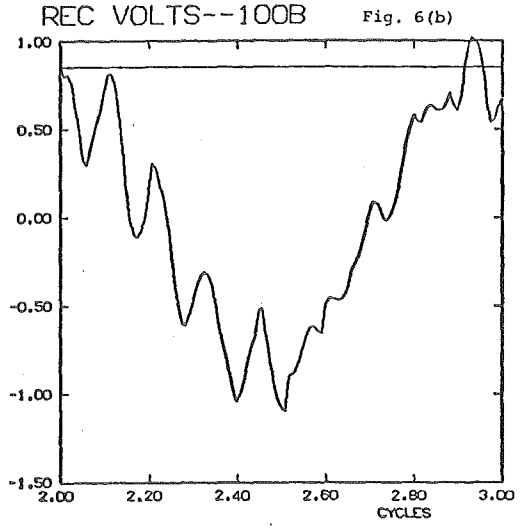

Fig. 6(b)

Fig. 6. Single cycles of one phase obtained from TCS waveforms of Figures 4 and 5.

$$g(t) = 1 \text{ for } |t| < \frac{T}{2} \quad (1)$$

$$g(t) = 0 \text{ for } |t| > \frac{T}{2} \quad (2)$$

Figure 7(a) shows the gate function and its spectrum, G(ω). In the frequency domain this multiplication is equivalent to the convolution of F(ω) with G(ω), i.e.

$$f_T(t) \longleftrightarrow F(\omega) \quad (3)$$

$$f_T(t) \cdot g(t) \longleftrightarrow F_g(\omega) \quad (4)$$

where $F_g(\omega) = F(\omega) \otimes G(\omega)$ (5)

and $\longleftrightarrow$ denotes a Fourier Transform pair.

When $f_T(t)$ contains only the fundamental frequency, ω_1, as shown in Figure 7(b), the convolution of F(ω)

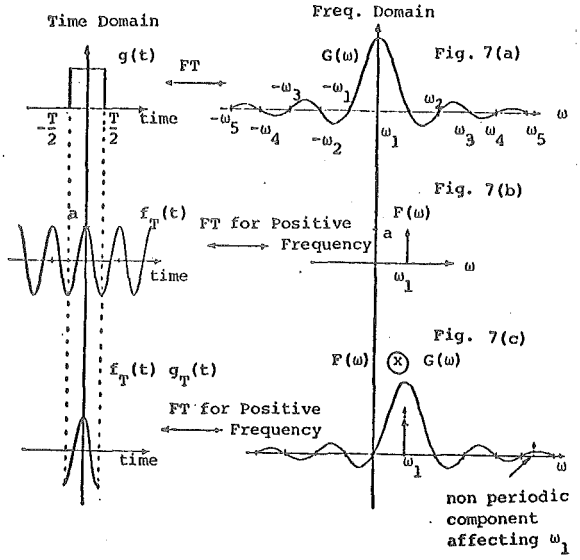

Fig. 7. Convolution and the effect of spectral leakage on the component at ω.

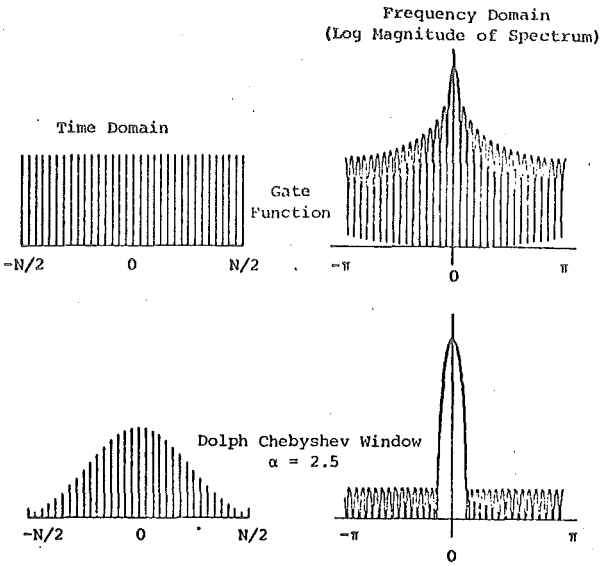

Fig. 8. Comparison of gate function and Dolph-Chebyshev window.

and $G(\omega)$ at ω_1 is illustrated in Figure 7(c). If other signals, which are periodic in aperture T, existed in $f_T(t)$, they would be present at the zero crossings of $G(\omega)$ and would not therefore contribute to the spectral component at ω_1. However non periodic frequencies exist at points other than the zero crossings of $G(\omega)$ and thereby contribute to the evaluation of periodic spectral components. This is spectral leakage and is illustrated in Figure 7(c) for the component at ω_1.

Because of the effect of spectral leakage, it is not possible to obtain the fundamental components of signals, such as those of Figures 6(a) and 6(b), with any degree of certainty by simple application of an FFT. The gate function is only one of a general class of functions, called windows. By the use of windows with special characteristics, spectral leakage can be minimized [2]. This then permits a comparison between a fundamental voltage, obtained from an unfiltered and a window filtered waveform, to provide an assessment of the magnitude of the spectral leakage effect.

Spectral Leakage Reduction

The objective in choosing a window to reduce spectral leakage is to obtain a narrow mainlobe with very low sidelobes in the frequency domain. Hence, when considering convolution, the weighting of the non periodic spectral components is very small and the contribution of these components to the periodic component being identified is reduced significantly. The Dolph-Chebyshev window provides the narrowest possible mainlobe width for a given sidelobe level [2] and was chosen for this filtering application. It is compared with a Unit Gate Function in Figure 8. Its discrete form is realised in the frequency domain by equation (6), and its time domain samples are obtained by performing a discrete inverse FFT on w(k).

$$w(k) = \frac{(-1)^k \cos\left(N\cos^{-1}\left[\beta \cos\left(\frac{\pi k}{N}\right)\right]\right)}{\cosh\left[N\cosh^{-1}(\beta)\right]} \qquad (6)$$

for $0 < k < N-1$ and k an integer

$$\beta = \cosh\left[\frac{1}{N}\cosh^{-1}(10^{\alpha})\right] \qquad (7)$$

and where the inverse hyperbolic cosine is defined by:

$$\cosh^{-1}x = \frac{\pi}{2} - \tan^{-1}\left(x/\sqrt{1-x^2}\right) \text{ for } |x| < 1.0$$

$$= \text{Ln}\left[x + \sqrt{x^2 - 1.0}\right] \text{ for } |x| > 1.0$$

and N = number of samples.

The sidelobe levels of this window remain below a specified constant maximum which can be controlled by the parameter α in equation (7). With α=4.0 the sidelobes are 80db (0.01%) down on the mainlobe magnitude. The very low and constant sidelobe level makes it possible to minimize the contributions due to non-periodic frequencies.

The use of such a low sidelobe level means a compromise in the width of the mainlobe. In the case with α=4.0, and with the window positioned for identification of ω_1 (by convolution), the 2nd and 3rd harmonics lie within the mainlobe. Although the d.c. component is also within the mainlobe, this bias can be removed from the discrete time domain data before it is weighted by the window in the time domain. The mainlobe width limitation is overcome by developing an algorithm in which three windows, each with different α parameters, are used on the same cycle of TCS data.

By applying the principle of convolution to the discrete TCS data and using the trigonometric form of the Fourier Transform (Appendix) the complex fundamental Fourier component of $[w(k).f(k)]_{k=1}^{N}$ is:

$$X_1 = w_0 C_1 + w_1 C_2 + w_2 C_3 + w_{-2} C_{-1} + w_{-3} C_{-2} + w_{-4} C_{-3} + w_{-1} C_0 + \sum_{n=3}^{N/2} w_n C_{n+1} + \sum_{n=4}^{N/2-1} w_{-n+1} C_{-n} \qquad (8)$$

where w = discrete window coefficients in the frequency domain
$C_n = C_{-n}$ - complex periodic Fourier components (subscript refers to harmonic order).

By neglecting the sidelobe contributions, i.e. the last two terms of equation (8) (these are weighted with window components in the order of 0.01%), and removing the d.c. component (i.e. C_o is zero), equation (8) reduces to:

$$X_1 = w_o C_1 + w_1 C_2 + w_2 C_3 + w_{-2} C_{-1} + w_{-3} C_{-2} + w_{-4} C_{-3} \quad (9)$$

The use of three different windows generates three simultaneous equations of the same form as equation (9) each with different window coefficients, the solution of which permits evaluation of the filtered fundamental component C_1.

The algorithm was tested on 32 sample discrete sinusoidal data of the form:

$$f_T(t) = c_1 \cos(\omega_1 t + \phi_1) + \sum_{n=2}^{7} c_n \cos(n\omega_1 t + \phi_n) \quad (10)$$

where $c_1 = 1.0$

$c_2 = 0.2$ for n=2 to 7.

On this purely sinusoidal data the window filtering introduced an error of 0.16% into the identification of C_1 due to the contributions from higher harmonics. When a non periodic component, magnitude 0.2, was introduced into $f_T(t)$ at $5.65\omega_1$ the error in identifying ω_1 by direct application of the FFT to the data was 2%, but by using window filtering this was reduced to 0.36%.

The series represented by equation (10) constitutes a severe test as it uses a high amplitude for every harmonic. Even so, the algorithm performance is well within the accuracy range of power system calculations.

The algorithm is therefore capable of providing an estimate of the effect of spectral leakage on the identification of fundamental voltage and current from TCS waveforms.

Spectral Leakage Effects in TCS Results

Window filtering was employed in analysing a number of TCS results including all cases presented in the companion papers (Parts I and III). In order to apply an FFT to the TCS results it is necessary to convert these results into an equally spaced sample sequence. Although higher order methods were used, linear interpolation was found to be quite acceptable considering the large number of TCS samples available.

The differences between direct and filtered Fourier analyses were small. Results showed differences of up to 0.7% and the maximum difference observed was 1%. These differences are not far outside the limits of accuracy of the filtering method itself and it can therefore be concluded that spectral leakage does not contribute significant errors when identifying the fundamental components of TCS waveforms.

It is therefore possible to obtain fundamental powers and voltages from TCS waveforms, in the presence of modulation, frequency mismatch and non periodic noise with the same degree of accuracy that other input data is obtained for transient stability studies.

EFFICIENT EVALUATION OF CONVERTOR VARIABLES

Approximations can be used to avoid the need to perform spectral analysis of the TCS results.

The evaluation of average or rms quantities from the convertor waveforms includes the effect of the harmonic components and thus violates the sinusoidal assumption made in transient stability studies. If the harmonic content is low then the rms quantity will represent a good approximation to the fundamental. The rms value of a voltage, V(t), is defined, over a period T as:

$$V_{rms} = \sqrt{\frac{1}{T} \int_o^T v(t)^2 \, dt} \quad (11)$$

For discrete data this becomes:

$$V_{rms} = \sqrt{\frac{1}{N} \sum_{n=1}^{N} (V_n)^2} \quad (12)$$

where N = the number of samples.

rms values for discrete data are easily and quickly evaluated in relation to spectral analysis.

RMS Approximation for Voltage

Figures 9(a) and 9(b) show a comparison of fundamental voltage (positive sequence) and rms voltage for the TCS waveforms of Figures 4 and 5. Figure 9(b) represents a severely distorted case with a 5% difference observed during the period immediately after disturbance initiation. This coincides with the period of maximum distortion in Figure 5 at which time harmonic content is high. The effect of using one cycle for obtaining the fundamental or rms voltage is clearly shown in Figure 9(a) during the cycle spanning fault application and removal, (i.e. at 2 and 7 cycles). While Figure 4 shows a sudden discontinuity at these times, Figure 9(a) demonstrates the averaging effect of processing, emphasising the need for extrapolation at discontinuities.

RMS Approximation for Power

Apparent power is defined as:

$$s(t) = v(t) \cdot i(t) \quad (13)$$

The real component of s(t) is the average value of s(t) taken over a period, T. i.e.

$$P_{rms} = \frac{1}{T} \int_o^T v(t) \cdot i(t) \, dt \quad (14)$$

This is readily evaluated from discrete signals using:

$$P_{rms} = \frac{1}{N} \sum_{n=1}^{N} V_n \, i_n \quad (15)$$

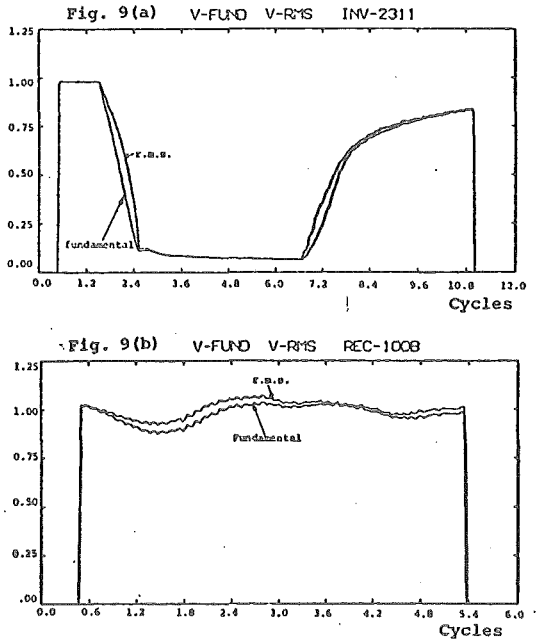

Fig. 9. Comparison of rms and fundamental voltages for the TCS waveforms of Figures 4 and 5.

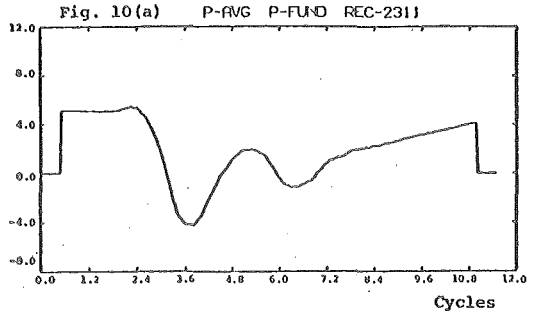

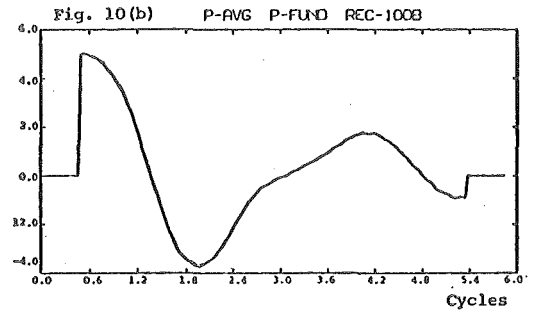

Fig. 10. Comparison of rms and fundamental powers for the cases present in Figures 4 and 5.

The real power evaluated in this way is the sum of fundamental and harmonic real powers. The results from a TCS have shown that, in general, the harmonic real power is small and that the rms approximation for real fundamental power is a good one. Figures 10(a) and 10(b) show two representative cases. In the case of Figure 10(a), although the maximum error is 4%, the cummulative error over the simulation period is small. The maximum error occurs for a short period when highly distorted signals exist.

The harmonic power flow can only result from in-phase components of harmonic currents and voltages. Considering the relatively low resistive component of the convertor transformer and the large X/R ratio of the a.c. system, the in-phase components of the harmonic currents and voltages are very small. Therefore the use of rms power is a good approximation and spectral analysis is not needed to derive the power variable.

CONCLUSIONS

An efficient technique has been developed for processing the aperiodic and distorted waveforms obtained from a Transient Convertor Simulation so that the information may be used directly in a Transient Stability study. From the choice of waveforms available it has been shown that power and voltage magnitude are suitable variables for transferring such information.

The information is transferred at each step of the TS study and the problem posed by system discontinuities has been considered and overcome. The use of spectral analysis and window filtering has shown that sufficient accuracy and considerable computing saving can be achieved by judicious approximations. It has been shown that the use of rms power in place of fundamental power introduces only very small errors. However in the case of the convertor voltage, the use of rms voltage can lead to significant errors.

It is therefore necessary to retain the spectral analysis to determine a fundamental voltage magnitude from the transient convertor simulation waveforms but the rms approximation for power avoids the need for spectral analysis of current.

The techniques developed have application wherever distorted and aperiodic waveform information requires analysis. One such application is harmonic analysis of waveforms obtained by fast digital sampling of power system data.

ACKNOWLEDGEMENTS

The authors wish to express their gratitude to the General Manager of New Zealand Electricity, Mr. K. D. McCool, to Dr. M.W. Kelly and to the staff of the Electrical Engineering Department and Computer Centre of the University of Canterbury for their help.

REFERENCES

[1] B.P. Lathi, "Signals, Systems and Communications", John Wiley & Sons Inc., 1965.

[2] F.J. Harris, "On the Use of Windows for Harmonic Analysis with the Discrete Fourier Transform", Proc. IEEE, Vol. 66, No. 1, January 1978.

[3] W. Shepherd and P. Zakikhani, "Suggested Definition of Reactive Power for Nonsinusoidal Systems", Proc. IEE, Vol. 119, No. 9, September 1972.

[4] D. Sharon, "Reactive Power Definitions and Power-Factor Improvement in Non Linear Systems", Proc. IEE, Vol. 120, No. 6, June 1973.

[5] W.T. Cochran et al, "What is the Fast Fourier Transform", Proc. IEEE, Vol. 55, No. 10, October 1967.

NOMENCLATURE

TS - Transient Stability
TCS - Transient Convertor Simulation
FFT - Fast Fourier Transform
db - Decibels
ω - Angular Frequency
T - Period of fundamental frequency
k - Sample index
v(t) - Instantaneous voltage
i(t) - Instantaneous current
s(t) - Instantaneous apparent power

APPENDIX

The Fourier transform pair of a periodic function $f_T(t)$ of period T can be written as:

$$f_T(t) = \sum_{n=-\infty}^{\infty} f(n\omega_1)\, e^{jn\omega_1 t} \qquad \text{(A1)}$$

$$F(n\omega_1) = \frac{1}{T} \int_{-\frac{T}{2}}^{\frac{T}{2}} f_T(t)\, e^{-jn\omega_1 t} dt \qquad \text{(A2)}$$

Equations (A1) and (A2) can be written in the familiar trigonometric form, i.e.

$$f_T(t) = \sum_{n=0}^{\infty} c_n \cos(n\omega_1 t + \phi_n) \qquad \text{(A3)}$$

$$c_o = a_o = \frac{1}{T} \int_{-\frac{T}{2}}^{\frac{T}{2}} f_T(t)\, dt \qquad \text{(A4)}$$

$$a_n = \frac{2}{T} \int_{-\frac{T}{2}}^{\frac{T}{2}} f_T(t) \cos(n\omega_1 t)\, dt \qquad \text{(A5)}$$

$$b_n = \frac{2}{T} \int_{-\frac{T}{2}}^{\frac{T}{2}} f_T(t) \sin(n\omega_1 t)\, dt \qquad \text{(A6)}$$

$$C_n = a_n + jbn = c_n(\cos n\omega_1 t + \phi_n) \qquad \text{(A7)}$$

Equation (A5) can be used to evaluate the effect of frequency mismatch. Given a small deviation from nominal frequency $\omega_1' = \omega_1 + \Delta\omega_1$ then

$$a_1 = \frac{2}{T} \int_{-\frac{T}{2}}^{\frac{T}{2}} \cos\omega_1' t \cos\omega_1 t\, dc \qquad \text{(A8)}$$

$$a_1 = \frac{2}{T(\omega_1'-\omega_1)} \sin\frac{(\omega_1'-\omega_1)T}{2} + \frac{2}{T(\omega_1'+\omega_1)} \sin\frac{(\omega_1'+\omega_1)T}{2} \qquad \text{(A9)}$$

For a fundamental frequency of 50 Hz (i.e. T=20 ms)

$$\omega_1 = 314.16$$

With a deviation of 0.25 ms in the period T

$$\omega_1' = 310.28$$

Hence $a_1 = 0.9935$.

The true amplitude of a_1 is 1.0 and therefore the error in identifying ω_1' at a frequency ω_1 is 0.65%.

APPENDIX A14

COMPUTATION OF AC-DC SYSTEM DISTURBANCES - PART III TRANSIENT STABILITY ASSESSMENT

COMPUTATION OF A.C.-D.C. SYSTEM DISTURBANCES. PT. III - TRANSIENT STABILITY ASSESSMENT

K.S. Turner
Student Mem., IEEE

M.D. Heffernan

New Zealand Electricity

C.P. Arnold
Member, IEEE

J. Arrillaga

University of Canterbury (N.Z.)

Abstract - Quasi-steady state and transient convertor simulation models of h.v.d.c. transmission are compared in multimachine transient stability studies. The paper analyses their respective a.c. and d.c. system responses to typical disturbances, discusses the limitations and extent of applicability of the quasi-steady state model and justifies the need for temporary transient convertor simulation. It is concluded that after preliminary transient convertor simulation studies in a particular system, a suitably modified quasi-steady state model can be used in the assessment of transient stability.

INTRODUCTION

It is generally accepted that some form of Transient Convertor Simulation (TCS), as discussed in a companion paper [1], is essential when assessing fault current levels, d.c. link response, recovery voltages [2], etc. On the other hand, in stability studies the h.v.d.c. link is normally represented by a Quasi-Steady State (QSS) behaviour [3][4]. This is justified by the fast controllability of the convertor plant as compared with the a.c. generator response.

However considering the relatively small time involved in first swing transient stability (TS), its accurate determination requires a correspondingly accurate representation of the d.c. link behaviour during and immediately after the disturbance.

The use of a small step transient simulation throughout the stability study has been proposed in a recent publication [5]. However the computational requirements appear to be prohibitive and the size of a.c. system representation restricted. It is thus apparent that a QSS model must be used for the d.c. link response if it can be justified.

It can not be established in advance whether a QSS model will provide realistic results. Only be attempting several worst case detailed convertor simulations can the validity of a QSS model be assessed.

This paper investigates the effect of different convertor models on the power behaviour of a d.c. link during disturbances and its relevance to the assessment of transient stability. The models are then used to investigate a worst case study, with a temporary d.c. current setting change, to explore the possibility of first swing stability improvement.

COMPARATIVE BEHAVIOUR OF THE QSS AND TCS MODELS

The differences between the two types of convertor

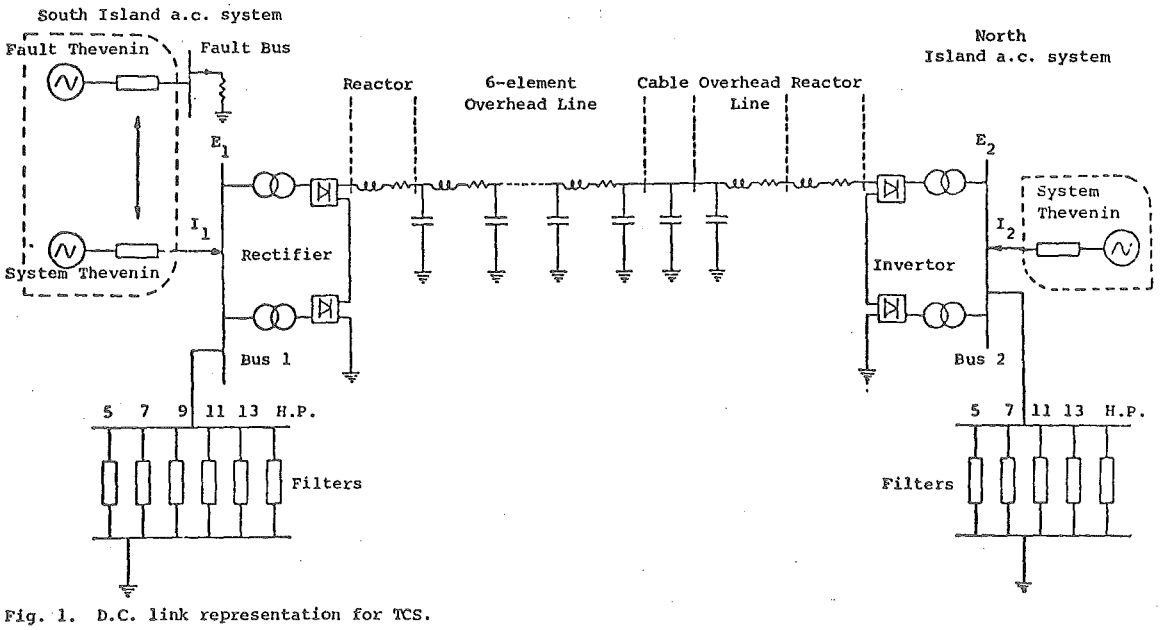

Fig. 1. D.C. link representation for TCS.

representation are examined using the results of four different worst case studies. These show progressively increasing differences between the QSS and TCS models.

A simplified circuit of the New Zealand d.c. link, (Figure 1), suitable for TCS, is used as a basis for the comparison. The figure illustrates the case of a fault in the South Island a.c. system, the normal power transmission being from south to north. In this representation a multimachine transient stability programme using the QSS d.c. link model and the New Zealand Primary transmission system, provides the time variant system equivalents for the TCS. In turn, the instant-

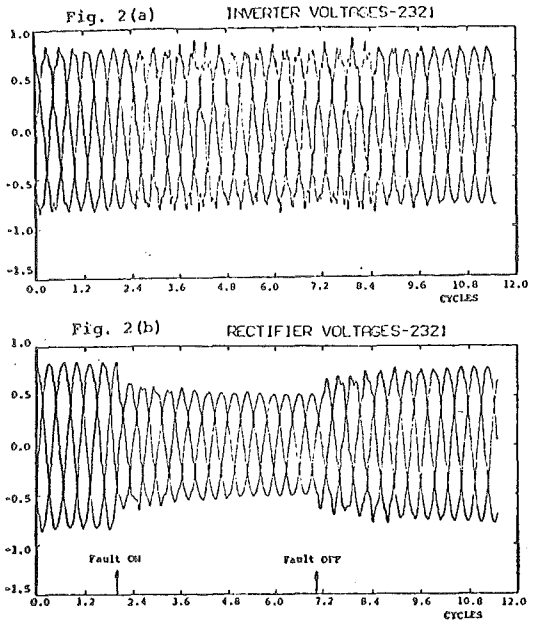

Fig. 2. Rectifier a.c. system fault - TCS voltage waveforms.

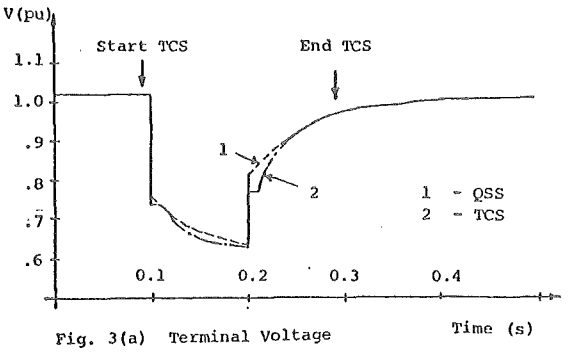

Fig. 3(a) Terminal Voltage

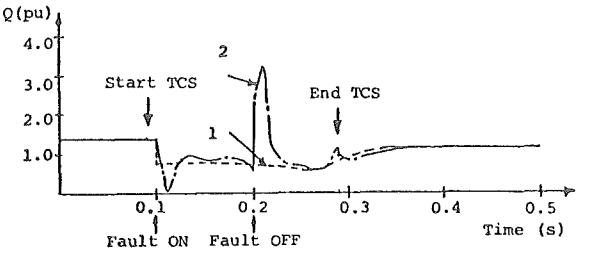

Fig. 3(b) Reactive Power

Fig. 3. Rectifier a.c. system fault - voltage and reactive power.

aneous values of I_1, I_2, E_1 and E_2 of Figure 1 are processed as described in a companion paper [6], to provide rms power and voltages at the convertor terminals for use in the transient stability programme.

The purpose of using transient convertor simulation in stability studies is to model accurately the d.c. link behaviour during the disturbance period, until the time when the link response and control have settled sufficiently to allow the QSS model to take over. In addition, there is little point in continuing detailed convertor simulation beyond the first swing maximum, unless subsequent swings are critical to the stability of the system.

The return to quasi-steady state behaviour of the transient convertor simulation can be evaluated by monitoring control action and d.c. current variations. Once control action has been settled and firing instants become equally spaced, the link terminal a.c. voltage waveforms lose most of their distortion. These effects are clearly illustrated by the voltage waveforms of Figure 2, which are taken from the results of the study carried out in the next section. In this case, most of the distortion has disappeared within 3 cycles of fault clearance.

Transient stability is assessed for the synchronous machines located closest to the d.c. link. These are the hydro turbine-generators in the south and relatively low inertia synchronous condensers in the north.

Where not otherwise specified, the graphical results presented are obtained from TS studies with either a QSS model used throughout or with TCS equivalents replacing the QSS model during the most disturbed period and the variables plotted are those at the interface between the d.c. link and the a.c. system.

The four different disturbances chosen for TS assessment are discussed in the following sections.

Rectifier a.c. System Fault

A three-phase fault of 5 cycle duration is applied at a bus central to a large proportion of the South Island generating capacity. This fault represents a very severe disturbance to the South Island a.c. system, but the voltage reduction at the rectifier terminals is only 25%.

The differences in rectifier terminal a.c. voltage are illustrated in Figure 3(a) for the two models. The use of a QSS model results in a higher voltage profile both during and immediately after the fault. The differences between the two models are even more noticeable in the reactive power profiles of Figure 3(b).

In the QSS model the filters are represented by a shunt admittance, while the TCS reflects the full dynamic response of the filters. For the TCS representation, the combination of the dynamic filter response and control action results in an initial drop in reactive power demand from the a.c. system. The mismatch is more pronounced following fault clearance.

Although the reactive power profile is useful in indicating the relative accuracy of the two convertor models, it is the real power transferred by the d.c. link which affects generator transient stability. Figures 4(a) and 4(b) show the real power flow to the link terminals. The invertor power (Figure 4(b)) is plotted for positive power flow out of the link terminal to facilitate a comparison between the two ends of the link.

Immediately after fault inception the TCS indicates that the rectifier d.c. power flow is considerably less than the level predicted by the QSS model (Curve 2 of Figure 4(a)). This is caused by the sudden drop in the rectifier d.c. voltage, giving rise to a corresponding reduction in d.c. current. However the control response at the invertor restores the d.c. current and the link recovers from the initial disturbance quickly. During the remaining fault period and in the post fault period, the TCS rectifier power exceeds that of the QSS model.

At the invertor end the immediate power response predicted by the QSS model (curve 1 of Figure 4(b)) deviates considerably from the TCS solution (curve 2), which reflects the delay effect caused by the d.c. line.

Although instantaneous power differences are ob-

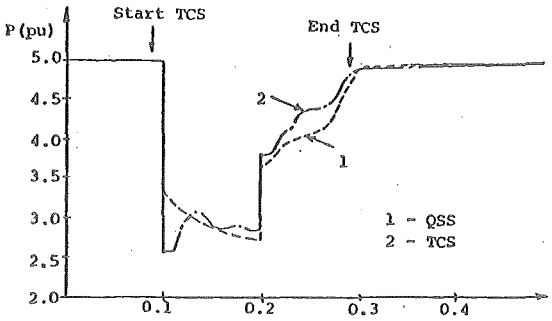

Fig. 4(a) Rectifier power.

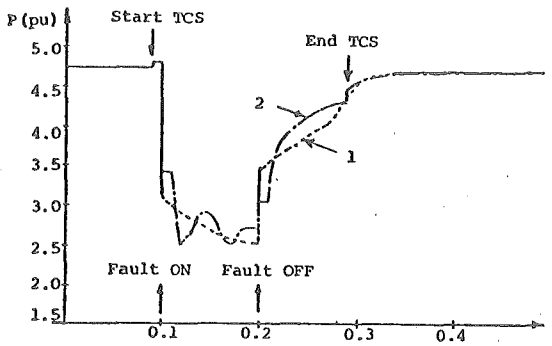

Fig. 4(b) Invertor power.

Fig. 4. Rectifier a.c. system fault - real power.

served, the nett energy transfer as calculated by the TCS and QSS models are similar, thus causing relatively small first swing maximum angle differences. For the high inertia machines at the rectifier terminals the difference is 3%, while for the low inertia synchronous condensers at the invertor, the difference is 12%. At both terminals the QSS model gives the larger maximum angles, and thus provides pessimistic but safe results.

D.C. Line Fault

A d.c. line fault is applied on the d.c. line, next to the rectifier smoothing reactor, which results in a complete loss of power transmission during the fault period.

The QSS model has severe limitations in its ability to represent this type of disturbance. A d.c. fault, using this model, is represented by instantaneous shutdown of the link at the prescribed time followed by restarting at the end of the specified fault period. Moreover the QSS model can not represent the timing of valve firings in relation to the fault occurrence and therefore gives no information regarding fault currents or subsequent control action.

For the TCS the d.c. fault is initiated immediately after a valve firing. This provides a worst case study since the control action influence is delayed for almost 30^{o} until the next firing. The TCS provides more detailed information of the d.c. link behaviour, as shown in the waveforms of Figure 5.

The fault is applied at cycle 2 and Figure 5(a) shows that the a.c. fault current flows for half a cycle after fault initiation. During this period the rectifier delay angle is retarded into the inverting region (between 120^{o} and 130^{o}), to accelerate the d.c. line discharge. Figure 5(b) shows that the fault is cleared rapidly as a result of this control action.

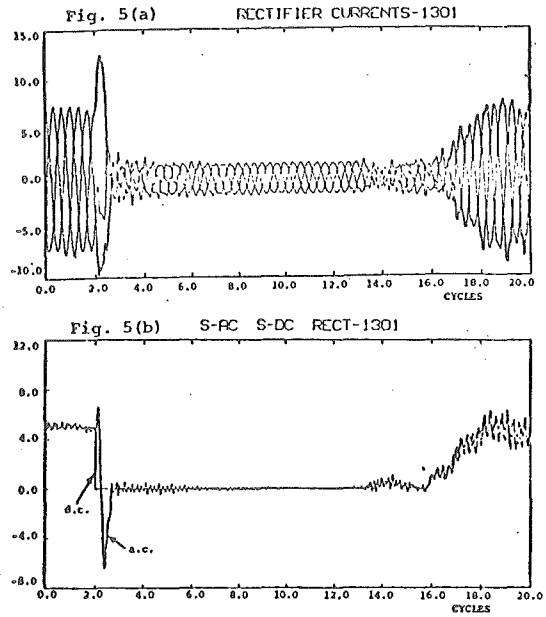

Fig. 5. D.C. line fault - TCS rectifier response.

Arc extinction and deionization times are greater for a d.c. fault than for an equivalent a.c. line fault and throughout this period no power can be transmitted.

The reactive power responses at the rectifier are illustrated in Figure 6(a). The TCS response indicates that at fault initiation the reactive power increases briefly, due to the half cycle of fault current. Once convertor action clears the fault current, the filters' total reactive power is fed to the a.c. network until d.c. line reenergization starts.

The real power responses are illustrated in Figure 6(b). There is little difference between the results of the QSS and TCS models at fault initiation.

The TCS results from the fault period indicate that extinction and deionization time require 11 cycles [7]. At the end of this period transmission recovery begins and in the absence of prior knowledge of the TCS response, the QSS model produces instantaneous power recovery at this time, as illustrated by curve 1 of Figure 6(b). As the transient convertor simulation of the recovery period progresses it becomes clear that, due to the line recharging delay, a considerable mismatch exists between the two models. The difference, clearly demonstrated by curves 1 and 4 in Figure 6(b), causes considerable error in the TS assessment as illustrated by the swing curves of Figure 7. The South Island machine shows a 16% error in the 1st swing peak of the QSS response.

By using interactive coordination between the models, as described in a companion paper [1], the QSS model start-up characteristic can be delayed to correspond with that of the TCS model. Curve 2 of Figure 6(b) shows a more accurate characteristic for the QSS model. With this approach, the differences in first swing maximum angles are reduced to less than 2%. This is due, in part, to the close correspondence of the two models throughout the fault period and also to the fact that the peak swing of the machines is very close to the transmission recovery time. Consequently the differences observed over the power recovery period do not affect the first swing significantly. By ramping, as well as delaying the restart, as illustrated by curve 3

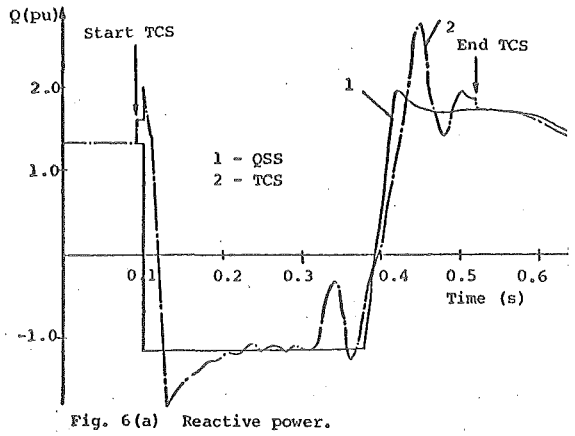

Fig. 6(a) Reactive power.

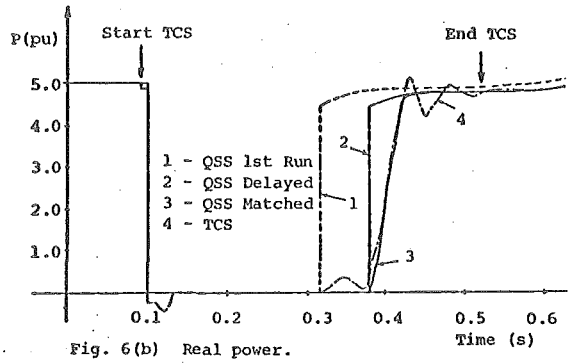

Fig. 6(b) Real power.

Fig. 6. D.C. line fault - rectifier power response.

of Figure 6(b) the first swing differences are reduced to less than 1%.

Figure 6 shows that, after transmission recovery, the controller response is oscillatory and the TCS is continued for several cycles beyond the first swing maximum to ensure that the oscillations are damped.

Invertor a.c. System Fault

Faults at invertor terminals provide a severe test for the d.c. link controls and often result in repeated commutation failures causing considerable disruption to the normal valve firing sequences at the invertor. A three phase fault, of 5 cycle duration, is thus applied at the invertor a.c. terminal busbar (Bus 2 of Figure 1). A 1 ohm fault impedance is used, causing an 80% voltage drop at the invertor terminals but providing sufficient source voltage for commutations to continue. For this fault location, the TCS variables E2 and I2, used to derive voltage and power equivalents for the TS study, include the effects of both the fault and the d.c. link. Since the fault is severe, it masks the convertor response, as illustrated in Figure 8.

In this case it is not necessary to obtain a separate fault Thevenin equivalent for the TCS since the system and fault equivalents are derived from the same bus. Moreover when TCS equivalents are used to represent the convertor behaviour, the variables obtained from the TCS can be used to specify the fault in the a.c. network of the TS model. Thus it is not necessary to represent the fault explicitly in the admittance matrix of the TS study. If explicit fault representation is required in the TS study, it is necessary to remove the effect of the fault from the TCS variables so that they can be used to represent the convertor only. Figure 9(a) illustrates the effect of the fault by comparing the apparent power at the a.c. and d.c. terminals of the invertor system. The difference between the two represents the power flowing to the fault.

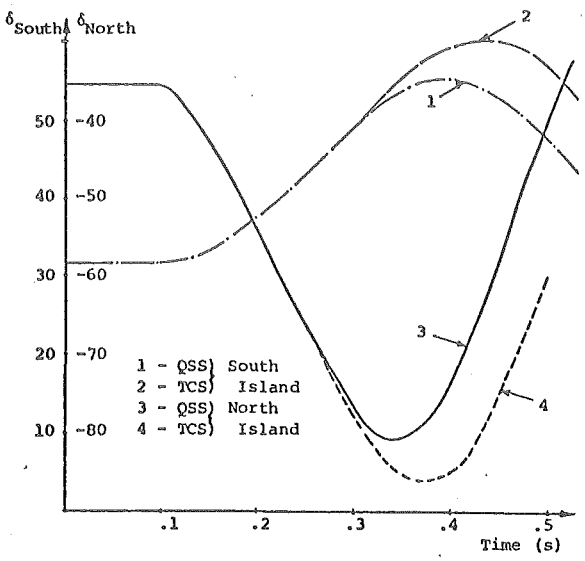

Fig. 7. D.C. line fault - swing curves.

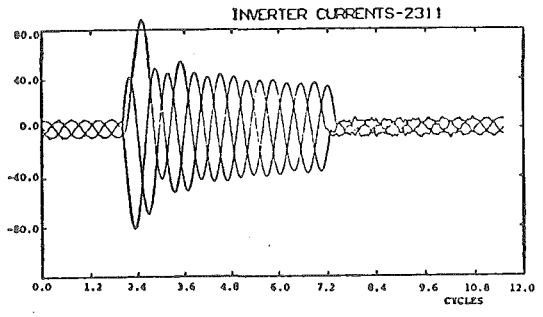

Fig. 8. Invertor a.c. system fault - TCS current (I_2) waveforms.

Immediately after the fault is applied, the invertor experiences repeated commutation failures which persist during the fault period. The commutation failures produce oscillations in the d.c. power at the invertor terminal. At the rectifier terminal the oscillations are smoothed by the d.c. line, as shown in Figure 9(b). These effects can not be represented by a QSS model.

The use of the QSS model produces responses which differ significantly from those obtained by TCS. The results from the two models are compared in Figure 10.

In order to compare directly the rectifier and invertor responses, the results plotted in figure 10(a) include the invertor power without the fault contribution. This is obtained by removing the fault power content from the TCS equivalent at each step of the TS study.

The differences between the TCS and QSS results are caused by a number of factors:

a) Due to the d.c. line response, power continues to be fed into the rectifier end of the line for one cycle after the fault occurs at the invertor bus.

b) At the invertor terminal, immediately before fault

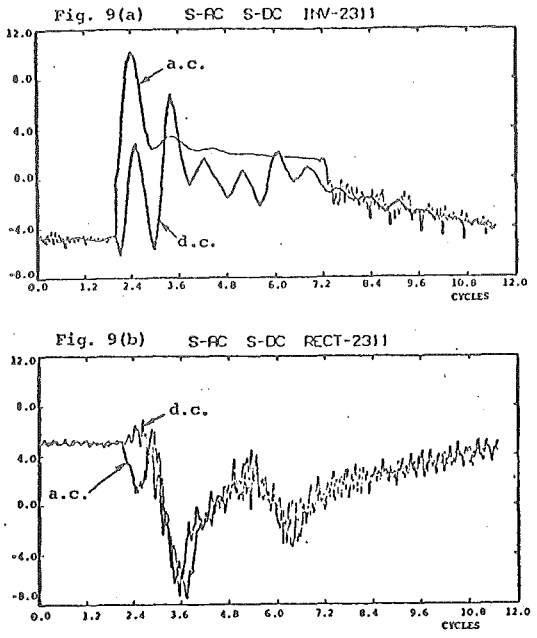

Fig. 9. Invertor a.c. system fault - TCS apparent powers.

clearance takes place, (i.e. the first detected current zero after breaker operation) a commutation failure occurs. This convertor disturbance delays the clearance time of the fault. It is impossible for a QSS model to detect this sequence of events.

c) In addition to the delay due to the commutation failure, invertor recovery is also affected by the response of the d.c. line and the controller at the rectifier end. As shown in Figure 10, the TCS rectifier response is slower than the QSS response.

The accurate response obtained from the TCS affects the results of the transient stability study as shown by the swing curves plotted in Figure 11. In this case, the maximum swing angle obtained using the QSS model is less than that obtained using the TCS model (i.e. optimistic) and this is especially noticeable for the low inertia machines at the invertor terminal. An accurate matching of the QSS and TCS responses cannot be generally applied to this disturbance because of the indeterminate nature of consequential convertor disturbances and their effect on normal valve firing sequences. In addition the QSS model cannot predict the oscillatory response at the rectifier terminal, illustrated in Figure 10(b) during the fault period.

The use of TCS equivalents is therefore essential in a TS study for this type of disturbance.

Invertor a.c. Fault with Current Setting Control

The fast controllability of d.c. links has long been recognised as a useful feature for stabilising a.c. power systems [8]. Moreover some consideration has been given to the use of temporary current setting changes for the purpose of improving first swing transient stability [3]. The interactive combination of TCS and TS models is an ideal technique for investigating such effects.

It has been demonstrated in previous sections that a 3-phase fault at the invertor terminal causes the largest disturbance to the a.c.-d.c. system. Since the invertor feeds power into the a.c. system, a generator

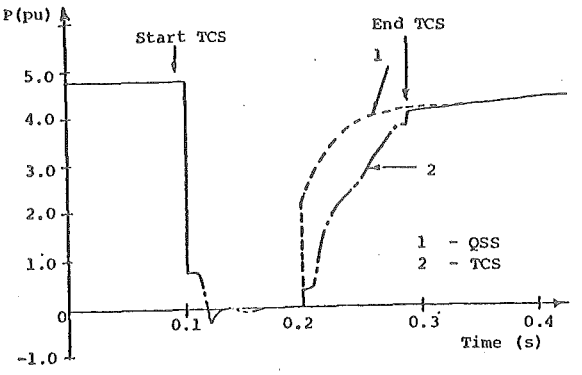

Fig. 10(a) Invertor power

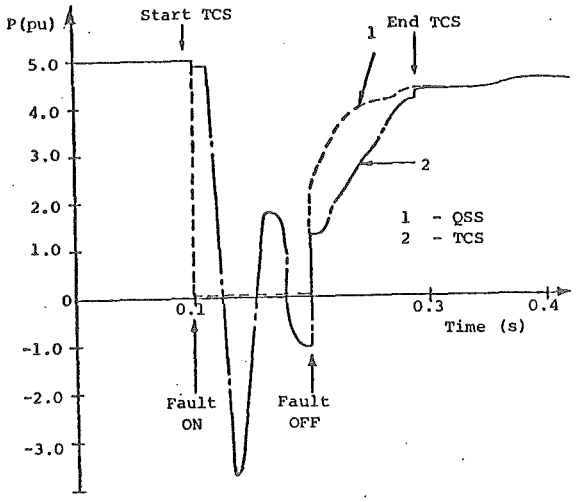

Fig. 10(b) Rectifier power

Fig. 10. Invertor a.c. system fault - real power.

near the invertor terminal may be stabilised, after a fault, by a period of reduced d.c. power infeed, (i.e. a drop in current setting). Similarly a synchronous motor may be stabilised by a period of increased power infeed, (i.e. an increase in current setting). The latter represents a worst case study, due to the increased possibility of commutation failure. It is used to investigate the possibility of first swing stability improvement with a 100% current setting increase of 6-cycles duration applied immediately after fault clearance.

The equivalent system used in the investigation, shown in Figure 12, consists of a simplified a.c. representation at each terminal and a large synchronous motor directly connected to the invertor terminal.

The TCS begins at fault clearance, as the previous case study has shown that the post fault clearance period produces the most significant difference between the two models for the purpose of assessing transient stability. This also saves 7-9 cycles of TCS computing time. Interactive coordination between the two models is used to match as closely as possible the QSS model performance with that of the TCS. The results obtained from the two models are compared in Figure 13.

Two transient convertor simulations are performed for this case. The first is carried out with the invertor control set to minimise the extinction angle, and the results (curve 2 of Figures 13(a) and 13(b)), differ markedly from the QSS model (curve 1). As a result of the low a.c. voltage and increased current

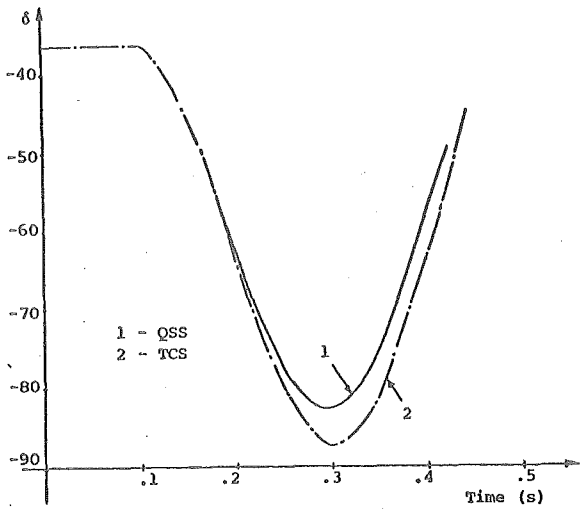

Fig. 11. Invertor a.c. system fault - North Island swing curves.

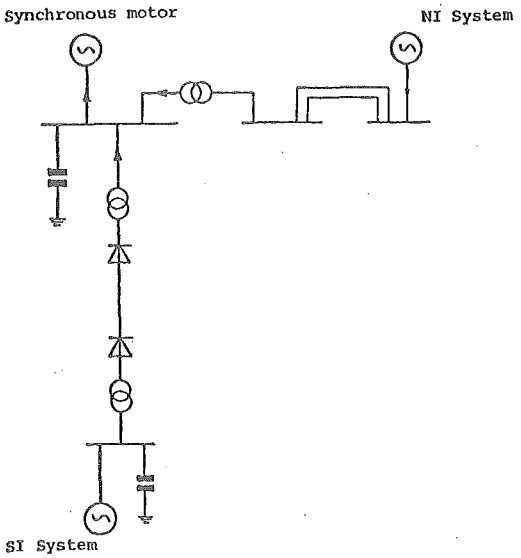

Fig. 12. Current setting control - equivalent circuit

setting, this type of control is unable to prevent commutation failures in the post fault period. These occur at cycles 12.5, 13.5 and 16.5 of Figure 14(a). The commutation failures create additional disturbances which would not have occurred without the step-up in current setting and therefore the d.c. power is severely reduced.

The repeated commutation failures of the first TCS are caused by the optimizing function of the extinction angle control. Since this type of control is only intended for steady state conditions, it can be modified to decrease the gain of the extinction angle controller during the transient period.

The second TCS with the modified control eliminates the commutation failures and, as illustrated in

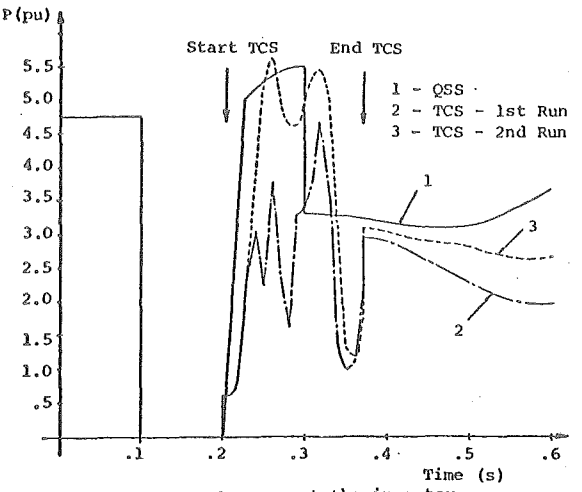

Fig. 13(a) Real power at the invertor

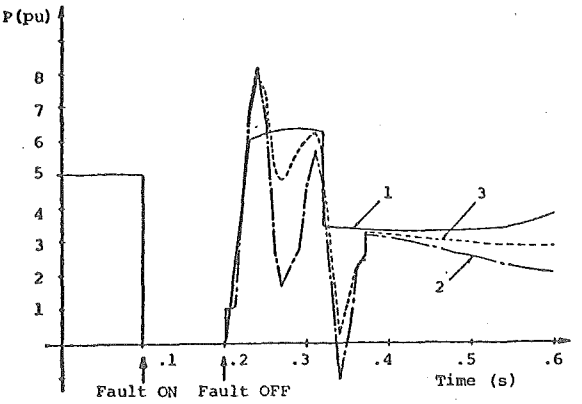

Fig. 13(b) Real power at the rectifier

Fig. 13. Current setting control - comparison of QSS and TCS results.

Figure 14(b), the invertor current waveforms are considerably improved. Much greater stabilising d.c. power is transmitted during the period of increased current setting, as shown by curve 3 of Figure 13.

Comparative swing curves for the synchronous motor are given in Figure 15. The motor is shown to be unstable for the first TCS study, the second TCS results indicate marginal stability and the QSS model gives extremely optimistic results which are totally unrealistic. This demonstrates the need for TCS studies when planning transient stability improvement.

The differences between the swing curves of Figure 15 also emphasise the problem of matching the QSS model performance to that of the TCS. Because the fault occurs at the invertor end, the rectifier maintains control of the d.c. current throughout the disturbance. However, due to the effect of the d.c. line delay in the TCS, accurate matching can only be achieved at one d.c. link terminal; in this case the rectifier terminal, as shown in Figure 13(b). The d.c. line delay results in a mismatch at the invertor terminal and the QSS restart is in advance of the TCS by almost a cycle.

CONCLUSIONS

For disturbances in the a.c. system and sufficiently far from the convertor terminals, the use of a QSS model will normally be accurate enough for the assessment of transient stability. In general, however,

Figure 14(a)
(First Run)

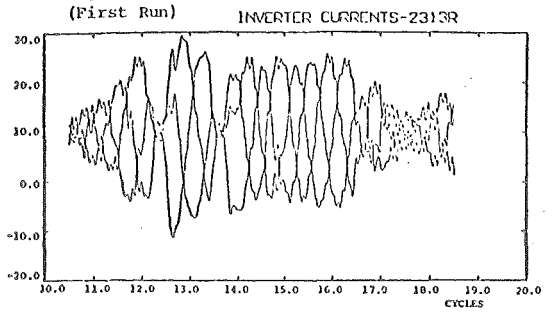

Fig. 14(b)
(Second Run)

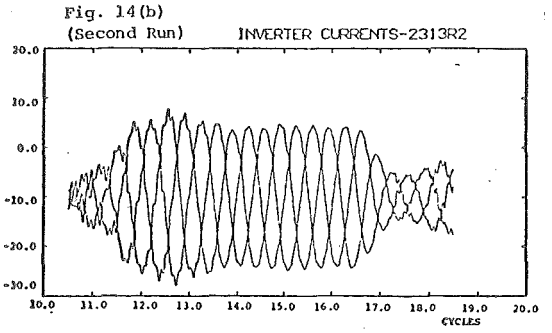

Fig. 14. Current setting control - TCS current waveforms.

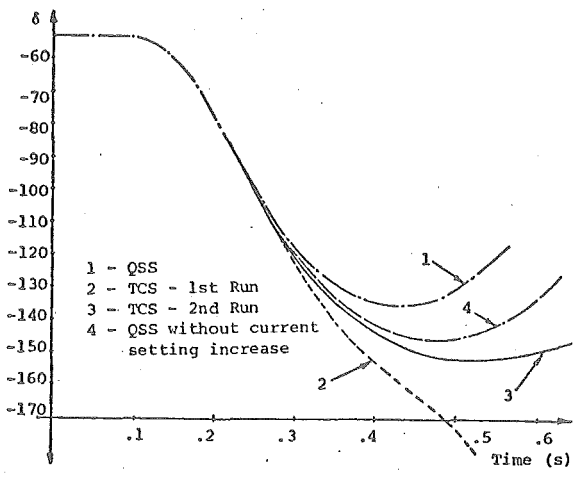

Fig. 15. Current setting control - swing curves.

it is not possible to decide on the applicability of a QSS model without some preliminary TCS case studies for the particular system under consideration. Moreover QSS results are not consistently optimistic or pessimistic.

A.C. short circuits close to the invertor end are likely to produce consequential convertor disturbances which affect the normal firing sequences. In such cases the use of TCS is essential.

It has also been demonstrated that in many cases appropriate matching between the two models can avoid the use of TCS for further disturbances in the same system. The use of TCS in a few selected cases will normally provide sufficient information to modify the QSS model for this purpose.

Results of several case studies obtained using the present New Zealand Primary transmission system indicate differences due to the QSS and TCS models of up to 16%. In more critical systems, it will be even more important to use the TCS model for accurate stability assessment.

ACKNOWLEDGEMENTS

The authors wish to express their gratitude to the General Manager of New Zealand Electricity, Mr. K. D. McCool and to the staff of the Electrical Engineering Department and Computer Centre of the University of Canterbury for their help.

REFERENCES

[1] Heffernan, M.D., Turner, K.S., Arrillaga, J. and Arnold, C.P. "Computation of a.c.-d.c. system disturbances - Part I: Interactive coordination of generator and convertor transient models" (Companion paper).

[2] Arrillaga, J., Heffernan, M.D., Lake, C.B. and Arnold, C.P. "Fault studies in a.c. systems interconnected by h.v.d.c. links", Proc. IEE, Part C, vol. 127, No. 1, Jan. 1980, pp. 14-19.

[3] Arrillaga, J. and El Amin, I.M. "Transient stability performance of a 3-machine system including an h.v.d.c. link", Proc. IEE, vol. 123, No. 11, Nov. 1976.

[4] Brameller, A., Yacamini, R., El Amin, I.M. and Lynch, C.A. "Transient stability of AC-HVDC systems using a direct solution", Paper A79074-6, PES Winter Meeting, N.Y., Feb. 1979.

[5] Vovos, N.A. and Galanos, G.D. "Transient stability of a.c.-d.c. systems", IEEE Transactions, vol. PAS-98, No. 4, July/Aug. 1979, pp. 1376-1383.

[6] Turner, K.S., Heffernan, M.D., Arnold, C.P. and Arrillaga, J. "Computation of a.c.-d.c. system disturbances - Part II: Derivation of power frequency variables from convertor transient response" (Companion paper).

[7] Heffernan, M.D., Arrillaga, J., Turner, K.S. and Arnold, C.P. "Recovery from temporary H.V.D.C. line faults", Paper 80SM 675-9, PES Summer Meeting, Minneapolis, July 1980.

[8] Uhlmann, E. "A.C. network stabilization by D.C. links", CIGRE, paper 32-01, Paris, 1970.